UAB
Universitat Autònoma de Barcelona

In vitro diagnostic designs for applications in health care

Mireia Bernuz Jimeno

ADVERTIMENT. L'accés als continguts d'aquesta tesi queda condicionat a l'acceptació de les condicions d'ús establertes per la següent llicència Creative Commons: https://creativecommons.org/licenses/?lang=ca

ADVERTENCIA. El acceso a los contenidos de esta tesis queda condicionado a la aceptación de las condiciones de uso establecidas por la siguiente licencia Creative Commons: https://creativecommons.org/licenses/?lang=es

WARNING. The access to the contents of this doctoral thesis it is limited to the acceptance of the use conditions set by the following Creative Commons license: https://creativecommons.org/licenses/?lang=en

UAB
Universitat Autònoma de Barcelona

In vitro diagnostic designs for applications in health care

Mireia Bernuz Jimeno

Directors:
Prof. María Isabel Pividori and Dr. Mercè Martí

Doctoral studies in Chemistry
Departament de Química
Facultat de Ciències
Universitat Autónoma de Barcelona
2024

Thesis submitted to aspire for the Doctor Degree

Mireia Bernuz Jimeno

Directors' approval

Dr. María Isabel Pividori Gurgo
Catedràtica d'Universitat
Departament de Química
Universitat Autònoma de Barcelona

Dr. Mercè Martí Ripoll
Professora titular
Departament de Biologia Cel·lular,
Fisiologia i Immunologia
Universitat Autònoma de Barcelona

Bellaterra (Cerdanyola del Vallès), February 2024

Resumen

El creciente interés por nuevas pruebas *in vitro* se justifica por la necesidad de nuevos diagnósticos rápidos específicos y sensibles. Esta demanda se ha vuelto particularmente importante en respuesta al aumento de la prevalencia de enfermedades emergentes. Por lo tanto, el objetivo de esta tesis es explorar el uso de diferentes biomarcadores para el diseño de pruebas *in vitro* en aplicaciones para la atención médica, incluyendo enfermedades tanto infecciosas como no infecciosas. Actualmente, existen diversas estrategias comerciales para su detección, pero su alto precio, instrumentación especializada y procedimientos complejos dificultan su accesibilidad en centros de atención primaria. Por lo tanto, surge la necesidad de desarrollar métodos alternativos de detección basados en biomarcadores novedosos para el diagnóstico temprano. Esta tesis se centra en explorar diferentes biomarcadores: los microRNAs (miRNAs), el RNA mensajero (mRNA) y los exosomas. Se han desarrollado métodos de detección específicos para cada biomarcador, utilizando biopsias líquidas y partículas magnéticas, que han permitido procedimientos mínimamente invasivos para la recolección de muestras y han simplificdo el protocolo al reducir la complejidad de los equipos usados. Además, el rendimiento analítico también se mejora al preconcentrar el analito y minimizar el efecto de la matriz. La primera aproximación se centra en los miRNAs como biomarcadores para la detección de cáncer. Se ha desarrollado un ensayo competitivo de miRNA magneto enzimático para detectar los miRNA21 y miRNA27a dentro de los exosomas, conocidos por tener un incremento en su expresión en el cáncer de mama. La segunda aproximación explora el RNA mensajero del interferón gamma para evaluar la respuesta inmune celular, especialmente relevante durante la pandemia de SARS-CoV-2. En este ensayo, se logró reducir el tiempo de incubación al medir los niveles de mRNA en lugar de las proteínas secretadas. Este método, probado con la infección por SARS-CoV-2, simplifica la evaluación y podría ayudar en el pronóstico. La tercera aproximación investiga los exosomas derivados de neuronas para el diagnóstico temprano de la enfermedad de Alzheimer. Para ello se ha desarrollado un inmunoensayo magnético para proteínas de membrana, utilizando biomarcadores específicos de neuronas y la detección de la proteína beta-secretasa. Todas las estrategias estudiadas en esta tesis acercan los diagnósticos a los centros de atención primaria y entornos con recursos limitados. En resumen, la tesis tiene

como objetivo contribuir al desarrollo de plataformas *in vitro* para la cuantificación de todo tipo de biomarcadores, que pueden adaptarse fácilmente a desafíos emergentes. Esta característica podría ser particularmente significativa con la llegada de otra pandemia, donde el rápido desarrollo de nuevas estrategias de diagnóstico podría ser necesario.

Abstract

The growing interest for novel *in vitro* testing is highlighted by the need for novel specific and sensitive rapid diagnostic. This demand has become particularly important in response to the rising prevalence of emerging diseases. Thereby, the aim of this thesis is exploring the use of different biomarkers for *in vitro* diagnostic designs in healthcare applications, including both communicable and non-communicable diseases. Currently, various approaches are commercially available, but their high cost, benchtop instrumentation, and complex procedures hinder their accessibility in point-of-care facilities. Therefore, there is a need for the development of alternative detection methods based on novel biomarkers for early diagnosis. This thesis is focused on different biomarkers: microRNAs (miRNAs), messenger RNA (mRNA), and exosomes. Specific detection methods were developed for each biomarker, utilizing liquid biopsies and magnetic particles. These allow minimally invasive procedures for sample collection and simplify the protocol, by reducing the complexity of the equipment. Moreover, the analytical performance is also improved by preconcentrating the analyte and minimizing the matrix effect. The first approach focuses on miRNAs as biomarkers for cancer detection. A competitive magneto enzyme-linked miRNA assay was developed to detect miRNA21 and miRNA27a within exosomes, known to be upregulated in breast cancer. The second approach explores interferon gamma mRNA for evaluating cellular immune response, particularly relevant during the SARS-CoV-2 pandemic. A shortened assay time was achieved by measuring mRNA levels instead of protein. This method, tested with SARS-CoV-2 infection, simplifies evaluation, and could aid in prognosis. The third approach investigates neuro-derived exosomes for early Alzheimer's disease diagnosis. A magneto-actuated immunoassay targeting membrane proteins was developed, utilizing neuron-specific biomarkers and beta-secretase detection. All the strategies studied in this thesis brings diagnostics closer to primary healthcare facilities and resource-constrained settings. To summarize, this thesis aims at contributing to the development of *in vitro* platform for the quantification of all types of biomarkers, which can be easily switched to emerging challenges. This feature could be particularly significant with the advent of another pandemic, wherein the rapid development of new diagnostic strategies could be imperative.

Table of content

Chapter 1. Introduction....9
1.1 Liquid biopsies....9
1.2 Biomarkers....11
1.2.1 Micro ribonucleic acid....12
1.2.2 Messenger RNA....14
1.2.3 Exosomes....15
1.2.3.1 Exosome isolation....18
1.2.3.2 Exosome physical characterization....21
1.3 Methodologies for the detection of biomarkers....24
1.3.1 Methods for the characterization and determination of nucleic acid sequences....24
1.3.1.1 Polymerase chain reaction....24
1.3.1.2. Northern blotting....27
1.3.1.3. In situ hybridization....27
1.3.1.4. Next generation sequencing....28
1.3.1.5. Microarrays....28
1.3.1.6. Nuclease protection assay....28
1.3.1.7. Emerging platforms for nucleic acids detection....29
1.3.2. Methods for the characterization and determination of proteins....32
1.3.2.1. Flow Cytometry....32
1.3.2.2. Enzyme-linked immunosorbent assay....33
1.3.2.3. Western blot....34
1.3.2.4. Proteomics....34
1.3.2.5. Emerging platforms for protein detection....35
1.4 Point-of-care devices for diagnosis in health care....38
1.4.1. Biosensors....39
1.4.1.1. Classification based on the bioreceptor....39
1.4.1.2. Classification based on the transducer....40
1.4.2. Trends in POC testing....41
1.4.2.1. Mobile health....41
1.4.2.2. Paper-based platforms....43
1.4.2.3. Magnetic particles....44
1.5 References....47
Chapter 2.Objectives....67

Chapter 3. Competitive magneto enzyme-linked miRNA assay for quantification of microRNAs in exosomes....73

3.1. Abstract....73

3.2. Introduction....73

3.3. Experimental....75

3.3.1. Instrumentation....75

3.3.2. Chemicals and biochemicals....75

3.3.4. Exosome isolation and characterization by nanoparticle tracking analysis and transmission electronic microscopy....76

3.3.5. Scaffold assembly on Oligo(dT) magnetic particles....76

3.3.6. Competitive magneto enzyme-linked miRNA assay....77

3.3.7. Specificity study....78

3.3.8. Quantification of miRNA1 and miRNA27a in breast cancer cell lines and derived exosomes....78

3.3.9. qPCR....79

3.3.10. Statistical Analysis....79

3.3.11. Safety Considerations....79

3.4. Results and discussion....79

3.4.1. Exosome isolation and characterization by nanoparticle tracking analysis and cryogenic transmission electronic microscopy....79

3.4.2. Competitive magneto enzyme-linked miRNA assay. Specificity study....80

3.4.3. Quantification of miRNA21 and miRNA27a in breast cancer cells and their derived exosomes....83

3.5. Conclusions....85

3.6. Supplementary data....87

3.6.1. Materials....87

3.6.2. Scaffold assembly on Oligo(dT) magnetic particles....90

3.6.3. miRNA extraction and quantification....96

3.6.4. qPCR....98

3.7 References....101

Chapter 4. Rapid diagnostic test for assessment of cellular immune response in a viral infection as a model....107

4.1. Abstract....107

4.2. Introduction....107

4.3. Experimental....109

4.3.1. Instrumentation....109

4.3.2. Chemicals and biochemicals....110

4.3.3. Rapid diagnostic test for assessment of cellular immune response 111
4.3.4. Whole blood stimulation, immunomagnetic separation of the lymphocytes and capturing of the transcripts 112
4.3.5. Double-tagging RT-PCR on magnetic beads 112
4.3.6. Lateral flow assay 113
4.3.7. Study design and ethics 113
4.3.8. Statistical Analysis 114
4.4. Results and discussion 114
4.4.1. Rapid diagnostic test for the assessment of cellular immune response 114
4.4.2. Rapid diagnostic test for the follow up of cellular immune response 117
4.5. Conclusions 120
4.6. Supplementary data 122
4.6.1. Experimental 122
4.6.2. Carbon nanoparticle modification with avidin 123
4.6.3. Demographic information of the study 124
4.6.4. Optimization of the rapid diagnostic test for the assessment of cellular immune response 124
4.6.5. Detection of IFN-γ expression by lateral flow assay in whole blood samples. Optimization of the assay conditions 127
4.6.6. Rapid diagnostic test for the assessment of cellular immune response 131
4.6.7. Statistical analysis 132
4.6.8. Future perspectives 134
4.6.9. Interferon gamma release assays 135
4.7 References 138
Chapter 5. Detection and characterization of neuroblastoma exosomes by magneto-actuated immunoassay for Alzheimer's Disease diagnosis 143
5.1. Abstract 143
5.2. Introduction 143
5.3. Experimental 146
5.3.1. Instrumentation 146
5.3.2. Chemicals and biochemicals 146
5.3.3. Cell culture 148
5.3.4. Exosomes isolation and purification 149
5.3.5. Exosomes characterization for nanoparticle tracking analysis and cryogenic transmission electronic microscopy 149
5.3.6. Immobilization of antibodies on magnetic particles 150
5.3.7. Flow cytometry 150

5.3.8. Magneto-actuated immunoassay 150
5.3.9. Statistical Analysis 152
5.3.10. Safety Considerations 152
5.4. Results and discussion 152
5.4.1. Characterization of exosomes by nanoparticle tracking analysis and cryogenic transmission electron microscopy 152
5.4.2. Characterization and comparative of the biomarkers expressed by SH-SY5Y cells and their derived exosomes. 153
5.4.3. Design of a combination of biomarkers for the neuronal derived exosomes detection 154
5.4.4. Magneto-actuated immunoassay 155
5.5. Future perspectives 158
5.6. Conclusions 158
5.7. Supplementary data 160
5.7.1. Experimental 160
5.7.2. Flow cytometry set up 160
5.7.3. Characterization of the SH-SY5Y and their derived exosomes 163
5.7.4. SH-SY5Y cell line differentiation 166
5.7.5. Characterization of human-derived exosomes from cerebrospinal fluid and plasma samples 168
5.8. References 174
Chapter 6. Final remarks 181

Glossary

AD	Alzheimer's disease
AgNC	Silver nanoclusters
ALP	Alkaline Phosphatase
ATCC	American type culture collection
AuNP	Gold nanoparticles
BACE1	Beta secretase
BIO	Biotin
BSA	Bovine serum albumin
CD	Cluster of diferentiation
cDNA	Complementary DNA
CFSE	Carboxyfluorescein succinimidyl ester
CNP	Carbon nanoparticles
Cryo-TEM	Cryogenic transmission electron microscopy
CSF	Cerebrospinal fluid
CTC	Circulating tumor cells
Cy5	Tetramethylindo(di)-carbocyanine-5
DIG	Digoxigenin
DLS	Dynamic light scattering
DNA	Deoxyribonucleic acid
EGFR	Epidermal growth factor receptor
ELISA	Enzyme-linked Immunosorbent Assay
EV	Extracellular vesicles
FBS	Foetal bovine serum
FDA	Food and Drug Administration
FITC / FLU	Fluorescein
HRP	Horseradish Peroxidase
IFNγ	Interferon gamma
ILV	Intraluminal vesicles
LFA	Lateral flow assay
LOD	Limit of detection
MCI	Mild cognitive impairement
mHealth	Mobile health
miRNA	Micro RNA
MP	Magnetic particles
mRNA	Messenger RNA
MVB	Multivesicular bodies
NDE	Neuron derived exosomes
NGS	Next generation sequencing
NTA	Nanoparticle tracking analysis
PBS	Phosphate buffer saline
PCR	Polymerase chain reaction
POC	Point-of-Care

qPCR	Quantitative PCR
RA	Retinoic Acid
RDT	Rapid diagnostic test
RNA	Ribonucleic Acid
RT	Reverse transcription
SARS-CoV-2	Severe acute respiratory syndrome coronavirus
SEM	Scanning electron microscopy
WHO	World Health Organization

Chapter 1.

Introduction

1.1. Liquid biopsies

In recent years, minimally invasive procedures have been gradually replacing invasive techniques in health care applications as for diagnosis, prognosis, and monitoring[1]. Considering the complications and challenges associated with traditional biopsies, liquid biopsies offer a promising alternative[2]. This term was first used for the analysis of circulating tumor cells (CTCs) but nowadays also include subcellular structures and circulating biomolecules, among others[3]. Liquid biopsies are based on the analysis of biological fluids, primarily involving blood sampling, but also including other fluids such as saliva, cerebrospinal fluid (CSF), or urine (Fig. 1.1). Its relevance was noticed in 2015, when it was considered one of the top ten breakthrough technologies by the MIT Technology Review[4].

When comparing liquid to tissue biopsies, the major advantage is the minimally invasive procedure for sample acquisition, as well as repeatability and reduced cost. Moreover, liquid biopsies can provide a more comprehensive view of the pathological state compared to a tissue biopsy, where the information is limited to the collected cells. However, tissue biopsies can provide histological information about the evaluated tissue, which is sometimes necessary for a final diagnosis[5]. Their easy obtention is also very useful for procedures like early treatment response evaluation or monitoring where repetitive sampling is required. Additionally, they have gained particular interest in children's healthcare, where less invasive procedures are continually developed, particularly for pediatric cancers. However, the liquid biopsies are not yet considered gold standard methodologies but complementary analysis[2].

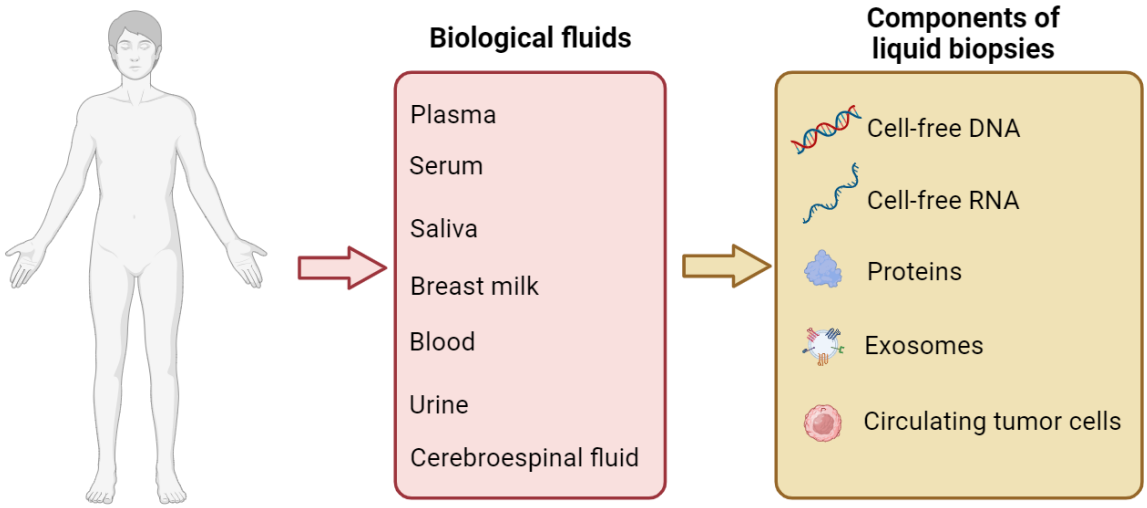


Figure 1.1. Biological fluids included in the liquid biopsies and the components found in them considered as biomarkers. Created with Biorender.com.

Liquid biopsies can be used for the analysis of a wide range of biomarkers with potential for health and disease evaluation. The main biomarkers involved in liquid biopsies include the following:

i. Circulating tumor cells (CTCs). CTCs were first described in 1869[6]. They are cells shed from the primary tumor during cancer development and are involved in metastasis seeding. Their release into the bloodstream allows their use as biomarkers in liquid biopsies containing tumor information[7]. There is an FDA-approved system for CTC detection called CellSearch, and it has been used in several studies for cancer prognosis[8,9].

ii. Cell-free DNA. This type of DNA can be detected in circulation, primarily in blood, but also in urine or CSF. It can circulate bound to proteins such as histones, lipids, forming macromolecules or be associated with extracellular vesicles (EVs)[5]. Cell-free DNA can be used to identify genetic alterations of affected cells including; mutations, epigenetic changes, or copy number variations[10].

iii. Cell-free RNA. Cell-free RNA can also be found in circulation, mainly noncoding RNA, including small RNAs and long noncoding RNAs[5]. MicroRNAs are the most studied given their implication in pathological dysregulations, as seen in heart failure where nearly 30 circulating miRNAs undergo expression changes, making them suitable for use as diagnostic biomarkers[11].

iv. Exosomes. Exosomes are small vesicles (ranging from 30 to 200 nm) secreted by most cell types, containing information from the originating cells. These vesicles, secreted via the endocytic pathway, contain proteins and nucleic acids and reflect the state of the cells from which they originate. Thus, they become suitable biomarkers in pathological processes. They have been studied for their use in neurodegenerative diseases early diagnosis[12] as well as in cancer[13], among other non-communicable and communicable diseases.

v. Proteins. Circulating proteins related to pathologies can be found in different body fluids, including communicable i.e. infectious diseases and non-communicable diseases as neoplasms or neurodegenerative diseases.

Regarding other biofluids, biomarkers in saliva and urine are being studied. Saliva has been determined to be useful for the evaluation of systemic diseases, buccal diseases and for pharmacotherapy[2,14]. On one hand, they can be evaluated in saliva, for example the EGFR gene mutation in CTCs of lung cancer patients[15], the dental caries etiology evaluation analyzing the pH levels as well as other parameters as bacterial load or saliva flow among others[16], or antiepileptic drugs detection for therapeutic monitoring of people with epilepsy[17]. On the other hand, urine has been used for urinary and non-urinary diseases. Analyzing free tumor DNA and an mRNA for the detection of bladder cancer[18,19] or by detecting it for the therapy evaluation in non-small cell lung cancer[20].

1.2. Biomarkers

A biomarkers, also known as biological marker, is described as '*a defined characteristic that is measured as an indicator of normal biological processes, pathogenic processes or responses to an exposure or intervention*.' by the National Institutes of Health Biomarkers Definitions Working Group as a basic definition[21]. Although, it has also been defined by the World Health Organization (WHO) as '*any substance, structure, or process that can be measured in the body or its products and influence or predict the incidence of outcome or disease'*. Through these definitions, biomarkers can include from pH levels or oxygen saturation in blood to proteins or gene expression patterns among many others. Biomarkers can be found in various types of body fluids, including blood, urine, saliva, as

well as tissues. The qualitative and quantitative analysis of these biomarkers is mainly performed in laboratory facilities by expert personnel.

Biomarkers analysis is nowadays a hot topic in bioanalytical chemistry. Enhancing clinical diagnostic capabilities in low-resource settings stands as the initial and crucial step toward advancing global health. Therefore, in response to this social challenge, the research into new rapid diagnostic tests (RDTs) closer to point-of-care (POC) testing are being developed.

Biomarkers utilized during this thesis, including micro RNAs, messenger RNAs and exosomes, will be described in detail below, including their detection methods, applications and relevance in POC testing.

1.2.1. Micro ribonucleic acid

Micro ribonucleic acid (microRNAs, or most common miRNAs) are short RNA molecules encompassed within the group of the small non-coding RNAs. They were firstly described in 1993 in *Caenorhabditis elegans*[22]. They were defined as small transcripts that did not encode for proteins but were responsible of the regulation of translation via antisense RNA-RNA interaction[22]. Although this regulation system was firstly found in *C. elegans*, through the years miRNAs have been described in a wide variety of species with some miRNA families being phylogenetically conserved e.g., lin-4 and let-7 among others[23,24]. Nowadays, they are described as evolutionary conserved non-coding RNA sequences with a length ranging from 19 to 24 nucleotides. Their function is the posttranscriptional regulation or silencing of their target genes. This way, a single miRNA can regulate the activity of more than one gen. Thus, abnormal expression of miRNAs is known to be associated with various communicable[25] and non-communicable[26,27] diseases.

The miRNA biogenesis can be divided either into the nuclear or the cytoplasmatic steps (Fig. 1.2). First, the miRNA sequences are transcribed, mainly by polymerase II, into a long primary transcript called pri-miRNA. This sequence adopts a harpin structure which suffers a first cleavage performed by the Drosha RNase III endonuclease and other associated proteins. The sequence is cleaved near to the base of the stem loop resulting in the formation of pre-miRNA (around 70 nt)[28,29]. Once this first cleavage is performed, the sequence is transported into the cytoplasm. In the cytoplasm, the pre-miRNA is further

processed RNase III and Dicer resulting in the formation of an RNA duplex through the loop cleavage. This RNA duplex interacts with the Argonaute protein 2 (Ago2) forming the RNA-induced silencing complex (RISC) in conjunction with the Hsp70/Hsp90[30]. During the complex maturation only one of the strands (miRNA), called the guide strand, is going to remain into the complex. The association of the miRNAs to the complex protect them of degradation. Mature RISC is then going to bind to the target mRNA for its regulation[29].

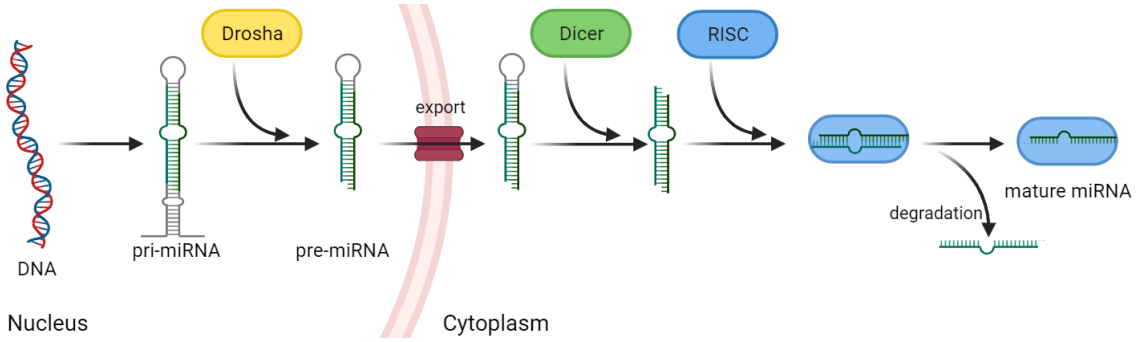


Figure 1.2. miRNA biogenesis, it is divided in subsequential steps of maturation in the nucleus and in the cytoplasm. First, the pri-miRNA is transcribed from the nuclear DNA and subsequently cleaved by Drosha to pre-miRNA to be exported to the cytoplasm. Pre-miRNA is cleaved and then assembled to the RISC complex to complete its maturation. Created with Biorender.com.

Micro RNAs are released by both healthy and dysregulated cells, opening the possibility of using them as potential biomarkers through minimally invasive procedures as liquid biopsies[31]. They can be detected in most of the body fluids such as plasma, serum, urine, tears, saliva, cerebrospinal fluid, breast milk, and bronchial lavage among others[32,33]. Circulating miRNAs are protected from RNase activity, this protection is hypothesized to happen due to their release, not only as free molecules to the extracellular space, but also associated to other molecules or encapsulated within exosomes[34]. These characteristics make the miRNAs as suitable biomarkers for health care purposes.

Despite the rising interest of miRNAs as potential biomarkers, the nature of the biomolecules carries some challenges for a robust and affordable detection, considering that miRNAs are short sequences with high homology levels and present at low concentration[31]. There are several detection methods currently in use for the detection of these miRNAs, including conventional PCR and real-time PCR (qPCR), miRNA microarrays[35], *in situ* hybridization analysis[36], northern blot analysis[37] and next-generation sequencing technology (NGS)[38]. Nowadays the RT-qPCR is considered the gold standard

method for the miRNA detection[39]. Preamplification steps are commonly added due to enlarge the sequences and to further increase the concentrations of the analyte. Considering that each miRNA is associated with the regulation of multiple genes, therefore, multiplexing-capable methodologies are of particular interest for this kind of biomarkers.

1.2.2. Messenger RNA

Messenger RNA (mRNA) was described long before the miRNA sequences. In 1961, two Nature distinctives papers reported for the first time unstable nucleic acid sequences encoding information for the protein synthesis[40–42]. Since then the knowledge of these RNA sequences have increased to the point that nowadays they can be synthesized, and used for therapeutic purposes as vaccines[43,44] and also as diagnostic biomarkers tools[45].

Nowadays, mRNAs are described as single-stranded ribonucleic acid sequences transcribed from DNA with short lifetime (between minutes to hours)[46] and that carry the information for the transcription into proteins. The mRNA biogenesis starts with the transcription, where the DNA is used as the template for the pre-mRNA synthesis through the RNA polymerase II, which must bound to the promoter of the gen along with the transcription factors[47,48]. This addition leads to a conformational change of the DNA unwinding it. This pre-mRNA maturing process starts while is being translated including the sequence capping (avoiding the degradation) and requiting complexes for the RNA processing[49]. Subsequently the splicing is performed removing the introns (non-coding sequences) and ligating the exons (coding sequences) by the spliceosome. Moreover, a poly(A) polymerase adds a poly A tail to the 3’ end. Previous to the exportation to the cytoplasm, the mRNA is packed into an RNA/protein complex containing export factors among others[50]. This complex crosses the nuclear membrane through the nuclear pore complex. Once in the cytoplasm, the mRNA will bind to ribosome for the translation, a process that involves converting the nucleic acid sequence into amino acids using the genetic code, with codons of three bases specific for each amino acid (Fig. 1.3).

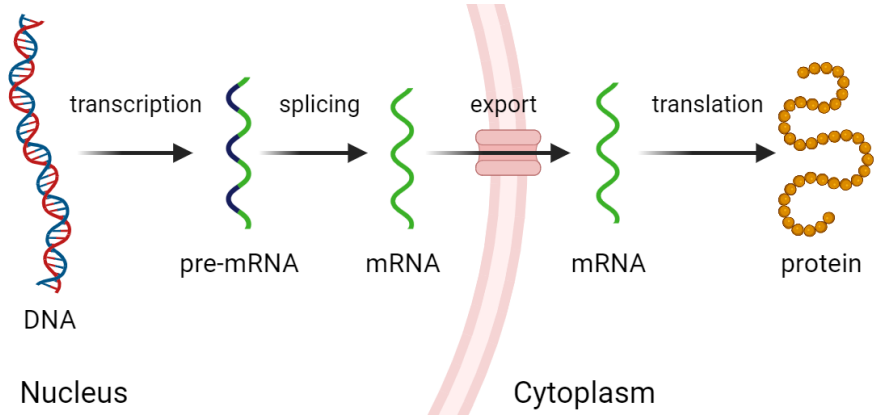


Figure 1.3. mRNA biogenesis, from the transcription of the DNA to the mRNA translation to protein. Created with Biorender.com.

The regulation of the mRNA sequences must be fine controlled due to their direct correlation to the protein synthesis. Thus, alterations in their regulation can lead to pathology. Moreover, changes in their expression can be monitored to determine cellular stages and processes, being suitable biomarkers in the homeostasis dysregulation.

1.2.3. Exosomes

The first time the terminology of exosomes was used regarding to extracellular vesicles (EV) was in 1987 by Johnstone *et al.*[51] in reference to vesicles released by reticulocytes, immature red blood cells. Nevertheless, the secretion of vesicles was previously observed. In the late 1960s, Wolf reported the release of extracellular vesicles by the platelets which he called "platelet dust"[52]. Since then, the study of exosomes and its knowledge have been rapidly expanded. In particular, after its origin in multivesicular bodies (MVB) was described, images of the exosomes were obtained through electron microscopy during the 1980s. During this period, their biological potential was identified. Previously, exosomes were described as '*a major route for externalization of obsolete membrane proteins'* and as cellular debris[53]. Thus, their content alteration depending on different physiological conditions open their potential use as biomarkers.

With the exponential growth of the field, nomenclature has become an issue due to the indiscriminate use of exosomes, microvesicles or microparticles as synonymous terms. Due to this, the International Society of Extracellular Vesicles (ISEV) was formed after an international EVs meeting, proposing an harmonization for the criteria[54]. The guidelines are periodically updated including and modifying the concepts and definitions. Since then,

many societies have been founded around the world focusing in EVs research. Nowadays, exosomes are described as bilipid vesicles classified as a subset of the extracellular vesicles. EVs classification has been controversial due to the heterogeneity of the expressed biomarkers. Thus, the classification has been determined by the size and origin of the vesicles dividing them into apoptotic bodies, ectosomes (or microvesicles) and exosomes.

Apoptotic bodies are the larger vesicles with sizes comprised between 200 and 5000 nm and a density of 1.16–1.28 g · mL^{-1} [55]. They are generated by the budding of the dying cells membrane containing subcellular fragments of the oncoming apoptotic cells such as organelles and nuclear content (Fig. 1.4). In contrast to the other EVs, apoptotic bodies are not involved in cell-to-cell communication but as hallmarks of apoptosis. They have also an important role in its correct development facilitating the clearance of the cells[56].

Ectosomes, also called microvesicles, are medium sized EVs (100 to 1000 nm, 1.04–1.07 g · mL^{-1} density) originated by the plasmatic membrane budding (Fig. 1.4). They contain cytoplasmatic material as well as adhesion molecules[55,57] and are known to be involved in the cell-to-cell communication through biomolecules trafficking. This can occur by their fusion with the membrane of their target cell, by being taken by endocytosis but also by releasing their content into the extracellular space[58,59].

Exosomes are the smallest EVs, between 30-200 nm size and a density among 1.13–1.19 g · mL^{-1} [55]. Exosomes, differentially of the other EV, are not released directly from the extracellular membrane but from the multivesicular bodies (MVB). MVB are intracellular endosomal organelles containing multiple intraluminal vesicles (ILVs) formed by the budding of the endosomal membrane abducting cytosolic components. Once ILVs are secreted into the extracellular space, they become exosomes[60] (Fig. 1.4).

Exosome biogenesis begins with the invagination of the extracellular membrane in an endocytosis process forming an early endosome. They can mature into late endosomes or MVBs with the formation of ILVs. However, not all ILVs are transported to the extracellular space (through the MVB fusion with the cell membrane) for their release via microtubules and the cytoskeletal network.

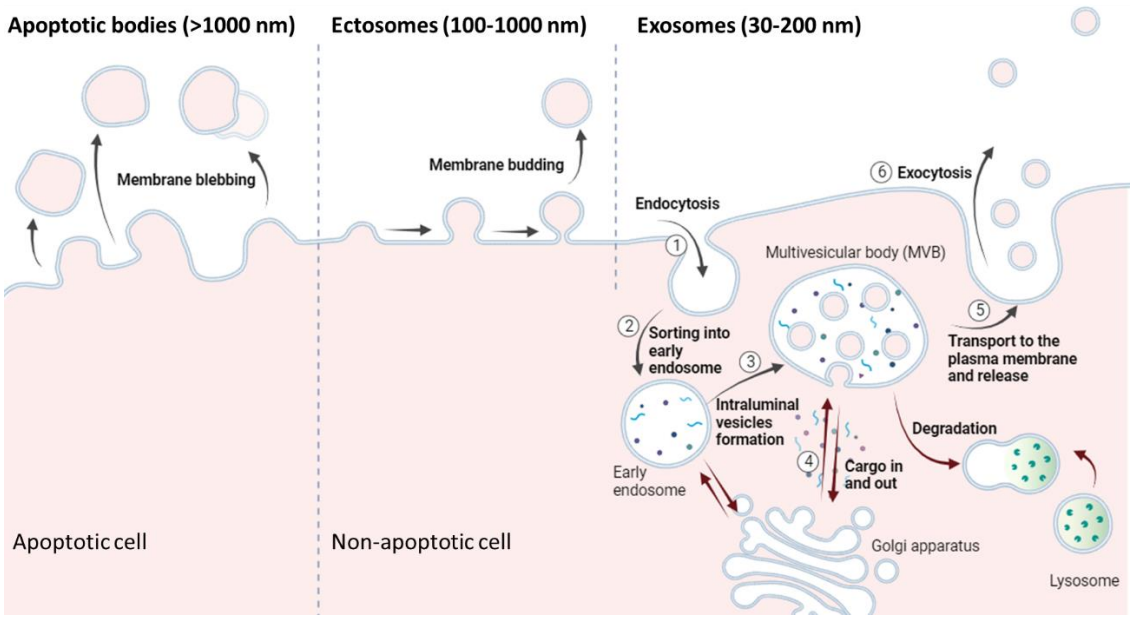


Figure 1.4. Types of extracellular vesicles and their biogenesis pathway: i) apoptotic bodies, the membrane blebbing during the cell apoptosis; ii) ectosomes, the budding of the plasmatic cell membrane; and iii) exosomes, the exocytosis of the intraluminal vesicles into the multivesicular bodies. Created with biorender.com.

The MVBs can also be fused with lysosomes to a degradation pathway. Due to this, biogenesis of the exosomes content is related to its transport and release, and also serve as a mirror of its oncoming cells and its physiological state[55]. Their cargo can include proteins and nucleic acids, among others. Tetraspanins (specifically CD9, CD63, and CD81) are the predominant proteins found in exosomes membrane. These proteins are well-known for their roles in facilitating the incorporation of cytoplasmatic cargo and interactions with cytosolic proteins. Other proteins involved in their transport and release as flotillin and caveolin-1, integrins and adhesion molecules, as well as soluble proteins in the inside as Alix protein, heat shot proteins (Hsp), cytoskeletal and associated proteins (actin, vimentin, annexin and talin) and enzymes (such as phosphoglycerate kinase 1 and glyceraldehyde3-phosphate dehydrogenase)[57,61]. In addition, exosomes are rich in nucleic acids such as DNA, RNA, and non-coding RNA[55]. Among these nucleic acids, miRNAs is the most abundant RNA species, playing crucial roles in various physiological processes through cell-to-cell communication[62]. Several lipids have been determined to be enriched in the membrane of the exosomes, such as lysobisphosphatidic acid, contributing to cholesterol accumulation in the membrane[59].

The majority of the cells produce exosomes and release them to the extracellular space. Thus, they can be found in various body fluids including blood[63], plasma[64], serum[65], saliva[66], breast milk[67], urine[68] or CSF[69], being possible to obtain information of the pathological hallmarks of their oncoming cells with minimally invasive procedures.

1.2.3.1. Exosome isolation

Exosome detection requires its separation from the complex matrix of the sample. This procedure is challenging due to the low concentration and the complexity of the biological matrices. Moreover, different isolation methods must be considered for the isolation of exosomes since not all the methods are suitable for all downstream applications.

Differential ultracentrifugation

Differential ultracentrifugation was the first described technique for exosomes isolation, and it is still the most used and considered as the gold standard method[70]. It was initially developed for isolation of the exosomes from reticulocytes[51]. Since then, the protocol has undergone minimal optimizations in terms of time and centrifugation rates, resulting in the current protocol[71]. The procedure is based on the use of subsequently centrifugations for the elimination of the particulate interferents until the exosomes are pelleted. It consists of four steps of serial centrifugation at: i) 300 *g* for the cell separation, ii) 2000 *g* centrifugation for the death cell and debris elimination, iii) 10,000 *g* centrifugation for the bigger EVs separation and iv) 100,000 *g* centrifugation for the exosomes pelleting[72]. Although, the centrifugation times are typically established, they can vary depending on the viscosity of the biological samples[73]. The detailed process is depicted in figure 1.5.

This well-stablished protocol yields a quite pure exosome recovery with low contamination of other EVs also present in the starting sample and without the need of pre-sample treatment, but it is moderately time-consuming. While the protocol itself is not expensive, it requires a benchtop equipment[74]. It requires the usage of ultracentrifuges and their associated rotors can be expensive to purchase and maintain, making them a significant investment for labs. Moreover, it is quite important to have an ultracentrifuge for low volume samples suitable for biological liquid biopsies. Operating an ultracentrifuge require specialized training and require regular maintenance and calibration to ensure accurate and safe operation. Finally, in some smaller or resource-constrained laboratories, the

availability of ultracentrifugation equipment may be limited, making this method less accessible.

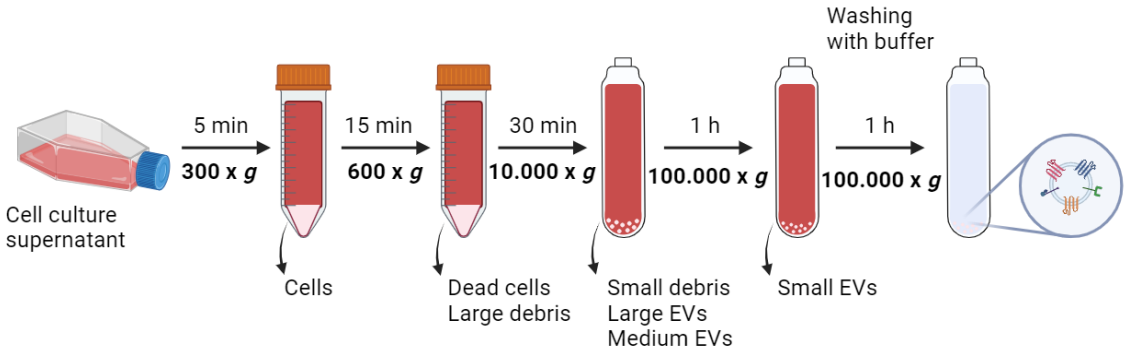


Figure 1.5. Protocol of the differential ultracentrifugation for the exosome isolation. Subsequently centrifugations for the elimination of the larger particles and cellular debris (from 300 x *g* to 100.000 x *g*), using cell culture supernatant as example. Created with Biorender.com.

Density gradient ultracentrifugation

This separation method is based on the use of a known density solution for the separation of exosomes. It allows the separation of the exosomes from other non-vesicular particles similar in size. Thus, it permits the obtention of very pure samples. The most used density gradient is sucrose[75], but others are used as iodixanol[73,76]. This method is suitable for complex and viscous samples.

The samples obtained through this method are high pure thus, suitable for high-sensitive downstream applications such as proteomics or transcriptomics. However, the ultracentrifugation used for the separation is very time consuming, it requires among 14-16 h at high speed (100,000-160,000 *g*). The density gradient is a key step for a good recovery and reproducibility. Moreover, this long-time ultracentrifugation can lead to vesicle aggregation and mechanical damage.

Size-exclusion chromatography

Size-exclusion chromatography is a method that separates the different components of a complex sample by size. The sample is loaded into a column containing heterosporous polymeric beads. As it passes through the column, different sample components are separated into fractions that can be collected[77]. It is a mild method that preserves the integrity of the exosomes, maintaining the functionality of the proteins (e.g., the enzymes

activity). To ensure this, the assay is performed at low pressure conditions or even gravimetrically. Sepharose columns are the most used, and they are readily commercially available for exosomes separation including Exopure™ (BioVision, Milpitas, CA, USA), qEV Exosome Isolation (Izon Science, Christchurch, Canterbury, NZ), and PURE-EVs Columns (HansaBioMed, Tallinn, EE).

Even though is a good method for the obtention of pure exosomes, the separation by size can cause the obtention of non-vesicular aggregates and their dilution, particularly in the Sepharose-based methods, compared to the polyethylene glycol[78]. The purity of the samples makes this method suitable for downstream applications as the "omics".

Filtration

The filtration of the samples through membranes can also be considered as size-exclusion physical separation method. Membranes retain any kind of particles larger than a determined size while allowing particles below the size pass through. This method is simple, but yields less pure exosomes compared to the other methodologies[79]. Moreover, the porous of the membranes can be clogged and bigger particles can pass through if they are malleable. It is usually carried out in combination with other isolation methods to increase the purity of the samples[77].

Polymer-based precipitation

With the increasing interest in the exosomes research, scientific suppliers have developed minimal equipment protocols for their obtention. One of the most popular is the polymer-based precipitation. Briefly, this method is based on the use of a polymeric matrix binding water molecules that force the precipitation of less soluble particles as EVs through a mild centrifugation step[80,81]. It is an easy separation method that conserves the structure and functionality of the exosomes. Nevertheless, the exosomes obtained are not pure, other EVs can be precipitated with the exosomes as well as non-vesicular particles as proteins. Thus, this methodology is not suitable for downstream applications that requires high purity exosomes as proteomic studies[74,82]. Some of the commercial kits available are ExoQuick™ (System Biosciences, Mountain View, CA, US), Total Exosome Isolation kit (Invitrogen, Waltham, MA, US) or ExoPure™ (BioVision, Waltham, MA, US).

Solid-phase separation based on magnetic particles

Immunomagnetic separation (IMS) is based on the use of biologically modified paramagnetic particles to attach specific targets and enables its isolation applying a magnetic field. It is a versatile technique that allows exosomes separation based on their surface markers. Thus, while the exosome population can be isolated by using exosome general markers, specific exosomes can be enriched by using an oncoming cell specific marker. It is a powerful tool for preconcentration and for matrix effect reduction, being an emerging tool for downstream applications as for biosensors.

The magnetic particles (MP) can be functionalized with different molecules. Antibodies are the most popular, but other affinity molecules can be also used[13,83,84]. Depending on the specific downstream application, additional steps may be necessary, including the elution of the exosomes attached on the MP. A prior centrifugation at 10,000 g for cell and cell debris removal is mandatory for successful separation and purification[13,85].

1.2.3.2. Exosome physical characterization

Prior to the determination of exosomes biomarkers in diagnostics, their purity and integrity must be assessed to guarantee the quality of the results. This characterization is also used for the comparison of the different separation methods assessing the robustness of the subsequently results obtained. This physical characterization is performed for the obtention of size and morphology information.

The methodologies used include electron microscopy techniques, such as transmission and scanning electron microscopy (TEM and SEM), providing information of the morphology and size of the EVs as well as the atomic force microscopy (AFM). Nanoparticle tracking analysis (NTA) and dynamic light scattering (DLS) which provide information of the size and concentration of the nanoparticles, and tunable resistive pulse sensing (TRPS) presented as an impedance-based alternative method to NTA for sizing and counting EVs.

Electron Microscopy

Transmission electron microscopy (TEM) and scanning electron microscopy (SEM) are employed to visualize exosome morphology and size. Specifically cryo-TEM microscopy is

the most popular technique for this purpose, replacing the negative staining which has traditionally been used for exosome visualization[86]. TEM techniques are based on the analysis of the electron beams that can either transmit or be diffracted when applied to a sample previously deposited on a carbon grid. Conventional TEM imaging includes a fixation and dehydration of the sample which can cause artifacts like the observation of cup-shaped exosomes. This was overcome with the cryo-TEM due to the sample preparation protocol. Samples are fixed by cryo-immobilization, vitrifying the water, and preventing crystals formation by liquid ethane cooling. This preserves the structure of the EVs and avoid the artifacts. Low temperature must be maintained during all the measuring procedure using liquid nitrogen (below -175ºC) (Fig. 1.6)[87].

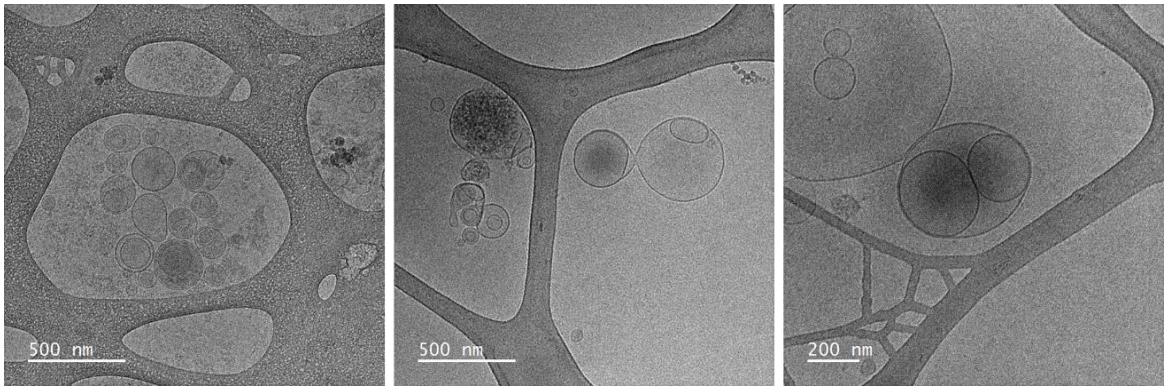


Figure 1.6. Cryo-TEM micrographs of exosomes and EVs obtained from the supernatants of cultured breast cancer cell lines MCF-7 and MDA-MB-231, obtained with a Jeol JEM 2011 microscope. Images obtained in the Service of Microscopy at Universitat Autònoma de Barcelona.

SEM is based on applying an electron beam to a sample to scan its surface, obtaining topography information. Samples must be previously fixed (chemically or cryogenically) and dehydrated. In addition, a thin layer of a conductive material must be deposited into the sample surface for their visualization[88]. Due to the small exosomes size this layer can affect its visualization[89]. Technological advances in SEM as Cryo-SEM and low voltage SEM allow the simplification of the sample preparation (no metallization required) and the preservation EV integrity.

Atomic force microscopy

Atomic force microscopy (AFM) is utilized for determining the morphology of EVs. It relies on scanning across the surface of a sample using a small cantilever. The tip at the end of

the cantilever contacts the surface, causing the cantilever to bend and altering the amount of laser light reflected into the photodiode generating topographic images with nanometric resolution. AFM requires minimal sample preparation, as they have to be adsorbed into a holder to a subsequently drying step previous to the procedure[90].

Nanoparticle Tracking Analysis

Nanoparticle tracking analysis (NTA) is a methodology based on the rate of Brownian motion of each individual particle, which can be used to calculate its hydrodynamic size. It is the currently gold standard method for the measurement of size distribution and concentration of nanoparticles in solution. Briefly, NTA uses a peristaltic pump to inject the sample into a chamber equipped with a laser light source and a CMOS (i.e., complementary metal oxide semiconductor) camera connected to an optical microscope. This provides a real-time analysis, recording videos of the scattered light of each particle tracked, which enables statistical calculation of particle size distribution by the Stokes-Einstein equation. Since the volume of the chamber is known, the concentration of the particles in the solution can be calculated[91] (Fig. 1.7).

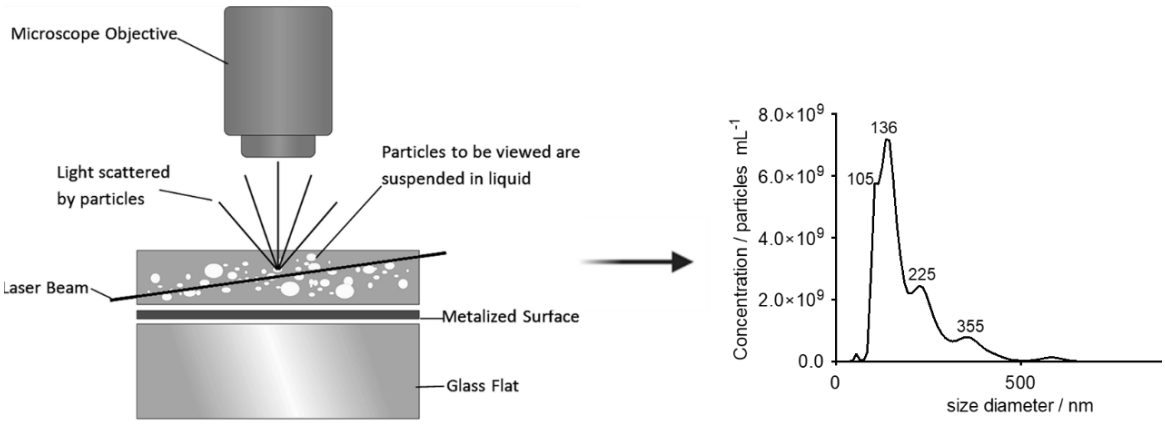


Figure 1.7. Schematic representation of the nanoparticle tracking analysis instrument[92] and graphical representation of the results obtained from the analysis of an exosome sample.

In addition, a fluorescence module can be integrated into the NTA, allowing the analysis of previously labelled populations. However, high expression biomarkers must be used for a proper detection.

Dynamic light scattering

Dynamic light scattering (DLS) is also a Brownian motion-based technique for calculating the size distribution of the EVs. DLS is based on the analysis of the motion of the nanoparticles hit by a polarized and monochromic light beam[90]. As opposed to the NTA, DLS cannot determine the concentration of the nanoparticles. However, it is able to detect smaller particles, below 10 nm[93].

Tunable resistive pulse sensing

Tunable resistive pulse sensing (TRPS) is a size distribution and concentration determination alternative to the NTA. It is based on the application of voltage into a flow chamber while the sample is passing through a porous membrane and measuring the impedance changes produced by the EVs. The magnitude of the signal is related to the particle size, giving also concentration of the sample[90].

1.3. Methodologies for the detection of biomarkers

Biomarkers can be detected through a wide variety of methods depending on the information wanted to obtain and the type of biomolecules to be determined. Methodologies for the detection of nucleic acids and proteins are going to be reviewed on the following section.

1.3.1. Methods for the characterization and determination of nucleic acid sequences

The detection methods for the nucleic acid sequences can be used for RNA and DNA sequences but they are more suitable for different nucleic acid species depending on their characteristics. Moreover, these methodologies will have slight differences depending on the sequences they will be applied. Each of the methods have their advantages and disadvantages, thus, depending on the purpose one method or another will provide better information.

1.3.1.1. Polymerase chain reaction

Reverse transcription polymerase chain reaction (RT-PCR) is a common technique for the RNA amplification and detection. It is one of the main techniques for the mRNA determination and it is used as a gold standard for miRNAs detection[39]. It has always a

previous step of synthesis of the cDNA though a reverse transcription and then it can be followed by a conventional PCR or by a real-time PCR or quantitative PCR (qPCR). As mentioned before, this technique is based on the amplification of cDNA though a polymerase. This amplification is performed by several consecutive cycles composed by three steps: i) denaturation, ii) annealing, and iii) elongation. The difference between the conventional PCR and qPCR is the readout method. Even though the qPCR is a very sensitive method it is expensive compared conventional PCR. Moreover, the RNA isolation methods used are crucial to avoid possible interferents or bias on the amplification.

Prior to the amplification, the mRNA is retrotranscribed, synthetizing double chain cDNA. The cDNA synthesis is performed by a reverse transcriptase using oligo(dT) primers which will attach to the polyA chain of the mRNA sequences and allow the transcription. In the case of the miRNAs amplification, due to its characteristics, additional steps are often necessary to ensure an adequate performance. To overcome the challenge of the short length of miRNAs during the reverse transcription, specialized primers such as stem-loop or linear retrotranscription (RT) primers, or the use of poly(A) polymerase, have been developed[39]. All these approaches have in common the elongation of the miRNA sequence using different strategies, as the ligation of adaptors in one of the extremes or the use of primers with tags as depicted in the Figure 1.8. Some of the commercial kits for the miRNAs amplification includes: TaqMan™ Advanced miRNA cDNA Synthesis Kit (Applied Biosystems™, Waltham, MA, US), and miRCURY LNA RT Kit (Qiagen, Hilden, NW, DE) among others.

Once the reverse transcription is performed and the cDNA is synthesized, the PCR can be carried out. The primers used for the amplification have to be designed tacking into account the length of the transcript that will be obtained through the PCR, their nucleotide sequences and length (affecting the denaturing temperature) as well as other characteristics. In the case of the miRNAs, depending on the cDNA synthesis strategy used, the primers selected will vary and will frequently be linked to the cDNA synthesis kit manufacturer.

As mentioned, the readout methods are different, while the conventional PCR is read when the amplification is finished using an agarose gel, the qPCR is being detected while

is being amplified by fluorescent probes[94]. These fluorescent probes must be specific to the selected sequences for its detection.

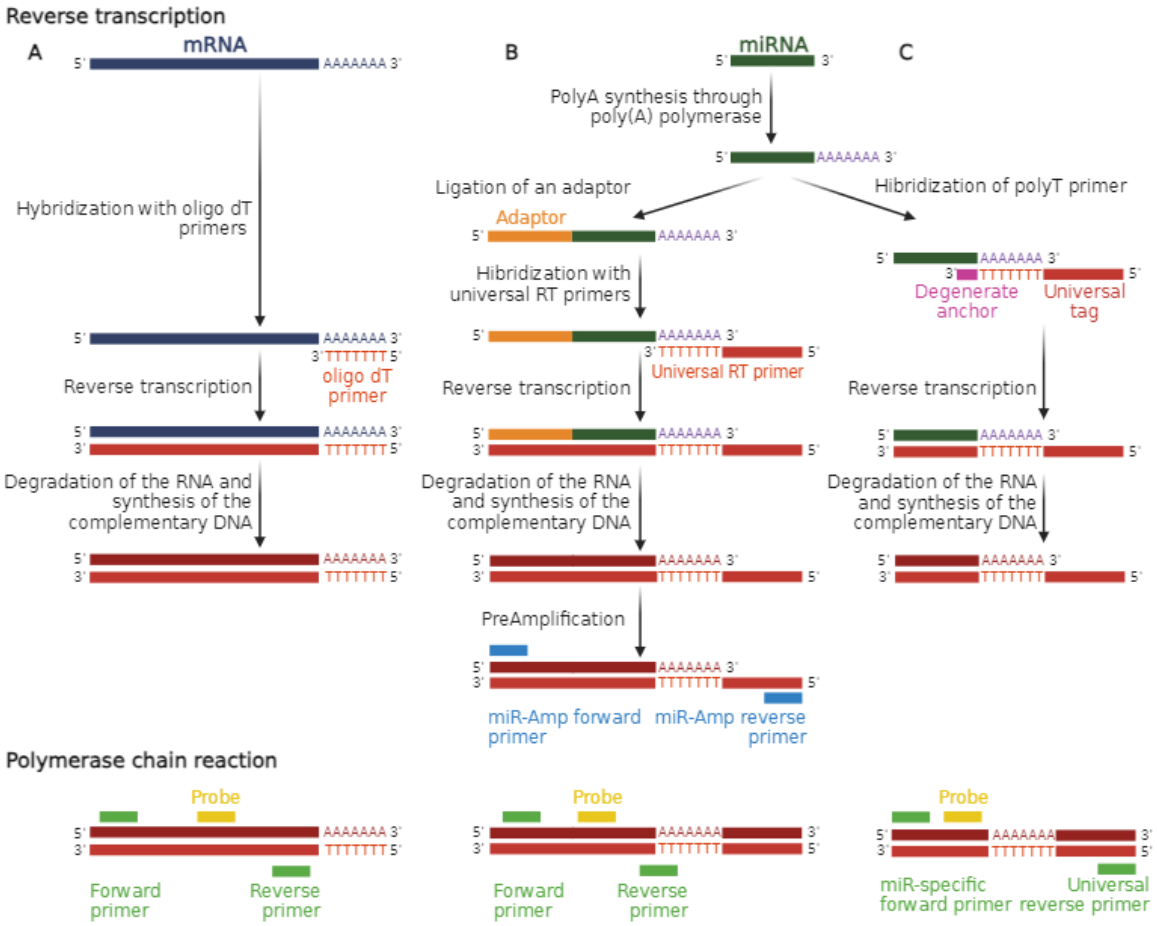


Figure 1.8. Reverse transcription and polymerase chain reaction of the mRNA and miRNA sequences, probes are only necessary for the qPCR but not for the conventional PCR. On one hand, Panel A describes a standard reverse transcription and PCR of the mRNA. On the other hand, two different miRNA reverse transcription approaches described in Panels B and C corresponding to the commercial kits TaqMan™ Advanced miRNA cDNA Synthesis Kit and miRCURY LNA RT Kit, respectively. Created with Biorender.com.

PCR detection method is used to identify the presence of nucleic acids in the exosomes cargo which is mainly RNA[55]. Even though DNA has been reported to be found by some studies[95]. Although the nucleic acid content is low an increasing interest have been generated and PCR amplification is suitable to increase the sensitivity of the detection. For that reason, qPCR is one of the most used amplification techniques for exosome miRNAs as it is the gold standard method.

Amplification PCR method is a well-known method available in most of the molecular biology laboratories. It is known to be reliable, versatile, and fast. Thus, has become the

most used method for the nucleic acid detection. While real-time qPCR is highly sensitive, it is also a time-consuming and complex procedure. To ensure the acquisition of robust and reproducible results, the different subsequential steps must be controlled. These steps include RNA extraction, RNA integrity assessment, cDNA synthesis, primer design, amplicon detection, and data normalization.

1.3.1.2. Northern blotting

Northern blotting is a method that can provide information about the size, sequence, and the amount of nucleic acid sequence in the sample. It is a useful methodology for detecting alternative splicing of mRNA and members of multigene families[96] as well as mature miRNAs and their precursor forms. It is based on the RNA size separation through a denaturing gel electrophoresis and its transference and fixation onto a membrane. Once the sample is separated and transferred the target miRNAs are labelled using nucleic acid probes complementary to the RNA sequence of the target[37,97]. However, this technique also has some limitations as the need of samples with high integrity for the quantification or the lower sensitivity compared to other methodologies due to the lack of amplification steps.

While this method does not require specialized equipment, it is time-consuming and is considered a semi-quantitative assay. However, it provides both information of sequence and length. It was the first method developed for miRNA detection[98]. Given the similarity of length of miRNA sequences, specific detection relies to the complementary probes. Moreover, the detection can be multiplexed using different fluorescent reporters.

1.3.1.3. *In situ* hybridization

In situ hybridization is a versatile methodology based on the use of nucleic acid-labelled probes for the detection of target sequences in cells and tissues. It was first described in the 60s and RNA probes were used to label DNA[99]. It provides information about subcellular distribution and expression of the nucleic acid sequencies including mRNAs and miRNAs[39] as well as DNA. There are different labels that can be used as fluorescence[100,101] or colorimetric methods[102] among others. These protocols are time-consuming and laborious even though it gives unique information about the sequences localization. However, high resolution instrumentation is need for their detection[103] and

the samples need to be pretreated for the fixation of the cell or tissue structure before the staining.

1.3.1.4. Next generation sequencing

This method is a sequence-based approach for the determination of nucleic acid sequences (including DNA, mRNAs and miRNAs). They require previous isolation of the DNA or RNAs, reverse transcription (in case is RNA), generation of a library and amplification. Although it is a very expensive methodology, the cost has lately decreased over time. The main advantage of next generation sequencing is that the high throughput sequencing do not restrict the researcher to look for a certain sequence but to analyze all the sequences that the sample contains. However, it is costly for routine use and requires extensive bioinformatic analysis due to the high-throughput data generated[39]. This approach allows the discovery of nucleic acid sequencies conforming the exosomes cargo.

1.3.1.5. Microarrays

For a rapid high throughput RNA determination, microarray technology is the most commonly used, primarily for the miRNAs[104]. This method is based on the use of solid-phase oligonucleotides complementary to the target RNA sequences. These RNAs must be previously reverse transcribed and labelled. Thus, when the RNAs are hybridized, the intensity of the signal in each well is proportional to the amount of the target. However, despite its multiplexing capabilities, microarray technology can be expensive and may not always distinguish between similar sequences[97].

1.3.1.6. Nuclease protection assay

Nuclease protection assay can be used for the detection and quantification of mainly mRNAs. This method is based on the antisense probe hybridization in solution to the target sequences[105]. Once the probes are hybridized to the mRNA sequences the single stranded remaining sequences are degraded with nucleases. The protected sequences are then loaded into an acrylamide gel for its subsequently detection. This method is useful for the simultaneous detection of several mRNA sequences[106]. They main limitation is the time consuming, low sensitivity and complexity of the protocol since the risk of the target sequence degradation.

1.3.1.7. Emerging platforms for nucleic acids detection

Even though conventional methods offer excellent analytical performance, they are often not suitable for rutinary clinical applications due to their high cost, complexity, and the need of high trained personnel. Because of this, the development of biosensors opens the door to a highly sensitive, specific, easy-to-use, and low-cost devices with a short assay time that asses physiological fluids in a non-invasive way[107,108]. Even though nowadays there is not a clear bench to bedside translation, recently multiple strategies have been proposed to deal with this challenge. These approaches can include well stablished strategies as the use of paper-based, electrochemical-based or microfluidic devices (Table 1.1).

It is also important to highlight the role of the integration of nanomaterials in the miRNA detection platforms, including gold nanoparticles (AuNP)[109], magnetic nanoparticles[110], silver nanoclusters (AgNC)[111], and quantum dots[112]. Their use in different approaches is based on taking advantage of the physicochemical properties of the materials for its transduction to quantifiable signals. Target sequences must be previously coupled to the mentioned nanomaterials using probes and readout is achieved through the properties of the nanomaterials. Some of the nanomaterials can emit fluorescence as AgNC; AuNP have optical properties; and others are suitable for their incorporation into different detection platforms, including biosensors[97]. These versatile techniques offer cost-effective detection methods suitable for POC methodologies.

Table 1.1. Nucleic acid detection methods

Methods	Specifications	Nucleic acid target	LOD	Detection time	Ref
Paper-based devices	Total RNA is extracted from human pancreatic carcinoma cell line EVs. mRNA is amplified and loaded to the LFA where it is visually detected through gold nanoparticles (AuNPs) with DNA probes immobilized on the strip.	glypican-1 (GPC1) mRNA	100 fM	2 h	[113]
	miRNA is incubated with biotinylated probes and ODN-modified AuNPs and then dropped into a LFA strip generating a sandwich hybridization. The detection is based on the visual readout.	miR21	5 amol for 50 µL reaction	70 min	[114]
	miRNA is hybridized into the LFA strip through an ODN probe. The visual readout is amplified through and enzymatic reaction using AuNP modified with HRP-and detection ODN.	miR224	7.5 pM	30 min	[115]
	DNA-Ag/Pt nanocluster (which showed peroxidase-like catalytic activity) is deposited in a paper-based strip. miRNA and TMB are dropped into the spot zone as well as TMB. H_2O_2 flows through the nanoclusters to the samples, producing blue color. miRNA inhibits the catalytic activity reaction and prevent the color formation.	miR21	4.1 pM	~ 30 min	[116]
Electrochemical-based devices	Serum exosomes are captured on functionalized magnetic particles with antibodies. Then, they are lysed and their mRNAs amplified and double-tagged for a electrochemical readout with a magneto-actuated graphite-epoxy composite electrode.	GAPDH mRNA	4×10^2 exosomes μL^{-1}	3 h	[117]
	Electrode is modified with DNA harpins. In presence of the miRNA, the harpins opened and the signal amplification readout system based on atom transfer radical polymerization (ATRP) coupled to them for a square wave voltammetry.	miR141	3.23 aM	7.5 h	[118]
	Electrode is functionalized with gold nanostructures and complementary oligonucleotide probes to detect specific miRNAs. In presence of the miRNAs, the hybridization was produced, and they detected by electrochemical Impedance Spectroscopy.	miR34a	39 pM	2.5 h	[119]

	Gold platinum bimetallic nanoparticles (AuPtBNPs)/3-aminopropyltriethoxy silane (APTS) nanocomposite coated fluorine-doped tin oxide electrode is functionalized with cDNA and upon miRNA-21 hybridization, the detection is based on differential pulse voltammetry.	miR21	0.63 fM	20 min	[120]
	The electrode is functionalized with biotinylated capture probe and hybridized with miR-29b. The DNA/RNA heteroduplexes are cleaved by DSN. The remaining biotin-modified capture probes form complexes with streptavidin-HRP and electrochemically detected by amperometry.	miR29b	0.79 pM	~ 4.5 h	[121]
Microfluidic devices	Single cells are lysed and the mixture with the RT-PCR master mix loaded into the SD chip inlet for the performance of a digital RT-PCR. The readout is based on fluorescence in situ hybridization.	GAPDH or TFRC mRNA	-	~ 45 min	[122]
	CTCs are captured and their CK-19 mRNA amplificated through loop-mediated isothermal amplification (LAMP) technique into the microfluidic device. The target is stained through immunofluorescence.	CK-19 mRNA	3×10^3 to 3×10^4 copies	~ 45 min	[123]
	miRNA is hybridized to ssDNA immobilized into a surface using a surface enhanced Raman scattering (SERS) substrate for the readout.	miR21	10 fM	~ 35 min	[124]
	miRNA reacts with the fluorescent DNA probes in the reaction chamber of the chip. After the incubation time, the mixture was flushed into the reaction chamber and detected.	miR191	0.146 aM	35 min	[125]

1.3.2. Methods for the characterization and determination of proteins

1.3.2.1. Flow Cytometry

Flow cytometry is a commonly used technique for protein characterization. It is used for proteins expressed on cells either on the surface (plasmatic membrane) or intracellularly (cytoplasm or nucleus). Similarly, this technique can also be used for the protein exosome characterization. The main challenge is the discrimination of the exosomes from the background signals due to their reduced size. To solve that difficulty, the exosomes can be directly labelled with a color tracer or attaching them to beads that function as a carrier to increase the exosome size. In the direct detection the vesicles are usually labelled with fluorescent cell staining as carboxyfluorescein succinimidyl ester (CFSE) or similar dyes for a better separation of the EVs to the noise signal. This is due to the capacity of the cytometer to determine the size and complexity of vesicles. However, the reduced size of this type of EVs can hinder its detection allowing this single approach to high resolution cytometers. To overcome this size handicap with conventional cytometry the exosomes can be coupled to bigger particles, thus allowing the cytometers detection (as latex, polystyrene, or magnetic particles) (Fig. 1.9).

Bead-coupled cytometry has been widely used for the exosomes characterization[85]. Exosomes can be directly coupled to the particles or the particles can be previously biofunctionalized to specifically capture the exosomes[85,126]. Following this approach, a commercial kit based in this principle has been commercialized by named MACSPlex EV Kit IO (Miltenyi Biotec) which allows the detection of 37 surface epitopes using different modified-bead populations which can be individually determined and using a labelling cocktail containing a mix for the tetraspanins detection. This approach allows the multiplexing of proteins characterization.

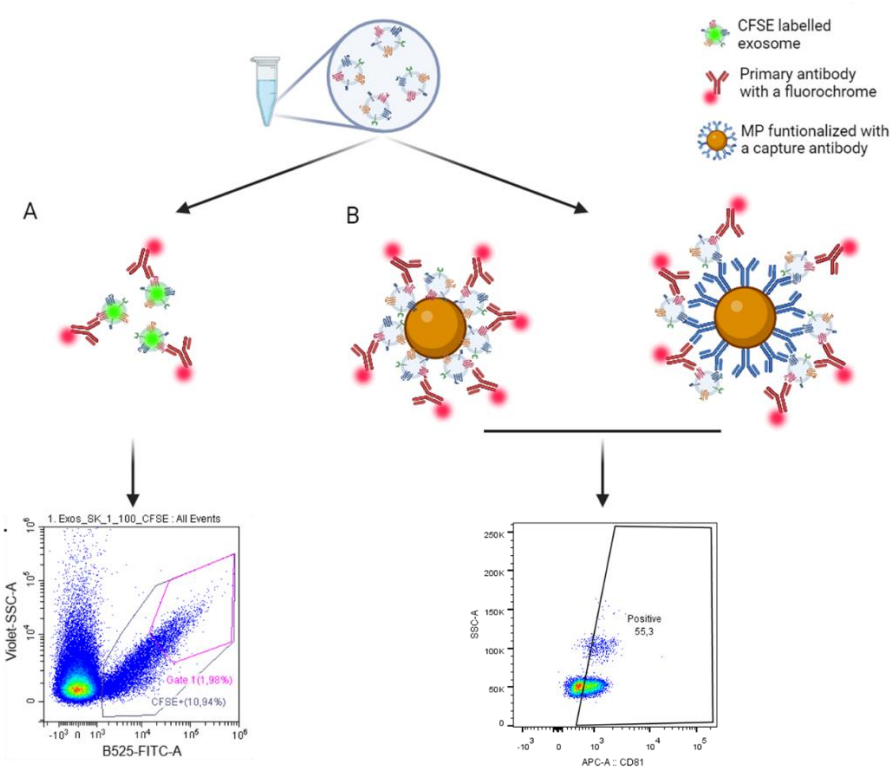


Figure 1.9. Strategies for the protein characterization for exosomes using flow cytometry: A) direct detection B) bead-coupled detection, with exosomes directly coupled to the MP or bind to the MP through specific antibodies. Flow cytometry plots are unpublished data from our group. Created with BioRender.com.

1.3.2.2. Enzyme-linked immunosorbent assay

Enzyme-linked immunosorbent assay (ELISA) is one of the most used methods for the protein detection including clinical and biological samples. Mainly two different approaches are performed, the immobilization of the antigen or the antibody on the plate, both using direct or indirect formats (Fig. 1.10). Alternatively, in our research group, magnetic particles have been used as functionalized surface instead of the plate surface. This approach leads to a magneto-actuated ELISA using magnetic fields for the washing steps instead of centrifugation. In addition, allows the preconcentration of the exosomes and increases the reactive surface for a better capture.

Concerning to the ELISA readout, different enzymatical reporters can be employed including horseradish peroxidase (HRP) and alkaline phosphatase (ALP) among others[127]. In addition, alternative approaches of the ELISA protocol can use other reporters obtaining different signals as in fluorescent immunoassays[128] or chemiluminescent immunoassays[129].

ELISA is a versatile methodology widely used in the laboratories due to its high throughput simplicity, low cost and the low equipment required. Moreover, commercial kits are available for huge number of proteins and samples simplifying the setup of the procedures. It is a suitable methodology for the detection of the surface proteins of the exosomes as well as the proteins inside the exosomes which required the previous lysis of the vesicles.

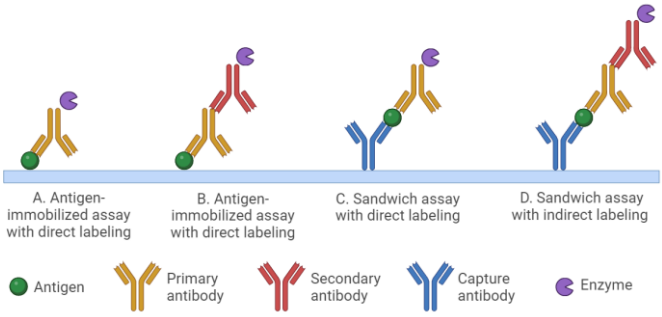


Figure 1.10. Schematic representation of the different ELISA formats. Panel A. Direct ELISA with the antigen immobilized into the plate. Panel B. Indirect ELISA with the antigen immobilized into the plate. Panel C. Direct sandwich ELISA. Panel D. Indirect sandwich ELISA. Created with BioRender.com.

1.3.2.3. Western blot

Western blot (WB) is a classical biochemical method for protein determination. This technique is based on the size separation of the previously denatured proteins by a SDS-PAGE gel electrophoresis transferred onto polyvinylidene difluoride membranes. Finally, the membrane is incubated with specific antibodies for the detection of the proteins to be determined. This technique is widely used for the validation of exosome isolation due to the cost-effectiveness and simplicity. However, the low protein concentration of the exosomes require high EVs amount especially for low expressed proteins into exosomes[130,131].

1.3.2.4. Proteomics

Proteomics is the study of the proteome i.e. the proteins expressed by an organism or a cell or tissue at a specific time at a large-scale. For this purpose, different high-throughput methodology approaches are used. Mass spectrometry is one of the most popular methodologies used for peptide and protein detection, identification, and characterization. This technique is based on the measurement of the mass-to-charge ratio of ions coming from previously broken molecules of the sample. This technique has been

evolving since it was developed ending in more accurate protein identification procedures[132]. To obtain robust data the sample, especially in exosomes, the samples must be pure to avoid interferents from the medium which can be a handicap for this technique. However, this is a useful high-throughput technique that can be used to obtain information of their cargo[133,134]. Mass spectrometers are divided into three parts; i) ion source, where the sample is ionized, ii) the mass analyzer, where the previously ionized sample is sorted by its mass-to-charge ratio, and iii) the detector, where the ions are measured. Once the data is obtained an extensive bioinformatic process must be performed.

In addition, other proteomic approaches are widely used as the immunoassays. These assays take advantage of the specificity of the antibodies for a high throughput protein identification. For the readout different strategies are used as fluorescence or DNA probes, which will be posteriorly amplified and detected by sequencing, among others. There are currently different companies in the market that offer proteomic services based on sequencing DNA probes linked to detection antibodies as Proximity Extension Assay (Olink, Uppsala, Sweden) or NULISA (Alamar bioscience, Fremont, CA, US). In addition, other proteomic services are based on fluorescent detection, they can be developed into microarray devices as the Kinex KAM microarray (Kinexus, Vancouver, Canada) or the scioDiscover protein profiling (Sciomics, Neckargemünd, Germany). These platforms generate big amounts of raw data that has to be subsequently processed and analyzed through bioinformatics.

1.3.2.5. Emerging platforms for protein detection

Despite the mentioned protein detection methods, there are other methodologies used for their detection. Paper-based biosensors, electrochemical based devices or microchips using microfluidics for the protein surface analysis among others can be used to determine them, these are usually based on ELISA sandwich protocols for the multiplex detection using antibodies[135] (Table 1.2).

Table 1.2 Protein detection methods

Devices	Specifications	Protein target	LOD	Detection time	Ref
Paper-based devices	IL-6 proteins in the serum get attached to the test line and the readout is performed through AuNPs conjugated with anti-IL-6 antibodies.	IL-6	76.85 pg/ml	20 min	[136]
	Purified exosomes are mixed with anti-CD63 modified AuNPs. The paper strip is dipped in the mixture and reacts in the test line containing a combination of anti-CD9 and anti-CD81 antibodies for the exosome capture.	Exosomes (CD9, CD81 and, CD63)	8.54×10^{5} exosomes $\mu L.^{-1}$	15 min	[137]
	Human plasma samples are dropped into the LFA and reacts with Au@Pt4L NP functionalized with specific antibodies for the readout. The test line is made of anti-PSA antibodies.	Prostate specific antigen (PSA)	20 pg mL^{-1}	15 min	[138]
	Serum CEA is quantified in a LFA with a colorimetric signal obtained by polydopamine-modified AuNP. The test zone is conformed by anti-CEA antibodies.	Carcinoembryonic antigen (CEA)	0.05 ng mL^{-1}	15 min	[139]
Electrochemical-based devices	Exosomes in human serum are captured with MP functionalized with cancer specific antibodies. The MP are captured on magnetic electrodes and then labelled with antiCD63-HRP for the amperometric readout	CD24, CD340, CD44, CD326 CD63,	10^{5} exosomes μL^{-1}	3 h	[140]
	Exosomes in human serum are captured to a magnetic electrode through MP modified with exosome specific antibodies. The ALP activity on exosomes is used for the electrochemical readout.	Exosome ALP	10^{5} exosomes μL^{-1}	~ 2 h	[141]

	Prostate specific antigen is detected in saliva using a hybrid nanocomposite of graphene nanoplatelets with diblock co-polymers and Au electrodes.	Prostate specific antigen	40 fg mL^{-1}	5 min	[142]
	Aptamers specific against cardiac troponin I are immobilized in MP through DNA probes. This complex was hybridized to the electrode as well as a partially complementary DNA probe which can also hybridize and activate the trans-cleavage activity of the CRISPR/Cas12a. The signal is inversely proportional to the protein presence due to the proportional free probe amount.	Cardiac troponin I	10 pg mL^{-1}	~ 30 min	[143]
Microfluidic devices	C-reactive protein is detected into a label-free 3D microfluidic biosensor based on the recognition of the protein through specific antibodies immobilized into Au electrode arrays.	C-reactive protein	1 pg mL^{-1}	Real-time	[144]
	The microfluidic system is based on the intrinsic fluorescence from aromatic amino acid tryptophan excited by a UV-LED (λ = 295 nm) to measure protein concentrations	Tryptophan, bovine serum albumin (BSA), bovine carbonic anhydrase (BCA)	72 nM 128 nM 250 nM	-	[145]
	Proteins in serum are detected using microscopic beads decorated with specific antibodies and labelling the immunocomplexes with a fluorescent generating reporter. In this study a streptavidin-β-galactosidase is used.	TNF-α	21 fM	~ 6 h	[146]

1.4. Point-of-care devices for diagnosis in health care

The medical diagnostic testing or healthcare approach that takes place at or near to the patient, instead of sending the samples to a centralized laboratory for analysis is performed by point-of-care devices[147]. POC testing areas include hospitals, clinics, and health departments, among others. In hospitals, POC test are necessary in emergency departments or critical care units where is need fast results outcome[148]. The use of POC testing reduces the time needed to make therapeutic decisions, minimizes the preanalytical errors and the cost per assay. However, POC testing is not yet available for a wide range of analysis, may have quality control issues and need a specialized training for the personnel performing the assays[149]. These tests can also be defined as rapid diagnostic tests (RDT) used at POC areas.

POC testing can be used for communicable and non-communicable diseases, for example measuring glucose in blood as in the glucometer, an hormone as in the pregnancy test, or the presence or absence of a pathogen[150]. Particularly, the glucometer was the first biosensor, commercialized in 1975[151]. It was based on the integration of the glucose oxidase into the membrane of an electrode for the measurement of the glucose levels in blood. Since then, the glucometer has been under constant revision for improvement until the nowadays formats. Another breaking point on the development of biosensors was the pregnancy test first commercialized by Unipath. This test is based on the detection of the human chorionic gonadotropin (hCG) in urine through a LFA, allowing the test performance at home.

The ideal RDT can be defined by the revised ASSURED criteria stablished by WHO to be adapted to the digital era by the reformulation into the acronym of REASSURED (Real-time connectivity, Easy specimen collection, Affordable; Sensitive; Specific; User friendly; Rapid; Robust; Equipment-free; Deliverable to end users or near patient care areas)[152]. These criteria stablish the paradigm for the development of new tests. For the accomplishment of these characteristics the scientific community considered innovative solutions to overcome the challenges.

1.4.1. Biosensors

A biosensor, as defined by the International Union of Pure and Applied Chemistry (IUPAC), "*is an integrated analytical device capable of providing specific quantitative or semiquantitative information using a biological o biomimetic receptor, which is in direct contact with a transducer*"[153]. Biosensors are constituted by three major components: i) a biological receptor, the interacting component with the analyte, ii) a transducer, transforming the interaction with the analyte to a measurable signal, and iii) a detector device, able to process the signal and displaying the sensor result (Fig. 1.11). Based on their components the biosensors can be classified according to their bioreceptor or by their transducer.

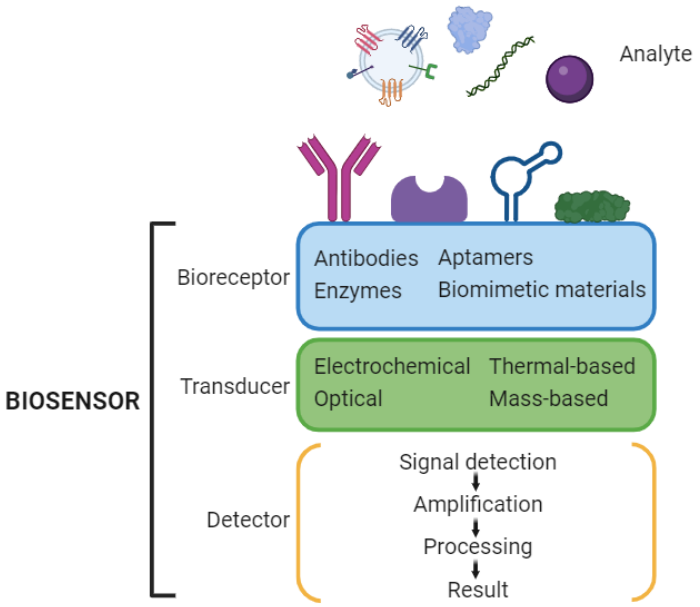


Figure 1.11. Schematic representation of the three major components of a biosensors, from the recognition of the analyte to the result obtention. Created with Biorender.com.

1.4.1.1. Classification based on the bioreceptor

The biorecognition element, situated in the bioreceptor, is the part of the biosensor that defines the specificity of the device. According to this property it can be define different categories of bioreceptors:

Enzymes are considered the first biorecognition element described in a biosensor: the glucose oxidase for the glucometer development[154]. Since then, other enzymes have also been used as biorecognition elements. The enzymes can be immobilized in the surface of

a the working electrochemical transducer, as in the previous example, or can also be used for optical biosensors generating colorimetric signals[155]. Even though they are sensitive and selective being biological active molecules are susceptible to be degraded or their activity altered through time[156].

Antibodies or immunoglobulins are proteins generated during the humoral response against foreign molecules by the plasma cells. These immune system molecules are generated to bind with high affinity a specific antigen. The antigen-antibody interaction is performed by a group of non-covalent bonds such as hydrogen bonds, Van der Waals forces, and electrostatic and hydrophobic interactions[157]. Due to the specificity against their target molecules, antibodies are wide used as a biorecognition element for different applications including health care but also for food analysis or environmental purposes. They can be integrated into a wide range of assays such as ELISA[158], paper-based lateral flow assay[159], immunosensors or flow cytometry[160].

Aptamers and nucleic acids are artificial short single stranded DNA or RNA sequences between 20-80 nucleotides, which have been used for the selective detection of not only oligonucleotide sequences but also peptides and metabolites among others due to their tridimensional conformation[161]. Their use has increased in the last decades due to their stability, versatility, and easy functionalization. They have been used for example, for pathogenic bacteria detection[162] or the biomarkers detection in blood[163].

Biomimetic materials are inorganic materials developed to substitute the biorecognition agents. Their interest increased around the 80s and 90s when the molecular imprinted polymers were developed. These polymers mimic the antigen-antibody recognition through tridimensional structure with selective recognition sites. Their advantages are their reduced cost and their stability. However, they have not reached a sensitivity and affinity comparable to the biorecognition agents yet[164]. They have already been used in some applications[165,166].

1.4.1.2. Classification based on the transducer

The transducer is the biosensor part responsible to generate a measurable signal after the biorecognition on the analyte. There are different transducers depending on the signalization, the energy conversion process that can be based on:

Electrochemical transduction transforms the bioreceptor signal into electrical signal. Among the electrical measurements, potentiometric, conductimetric and amperometric readouts are the most popular. They have been used for the detection of DNA amplimers[167] or exosomes[168] among others.

Optical transduction refers to measuring changes in the wavelength of a light source when an analyte binds to the biosensing surface through a specific recognition element[127]. There are different transduction techniques such as the surface plasmon resonance (SPR) based on the change of the refracting index of a metallic surface due to the target molecule interaction when a light beam interact with it[169]. Different applications have been developed as for the quantification of antibodies[170], viral detection[171], or for cancer biomarkers detection[172], among many others.

Thermal-based transduction is based on the transformation of the temperature changes produced by chemical reactions into quantifiable signals. They are primary associated to enzymatic bioreceptors such as oxidases and catalases. Some of their applications are the detection of metabolites such as glucose, ethanol or lactate among others[173,174].

Mass-based transduction relies on the measurement of piezoelectric signal changes. This transduction can be achieved through a quartz crystal microbalance or a cantilever. This method is suitable for combining with several recognition elements and can be applied in the detection of a wide range of molecules[175,176].

1.4.2. Trends in POC testing

Over the past few years, due to the pandemic, there has been a significant increase in interest in POC testing. The need for diagnostic tools has become evident, and the convergence of biosensors with Rapid Diagnostic Tests (RDTs) has become a pressing need.

1.4.2.1. Mobile health

One of the trends in the development of POC testing is the integration of smartphones into healthcare platforms to achieve either data transmission and processing and the readout. There has been an exponential growth in the development of mobile applications (apps), often available at little to no cost. These applications include those used by patients for self-monitoring, as well as apps designed for scientific purposes such as healthcare diagnostics, environmental monitoring, or food evaluation. This represents a significant

advancement, when integrated in diagnostic platforms in terms of result readout, analysis, and display, which can now be overcome with smartphone technology[177]. Mobile health (mHealth) has the potential to replace some expensive and benchtop instrumentation, making it suitable for POC testing. In some cases, additional accessories need to be attached to the phones, such as illumination sources or simplified biosensor devices. The smartphone can be essentially used as a detector or as instrumental interface[178].

Smartphone as detector

In this case, the smartphone can be integrated to a device containing the instrumentation in a simplified format or the smartphone intrinsic components, for instance the camera can be used for the optical readout.

Microscopic imaging. Using the smartphone camera as well as external accessories such as LED illuminating source, and optical components, it is possible to obtain information about the morphology of the samples. Based on this, bright-field microscopic and fluorescent microscopic imaging biosensors were reported. On one hand, they can be used for example for the blood cells observation in blood smears or helminth eggs[179]. On the other hand, fluorescence can be used for the detection of bacteria using FISH methodology with probes against bacterial RNA[180] or cancer cells in blood samples incorporating this system to a microfluidic chip[181]. For this approach LEDs are usually employed to excite the fluorescent molecules.

Colorimetric sensor. For the colorimetric detection, the smartphone itself can be used without the need of external devices. However, complementary devices can be used to control external variables as camera position or environmental light. It can be used for the hemoglobin quantification in blood without any sample pretreatment[182] as well as for the nitrite concentration and pH in a paper-based device[183].

Electrochemical sensor. Through the coupling of simple devices, the smartphone can act as a receiver and analyzed of the electrochemical signal, including amperometric, potentiometric and impedimetric biosensors. These biosensors can include the detection of wide variety of biomolecules through screen-printed electrodes[184,185] among other approaches.

Electrochemiluminescence sensor. There are few sensors using this technology that combines electrochemistry and chemiluminescence. It is based on the application of a specific voltage to pre-buried electrodes where these molecules will react. For instance, palm-sized paper-based bipolar electrode electrochemiluminescence device for the measurement of several biomolecules was reported [186].

Smartphone as instrumental interface

In addition, smartphones can be also used for the control and display of the analytical device. They can be connected to each other using USB port, wi-fi or bluetooth connection. Nowadays there are commercial application platforms available for the smartphone connection, mainly glucometers and ethylometers. The first commercially available ethylometer, Floome, can be connected to a smartphone via audio jack and measure the alcohol concentration in breath. In addition, small glucometers are being developed to be placed under the skin to deliver real-time information to smartphones.

1.4.2.2. Paper-based platforms

Paper-based devices have unique characteristics such as affordability, portability, disposability, and user-friendliness, which make them well suited bioanalytical platforms for POC. In addition, the device structure able the preservation of the reagent and the materials for long-time storage. Lateral flow assay (LFA) is the most used technique since the development of the pregnancy test in 1988. However, through the pandemic outcome the antigen test against SARS-CoV-2 virus have also become a current self-testing to be done at-home or anywhere[187]. LFA is a versatile platform that can be used to detect a wide variety of biomolecules including viral particles, nucleic acid sequences and proteins. Most LFA are formed by four parts i) sample pad, where the sample is loaded; ii) conjugate pad, containing mainly the readout nanoparticles functionalized with biomolecules specific to the target analyzed; iii) detection zone, usually formed by a nitrocellulose membrane, containing the test and the control lines (antibodies or antigens immobilized); and iv) the absorbent pad, to wick the excess of reagents (Fig. 1.12). Besides the LFA, there are other paper-based platforms such as the pH universal indicator paper or the vertical flow assays as well as paper-printed microfluidic devices[186].

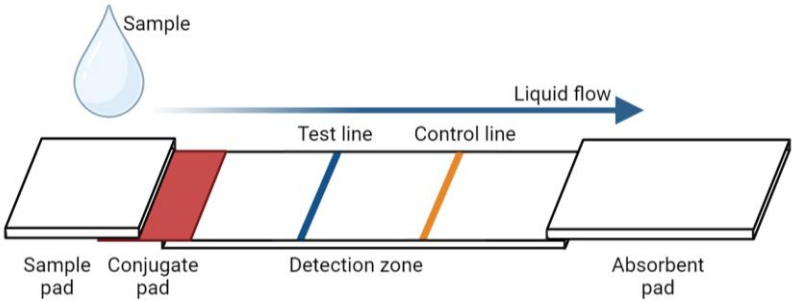


Figure 1.12. Schematic representation of the components of the lateral flow assay including the different parts and the liquid flow direction. Created with biorender.com.

There are several types of paper used for the fabrication these devices, choosing correctly the paper is important due to their intrinsic characteristics, as the pore size. In addition, the flow rate can also be modified using different strategies as the use of wax or the modification of the shape of the detection zone. In the test line, the antigen detected is captured primarily by specific antibodies due to the high specificity and wide versatility. However, and depending on the analyte, the capture can be performed by immobilizing antigens, aptamers, DNA probes or biomimetic materials as molecular imprinted polymers. The most used strategy for the visual readout in the commercial paper-based assays is the use of modified gold nanoparticles. However, there are alternative readout strategies as the use of other types of particles (latex particles or carbon nanoparticles among others, as it is studied in this doctoral thesis), enzymatic labels or fluorescent labels. The LFA versatility will be explored in chapter 4 through nucleic acid lateral flow assay development for intracellular infections.

1.4.2.3. Magnetic particles

Magnetic particles have been widely integrated in POC. They present useful characteristics as their easy use, versatility, and stability, which makes them suitable for their use in platforms with reduced instrumentation and with a reduced cost. They are composed by three parts: i) a paramagnetic core, ii) a polymeric shell, and iii) a coating containing the functionalized molecules[188] (Fig. 1.13). Their paramagnetic core, usually magnetite iron oxide (Fe_3O_4) but also ferrites (MFe_2O_4 being M a divalent cation) allows their separation through the application of a magnetic field to the sample solution. Thus, becoming perfect candidates for target molecules separation with minimal instrumentation required[189]. Moreover, outside the polymeric shell recovering the core there can be a coat constituted

by chemicals and biochemicals that can be functionalized. This coating adds to the magnetic particles huge versatility due to the possibility of antibody functionalization as well as other biomolecules as aptamers, proteins or MIPs and functional groups[190],being able to capture proteins, nucleic acids[167] and EVs[85] among others.

There are ready-to-use MP commercially available. First commercialized were the Dynabeads (Invitrogen, Thermo Fisher Scientific), with a wide variety of MP including streptavidin-MP, antibody-MP and oligo(dT)-MP among others. MP can also be purchased from Miltenyi Biotec (Bergisch Gladbach, NW, DE), for cell isolation. Other common MPs are the CD bioparticles (New York, NY, USA) and PureProteome from Sigma-Aldrich (Merck KGaA) among many others.

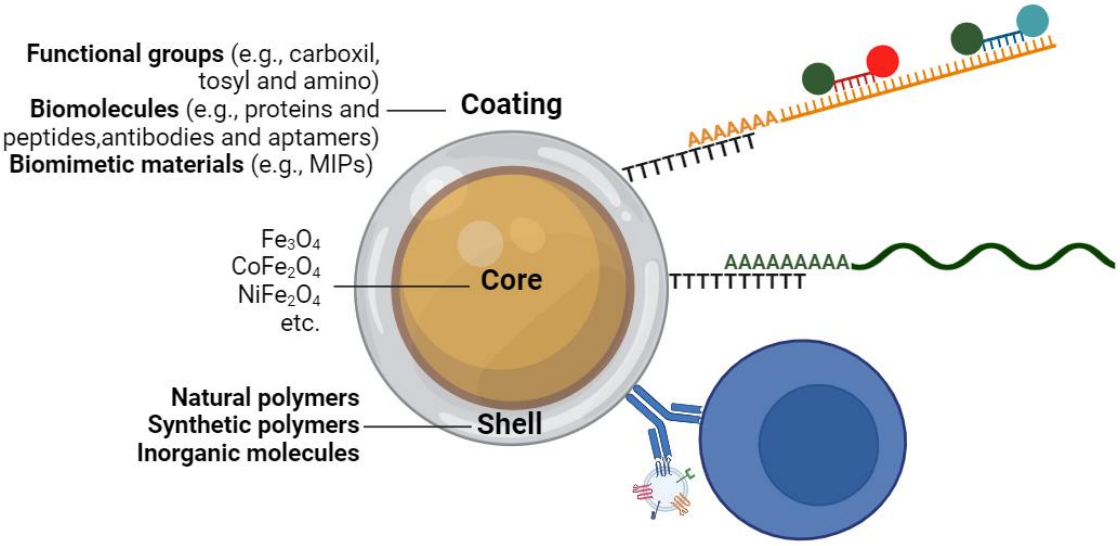


Figure 1.13. Schematic representation of a magnetic particle with its different components. Including the main three parts (core, shell, and coating) and their composition as well as the different approaches that will be explored during the thesis. Created with biorender.com.

Their use is not only limited for separation and preconcentration of analytes, but they can also be integrated to biosensors as recognizing agents in magnetic electrodes[13] or integrating on magnetic ELISA as solid-phase surface[127]. Moreover, they have been used with medical purposes as for drug delivery, hyperthermia treatment or radioimmunotherapy among others[191]. Magnetic particles have also been integrated to microfluidic devices where they have been used for the separation and preconcentration of targeted biomolecules[192].

Our group has a wide previous experience in the integration of the MP in different methodologies. Previous work performed in the lab has integrated MPs in electrochemical biosensors for different applications such as the detection of pathogenic bacteria[193], cDNA amplimers[13] or pesticides[194] among others. In addition, MPs have also been used for protein characterization in breast cancer derived exosomes[140,195] and the isolation and preconcentration of pathogenic bacteria as *Mycobacterium fortuitum*[196].

In this thesis, MPs have been employed for the first time in our research group for miRNA detection, thereby expanding the group's expertise including another valuable biomarker. For the miRNA detection, a competitive magneto enzyme-linked miRNA (ELmiRNA) assay with optical readout has been developed in chapter 3. Incorporating the oligo(dT)-MP in the detection system reducing the complex instrumentation needed and the matrix effect. Furthermore, MPs have been integrated into a Rapid Diagnostic Test (RDT), specifically a paper-based LFA, for the detection of the cellular immune response. MPs have been used for T cell separation and mRNA isolation, combining in the same protocol different types of magnetic particles. This methodology has been further validated using human samples as discussed in Chapter 4. Additionally, neuron-derived exosomes have been isolated by functionalizing MPs with antibodies capturing them in the context of neurodegenerative diseases. Subsequently performing a magneto-ELISA, outlined in chapter 5. The versatility of MPs has been demonstrated in this thesis by their integration into various *in vitro* platforms, as represented in Figure 1.13. In addition, the wide variety of magnetic particles allows for the adaptation of the developed methodologies to different targets than those already proposed, enabling the customization of the coating according to the specific requirements of the biomarker.

1.5 References

(1) Perakis, S.; Speicher, M. R. Emerging Concepts in Liquid Biopsies. *BMC Med.* **2017**, *15* (1), 1–12. https://doi.org/10.1186/s12916-017-0840-6.

(2) Lone, S. N.; Nisar, S.; Masoodi, T.; Singh, M.; Rizwan, A.; Hashem, S.; El-Rifai, W.; Bedognetti, D.; Batra, S. K.; Haris, M.; Bhat, A. A.; Macha, M. A. Liquid Biopsy: A Step Closer to Transform Diagnosis, Prognosis and Future of Cancer Treatments. *Mol. Cancer* **2022**, *21* (1), 1–22. https://doi.org/10.1186/s12943-022-01543-7.

(3) Engell, H. C. Cancer Cells in the Circulating Blood; a Clinical Study on the Occurrence of Cancer Cells in the Peripheral Blood and in Venous Blood Draining the Tumour Area at Operation. *Ugeskr. Laeger* **1955**, *117* (25), 822–823.

(4) *10 Breakthrough Technologies of 2015: Where Are They Now? | MIT Technology Review*.https://www.technologyreview.com/2015/12/26/247170/10-breakthrough-technologies-of-2015-where-are-they-now/ (accessed 2023-09-19).

(5) Macías, M.; Alegre, E.; Díaz-Lagares, A.; Patiño, A.; Pérez-Gracia, J. L.; Sanmamed, M.; López-López, R.; Varo, N.; González, A. Liquid Biopsy: From Basic Research to Clinical Practice. *Adv. Clin. Chem.* **2018**, *83*, 73–119. https://doi.org/10.1016/BS.ACC.2017.10.003.

(6) Park, Y.; Luo, L.; Parhi, K. K.; Netoff, T. Seizure Prediction with Spectral Power of EEG Using Cost-Sensitive Support Vector Machines. *Epilepsia* **2011**, *52* (10), 1761–1770. https://doi.org/10.1111/j.1528-1167.2011.03138.x.

(7) Lin, D.; Shen, L.; Luo, M.; Zhang, K.; Li, J.; Yang, Q.; Zhu, F.; Zhou, D.; Zheng, S.; Chen, Y.; Zhou, J. Circulating Tumor Cells: Biology and Clinical Significance. *Signal Transduct. Target. Ther.* **2021**, *6* (1), 1–24. https://doi.org/10.1038/s41392-021-00817-8.

(8) Magbanua, M. J. M.; Yau, C.; Wolf, D. M.; Lee, J. S.; Chattopadhyay, A.; Scott, J. H.; Bowlby-Yoder, E.; Hwang, E. S.; Alvarado, M.; Ewing, C. A.; Delson, A. L.; Van'T Veer, L. J.; Esserman, L.; Park, J. W. Synchronous Detection of Circulating Tumor Cells in Blood and Disseminated Tumor Cells in Bone Marrow Predicts Adverse Outcome in Early Breast Cancer. *Clin. Cancer Res.* **2019**, *25* (17), 5388–5397. https://doi.org/10.1158/1078-0432.CCR-18-3888.

(9) Wang, C.; Mu, Z.; Ye, Z.; Zhang, Z.; Abu-Khalaf, M. M.; Silver, D. P.; Palazzo, J. P.; Jagannathan, G.; Fellin, F. M.; Bhattacharya, S.; Jaslow, R. J.; Tsangaris, T. N.; Berger, A.; Neupane, M.; Cescon, T. P.; Lopez, A. M.; Yao, K.; Chong, W.; Lu, B.; Myers, R. E.; Hou, L.; Wei, Q.; Li, B.; Cristofanilli, M.; Yang, H. Prognostic Value of HER2 Status on Circulating Tumor Cells in Advanced-Stage Breast Cancer Patients with HER2-Negative Tumors. *Breast Cancer Res. Treat.* **2020**, *181* (3), 679–689. https://doi.org/10.1007/S10549-020-05662.

(10) Ray, S. K.; Mukherjee, S. Cell Free DNA as an Evolving Liquid Biopsy Biomarker for Initial Diagnosis and Therapeutic Nursing in Cancer- An Evolving Aspect in Medical Biotechnology. *Curr. Pharm. Biotechnol.* **2020**, *23* (1), 112–122. https://doi.org/10.2174/1389201021666201211102710.

(11) Ovchinnikova, E. S.; Schmitter, D.; Vegter, E. L.; Ter Maaten, J. M.; Valente, M. A. E.; Liu, L. C. Y.; Van Der Harst, P.; Pinto, Y. M.; De Boer, R. A.; Meyer, S.; Teerlink, J. R.; O'Connor, C. M.; Metra, M.; Davison, B. A.; Bloomfield, D. M.; Cotter, G.; Cleland, J. G.; Mebazaa, A.; Laribi, S.; Givertz, M. M.; Ponikowski, P.; Van Der Meer, P.; Van Veldhuisen, D. J.; Voors, A. A.; Berezikov, E. Signature of Circulating MicroRNAs in Patients with Acute Heart Failure. *Eur. J. Heart Fail.* **2016**, *18* (4), 414–423. https://doi.org/10.1002/EJHF.332.

(12) Cano, A.; Esteban-de-Antonio, E.; Bernuz, M.; Puerta, R.; García-González, P.; de Rojas, I.; Olivé, C.; Pérez-Cordón, A.; Montrreal, L.; Núñez-Llaves, R.; Sotolongo-Grau, Ó.; Alarcón-Martín, E.; Valero, S.; Alegret, M.; Martín, E.; Martino-Adami, P. V.; Ettcheto, M.; Camins, A.; Vivas, A.; Gomez-Chiari, M.; Tejero, M. Á.; Orellana, A.; Tárraga, L.; Marquié, M.; Ramírez, A.; Martí, M.; Pividori, M. I.; Boada, M.; Ruíz, A. Plasma Extracellular Vesicles Reveal Early Molecular Differences in Amyloid Positive Patients with Early-Onset Mild Cognitive Impairment. *J. Nanobiotechnology* **2023**, *21* (1), 1–19. https://doi.org/10.1186/S12951-023-01793-7.

(13) Pallares-Rusiñol, A.; Moura, S. L.; Martí, M.; Pividori, M. I. Electrochemical Genosensing of Overexpressed GAPDH Transcripts in Breast Cancer Exosomes. *Anal. Chem.* **2023**, *95* (4), 2487–2495. https://doi.org/10.1021/acs.analchem.2c04773.

(14) Aro, K.; Wei, F.; Wong, D. T.; Tu, M. Saliva Liquid Biopsy for Point-of-Care Applications. *Front. Public Heal.* **2017**, *5*, 77. https://doi.org/10.3389/FPUBH.2017.00077.

(15) Wei, F.; Lin, C. C.; Joon, A.; Feng, Z.; Troche, G.; Lira, M. E.; Chia, D.; Mao, M.; Ho, C. L.; Su, W. C.; Wong, D. T. W. Noninvasive Saliva-Based EGFR Gene Mutation Detection in Patients with Lung Cancer. *Am. J. Respir. Crit. Care Med.* **2014**, *190* (10), 1117–1126. https://doi.org/10.1164/RCCM.201406-1003OC.

(16) Kutsch, V. K.; Young, D. A. New Directions in the Etiology of Dental Caries Disease. *J. Calif. Dent. Assoc.* **2011**, *39* (10), 716–721. https://doi.org/10.1080/19424396.2011.12221949.

(17) Dwivedi, R.; Gupta, Y. K.; Singh, M.; Joshi, R.; Tiwari, P.; Kaleekal, T.; Tripathi, M. Correlation of Saliva and Serum Free Valproic Acid Concentrations in Persons with Epilepsy. *Seizure* **2015**, *25*, 187–190. https://doi.org/10.1016/j.seizure.2014.10.010.

(18) Patel, K. M.; Van Der Vos, K. E.; Smith, C. G.; Mouliere, F.; Tsui, D.; Morris, J.; Chandrananda, D.; Marass, F.; Van Den Broek, D.; Neal, D. E.; Gnanapragasam, V. J.; Forshew, T.; Van Rhijn, B. W.; Massie, C. E.; Rosenfeld, N.; Van Der Heijden, M. S. Association of Plasma and Urinary Mutant DNA with Clinical Outcomes in Muscle Invasive Bladder Cancer. *Sci. Rep.* **2017**, *7* (1), 5554. https://doi.org/10.1038/s41598-017-05623-3.

(19) Valenberg, F. J. P. va.; Hiar, A. M.; Wallace, E.; Bridge, J. A.; Mayne, D. J.; Beqaj, S.; Sexton, W. J.; Lotan, Y.; Weizer, A. Z.; Jansz, G. K.; Stenzl, A.; Danella, J. F.; Cline, K. J.; Williams, M. B.; Montgomery, S.; David, R. D.; Harris, R.; Klein, E. W.; Bradford, T. J.; Wolk, F. N.; Westenfelder, K. R.; Trainer, A. F.; Richardson, T. A.; Egerdie, R. B.;

Goldfarb, B.; Zadra, J. A.; Lu, X.; Simon, I. M.; Campbell, S. A.; Bates, M. P.; Higuchi, R. G.; Witjes, J. A. Validation of an MRNA-Based Urine Test for the Detection of Bladder Cancer in Patients with Haematuria. *Eur. Urol. Oncol.* **2021**, *4* (1), 93–101. https://doi.org/10.1016/j.euo.2020.09.001.

(20) Husain, H.; Melnikova, V. O.; Kosco, K.; Woodward, B.; More, S.; Pingle, S. C.; Weihe, E.; Park, B. H.; Tewari, M.; Erlander, M. G.; Cohen, E.; Lippman, S. M.; Kurzrock, R. Monitoring Daily Dynamics of Early Tumor Response to Targeted Therapy by Detecting Circulating Tumor DNA in Urine. *Clin. Cancer Res.* **2017**, *23* (16), 4716–4723. https://doi.org/10.1158/1078-0432.CCR-17-0454.

(21) Silver Spring (MD): Food and Drug Administration (US); Bethesda (MD): National Institutes of Health (US). *FDA-NIH Biomarker Working Group. BEST (Biomarkers, EndpointS, and Other Tools) Resource.*; Food and Drug Administration (US), 2016.

(22) Lee, R. C.; Feinbaum, R. L.; Ambros, V. The C. Elegans Heterochronic Gene Lin-4 Encodes Small RNAs with Antisense Complementarity to Lin-14. *Cell* **1993**, *75* (5), 843–854. https://doi.org/10.1016/0092-8674(93)90529-Y.

(23) Roush, S.; Slack, F. J. The Let-7 Family of MicroRNAs. *Trends Cell Biol.* **2008**, *18* (10), 505–516. https://doi.org/10.1016/j.tcb.2008.07.007.

(24) Bracht, J. R.; Van Wynsberghe, P. M.; Mondol, V.; Pasquinelli, A. E. Regulation of Lin-4 MiRNA Expression, Organismal Growth and Development by a Conserved RNA Binding Protein in C. Elegans. *Dev. Biol.* **2010**, *348* (2), 210. https://doi.org/10.1016/J.YDBIO.2010.10.003.

(25) Tribolet, L.; Kerr, E.; Cowled, C.; Bean, A. G. D.; Stewart, C. R.; Dearnley, M.; Farr, R. J. MicroRNA Biomarkers for Infectious Diseases: From Basic Research to Biosensing. *Front. Microbiol.* **2020**, *11*, 1197. https://doi.org/10.3389/FMICB.2020.01197.

(26) da Silva, D. C. P.; Carneiro, F. D.; Almeida, K. C. de; Bottino, C. F. D. S. Role of MiRNAs on the Pathophysiology of Cardiovascular Diseases. *Arq. Bras. Cardiol.* **2018**, *111* (5), 738–746. https://doi.org/10.5935/ABC.20180215.

(27) Li, Y.; Yin, Z.; Fan, J.; Zhang, S.; Yang, W. The Roles of Exosomal MiRNAs and LncRNAs in Lung Diseases. *Signal Transduct. Target. Ther.* **2019**, *4* (1), 47. https://doi.org/10.1038/S41392-019-0080-7.

(28) Vishnoi, A.; Rani, S. MiRNA Biogenesis and Regulation of Diseases: An Overview. *Methods Mol. Biol.* **2017**, *1509*, 1–10. https://doi.org/10.1007/978-1-4939-6524-3_1.

(29) Matsuyama, H.; Suzuki, H. I. Systems and Synthetic MicroRNA Biology: From Biogenesis to Disease Pathogenesis. *Int. J. Mol. Sci.* **2020**, *21* (1), 132. https://doi.org/10.3390/ijms21010132.

(30) Michlewski, G.; Cáceres, J. F. Post-Transcriptional Control of MiRNA Biogenesis. *RNA* **2019**, *25* (1), 1. https://doi.org/10.1261/RNA.068692.118.

(31) Jet, T.; Gines, G.; Rondelez, Y.; Taly, V. Advances in Multiplexed Techniques for the Detection and Quantification of MicroRNAs. *Chem. Soc. Rev.* **2021**, *50* (6), 4141–4161. https://doi.org/10.1039/d0cs00609b.

(32) O'Brien, J.; Hayder, H.; Zayed, Y.; Peng, C. Overview of MicroRNA Biogenesis, Mechanisms of Actions, and Circulation. *Front. Endocrinol. (Lausanne).* **2018**, *9*, 402. https://doi.org/10.3389/fendo.2018.00402.

(33) Weber, J. A.; Baxter, D. H.; Zhang, S.; Huang, D. Y.; Huang, K. H.; Lee, M. J.; Galas, D. J.; Wang, K. The MicroRNA Spectrum in 12 Body Fluids. *Clin. Chem.* **2010**, *56* (11), 1733. https://doi.org/10.1373/CLINCHEM.2010.147405.

(34) Chevillet, J. R.; Kang, Q.; Ruf, I. K.; Briggs, H. A.; Vojtech, L. N.; Hughes, S. M.; Cheng, H. H.; Arroyo, J. D.; Meredith, E. K.; Gallichotte, E. N.; Pogosova-Agadjanyan, E. L.; Morrissey, C.; Stirewalt, D. L.; Hladik, F.; Yu, E. Y.; Higano, C. S.; Tewari, M. Quantitative and Stoichiometric Analysis of the MicroRNA Content of Exosomes. *Proc. Natl. Acad. Sci. U. S. A.* **2014**, *111* (41), 14888–14893. https://doi.org/10.1073/PNAS.1408301111/.

(35) Fabri-Faja, N.; Calvo-Lozano, O.; Dey, P.; Terborg, R. A.; Estevez, M. C.; Belushkin, A.; Yesilköy, F.; Duempelmann, L.; Altug, H.; Pruneri, V.; Lechuga, L. M. Early Sepsis Diagnosis via Protein and MiRNA Biomarkers Using a Novel Point-of-Care Photonic Biosensor. *Anal. Chim. Acta* **2019**, *1077*, 232–242. https://doi.org/10.1016/j.aca.2019.05.038.

(36) Krzywkowski, T.; Nilsson, M. Padlock Probes to Detect Single Nucleotide Polymorphisms. *Methods Mol. Biol.* **2018**, *1649*, 209–229. https://doi.org/10.1007/978-1-4939-7213-5_14.

(37) Trayhurn, P. Northern Blotting. *Proc. Nutr. Soc.* **1996**, *55* (1B), 583–589. https://doi.org/10.1079/pns19960051.

(38) Yaylak, B.; Akgül, B. Experimental MicroRNA Detection Methods. *Methods Mol. Biol.* **2022**, *2257*, 33–55. https://doi.org/10.1007/978-1-0716-1170-8_2.

(39) Bawazeer, A.; Prince, D. C. Detection of MiRNAs. *Methods Mol. Biol.* **2023**, *2630*, 1–11. https://doi.org/10.1007/978-1-0716-2982-6_1.

(40) Brenner, S.; Jacob, F.; Meselson, M. An Unstable Intermediate Carrying Information from Genes to Ribosomes for Protein Synthesis. *Nature* **1961**, *190* (4776), 576–581. https://doi.org/10.1038/190576a0.

(41) Gros, F.; Hiatt, H.; Gilbert, W.; Kurland, C. G.; Risebrough, R. W.; Watson, J. D. Unstable Ribonucleic Acid Revealed by Pulse Labelling of Escherichia Coli. *Nature* **1961**, *190* (4776), 581–585. https://doi.org/10.1038/190581a0.

(42) Jacob, F.; Monod, J. Genetic Regulatory Mechanisms in the Synthesis of Proteins. *J. Mol. Biol.* **1961**, *3* (3), 318–356. https://doi.org/10.1016/S0022-2836(61)80072-7.

(43) An, D.; Frassetto, A.; Jacquinet, E.; Eybye, M.; Milano, J.; DeAntonis, C.; Nguyen, V.; Laureano, R.; Milton, J.; Sabnis, S.; Lukacs, C. M.; Guey, L. T. Long-Term Efficacy and Safety of MRNA Therapy in Two Murine Models of Methylmalonic Acidemia. *EBioMedicine* **2019**, *45*, 519–528. https://doi.org/10.1016/j.ebiom.2019.07.003.

(44) Baden, L. R.; El Sahly, H. M.; Essink, B.; Kotloff, K.; Frey, S.; Novak, R.; Diemert, D.; Spector, S. A.; Rouphael, N.; Creech, C. B.; McGettigan, J.; Khetan, S.; Segall, N.; Solis, J.; Brosz, A.; Fierro, C.; Schwartz, H.; Neuzil, K.; Corey, L.; Gilbert, P.; Janes, H.;

Follmann, D.; Marovich, M.; Mascola, J.; Polakowski, L.; Ledgerwood, J.; Graham, B. S.; Bennett, H.; Pajon, R.; Knightly, C.; Leav, B.; Deng, W.; Zhou, H.; Han, S.; Ivarsson, M.; Miller, J.; Zaks, T. Efficacy and Safety of the MRNA-1273 SARS-CoV-2 Vaccine. *N. Engl. J. Med.* **2021**, *384* (5), 403–416. https://doi.org/10.1056/NEJMOA2035389.

(45) Al-Harithy, R. N.; Alomari, A. S. Expression of Leptin MRNA as Non-Invasive Biomarker in Type 2 Diabetes Mellitus. *Int. J. Clin. Pract.* **2021**, *75* (12), e14844. https://doi.org/10.1111/IJCP.14844.

(46) Chen, C. Y. A.; Ezzeddine, N.; Shyu, A. Bin. Messenger RNA Half-Life Measurements in Mammalian Cells. *Methods Enzymol.* **2008**, *448*, 335. https://doi.org/10.1016/S0076-6879(08)02617-7.

(47) Le, N. Q. K.; Yapp, E. K. Y.; Nagasundaram, N.; Yeh, H. Y. Classifying Promoters by Interpreting the Hidden Information of DNA Sequences via Deep Learning and Combination of Continuous FastText N-Grams. *Front. Bioeng. Biotechnol.* **2019**, *7*, 491279. https://doi.org/10.3389/fbioe.2019.00305.

(48) Taguchi, Y. H. Regulation of Gene Expression. *Encycl. Bioinforma. Comput. Biol. ABC Bioinforma.* **2018**, *1–3*, 806–813. https://doi.org/10.1016/B978-0-12-809633-8.20667-5.

(49) Bentley, D. L. Coupling MRNA Processing with Transcription in Time and Space. *Nat. Rev. Genet.* **2014**, *15* (3), 163–175. https://doi.org/10.1038/nrg3662.

(50) Cole, C. N. Choreographing MRNA Biogenesis. *Nat. Genet.* **2001**, *29* (1), 6–7. https://doi.org/10.1038/ng0901-6.

(51) Johnstone, R. M.; Adam, M.; Hammond, J. R.; Orr, L.; Turbide, C. Vesicle Formation during Reticulocyte Maturation. Association of Plasma Membrane Activities with Released Vesicles (Exosomes). *J. Biol. Chem.* **1987**, *262* (19), 9412–9420. https://doi.org/10.1016/s0021-9258(18)48095-7.

(52) Wolf, P. The Nature and Significance of Platelet Products in Human Plasma. *Br. J. Haematol.* **1967**, *13* (3), 269–288. https://doi.org/10.1111/j.1365-2141.1967.tb08741.x.

(53) Johnstone, R. M.; Mathew, A.; Mason, A. B.; Teng, K. Exosome Formation during Maturation of Mammalian and Avian Reticulocytes: Evidence That Exosome Release Is a Major Route for Externalization of Obsolete Membrane Proteins. *J. Cell. Physiol.* **1991**, *147* (1), 27–36. https://doi.org/10.1002/JCP.1041470105.

(54) Lötvall, J.; Hill, A. F.; Hochberg, F.; Buzás, E. I.; Vizio, D. Di; Gardiner, C.; Gho, Y. S.; Kurochkin, I. V.; Mathivanan, S.; Quesenberry, P.; Sahoo, S.; Tahara, H.; Wauben, M. H.; Witwer, K. W.; Théry, C. Minimal Experimental Requirements for Definition of Extracellular Vesicles and Their Functions: A Position Statement from the International Society for Extracellular Vesicles. *J. Extracell. Vesicles* **2014**, *3* (1), 26913. https://doi.org/10.3402/jev.v3.26913.

(55) Gurung, S.; Perocheau, D.; Touramanidou, L.; Baruteau, J. The Exosome Journey: From Biogenesis to Uptake and Intracellular Signalling. *Cell Commun. Signal.* **2021**, *19* (1), 1–19. https://doi.org/10.1186/s12964-021-00730-1.

(56) Battistelli, M.; Falcieri, E. Apoptotic Bodies: Particular Extracellular Vesicles Involved in Intercellular Communication. *Biology (Basel).* **2020**, *9* (1), 21. https://doi.org/10.3390/biology9010021.

(57) Cocucci, E.; Meldolesi, J. Ectosomes and Exosomes: Shedding the Confusion between Extracellular Vesicles. *Trends Cell Biol.* **2015**, *25* (6), 364–372. https://doi.org/10.1016/J.TCB.2015.01.004.

(58) Cocucci, E.; Meldolesi, J. Ectosomes. *Curr. Biol.* **2011**, *21* (23), R940–R941. https://doi.org/10.1016/j.cub.2011.10.011.

(59) Meldolesi, J. Exosomes and Ectosomes in Intercellular Communication. *Curr. Biol.* **2018**, *28* (8), R435–R444. https://doi.org/10.1016/j.cub.2018.01.059.

(60) Théry, C.; Zitvogel, L.; Amigorena, S. Exosomes: Composition, Biogenesis and Function. *Nat. Rev. Immunol.* **2002**, *2* (8), 569–579. https://doi.org/10.1038/nri855.

(61) Pegtel, D. M.; Gould, S. J. Exosomes. *Annu. Rev. Biochem.* **2019**, *88*, 487–514. https://doi.org/10.1146/annurev-biochem-013118-111902.

(62) Foster, B. P.; Balassa, T.; Benen, T. D.; Dominovic, M.; Elmadjian, G. K.; Florova, V.; Fransolet, M. D.; Kestlerova, A.; Kmiecik, G.; Kostadinova, I. A.; Kyvelidou, C.; Meggyes, M.; Mincheva, M. N.; Moro, L.; Pastuschek, J.; Spoldi, V.; Wandernoth, P.; Weber, M.; Toth, B.; Markert, U. R. Extracellular Vesicles in Blood, Milk and Body Fluids of the Female and Male Urogenital Tract and with Special Regard to Reproduction. *Crit. Rev. Clin. Lab. Sci.* **2016**, *53* (6), 379–395. https://doi.org/10.1080/10408363.2016.1190682.

(63) Cheng, Y.; Chang, F.; Gong, Y.; Lu, P. A Study on the Clinical Significance of Blood Exosomal PD-L1 in Non-Small Cell Lung Cancer Patients and Its Correlation with PD-L1 in Tumor Tissues. *Horm. Metab. Res.* **2023**, *55* (11), 788–793. https://doi.org/10.1055/a-2110-7497.

(64) Han, H.; Zhang, L.; Fu, Q.; Zhang, B.; Chen, J. Plasma Exosomes Aggravate Acute Pancreatitis by Promoting M1 Polarization of Adipose Tissue Macrophages in Obesity-Related Severe Acute Pancreatitis. *Dig. Dis. Sci.* **2023**, *68* (9), 3660–3670. https://doi.org/10.1007/s10620-023-08021-0.

(65) Graham, R.; Gazinska, P.; Zhang, B.; Khiabany, A.; Sinha, S.; Alaguthurai, T.; Flores-Borja, F.; Vicencio, J.; Beuron, F.; Roxanis, I.; Matkowski, R.; Liam-Or, R.; Tutt, A.; Ng, T.; Al-Jamal, K. T.; Zhou, Y.; Irshad, S. Serum-Derived Extracellular Vesicles from Breast Cancer Patients Contribute to Differential Regulation of T-Cell-Mediated Immune-Escape Mechanisms in Breast Cancer Subtypes. *Front. Immunol.* **2023**, *14*, 1204224. https://doi.org/10.3389/fimmu.2023.1204224.

(66) Kaczor-Urbanowicz, K. E.; Wei, F.; Rao, S. L.; Kim, J.; Shin, H.; Cheng, J.; Tu, M.; Wong, D. T. W.; Kim, Y. Clinical Validity of Saliva and Novel Technology for Cancer Detection. *Biochim. Biophys. Acta - Rev. Cancer* **2019**, *1872* (1), 49–59. https://doi.org/10.1016/j.bbcan.2019.05.007.

(67) Miyake, H.; Lee, C.; Chusilp, S.; Bhalla, M.; Li, B.; Pitino, M.; Seo, S.; O'Connor, D. L.; Pierro, A. Human Breast Milk Exosomes Attenuate Intestinal Damage. *Pediatr. Surg.*

Int. **2020**, *36* (2), 155–163. https://doi.org/10.1007/S00383-019-04599-7.

(68) McKiernan, J.; Donovan, M. J.; O'Neill, V.; Bentink, S.; Noerholm, M.; Belzer, S.; Skog, J.; Kattan, M. W.; Partin, A.; Andriole, G.; Brown, G.; Wei, J. T.; Thompson, I. M.; Carroll, P. A Novel Urine Exosome Gene Expression Assay to Predict High-Grade Prostate Cancer at Initial Biopsy. *JAMA Oncol.* **2016**, *2* (7), 882–889. https://doi.org/10.1001/jamaoncol.2016.0097.

(69) Chen, W. W.; Balaj, L.; Liau, L. M.; Samuels, M. L.; Kotsopoulos, S. K.; Maguire, C. A.; LoGuidice, L.; Soto, H.; Garrett, M.; Zhu, L. D.; Sivaraman, S.; Chen, C.; Wong, E. T.; Carter, B. S.; Hochberg, F. H.; Breakefield, X. O.; Skog, J. Beaming and Droplet Digital Pcr Analysis of Mutant Idh1 Mrna in Glioma Patient Serum and Cerebrospinal Fluid Extracellular Vesicles. *Mol. Ther. Nucleic Acids* **2013**, *2*, e109. https://doi.org/10.1038/mtna.2013.28.

(70) Langevin, S. M.; Kuhnell, D.; Orr-Asman, M. A.; Biesiada, J.; Zhang, X.; Medvedovic, M.; Thomas, H. E. Balancing Yield, Purity and Practicality: A Modified Differential Ultracentrifugation Protocol for Efficient Isolation of Small Extracellular Vesicles from Human Serum. *RNA Biol.* **2019**, *16* (1), 5–12. https://doi.org/10.1080/15476286.2018.1564465.

(71) Swatler, J.; Dudka, W.; Piwocka, K. Isolation and Characterization of Extracellular Vesicles from Cell Culture Conditioned Medium for Immunological Studies. *Curr. Protoc. Immunol.* **2020**, *129* (1), e96. https://doi.org/10.1002/cpim.96.

(72) Livshts, M. A.; Khomyakova, E.; Evtushenko, E. G.; Lazarev, V. N.; Kulemin, N. A.; Semina, S. E.; Generozov, E. V.; Govorun, V. M. Isolation of Exosomes by Differential Centrifugation: Theoretical Analysis of a Commonly Used Protocol. *Sci. Rep.* **2015**, *5*. https://doi.org/10.1038/srep17319.

(73) Théry, C.; Amigorena, S.; Raposo, G.; Clayton, A. Isolation and Characterization of Exosomes from Cell Culture Supernatants and Biological Fluids. *Curr. Protoc. cell Biol.* **2006**, *Chapter 3* (1). https://doi.org/10.1002/0471143030.CB0322S30.

(74) Tang, Y. T.; Huang, Y. Y.; Zheng, L.; Qin, S. H.; Xu, X. P.; An, T. X.; Xu, Y.; Wu, Y. S.; Hu, X. M.; Ping, B. H.; Wang, Q. Comparison of Isolation Methods of Exosomes and Exosomal RNA from Cell Culture Medium and Serum. *Int. J. Mol. Med.* **2017**, *40* (3), 834–844. https://doi.org/10.3892/IJMM.2017.3080.

(75) Keller, S.; Ridinger, J.; Rupp, A. K.; Janssen, J. W. G.; Altevogt, P. Body Fluid Derived Exosomes as a Novel Template for Clinical Diagnostics. *J. Transl. Med.* **2011**, *9* (1), 1–9. https://doi.org/10.1186/1479-5876-9-86.

(76) Van Deun, J.; Mestdagh, P.; Sormunen, R.; Cocquyt, V.; Vermaelen, K.; Vandesompele, J.; Bracke, M.; De Wever, O.; Hendrix, A. The Impact of Disparate Isolation Methods for Extracellular Vesicles on Downstream RNA Profiling. *J. Extracell. Vesicles* **2014**, *3* (1), 24858. https://doi.org/10.3402/jev.v3.24858.

(77) Witwer, K. W.; Buzás, E. I.; Bemis, L. T.; Bora, A.; Lässer, C.; Lötvall, J.; Nolte-'t Hoen, E. N.; Piper, M. G.; Sivaraman, S.; Skog, J.; Théry, C.; Wauben, M. H.; Hochberg, F. Standardization of Sample Collection, Isolation and Analysis Methods in Extracellular Vesicle Research. *J. Extracell. Vesicles* **2013**, *2* (1), 20360.

https://doi.org/10.3402/jev.v2i0.20360.

(78) de Menezes-Neto, A.; Sáez, M. J.; Lozano-Ramos, I.; Segui-Barber, J.; Martin-Jaular, L.; Ullate, J. M. E.; Fernandez-Becerra, C.; Borrás, F. E.; del Portillo, H. A. Size-Exclusion Chromatography as a Stand-Alone Methodology Identifies Novel Markers in Mass Spectrometry Analyses of Plasma-Derived Vesicles from Healthy Individuals. *J. Extracell. Vesicles* **2015**, *4* (1), 27378. https://doi.org/10.3402/JEV.V4.27378.

(79) Lobb, R. J.; Becker, M.; Wen, S. W.; Wong, C. S. F.; Wiegmans, A. P.; Leimgruber, A.; Möller, A. Optimized Exosome Isolation Protocol for Cell Culture Supernatant and Human Plasma. *J. Extracell. Vesicles* **2015**, *4* (1), 27031. https://doi.org/10.3402/jev.v4.27031.

(80) Lewis, G. D.; Metcalf, T. G. Polyethylene Glycol Precipitation for Recovery of Pathogenic Viruses, Including Hepatitis A Virus and Human Rotavirus, from Oyster, Water, and Sediment Samples. *Appl. Environ. Microbiol.* **1988**, *54* (8), 1983–1988. https://doi.org/10.1128/AEM.54.8.1983-1988.1988.

(81) Niu, Z.; Pang, R. T. K.; Liu, W.; Li, Q.; Cheng, R.; Yeung, W. S. B. Polymer-Based Precipitation Preserves Biological Activities of Extracellular Vesicles from an Endometrial Cell Line. *PLoS One* **2017**, *12* (10), e0186534. https://doi.org/10.1371/journal.pone.0186534.

(82) Brennan, K.; Martin, K.; FitzGerald, S. P.; O'Sullivan, J.; Wu, Y.; Blanco, A.; Richardson, C.; Mc Gee, M. M. A Comparison of Methods for the Isolation and Separation of Extracellular Vesicles from Protein and Lipid Particles in Human Serum. *Sci. Rep.* **2020**, *10* (1), 1–13. https://doi.org/10.1038/s41598-020-57497-7.

(83) Cheeveewattanagul, N.; Guajardo Yévenes, C. F.; Bamrungsap, S.; Japrung, D.; Chalermwatanachai, T.; Siriwan, C.; Warachit, O.; Somasundrum, M.; Surareungchai, W.; Rijiravanich, P. Aptamer-Functionalised Magnetic Particles for Highly Selective Detection of Urinary Albumin in Clinical Samples of Diabetic Nephropathy and Other Kidney Tract Disease. *Anal. Chim. Acta* **2021**, *1154*, 338302. https://doi.org/10.1016/J.ACA.2021.338302.

(84) Guo, Q. Y.; Ren, S. Y.; Wang, J. Y.; Li, Y.; Yao, Z. Y.; Huang, H.; Gao, Z. X.; Yang, S. P. Low Field Nuclear Magnetic Sensing Technology Based on Hydrogel-Coated Superparamagnetic Particles. *Anal. Chim. Acta* **2020**, *1094*, 151–159. https://doi.org/10.1016/j.aca.2019.10.013.

(85) Moura, S. L.; Martí, M.; Pividori, M. I. Matrix Effect in the Isolation of Breast Cancer-Derived Nanovesicles by Immunomagnetic Separation and Electrochemical Immunosensing— A Comparative Study. *Sensors* **2020**, *20* (4), 965. https://doi.org/10.3390/s20040965.

(86) Choi, H.; Mun, J. Y. Structural Analysis of Exosomes Using Different Types of Electron Microscopy. *Appl. Microsc.* **2017**, *47* (3), 171–175. https://doi.org/10.9729/am.2017.47.3.171.

(87) Chuo, S. T. Y.; Chien, J. C. Y.; Lai, C. P. K. Imaging Extracellular Vesicles: Current and Emerging Methods. *J. Biomed. Sci.* **2018**, *25* (1), 1–10. https://doi.org/10.1186/

S12929-018-0494-5.

(88) Kondratov, K. A.; Petrova, T. A.; Mikhailovskii, V. Y.; Ivanova, A. N.; Kostareva, A. A.; Fedorov, A. V. A Study of Extracellular Vesicles Isolated from Blood Plasma Conducted by Low-Voltage Scanning Electron Microscopy. *Cell tissue biol.* **2017**, *11* (3), 181–190. https://doi.org/10.1134/S1990519X17030051.

(89) Shao, H.; Chung, J.; Balaj, L.; Charest, A.; Bigner, D. D.; Carter, B. S.; Hochberg, F. H.; Breakefield, X. O.; Weissleder, R.; Lee, H. Protein Typing of Circulating Microvesicles Allows Real-Time Monitoring of Glioblastoma Therapy. *Nat. Med.* **2012**, *18* (12), 1835–1840. https://doi.org/10.1038/nm.2994.

(90) Szatanek, R.; Baj-Krzyworzeka, M.; Zimoch, J.; Lekka, M.; Siedlar, M.; Baran, J. The Methods of Choice for Extracellular Vesicles (EVs) Characterization. *Int. J. Mol. Sci.* **2017**, *18* (6), 1153. https://doi.org/10.3390/ijms18061153.

(91) Gardiner, C.; Ferreira, Y. J.; Dragovic, R. A.; Redman, C. W. G.; Sargent, I. L. Extracellular Vesicle Sizing and Enumeration by Nanoparticle Tracking Analysis. *J. Extracell. Vesicles* **2013**, *2* (1), 19671. https://doi.org/10.3402/jev.v2i0.19671.

(92) Griffiths, D.; Carnell-Morris, P.; Wright, M. Nanoparticle Tracking Analysis for Multiparameter Characterization and Counting of Nanoparticle Suspensions. *Methods Mol. Biol.* **2020**, *2118*, 289–303. https://doi.org/10.1007/978-1-0716-0319-2_22.

(93) Lyu, T. S.; Ahn, Y.; Im, Y. J.; Kim, S. S.; Lee, K. H.; Kim, J.; Choi, Y.; Lee, D.; Kang, E. S.; Jin, G.; Hwang, J.; Lee, S. I.; Cho, J. A. The Characterization of Exosomes from Fibrosarcoma Cell and the Useful Usage of Dynamic Light Scattering (DLS) for Their Evaluation. *PLoS One* **2021**, *16* (11), e0231994. https://doi.org/10.1371/journal.pone.0231994.

(94) Wong, M. L.; Medrano, J. F. Real-Time PCR for MRNA Quantitation. *Biotechniques* **2005**, *39* (1), 75–85. https://doi.org/10.2144/05391RV01.

(95) Allenson, K.; Castillo, J.; San Lucas, F. A.; Scelo, G.; Kim, D. U.; Bernard, V.; Davis, G.; Kumar, T.; Katz, M.; Overman, M. J.; Foretova, L.; Fabianova, E.; Holcatova, I.; Janout, V.; Meric-Bernstam, F.; Gascoyne, P.; Wistuba, I.; Varadhachary, G.; Brennan, P.; Hanash, S.; Li, D.; Maitra, A.; Alvarez, H. High Prevalence of Mutant KRAS in Circulating Exosome-Derived DNA from Early-Stage Pancreatic Cancer Patients. *Ann. Oncol.* **2017**, *28* (4), 741–747. https://doi.org/10.1093/annonc/mdx004.

(96) Dvorák, Z.; Pascussi, J. M.; Modrianský, M. Approaches to Messenger RNA Detection - Comparison of Methods. *Biomed. Pap. Med. Fac. Univ. Palacky. Olomouc. Czech. Repub.* **2003**, *147* (2), 131–135. https://doi.org/10.5507/bp.2003.018.

(97) Ye, J.; Xu, M.; Tian, X.; Cai, S.; Zeng, S. Research Advances in the Detection of MiRNA. *J. Pharm. Anal.* **2019**, *9* (4), 217–226. https://doi.org/10.1016/J.JPHA.2019.05.004.

(98) Lee, R. C.; Feinbaum, R. L.; Ambros, V. The C. Elegans Heterochronic Gene Lin-4

Encodes Small RNAs with Antisense Complementarity to Lin-14. *Cell* **1993**, *75* (5), 843–854. https://doi.org/10.1016/0092-8674(93)90529-Y.

(99) Gall, J. G.; Pardue, M. L. Formation and Detection of RNA-DNA Hybrid Molecules in Cytological Preparations. *Proc. Natl. Acad. Sci. U. S. A.* **1969**, *63* (2), 378–383. https://doi.org/10.1073/pnas.63.2.378.

(100) Young, A. P.; Jackson, D. J.; Wyeth, R. C. A Technical Review and Guide to RNA Fluorescence in Situ Hybridization. *PeerJ* **2020**, *8*, e8806. https://doi.org/10.7717/peerj.8806.

(101) Raj, A.; van den Bogaard, P.; Rifkin, S. A.; van Oudenaarden, A.; Tyagi, S. Imaging Individual MRNA Molecules Using Multiple Singly Labeled Probes. *Nat. Methods* **2008**, *5* (10), 877–879. https://doi.org/10.1038/nmeth.1253.

(102) Barroso-Chinea, P.; Aymerich, M. S.; Castle, M. M.; Pérez-Manso, M.; Tuñón, T.; Erro, E.; Lanciego, J. L. Detection of Two Different MRNAs in a Single Section by Dual in Situ Hybridization: A Comparison between Colorimetric and Fluorescent Detection. *J. Neurosci. Methods* **2007**, *162* (1–2), 119–128. https://doi.org/10.1016/J.JNEUMETH.2006.12.017.

(103) Dave, V. P.; Ngo, T. A.; Pernestig, A. K.; Tilevik, D.; Kant, K.; Nguyen, T.; Wolff, A.; Bang, D. D. MicroRNA Amplification and Detection Technologies: Opportunities and Challenges for Point of Care Diagnostics. *Lab. Investig.* **2019**, *99* (4), 452–469. https://doi.org/10.1038/s41374-018-0143-3.

(104) Li, W.; Ruan, K. MicroRNA Detection by Microarray. *Anal. Bioanal. Chem.* **2009**, *394* (4), 1117–1124. https://doi.org/10.1007/S00216-008-2570-2.

(105) Goldrick, M.; Kessler, D. RNA Analysis by Nuclease Protection. *Curr. Protoc. Neurosci.* **2003**, *Chapter 5* (1), 5.1.1-5.1.30. https://doi.org/10.1002/0471142301.ns0501s23.

(106) Farrell, R. E. Quantification of Specific MRNAs by Nuclease Protection. *RNA Methodol.* **2017**, 545–567. https://doi.org/10.1016/B978-0-12-804678-4.00018-X.

(107) Qian, L.; Li, Q.; Baryeh, K.; Qiu, W.; Li, K.; Zhang, J.; Yu, Q.; Xu, D.; Liu, W.; Brand, R. E.; Zhang, X.; Chen, W.; Liu, G. Biosensors for Early Diagnosis of Pancreatic Cancer: A Review. *Transl. Res.* **2019**, *213*, 67–89. https://doi.org/10.1016/j.trsl.2019.08.002.

(108) Wu, Y.; Zhang, Y.; Zhang, X.; Luo, S.; Yan, X.; Qiu, Y.; Zheng, L.; Li, L. Research Advances for Exosomal MiRNAs Detection in Biosensing: From the Massive Study to the Individual Study. *Biosens. Bioelectron.* **2021**, *177*, 112962. https://doi.org/10.1016/j.bios.2020.112962.

(109) Coutinho, C.; Somoza, Á. MicroRNA Sensors Based on Gold Nanoparticles. *Anal. Bioanal. Chem.* **2019**, *411* (9), 1807–1824. https://doi.org/10.1007/s00216-018-1450-7.

(110) Gessner, I.; Fries, J. W. U.; Brune, V.; Mathur, S. Magnetic Nanoparticle-Based Amplification of MicroRNA Detection in Body Fluids for Early Disease Diagnosis. *J. Mater. Chem. B* **2021**, *9* (1), 9–22. https://doi.org/10.1039/D0TB02165B.

(111) Shah, P.; Thulstrup, P. W.; Cho, S. K.; Bhang, Y. J.; Ahn, J. C.; Choi, S. W.; Bjerrum, M. J.; Yang, S. W. In-Solution Multiplex MiRNA Detection Using DNA-Templated Silver Nanocluster Probes. *Analyst* **2014**, *139* (9), 2158–2166. https://doi.org/10.1039/c3an02150e.

(112) Goryacheva, O. A.; Mishra, P. K.; Goryacheva, I. Y. Luminescent Quantum Dots for MiRNA Detection. *Talanta* **2018**, *179*, 456–465. https://doi.org/10.1016/j.talanta.2017.11.011.

(113) Li, H.; Warden, A. R.; Su, W.; He, J.; Zhi, X.; Wang, K.; Zhu, L.; Shen, G.; Ding, X. Highly Sensitive and Portable MRNA Detection Platform for Early Cancer Detection. *J. Nanobiotechnology* **2021**, *19* (1), 1–10. https://doi.org/10.1186/s12951-021-01039-4.

(114) Hou, S. Y.; Hsiao, Y. L.; Lin, M. S.; Yen, C. C.; Chang, C. S. MicroRNA Detection Using Lateral Flow Nucleic Acid Strips with Gold Nanoparticles. *Talanta* **2012**, *99*, 375–379. https://doi.org/10.1016/J.TALANTA.2012.05.067.

(115) Gao, X.; Xu, L. P.; Wu, T.; Wen, Y.; Ma, X.; Zhang, X. An Enzyme-Amplified Lateral Flow Strip Biosensor for Visual Detection of MicroRNA-224. *Talanta* **2016**, *146*, 648–654. https://doi.org/10.1016/j.talanta.2015.06.060.

(116) Fakhri, N.; Abarghoei, S.; Dadmehr, M.; Hosseini, M.; Sabahi, H.; Ganjali, M. R. Paper Based Colorimetric Detection of MiRNA-21 Using Ag/Pt Nanoclusters. *Spectrochim. Acta Part A Mol. Biomol. Spectrosc.* **2020**, *227*, 117529. https://doi.org/10.1016/J.SAA.2019.117529.

(117) Pallares-Rusiñol, A.; Moura, S. L.; Martí, M.; Pividori, M. I. Electrochemical Genosensing of Overexpressed GAPDH Transcripts in Breast Cancer Exosomes. *Anal. Chem.* **2023**, *95* (4), 2487–2495. https://doi.org/10.1021/acs.analchem.2c04773.

(118) Wang, Q.; Sun, H.; Wen, D.; Wang, L.; Li, L.; Kong, J.; Zhang, X. Ultrasensitive Electrochemical Detection of MiRNA Based on Polymerization Signal Amplification. *Talanta* **2021**, *235*, 122744. https://doi.org/10.1016/j.talanta.2021.122744.

(119) Pereira, R. L.; Oliveira, D.; Pêgo, A. P.; Santos, S. D.; Moreira, F. T. C. Electrochemical MiRNA-34a-Based Biosensor for the Diagnosis of Alzheimer's Disease. *Bioelectrochemistry* **2023**, *154*, 108553. https://doi.org/10.1016/j.bioelechem.2023.108553.

(120) Bharti, A.; Mittal, S.; Rana, S.; Dahiya, D.; Agnihotri, N.; Prabhakar, N. Electrochemical Biosensor for MiRNA-21 Based on Gold-Platinum Bimetallic Nanoparticles Coated 3-Aminopropyltriethoxy Silane. *Anal. Biochem.* **2020**, *609*, 113908. https://doi.org/10.1016/j.ab.2020.113908.

(121) Yan, J.; Wang, J.; Liu, H.; Wang, L.; Yu, K.; Deng, L.; Su, J.; Chen, H. MiR-29b Detection in Serum Using an Electrochemical Biosensor for the Early Diagnosis of Gestational Diabetes. *Anal. Biochem.* **2023**, *674*, 115209. https://doi.org/10.1016/J.AB.2023.115209.

(122) Thompson, A. M.; Gansen, A.; Paguirigan, A. L.; Kreutz, J. E.; Radich, J. P.; Chiu, D. T.

Self-Digitization Microfluidic Chip for Absolute Quantification of MRNA in Single Cells. *Anal. Chem.* **2014**, *86* (24), 12308–12314. https://doi.org/10.1021/ac5035924.

(123) Wang, J.; Lu, W.; Tang, C.; Liu, Y.; Sun, J.; Mu, X.; Zhang, L.; Dai, B.; Li, X.; Zhuo, H.; Jiang, X. Label-Free Isolation and MRNA Detection of Circulating Tumor Cells from Patients with Metastatic Lung Cancer for Disease Diagnosis and Monitoring Therapeutic Efficacy. *Anal. Chem.* **2015**, *87* (23), 11893–11900. https://doi.org/10.1021/acs.analchem.5b03484.

(124) Ma, W.; Liu, L.; Zhang, X.; Liu, X.; Xu, Y.; Li, S.; Zeng, M. A Microfluidic-Based SERS Biosensor with Multifunctional Nanosurface Immobilized Nanoparticles for Sensitive Detection of MicroRNA. *Anal. Chim. Acta* **2022**, *1221*, 340139. https://doi.org/10.1016/j.aca.2022.340139.

(125) Chu, Y.; Gao, Y.; Tang, W.; Qiang, L.; Han, Y.; Gao, J.; Zhang, Y.; Liu, H.; Han, L. Attomolar-Level Ultrasensitive and Multiplex MicroRNA Detection Enabled by a Nanomaterial Locally Assembled Microfluidic Biochip for Cancer Diagnosis. *Anal. Chem.* **2021**, *93* (12), 5129–5136. https://doi.org/doi.org/10.1021/acs.analchem.0c04896.

(126) Theodoraki, M. N.; Hong, C. S.; Donnenberg, V. S.; Donnenberg, A. D.; Whiteside, T. L. Evaluation of Exosome Proteins by On-Bead Flow Cytometry. *Cytom. Part A* **2021**, *99* (4), 372–381. https://doi.org/10.1002/cyto.a.24193.

(127) Moura, S. L.; Martín, C. G.; Martí, M.; Pividori, M. I. Multiplex Detection and Characterization of Breast Cancer Exosomes by Magneto-Actuated Immunoassay. *Talanta* **2020**, *211*, 120657. https://doi.org/10.1016/J.TALANTA.2019.120657.

(128) Xia, Y.; Chen, T.; Chen, G.; Weng, Y.; Zeng, L.; Liao, Y.; Chen, W.; Lan, J.; Zhang, J.; Chen, J. A Nature-Inspired Colorimetric and Fluorescent Dual-Modal Biosensor for Exosomes Detection. *Talanta* **2020**, *214*, 120851. https://doi.org/10.1016/j.talanta.2020.120851.

(129) Roda, A.; Mirasoli, M.; Michelini, E.; Di Fusco, M.; Zangheri, M.; Cevenini, L.; Roda, B.; Simoni, P. Progress in Chemical Luminescence-Based Biosensors: A Critical Review. *Biosens. Bioelectron.* **2016**, *76*, 164–179. https://doi.org/10.1016/J.BIOS.2015.06.017.

(130) Chen, S.; Zhang, M.; Li, J.; Huang, J.; Zhou, S.; Hou, X.; Ye, H.; Liu, X.; Xiang, S.; Shen, W.; Miao, J.; Hou, F. F.; Liu, Y.; Zhou, L. β-Catenin-Controlled Tubular Cell-Derived Exosomes Play a Key Role in Fibroblast Activation via the OPN-CD44 Axis. *J. Extracell. Vesicles* **2022**, *11* (3), e12203. https://doi.org/10.1002/jev2.12203.

(131) Paolini, L.; Zendrini, A.; Noto, G. Di; Busatto, S.; Lottini, E.; Radeghieri, A.; Dossi, A.; Caneschi, A.; Ricotta, D.; Bergese, P. Residual Matrix from Different Separation Techniques Impacts Exosome Biological Activity. *Sci. Rep.* **2016**, *6* (1), 1–11. https://doi.org/10.1038/srep23550.

(132) Domon, B.; Aebersold, R. Mass Spectrometry and Protein Analysis. *Science (80-.).* **2006**, *312* (5771), 212–217. https://doi.org/10.1126/science.1124619.

(133) Brown, B. A.; Zeng, X.; Todd, A. R.; Barnes, L. F.; Winstone, J. M. A.; Trinidad, J. C.; Novotny, M. V.; Jarrold, M. F.; Clemmer, D. E. Charge Detection Mass Spectrometry Measurements of Exosomes and Other Extracellular Particles Enriched from Bovine Milk. *Anal. Chem.* **2020**, *92* (4), 3285. https://doi.org/10.1021/ACS.ANALCHEM.9B05173.

(134) Cai, H.; Pang, Y.; Wang, Q.; Qin, W.; Wei, C.; Li, Y.; Li, T.; Li, F.; Wang, Q.; Li, Y.; Wei, Y.; Jia, L. Proteomic Profiling of Circulating Plasma Exosomes Reveals Novel Biomarkers of Alzheimer's Disease. *Alzheimer's Res. Ther.* **2022**, *14* (1), 181. https://doi.org/10.1186/s13195-022-01133-1.

(135) Lin, S.; Yu, Z.; Chen, D.; Wang, Z.; Miao, J.; Li, Q.; Zhang, D.; Song, J.; Cui, D. Progress in Microfluidics-Based Exosome Separation and Detection Technologies for Diagnostic Applications. *Small* **2020**, *16* (9), e1903916. https://doi.org/10.1002/smll.201903916.

(136) Lin, S. W.; Shen, C. F.; Liu, C. C.; Cheng, C. M. A Paper-Based IL-6 Test Strip Coupled With a Spectrum-Based Optical Reader for Differentiating Influenza Severity in Children. *Front. Bioeng. Biotechnol.* **2021**, *9*, 752681. https://doi.org/10.3389/FBIOE.2021.752681/BIBTEX.

(137) Oliveira-Rodríguez, M.; López-Cobo, S.; Reyburn, H. T.; Costa-García, A.; López-Martín, S.; Yáñez-Mó, M.; Cernuda-Morollón, E.; Paschen, A.; Valés-Gómez, M.; Blanco-López, M. C. Development of a Rapid Lateral Flow Immunoassay Test for Detection of Exosomes Previously Enriched from Cell Culture Medium and Body Fluids. *J. Extracell. Vesicles* **2016**, *5* (1), 5. https://doi.org/10.3402/jev.v5.31803.

(138) Gao, Z.; Ye, H.; Tang, D.; Tao, J.; Habibi, S.; Minerick, A.; Tang, D.; Xia, X. Platinum-Decorated Gold Nanoparticles with Dual Functionalities for Ultrasensitive Colorimetric in Vitro Diagnostics. *Nano Lett.* **2017**, *17* (9), 5572–5579. https://doi.org/10.1021/acs.nanolett.7b02385.

(139) Mahmoudi, T.; Pourhassan-Moghaddam, M.; Shirdel, B.; Baradaran, B.; Morales-Narváez, E.; Golmohammadi, H. On-Site Detection of Carcinoembryonic Antigen in Human Serum. *Biosensors* **2021**, *11* (10). https://doi.org/10.3390/bios11100392.

(140) Moura, S. L.; Martín, C. G.; Martí, M.; Pividori, M. I. Electrochemical Immunosensing of Nanovesicles as Biomarkers for Breast Cancer. *Biosens. Bioelectron.* **2020**, *150*, 111882. https://doi.org/10.1016/j.bios.2019.111882.

(141) Moura, S. L.; Pallarès-Rusiñol, A.; Sappia, L.; Martí, M.; Pividori, M. I. The Activity of Alkaline Phosphatase in Breast Cancer Exosomes Simplifies the Biosensing Design. *Biosens. Bioelectron.* **2022**, *198*, 113826. https://doi.org/10.1016/j.bios.2021.113826.

(142) Khan, M. S.; Dighe, K.; Wang, Z.; Srivastava, I.; Daza, E.; Schwartz-Dual, A. S.; Ghannam, J.; Misra, S. K.; Pan, D. Detection of Prostate Specific Antigen (PSA) in Human Saliva Using an Ultra-Sensitive Nanocomposite of Graphene Nanoplatelets with Diblock-: Co -Polymers and Au Electrodes. *Analyst* **2018**, *143* (5), 1094–1103. https://doi.org/10.1039/c7an01932g.

(143) Chen, H.; Li, Z. yin; Chen, J.; Yu, H.; Zhou, W.; Shen, F.; Chen, Q.; Wu, L.

CRISPR/Cas12a-Based Electrochemical Biosensor for Highly Sensitive Detection of CTnI. *Bioelectrochemistry* **2022**, *146*, 108167. https://doi.org/10.1016/J.BIOELECHEM.2022.108167.

(144) Liu, D.; Zhou, L.; Huang, L.; Zuo, Z.; Ho, V.; Jin, L.; Lu, Y.; Chen, X.; Zhao, J.; Qian, D.; Liu, H.; Mao, H. Microfluidic Integrated Capacitive Biosensor for C-Reactive Protein Label-Free and Real-Time Detection. *Analyst* **2021**, *146* (17), 5380–5388. https://doi.org/10.1039/d1an00464f.

(145) Lee, J.; Tripathi, A. Measurements of Label Free Protein Concentration and Conformational Changes Using a Microfluidic UV-LED Method. *Biotechnol. Prog.* **2007**, *23* (6), 1506–1512. https://doi.org/10.1021/BP0701970.

(146) Rissin, D. M.; Kan, C. W.; Campbell, T. G.; Howes, S. C.; Fournier, D. R.; Song, L.; Piech, T.; Patel, P. P.; Chang, L.; Rivnak, A. J.; Ferrell, E. P.; Randall, J. D.; Provuncher, G. K.; Walt, D. R.; Duffy, D. C. Single-Molecule Enzyme-Linked Immunosorbent Assay Detects Serum Proteins at Subfemtomolar Concentrations. *Nat. Biotechnol.* **2010**, *28* (6), 595–599. https://doi.org/10.1038/nbt.1641.

(147) Fiallos, M. R.; Hanhan, U. A.; Orlowski, J. P. POINT-OF-CARE TESTING. *Pediatr. Clin. North Am.* **2001**, *48* (3), 589–600. https://doi.org/10.1016/S0031-3955(05)70329-1.

(148) Gauglitz, G. Point-of-Care Platforms. *Annu. Rev. Anal. Chem.* **2014**, *7*, 297–315. https://doi.org/10.1146/annurev-anchem-071213-020332.

(149) Goble, J. A.; Rocafort, P. T. Point-of-Care Testing: Future of Chronic Disease State Management? *J. Pharm. Pract.* **2017**, *30* (2), 229–237. https://doi.org/10.1177/0897190015587696.

(150) Park, S. H.; Jegal, S.; Ahn, S. K.; Jung, H.; Lee, J.; Na, B. K.; Hong, S. J.; Bahk, Y. Y.; Kim, T. S. Diagnostic Performance of Three Rapid Diagnostic Test Kits for Malaria Parasite Plasmodium Falciparum. *Korean J. Parasitol.* **2020**, *58* (2), 147–152. https://doi.org/10.3347/kjp.2020.58.2.147.

(151) Clark, L. C.; Lyons, C. Electrode Systems for Continuous Monitoring in Cardiovascular Surgery. *Ann. N. Y. Acad. Sci.* **1962**, *102* (1), 29–45. https://doi.org/10.1111/j.1749-6632.1962.tb13623.x.

(152) Land, K. J.; Boeras, D. I.; Chen, X. S.; Ramsay, A. R.; Peeling, R. W. REASSURED Diagnostics to Inform Disease Control Strategies, Strengthen Health Systems and Improve Patient Outcomes. *Nat. Microbiol.* **2019**, *4* (1), 46–54. https://doi.org/10.1038/s41564-018-0295-3.

(153) Mc Naught, a. D.; Wilkinson, A. *The IUPAC Compendium of Chemical Terminology*; International Union of Pure and Applied Chemistry (IUPAC), 2019. https://doi.org/10.1351/goldbook.

(154) Clark, L. C.; Lyons, C. Electrode Systems for Continuous Monitoring in Cardiovascular Surgery. *Ann. N. Y. Acad. Sci.* **1962**, *102* (1), 29–45. https://doi.org/10.1111/j.1749-6632.1962.tb13623.x.

(155) Lolekha, P. H.; Srisawasdi, P.; Jearanaikoon, P.; Wetprasit, N.; Sriwanthana, B.; Kroll,

M. H. Performance of Four Sources of Cholesterol Oxidase for Serum Cholesterol Determination by the Enzymatic Endpoint Method. *Clin. Chim. Acta* **2004**, *339* (1–2), 135–145. https://doi.org/10.1016/j.cccn.2003.10.005.

(156) Newman, J. D.; Setford, S. J. Enzymatic Biosensors. *Mol. Biotechnol.* **2006**, *32* (3), 249–268. https://doi.org/10.1385/MB:32:3:249.

(157) Ma, H.; O'Kennedy, R. The Structure of Natural and Recombinant Antibodies. *Methods Mol. Biol.* **2015**, *1348*, 7–11. https://doi.org/10.1007/978-1-4939-2999-3_2.

(158) Ding, S.; Zhou, H.; Gu, Y.; Shen, Y.; Zhang, L.; Zhao, H.; Wu, J.; Zhang, X.; Chang, X.; Liu, C. Establishment of a Novel Double-Monoclonal Antibody Sandwich Enzyme-Linked Immunosorbent Assay (ELISA): Tool for Human B7-H4 Detection in Autoimmune Diseases. *Clin. Exp. Immunol.* **2021**, *205* (2), 150–159. https://doi.org/10.1111/cei.13610.

(159) Corstjens, P. L. A. M.; de Dood, C. J.; van der Ploeg-van Schip, J. J.; Wiesmeijer, K. C.; Riuttamäki, T.; van Meijgaarden, K. E.; Spencer, J. S.; Tanke, H. J.; Ottenhoff, T. H. M.; Geluk, A. Lateral Flow Assay for Simultaneous Detection of Cellular- and Humoral Immune Responses. *Clin. Biochem.* **2011**, *44* (14–15), 1241–1246. https://doi.org/10.1016/j.clinbiochem.2011.06.983.

(160) Egri, N.; Olivé, V.; Hernández-Rodríguez, J.; Castro, P.; De Guzman, C.; Heredia, L.; Segura, A. C.; Fernandez, M. D.; de Moner, N.; Torradeflot, M.; Ballús, J.; Martinez, R.; Vazquez, M.; Costa, M. V.; Dobaño, C.; Mazza, M.; Mazzotti, L.; Pascal, M.; Juan, M.; González-Navarro, E. A.; Calderón, H. CoVITEST: A Fast and Reliable Method to Monitor Anti-SARS-CoV-2 Specific T Cells From Whole Blood. *Front. Immunol.* **2022**, *13*, 848586. https://doi.org/10.3389/fimmu.2022.848586.

(161) Guan, B.; Zhang, X. Aptamers as Versatile Ligands for Biomedical and Pharmaceutical Applications. *Int. J. Nanomedicine* **2020**, *15*, 1059–1071. https://doi.org/10.2147/IJN.S237544.

(162) Zhao, Y. W.; Wang, H. X.; Jia, G. C.; Li, Z. Application of Aptamer-Based Biosensor for Rapid Detection of Pathogenic Escherichia Coli. *Sensors (Basel).* **2018**, *18* (8). https://doi.org/10.3390/S18082518.

(163) Xiao, Y.; Lubin, A. A.; Heeger, A. J.; Plaxco, K. W. Label-Free Electronic Detection of Thrombin in Blood Serum by Using an Aptamer-Based Sensor. *Angew. Chemie - Int. Ed.* **2005**, *44* (34), 5456–5459. https://doi.org/10.1002/anie.200500989.

(164) Andersson, L.; Sellergren, B.; Mosbach, K. Imprinting of Amino Acid Derivatives in Macroporous Polymers. *Tetrahedron Lett.* **1984**, *25* (45), 5211–5214. https://doi.org/10.1016/S0040-4039(01)81566-5.

(165) Lu, Y.; Liu, Q.; Fu, B.; Li, P.; Xu, W. Label-Free MIP-SERS Biosensor for Sensitive Detection of Colorectal Cancer Biomarker. *Talanta* **2023**, *258*, 124461. https://doi.org/10.1016/j.talanta.2023.124461.

(166) Yarman, A.; Kurbanoglu, S.; Jetzschmann, K. J.; Ozkan, S. A.; Wollenberger, U.; Scheller, F. W. Electrochemical MIP-Sensors for Drugs. *Curr. Med. Chem.* **2017**, *25*

(33), 4007–4019. https://doi.org/10.2174/092986732466617100510371 2.

(167) Carinelli, S.; Xufré, C.; Martí, M.; Pividori, M. I. Interferon Gamma Transcript Detection on T Cells Based on Magnetic Actuation and Multiplex Double-Tagging Electrochemical Genosensing. *Biosens. Bioelectron.* **2018**, *117*, 183–190. https://doi.org/10.1016/j.bios.2018.05.030.

(168) Chang, K.; Sun, P.; Dong, X.; Zhu, C.; Liu, X.; Zheng, D.; Liu, C. Aptamers as Recognition Elements for Electrochemical Detection of Exosomes. *Chem. Res. Chinese Univ.* **2022**, *38* (4), 879–885. https://doi.org/10.1007/S40242-022-2088-8.

(169) Olaru, A.; Bala, C.; Jaffrezic-Renault, N.; Aboul-Enein, H. Y. Surface Plasmon Resonance (SPR) Biosensors in Pharmaceutical Analysis. *Crit. Rev. Anal. Chem.* **2015**, *45* (2), 97–105. https://doi.org/10.1080/10408347.2014.881250.

(170) Ly, T. T.; Ruan, Y.; Du, B.; Jia, P.; Zhang, H. Fibre-Optic Surface Plasmon Resonance Biosensor for Monoclonal Antibody Titer Quantification. *Biosensors* **2021**, *11* (10), 383. https://doi.org/10.3390/bios11100383.

(171) Dai, Z.; Xu, X.; Wang, Y.; Li, M.; Zhou, K.; Zhang, L.; Tan, Y. Surface Plasmon Resonance Biosensor with Laser Heterodyne Feedback for Highly-Sensitive and Rapid Detection of COVID-19 Spike Antigen. *Biosens. Bioelectron.* **2022**, *206*, 114163. https://doi.org/10.1016/j.bios.2022.114163.

(172) Das, S.; Devireddy, R.; Gartia, M. R. Surface Plasmon Resonance (SPR) Sensor for Cancer Biomarker Detection. *Biosensors* **2023**, *13* (3), 396. https://doi.org/10.3390/bios13030396.

(173) Ramanathan, K.; Danielsson, B. Principles and Applications of Thermal Biosensors. *Biosens. Bioelectron.* **2001**, *16* (6), 417–423. https://doi.org/10.1016/S0956-5663(01)00124-5.

(174) Zhang, Y.; Tadigadapa, S. Calorimetric Biosensors with Integrated Microfluidic Channels. *Biosens. Bioelectron.* **2004**, *19* (12), 1733–1743. https://doi.org/10.1016/j.bios.2004.01.009.

(175) Pohanka, M. Overview of Piezoelectric Biosensors, Immunosensors and DNA Sensors and Their Applications. *Materials (Basel).* **2018**, *11* (3), 448. https://doi.org/10.3390/ma11030448.

(176) Lim, H. J.; Saha, T.; Tey, B. T.; Tan, W. S.; Ooi, C. W. Quartz Crystal Microbalance-Based Biosensors as Rapid Diagnostic Devices for Infectious Diseases. *Biosens. Bioelectron.* **2020**, *168*, 112513. https://doi.org/10.1016/J.BIOS.2020.112513.

(177) Huang, X.; Xu, D.; Chen, J.; Liu, J.; Li, Y.; Song, J.; Ma, X.; Guo, J. Smartphone-Based Analytical Biosensors. *Analyst* **2018**, *143* (22), 5339–5351. https://doi.org/10.1039/C8AN01269E.

(178) Roda, A.; Michelini, E.; Zangheri, M.; Di Fusco, M.; Calabria, D.; Simoni, P. Smartphone-Based Biosensors: A Critical Review and Perspectives. *TrAC - Trends Anal. Chem.* **2016**, *79*, 317–325. https://doi.org/10.1016/j.trac.2015.10.019.

(179) Switz, N. A.; D'Ambrosio, M. V.; Fletcher, D. A. Low-Cost Mobile Phone Microscopy

with a Reversed Mobile Phone Camera Lens. *PLoS One* **2014**, *9* (5), e95330. https://doi.org/10.1371/journal.pone.0095330.

(180) Müller, V.; Sousa, J. M.; Ceylan Koydemir, H.; Veli, M.; Tseng, D.; Cerqueira, L.; Ozcan, A.; Azevedo, N. F.; Westerlund, F. Identification of Pathogenic Bacteria in Complex Samples Using a Smartphone Based Fluorescence Microscope. *RSC Adv.* **2018**, *8* (64), 36493–36502. https://doi.org/10.1039/c8ra06473c.

(181) Ulep, T. H.; Zenhausern, R.; Gonzales, A.; Knoff, D. S.; Lengerke Diaz, P. A.; Castro, J. E.; Yoon, J. Y. Smartphone Based On-Chip Fluorescence Imaging and Capillary Flow Velocity Measurement for Detecting ROR1+ Cancer Cells from Buffy Coat Blood Samples on Dual-Layer Paper Microfluidic Chip. *Biosens. Bioelectron.* **2020**, *153*, 112042. https://doi.org/10.1016/j.bios.2020.112042.

(182) Meng, Z.; Tayyab, M.; Lin, Z.; Raji, H.; Javanmard, M. A Smartphone-Based Disposable Hemoglobin Sensor Based on Colorimetric Analysis. *Sensors* **2023**, *23* (1), 394. https://doi.org/10.3390/s23010394.

(183) Lopez-Ruiz, N.; Curto, V. F.; Erenas, M. M.; Benito-Lopez, F.; Diamond, D.; Palma, A. J.; Capitan-Vallvey, L. F. Smartphone-Based Simultaneous PH and Nitrite Colorimetric Determination for Paper Microfluidic Devices. *Anal. Chem.* **2014**, *86* (19), 9554–9562. https://doi.org/10.1021/ac5019205.

(184) Zeng, R.; Qiu, M.; Wan, Q.; Huang, Z.; Liu, X.; Tang, D.; Knopp, D. Smartphone-Based Electrochemical Immunoassay for Point-of-Care Detection of SARS-CoV-2 Nucleocapsid Protein. *Anal. Chem.* **2022**, *94* (43), 15155–15161. https://doi.org/10.1021/acs.analchem.2c03606.

(185) Su, J.; Chen, S.; Dou, Y.; Zhao, Z.; Jia, X.; Ding, X.; Song, S. Smartphone-Based Electrochemical Biosensors for Directly Detecting Serum-Derived Exosomes and Monitoring Their Secretion. *Anal. Chem.* **2022**, *94* (7), 3235–3244. https://doi.org/10.1021/acs.analchem.1c04910.

(186) Ma, T.; Ren, S.; Wang, Y.; Yu, H.; Li, L.; Li, X.; Zhang, L.; Yu, J.; Zhang, Y. Paper-Based Bipolar Electrode Electrochemiluminescence Sensors for Point-of-Care Testing. *Biosens. Bioelectron.* **2023**, *235*, 115384. https://doi.org/10.1016/j.bios.2023.115384.

(187) Antiochia, R. Paper-Based Biosensors: Frontiers in Point-of-Care Detection of Covid-19 Disease. *Biosensors* **2021**, *11* (4), 110. https://doi.org/10.3390/bios11040110.

(188) Mittal, A.; Roy, I.; Gandhi, S. Magnetic Nanoparticles: An Overview for Biomedical Applications. *Magnetochemistry* **2022**, *8* (9), 107. https://doi.org/10.3390/magnetochemistry8090107.

(189) Pohanka, M. Biosensors and Bioanalytical Devices Based on Magnetic Particles: A Review. *Curr. Med. Chem.* **2020**, *28* (14), 2828–2841. https://doi.org/10.2174/0929867327666200730213721.

(190) Kralj, S.; Drofenik, M.; Makovec, D. Controlled Surface Functionalization of Silica-Coated Magnetic Nanoparticles with Terminal Amino and Carboxyl Groups. *J. Nanoparticle Res.* **2011**, *13* (7), 2829–2841. https://doi.org/10.1007/s11051-010-

0171-4.

(191) Mohammed, L.; Gomaa, H. G.; Ragab, D.; Zhu, J. Magnetic Nanoparticles for Environmental and Biomedical Applications: A Review. *Particuology* **2017**, *30*, 1–14. https://doi.org/10.1016/j.partic.2016.06.001.

(192) Abedini-nassab, R.; Pouryosef Miandoab, M.; Şaşmaz, M. Microfluidic Synthesis, Control, and Sensing of Magnetic Nanoparticles: A Review. *Micromachines* **2021**, *12* (7), 768. https://doi.org/10.3390/mi12070768.

(193) Liébana, S.; Brandão, D.; Cortés, P.; Campoy, S.; Alegret, S.; Pividori, M. I. Electrochemical Genosensing of Salmonella, Listeria and Escherichia Coli on Silica Magnetic Particles. *Anal. Chim. Acta* **2016**, *904*, 1–9. https://doi.org/10.1016/j.aca.2015.09.044.

(194) Zacco, E.; Pividori, M. I.; Alegret, S.; Galve, R.; Marco, M. P. Electrochemical Magnetoimmunosensing Strategy for the Detection of Pesticides Residues. *Anal. Chem.* **2006**, *78* (6), 1780–1788. https://doi.org/10.1021/ac0512610.

(195) Moura, S. L.; Martín, C. G.; Martí, M.; Pividori, M. I. Multiplex Detection and Characterization of Breast Cancer Exosomes by Magneto-Actuated Immunoassay. *Talanta* **2020**, *211*, 120657. https://doi.org/10.1016/j.talanta.2019.120657.

(196) Mesas Gómez, M.; Molina-Moya, B.; de Araújo, B. C.; Pallarès-Rusiñol, A.; Ferrer-Dalmau, J.; Boldrín Zanoni, M. V.; Domínguez, J.; Julian, E.; Pividori, M. I. Mycobacterium Detection Method Combining Filtration, Immunomagnetic Separation, and Electrochemical Readout in a Portable Biosensing Device. *Sensors Actuators B Chem.* **2024**, *403*, 135211. https://doi.org/10.1016/j.snb.2023.135211.

Chapter 2.

Objectives

2. Objectives

The development of *in vitro* diagnostic tests for health care is crucial to bring testing closer to point-of-care facilities. While high-throughput strategies exist commercially, their implementation in low and middle-income primary healthcare centers is hindered by their high cost and complexity. Hence, the exploration of alternative approaches and the investigation of novel biomarkers, alongside the utilization of less invasive samples such as liquid biopsies, are significant areas of focus. This dissertation is dedicated to designing and developing diagnostic approaches for the detection of biomarkers in healthcare samples. The general objectives of this dissertation are outlined as follows:

- To explore biomarkers of different natures for diagnosing both communicable and non-communicable diseases, aiming to identify markers that can reliably indicate disease presence, progression, or treatment response.
- To design innovative diagnostic approaches for detecting and quantifying biomarkers, focusing on developing reliable, accurate, and efficient methods for disease diagnosis and monitoring.
- To integrate magnetic particles into diagnostic methodologies for simplifying instrumentation requirements and mitigate sample matrix effects, enhancing the robustness and reliability of diagnostic assays.
- To develop streamlined approaches for reducing the complexity of diagnostic assays, making them more accessible and user-friendly for healthcare personnel with varying levels of expertise. This includes designing protocols that require minimal sample processing and technical skill, facilitating broader adoption in diverse healthcare settings.
- To contribute to reducing healthcare disparities by developing affordable, scalable, and adaptable diagnostic approaches to different healthcare settings. By focusing on simplicity, accessibility, and cost-effectiveness, aim to ensure that all individuals, regardless of socioeconomic status or geographical location, have access to high-quality diagnostic testing.
- To enhance patient outcomes by developing diagnostic approaches that facilitate early detection, accurate diagnosis, and timely intervention for a range of healthcare conditions. By providing healthcare providers with rapid and reliable

diagnostic tools, aim to improve patient management, treatment decisions, and overall healthcare outcomes.

Chapter 3 addresses the development of competitive magneto enzyme-linked assay for the quantification of specific miRNAs in exosomes, being the specific objectives the following:

- To design and assemble a competitive magneto enzyme-linked miRNA (ELmiRNA) assay scaffold.
- To assess the sensitivity and the limit of detection of the proposed methodology using synthetic ODN counterpart.
- To assess the specificity of the ELmiRNA assay using a synthetic miRNA complex matrix sample.
- To evaluate the analytical performance of the competitive ELmiRNA assay using miRNAs isolated from breast cancer cell lines (MCF-7 and MDA-MB-231) and their derived exosomes.
- To validate the results performing a qPCR as the gold standard method.

Chapter 4 develops the design of a lateral flow assay (LFA) for the determination of the cellular immune response in whole blood samples, using the SARS-CoV-2 as a model of viral infection, being the specific objectives the following:

- To synthetise avidin carbon nanoparticles for their incorporation in LFA as a readout alternative.
- To reduce the sample incubation time using the mRNA instead of the released proteins.
- To detect the IFNγ transcripts through LFA, using gold nanoparticles and carbon nanoparticles.
- To compare the IFNγ expression between infected and non-infected individuals, both vaccinated.
- To determine the time window after the infection the assay can be performed.
- To assess which miRNA sequence can be used as intern control for exosomes qPCR expression normalization.

Chapter 5 is focused on the development of a magneto-actuated enzyme-linked immunosorbent assay for the early diagnosis of Alzheimer's disease, using the exosomes of a neuroblastoma cell line (SH-SY5Y) as a model, being the specific objectives the following:

- To find an *in vitro* model that allows a stable and homogeneous source of neuronal-like exosomes resembling Alzheimer's Disease individuals.
- To isolate and characterize exosomes and finding proteins that allow a selective capture of neural-derived exosomes.
- To compare the expression of key exosome proteins (general and neuron specific) between the cell lines and their derived exosomes.
- To study different combinations of biomarkers in order to achieve a selective capture of neuroblastoma-derived exosomes.
- To develop a novel magneto actuated enzyme-linked immunosorbent assay (magneto-ELISA) for the capture and detection of NDEs using specific neuronal and AD-related biomarkers for their capture and detection.
- To isolate and characterize exosomes from human liquid biopsies as cerebrospinal fluid and plasma

Chapter 3.

Competitive magneto enzyme-linked miRNA assay for quantification of microRNAs in exosomes

3.1. Abstract

MicroRNAs are short sequences lacking coding function and involved in gene expression regulation. miRNAs are under intensive study as novel and promising diagnostic and prognostic biomarkers, given their presence in many biological fluids. They are shielded from RNase activity through association with proteins or encapsulated within exosomes. Current methods for miRNA detection, from sample preparation to data interpretation, are technically complex and resource-intensive, requiring long and multiple incubation steps. To address these challenges, this chapter proposes a competitive magneto enzyme-linked miRNA (ELmiRNA) assay for the detection and quantification of miRNAs in exosomes. To achieve this, a scaffold was designed on magnetic particles by hybridizing biotin/fluorescein and biotin/digoxigenin-tagged miRNA synthetic DNA probes. Further incubation with the sample containing miRNA results in the displacement of the tagged probes, allowing the subsequent detection of the non-displaced probes remaining attached to the magnetic particles. As a proof of concept, the scaffold was designed for measuring the presence of miRNA21 and miRNA27a, previously associated with breast cancer upregulation, in exosomes-derived from cell cancer lines MCF-7 and MDA-MB-231. Results demonstrated the capacity of the miRNA-magneto assay to quantify miRNAs in exosomes. ELmiRNA assay provides a sensitive approach using affordable instrumentation readily available in low-resource settings laboratories and requiring minimal maintenance by a microplate reader equipped with filters. This method exhibits promising features in improving the analytical simplification for miRNA analysis as an alternative diagnostic tool to RT-qPCR.

3.2. Introduction

MicroRNAs are short sequences 19 to 24 nucleotides in length, lacking coding function[1]. Dysregulated values of miRNAs are associated with communicable[2] and non-communicable[3,4] diseases. Importantly, they can be found in almost all biological fluids, including plasma, serum, urine, tears, and saliva, among others[5,6]. In biologic fluids, RNase activity against circulating miRNA is prevented by their release in association with proteins or within the exosomes[7]. Exosomes are bilipid extracellular vesicles ranging between 30 and 200 nm, secreted to the extracellular space by almost every cell type via the

multivesicular body secreting pathway. Their interest as biomarkers is growing due to their molecular signature, directly related to their origin cells. Among them, miRNAs in exosomes have gained attention, with around 50% of the total non-coding RNA cargo in exosomes being miRNAs[8]. These features make them as potential diagnostic biomarkers for different conditions including cancer[9], neurodegenerative diseases[10], sepsis or SIRS (systemic inflammatory response syndrome)[11]. Several miRNA detection methods are currently under development. However, none of them has been universally accepted as a gold standard for miRNA detection in exosomes, primarily due to the challenge of achieving reliable absolute quantification. Advances in detection technologies, such as quantitative PCR (RT-qPCR), miRNA microarrays, *in situ* hybridization analysis, high sensitive northern blot analysis, and next-generation sequencing technology (NGS), show promise in improving miRNA detection[12]. However, challenges remain, especially for low-abundance or highly redundant miRNAs.

Among these methods, qPCR is commonly used, relying on a retro transcription first step followed by qPCR fluorescence detection. Preamplification steps are often used to extend short sequences, which can then be incorporated into conventional PCR amplification using standard primers. However, there is no universally accepted standard for quantification, and results are typically presented as normalized relative values using reference designed antisense ODN (oligodeoxynucleotides) miRNAs. This practice assumes that the expression of these reference miRNAs remains relatively constant under the experimental conditions. Although qPCR have an excellent analytical performance, it is not suitable for rutinary clinical applications fundamentally due to their high cost, complex operation, and the need of highly trained personnel. In contrast, enzyme-linked immunosorbent assays (ELISA) are routinely implemented in low complexity clinical laboratories worldwide[13,14]. This high throughput screening assay can process many samples simultaneously because it is performed in microplates. This is very useful for large-scale testing and screening. In addition, magnetic particles (MPs) have been integrated into immunoassays to improve target separation, preconcentration, or removal for various applications[15]. The most striking feature is the preconcentration of the target upon specific reaction and further magnetic actuation, even in complex samples[9]. They also allow target separation from other sample components in complex matrices such as

biological fluids, compared to conventional immunoassays. Moreover, the use of MPs provides wider active areas, while mixing efficiently with the sample.

This chapter describes ELmiRNA (competitive magneto enzyme-linked miRNA) assay, a high-throughput, simple and rapid method for quantifying miRNA in exosomes. The assay is demonstrated for miRNA21 and miRNA27a, which dysregulation has been reported in breast cancer derived exosomes[16–18]. Their functions have been related with angiogenesis induction[19] and cell cycle regulation[17]. The competition is performed on a designed scaffold and the quantification, based on double-tagged probes[20–22]. This method offers a highly suitable alternative diagnostic tool to RT-qPCR, providing sensitivity while using readily available instrumentation in low-resource laboratories and requiring minimal maintenance, such as a microplate reader equipped with filters.

3.3. Experimental

3.3.1. Instrumentation

Optical measurements were performed on the spectrophotometer (Infinite F50) from Tecan (Männedorf, CH) microplate reader with Magellan v7.0 software. The exosome ultracentrifugation was performed using the ultracentrifuge Beckman Coulter OptimaTM L-80XP. Exosomes were then characterized by nano tracking particle analysis (NTA) using the NanoSight LM10-HS system (NanoSight Ltd., Malvern, GB) and the cryogenic transmission electron microscopy (CryoTEM) images were obtained using a Jeol JEM 2011 with a 200 kV accelerating voltage (JEOL USA Inc., MA, USA). qPCR was performed with the C1000 touch Thermal Cycler (Bio-Rad, CA, USA). All further instrumentation is detailed described in §3.6.1 supplementary data.

3.3.2. Chemicals and biochemicals

All chemicals and biochemical are described in § 3.6.1 supplementary data including buffers and solutions. For scaffold assembling, magnetic particles oligo(dT)-MPs (Dynabeads™ Oligo(dT)25, Ref. 61002) were purchased from ThermoFisher Scientific. The synthetic miRNAs, the scaffold and the probes were purchased in Merck (Darmstadt, DE), and the sequences are described in Table 1.

Table 3.1. Sequences used for the scaffold assembly on oligo(dT)$_{25}$ magnetic particles, as shown in Fig. 3.1.

Name	Sequence (5'- 3')	Oligo	Tm (°C)
double-tagged miRNA27a probe	BIO-TTCACAGTGGCT-6FAM	5' biotin 3' 6FAM	29
double-tagged miRNA21 probe	BIO-TAGCTTATCAGAC-DIG	5' biotin 3' digoxigenin	29
miRNA27a (synthetic ODN counterpart)	TTCACAGTGGCTAAGTTCCGC	none	66.3
miRNA21 (synthetic ODN counterpart)	TAGCTTATCAGACTGATGTTGA	none	56.7
miRNAlet7a (synthetic non-specific ODN counterpart)	TGAGGTAGTAGGTTGTATAGTT	none	51.4
miRNA320a (synthetic non-specific ODN counterpart)	AAAAGCTGGGTTGAGAGGGCGA	none	71.8
ODN backbone miRNA 21/27a	$(A)_{15}(N)_5$TCAACATCAGTCTGATAAGCTA$(N)_{10}$GC GGAACTTAGCCACTGTGAA	none	82.7

3.3.4. Exosome isolation and *characterization by nanoparticle tracking analysis and transmission electronic microscopy*

Cell lines MDA-MB-231 (breast adenocarcinoma, ATCC, ref. HTB-26) and MCF-7 (breast adenocarcinoma, ATCC, ref. HTB-22) were cultured in Dulbecco's Modified Eagle Medium (DMEM) medium supplemented with a 10% of decomplemented exosome-free fetal bovine serum (FBS) and with a 100 U mL^{-1} of penicillin-streptomycin. The exosomes were purified by differential ultracentrifugation from cell line cultured supernatant[23], as detailed described in § 3.6.1 (Supp. data). For further characterization of purified exosomes, nanoparticle tracking analysis (NTA) was performed by triplicate to obtain a size distribution histogram and the exosomes concentration. Cryogenic transmission electronic microscopy (Cryo-TEM) was performed for the characterization of the exosome morphology. More detailed information is available in § 3.6.1 (Supp. data).

3.3.5. Scaffold assembly on Oligo(dT) magnetic particles

Before conducting the competitive magneto enzyme-linked miRNA (ELmiRNA) assay, scaffold assembly was prepared, as illustrated in Figure 3.1, Panel A and detailed described

in § 3.6.2 and Fig. 3.6 therein (Supp. data). The optimization of all the concentration, as well as the amount per assay is also shown in Fig. 3.7 and 3.8 (Supp. data).

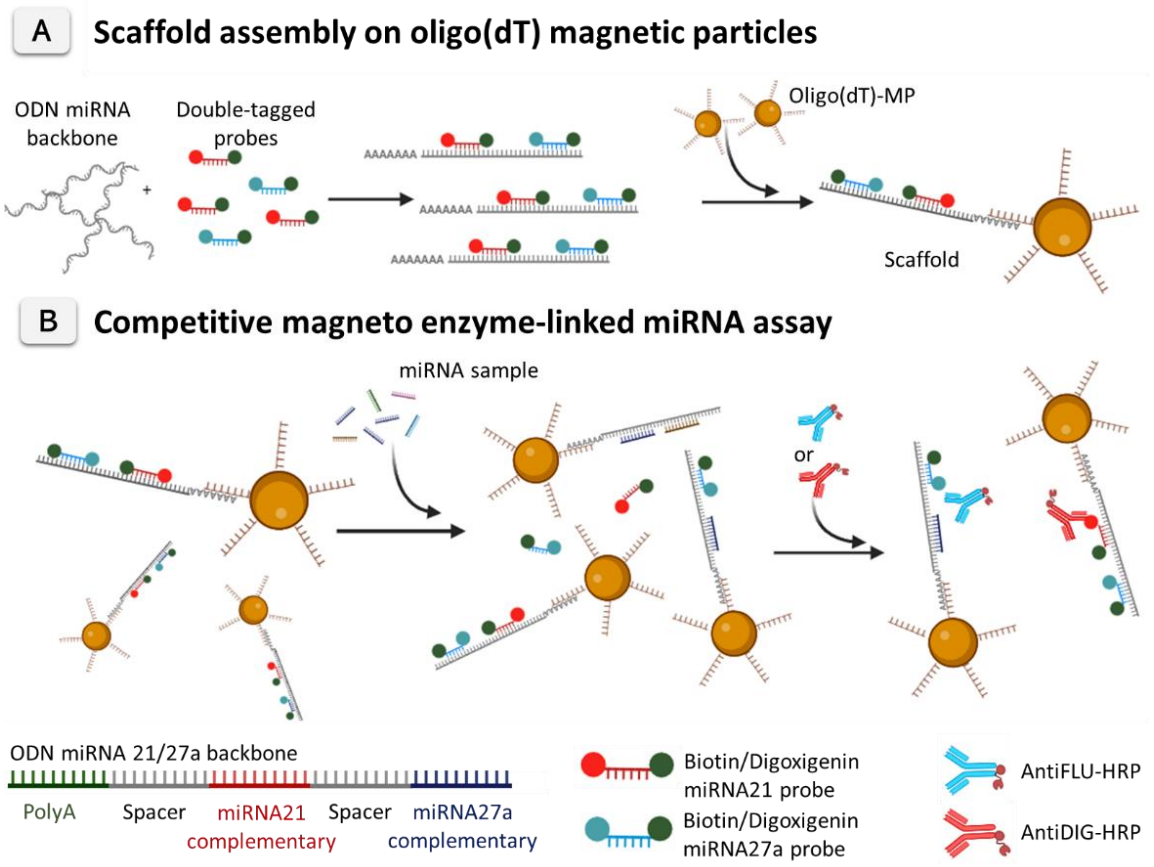


Figure 3.1. Schematic representation of the Scaffold assembly on oligo(dT)-MPs (Panel A) and the competitive magneto enzyme-linked miRNA (ELmiRNA) assay for the detection of miRNA27a and miRNA21 (Panel B). Created with biorender.com.

3.3.6. Competitive magneto enzyme-linked miRNA assay

The ELmiRNA assay procedure is outlined in Figure 3.1, Panel B, and involves the following steps: i) incubation of the sample containing miRNA and the backbone assembled on oligo(dT)-MPs to achieve the displacement of the tagged-probes; ii) enzymatic labelling of the remaining tagged probed on the scaffold with antiDIG-HRP or antiFLU-HRP, coding for miRNA21 and miRNA27a, respectively; iii) optical readout.

Briefly, the sample containing miRNA (for instance, from the lysed exosomes) was previously treated for 5 min at 75 °C. Then, 15 mg of the oligo(dT)-MP with the backbone assembled was added, and the incubation was performed in polypropylene 96-well plate in a final volume of 100 mL. The microplate was then placed into a thermomixer and

heated for 5 minutes at 37° and cooled down for 30 min until it reached 10°C, followed by washing steps with washing buffer (3X). The remaining tagged probes on the scaffold coding for miRNA21 and miRNA27a were identified by incubation with antiDIG-HRP (10 mU mL^{-1}) or antiFLU-HRP (7.14 mU mL^{-1}) antibodies, respectively, for 30 min at 10°C in a shaker at 750 rpm. Finally, the optical readout was performed with the TMB substrate kit as recommended by the manufacturer. After 30 min of reaction, a volume of stop solution was added. Finally, the absorbance measurement of the supernatants was thus performed with the microplate reader using a 450 nm filter. After each incubation or washing step, a 96-well magnet plate separator was positioned under the microtiter plate until pellet formation on the bottom corner, followed by supernatant separation.

3.3.7. Specificity study

Specificity study was performed by challenging the approach to a high concentration of interferences. Therefore, the ELmiRNA assay was carried out with a matrix of other miRNAs. Beside the negative control, the positive sample containing the specific sequences, as well as the interferences containing only the non-specific sequences, and a mix containing the specific and non-specific sequences (at a total 100-fold higher concentration compared to the specific sequence), were processed. Specific miRNAs were tested at 25 pmol (250 nM), and were mixed with non-specific sequences, including miRNAlet7a and miRNA320a synthetic ODN counterpart, at a total 100-fold higher concentration compared to the specific corresponding to 2.5 nmol (25 µM).

3.3.8. Quantification of miRNA1 and miRNA27a in breast cancer cell lines and derived exosomes

For the determination of miRNA in cells, the extraction was performed in 5 x 10^6 cell pellets with commercial miRNA isolation kit, following the instructions provided by the manufacturer with slight modification, as described in § 3.6.3 (Supp. data). Briefly, after the cell lysis with a denaturing lysis buffer, the sample was extracted with acid-phenol:chlorophorm (125:24:1, with isoamyl alcohol) followed by purification on a glass-fiber filter, providing a sample enriched in miRNAs with low quantity of RNAs larger than 200 bases. For the exosomes, the extraction was performed in 10^{11} exosomes with the Total Exosome RNA and Protein Isolation Kit as described in § 3.6.3 (Supp. data). For either

cell or exosomes-derived miRNA, the quantification of total miRNA was performed by Qubit 4 using the microRNA assay kit, as described in § 3.6.3 (Supp. data).

3.3.9. qPCR

qPCR was used as the gold standard method for the validation of the results obtained with the ELmiRNA assay. The normalization of the expression of the miRNAs was performed using the miRNA-let7a, which was previously selected among other candidates as described in § 3.6.5 Supp. data. For the qPCR performance a previous reverse transcription was carried out using the TaqMan™ Advanced miRNA cDNA Synthesis Kit and further the TaqMan® Fast Advanced Master Mix for the qPCR, both protocols performed as described § 3.6.5 (Supp. data).

3.3.10. Statistical Analysis

The statistical analyses and calculations were performed using Prism v 10.0.1 (GraphPad, San Diego, USA). The calibration curves were adjusted to a non-linear regression fitting, using the four-parameter logistic curve, abbreviated 4PL. The limit of detection was calculated considering the number of negative controls for each curve, using the one-tailed test with a significance level of $p > 0.05$ (*t*-student, $p > 0.05$). Two-way ANOVA was performed to determine statistical differences between the different conditions in specificity study with a significance level of $p > 0.05$.

3.3.11. Safety Considerations

All works were performed in a Biosafety cabinet, and all material was decontaminated by autoclaving or disinfected before discarding following U.S. Department of Health and Human Services guidelines for level 2 laboratory Biosafety.

3.4. Results and discussion

3.4.1. Exosome isolation and characterization by nanoparticle tracking analysis and cryogenic transmission electronic microscopy

Exosomes were first isolated and characterized through nanoparticle tracking analysis (NTA) and cryogenic transmission electronic microscopy (Cryo-TEM). The diameter size distribution of breast cancer-derived nanovesicles from MCF-7 and MDA-MB-231 cell lines is shown in Figure 3.2, Panels A and B, respectively. The highest peaks are enriched with

exosomes and correspond to 136 and 125 nm in diameter, respectively). The particle concentration after preconcentration by ultracentrifugation in the sample was determined by NTA, being approximately 8.09 x 10^{10} (SD 1.93 x 10^{10}) particles/mL and 1.14 x 10^{11} (SD 2.72 x 10^{9}) particles/mL, respectively, for exosomes derived from MCF-7 and MDA-MB-231 cell lines. Further information of size diameter distribution was obtained by Cryo-TEM. Micrographs of the exosome sample show well-shape exosome vesicles with closed circular lipid bilayers (Fig. 3.2, Panel C). Cryo-TEM micrographs also reveal the presence of some exosome aggregates (Fig. 3.2, Panel D). Results obtained with the NTA and the micrographs obtained with Cryo-TEM showed concordant results.

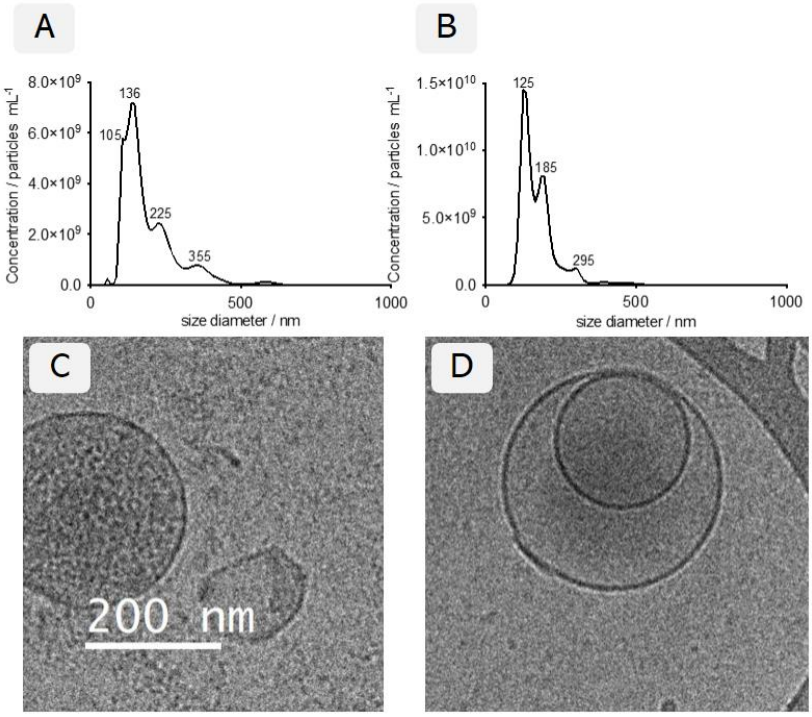


Figure 3.2. Characterization by NTA of purified exosomes derived from the MCF-7 breast cancer cell line (Panel A) and MDA-MB-231 (Panel B). Panels C and D show the cryo-TEM images of purified exosomes at an acceleration voltage of 200 kV.

3.4.2. Competitive magneto enzyme-linked miRNA assay. Specificity study

First, the reagents involved in the assembly of the scaffold were set up, and the reagent concentration optimized, as outlined in Figures 3.7 and 3.8 (Supp. data). In summary, the reagent amount per assay was set up at 0.5 pmol of the ODN backbone miRNA 21/27a, 1 pmol of each of the double-tagged probes, and 15 μg of the oligo(dT)-MP.

In order to stablish the LOD for the assay, a calibration plot was performed, as shown in Figure 3.3 (Panel A) with miRNA27a and miRNA21 synthetic ODN counterpart, due to the difficulties inherent to the synthesis and stability of these short RNA sequences[24,25]. Figure 3.3, Panel A shows the calibration plot from 0 to 2500 nM for the detection of miRNA21 and miRNA27a with the ELmiRNA assay. The data was fitted with a non-linear regression (Sigmoidal 4PL, GraphPad Prism Software v 10.0.1, R^2= 0,9861 and 0,9938) and the limits of detection (LODs) were calculated, resulting in a value of 1.5 nM or 9.6 pg μL^{-1} (corresponding to an amount per assay of 0.15 pmol) and 2.7 nM or 16.2 pg μL^{-1} (0.266 pmol) for miRNA21 and miRNA27a, respectively, by processing 100 mL of sample. In all cases, the LODs were calculated after normalization of the raw data as 10% inhibitory concentration (IC10). As shown in Figure 3.3, Panel A, data show an inversely correlation between the concentration of the synthetic miRNAs ODN counterpart and the absorbance values, demonstrating the displacement of the tagged probes from the scaffold and good performance of the ELmiRNA assay designed in this work.

The concentration of miRNA in different samples can vary widely depending on the source, tissue, or biological sample being analyzed. Moreover, different miRNA species vary widely in concentration over a dynamic range in biological fluids[26]. For instance, some studies had estimated that their concentrations could vary between 10^5 – 10^8 copies mL^{-1} (corresponding to the range between pg to ng mL^{-1})[27]. The LODs reached in this work (around 9 and 16 pg μL^{-1} for miRNA21 and miRNA27a respectively) are thus included in this range.

Although miRNA detection methods has evolved significantly, offering a range of techniques with varying levels of sensitivity, specificity, throughput, and complexity, the methods still rely on high complexity and benchtop equipment such as RT-qPCR amplification and fluorescent readout[28,29]. However, no amplification step or fluorescence readout are used in this approach. Accordingly, the use of an optical readout without any DNA amplification simplifies the analytical procedure.

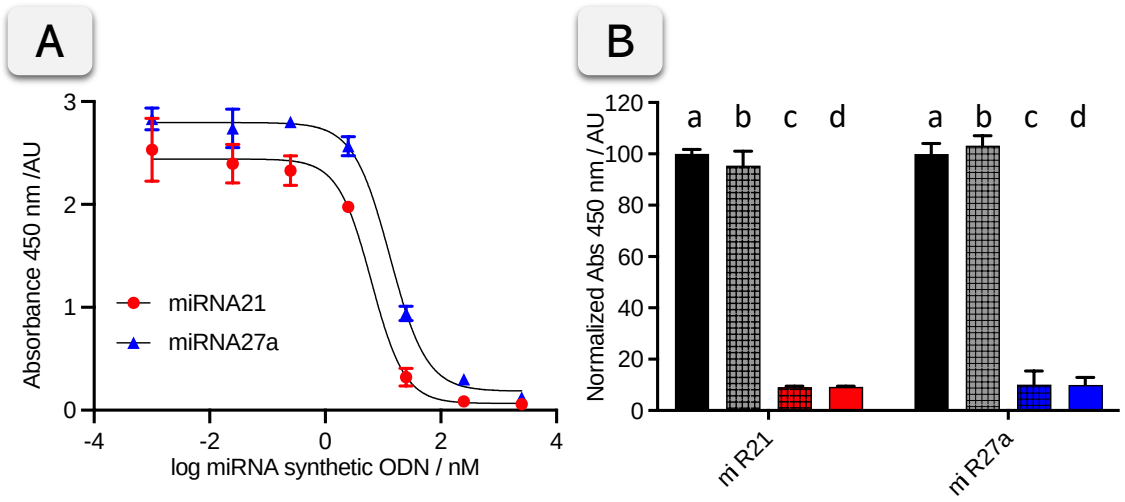


Figure 3.3. Panel A. Calibration plot for miRNA21 (red) and miRNA27a (blue) from 0 to 2500 nM, with the ELmiRNA assay approach (R^2= 0.9861 and 0.9938, respectively). Panel B. Specificity study including (a) negative control; (b) only non-specific microRNA); (c) non-specific microRNA and specific miRNA21 or miRNA27a; (d) only specific miRNA21 or miRNA27a ODN counterpart. In all cases, specific sequence (miRNA21 or miRNA27a) was added at 250 nM, while non-specific microRNA sequences (miRNAlet7a and miRNA320a) were added at a 100-fold excess at 25 mM. In all cases, the enzymatic labelling was performed with antiDIG-HRP (10 mU mL^{-1}) and coding for miRNA21, and antiFLU-HRP (7.14 mU mL^{-1}), coding for miRNA27a. Further experimental details can be found in the text. The error bars show the standard deviation for n=3.

The specificity of the ELmiRNA assay towards a high concentration of non-complementary microRNA sequences was also studied, and the results are shown in Figure 3.3, Panel B. The signal of the negative control containing no microRNA was found to be comparable with non-specific miRNA samples at a high concentration of 25 mM ($p < 0.05$) according to a One-way ANOVA test. Furthermore, the obtained signals when miRNA21 or miRNA27a was mixed with non-specific miRNAs (miRNAlet7a and miRNA320a) were also comparable ($p < 0.05$) to those obtained only with the specific miRNA21 or miRNA27a, showing a good specificity for the assay. The ELmiRNA assay was specifically designed for the detection of miRNA21 and miRNA27a by utilizing a specific ODN backbone miRNA21 and miRNA27a for the assembly of the scaffold, which contains the complementary sequences for both miRNA21 and miRNA27a. As expected, other microRNAs were not interfering in the ELmiRNA assay.

3.4.3. Quantification of miRNA21 and miRNA27a in breast cancer cells and their derived exosomes

After the optimization of the reagent amounts for both miRNAs, the ELmiRNA assays were performed, to measure miRNA extracted from MCF-7 and MDA-MB-231 cell lines, as well as in their derived-exosomes. To achieve that, total miRNA extracted from 5 million MCF-7 and MDA-MB-231 cells, and 10^{11} exosomes derived from MCF-7 and MDA-MB-231 cells was quantified with Qubit test, being 66 µg mL^{-1} and 63 µg mL^{-1} for the MCF-7 and MDA-MB-231 cells and 3.54 µg mL^{-1} and 0.235 µg mL^{-1} from their derived exosomes, respectively. The ELmiRNA assay was thus performed, and the absorbance values were interpolated in then calibration plot. After interpolation, the amount of miRNA in MCF-7 cells was determined to be 15.79 pg μL^{-1} miRNA21 and 16.38 pg μL^{-1} miRNA27a, corresponding to 27,821 and 32,440 copies per cell, respectively. In the case of MDA-MB-231 cells, the interpolation with the calibration plot provides a concentration of 11.44 pg μL^{-1} for miRNA21 and 27.37 pg μL^{-1} for miRNA27a, corresponding to 21,077 and 54,920 copies per cell (Fig. 3.4, Panel A), respectively. These values are in line with other previous reports which describe a wide dynamic range of concentrations of miRNAs from around 500 copies per cell to more than 10.000 copies per cell[30]. To validate the results obtained with the ELmiRNA assay, the samples were tested using qPCR, considered the gold standard method. A miRNA endogenous control was employed for normalization, as selected in Figure 3.9 (Supp. data). While the ELmiRNA method allows expressing the absolute number of copies per entity (either cell or exosome), qPCR allows expressing relative values compared to the miRNA endogenous control. However, as depicted in Figure 3.4, the results obtained with the ELmiRNA assay align with the relative expression determined by qPCR (Fig. 3.4, Panel B). In summary, a correlation was observed between the measurements by the ELmiRNA assay and qPCR determination, indicating higher expression of miRNA21 in MCF-7 cells, whereas miRNA27a was more expressed in the MDA-MB-231 cell line.

In the case of the exosomes derived from MCF-7 cells, the interpolation on the calibration plot, provides 150.96 pg μL^{-1} miRNA21 and 97.62 pg μL^{-1} miRNA27a. Thus, for miRNA21, there are approximately 17 copies per exosome, and for miRNA27a, there are approximately 12 copies per MCF-7 derived exosomes. In the case of the exosomes

derived from MDA-MB-231 cells, the results provide 140.45 pg μL^{-1} miRNA21 and 178.16 pg μL^{-1} miRNA27a. So, for miRNA21, there are approximately 11 copies per exosome, and for miRNA27a, there are approximately 15 copies per MDA-MB-231 derived exosomes (Fig. 3.4, Panel B), in agreement to other reports[31]. As determined in the cells, the results obtained with the ELmiRNA assay correlates with the expression values obtained with the qPCR (Figure 3.4, dashed bars).

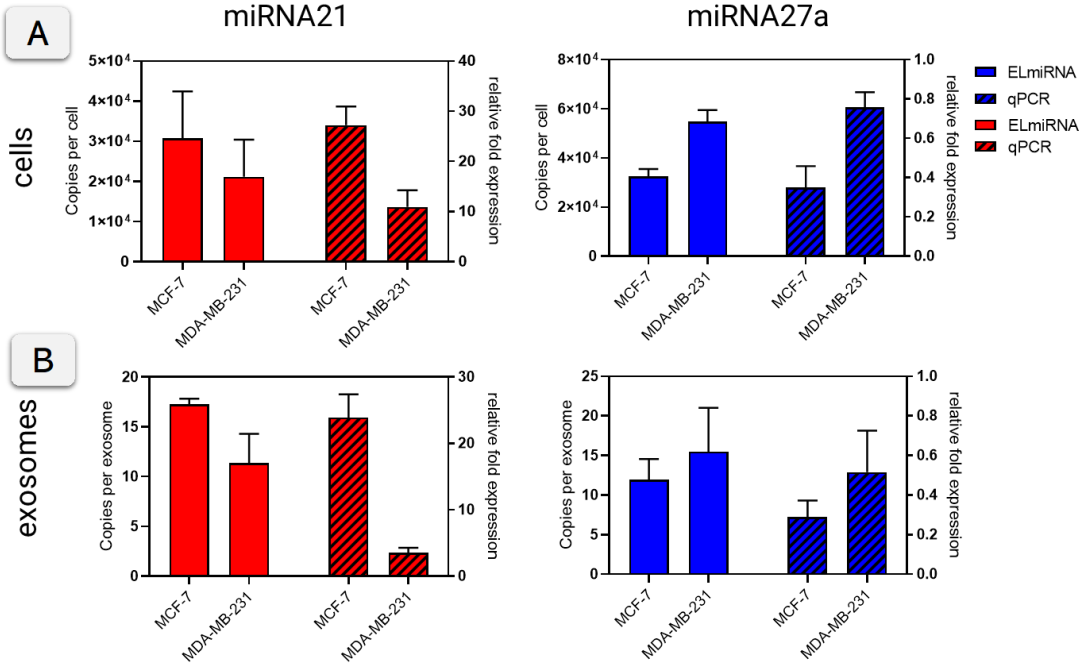


Figure 3.4. Bar plots showing comparatively results for the determination of miRNA 21 (red bars) and miRNA27a (blue bars) by ELmiRNA assay (open bars) and qPCR technique (dashed bars). Panel A shows the results for the MCF-7 and MDA-MB-231 cell, while Panel B shows the results for the derived exosomes.

These results demonstrate the suitability for detecting miRNAs in exosomes. The presence of both types of miRNAs was detected in the exosomes of both cell lines, as previously reported in the literature, which have been determined to be upregulated in breast cancer exosomes[24,32,33].

Given the communicative functionality of exosomes and the regulatory role of miRNAs, they are postulated to be responsible for decreasing apoptosis and accelerating proliferation in non-carcinogenic cells. Therefore, the capability to quantify the exosomes released by the carcinogenic cells opens the possibility of a time-course analysis to track cancer evolution and, consequently, its prognosis in liquid biopsies.

There is a lack of consensus on the concentration of miRNAs in body fluids due to the absence of standardization in RNA extraction and quantification methods, as well as variations in exosome concentration in different biological fluids. To ensure an adequate concentration of exosomes when performing the assay in biological fluids, the quantification procedure can be integrated to a sample procedure to preenrich exosomes[34].

The results align with previous studies indicating that certain miRNAs are enriched in exosomes, and showing a lower variability compared to their oncoming cells[35,36], since despite the initial total miRNA low concentration, the miRNAs were detected in significant concentrations. Specific miRNA-binding motifs have been identified as contributors to their selective loading into exosomes[37]. Similarly, proteins commonly associated with miRNAs are less represented than expected based on their cellular expression. However, the precise selective pathways through which miRNAs are loaded into exosomes remain unclear[37,38]. Consequently, predicting the concentration of specific miRNAs in exosomes solely based on their molecular signature in the parent cells remains a challenge.

3.5. Conclusions

Circulating miRNAs associated to exosomes have emerged as promising biomarkers for both diagnostic and monitoring purposes across various pathological conditions. Moreover, their presence in many biological fluids opens the possibility of a minimally invasive procedure for the sample collection. Unfortunately, the gold standard method for the quantification presents some drawbacks. Consequently, a novel approach to miRNA quantification has been developed to address some of these shortcomings by using less complex instrumentation and a more cost-effective procedure.

This is achieved through the development and optimization of the ELmiRNA assay, in which the displacement of DNA probes by competitive binding on a backbone bound to magnetic particles is demonstrated, showing good limits of detection and selectivity. Moreover, the method has been demonstrated to perform well in detecting miRNA21 and miRNA27a in exosomes.

The integration of magnetic particles in the scaffold reduces the matrix effect and enhanced analytical features regarding sensitivity and selectivity. The ELmiRNA assay is not affected by the presence of other miRNAs in the samples, allowing it to be used in complex miRNA samples. Despite other methods, the main advantage of ELmiRNA assay is that no amplification is required. Moreover, the competitive magneto enzyme-linked miRNA assay reported here represent a good alternative to the costly gold standard qPCR for the simultaneous detection of multiple samples by using a conventional microplate reader operated by filters. Since ELISA is a technique widely used in laboratories, special equipment or personnel training are not required. Moreover, due to the versatility of the scaffold generated, it permits the change of the sequence of the backbones and the probes for the detection of other miRNA sequences. Thus, being able to be easily adapted for other communicable and non-communicable diseases implying miRNAs dysregulation.

3.6. Supplementary data

3.6.1. Materials

Instrumentation

The scaffold assembly was carried out in the SimpliAmp thermal cycler (Product N° 2720, Applied Biosystems). Competitive magneto Enzyme-Linked miRNA Assay (ELmiRNA) was performed using an Eppendorf ThermoMixer C (Eppendorf AG, DE) for incubation, while the magnetic separation was performed with a magnetic separator DynaMag™-96 Side Skirted Magnet (ref. 12027, Thermo Fisher Scientific). Optical measurements were performed on the spectrophotometer (Infinite F50) purchased from Tecan (Männedorf, CH) microplate reader with Magellan v7.0 software. The exosome ultracentrifugation was performed using the ultracentrifuge Beckman Coulter OptimaTM L-80XP. Exosomes were then characterized by nanotracking particle analysis (NTA) using the NanoSight LM10-HS system (NanoSight Ltd., Malvern, GB) and the cryogenic transmission electron microscopy (CryoTEM) images were obtained using a Jeol JEM 2011 with a 200 kV accelerating voltage (JEOL USA Inc., MA, USA). qPCR was performed with the C1000 touch Thermal Cycler (Bio-rad, CA, USA). MiRNA quantification after the extraction was performed with the Qubit 4 Fluorometer (Thermo Fisher Scientific, WA, USA).

Chemicals and biochemicals

For cell culture the following reagents were purchased: Dulbecco's Modified Eagle Medium (DMEM, ref. 31966-047, Thermo Fisher Scientific) medium, fetal bovine serum (FBS, ref. 12007C, Sigma-Aldrich) and penicillin-streptomycin (ref. 15140122, Thermo Fisher Scientific). For miRNA extraction and quantification, the following commercial kits were used: mirVana miRNA isolation kit (ref. AM1561, Invitrogen, USA), Total Exosome RNA and Protein Isolation Kit (ref. 447845, Invitrogen), and miRNA quantification kit (Ref. Q32880, Invitrogen). For enzymatic labelling, antiDigoxigenin-HRP (andiDIG-HRP) and antiFluorescein-HRP (antiFLU-HRP), and streptavidin-HRP were purchased from Roche (Basel, Switzerland) while for the optical readout, Pierce™ TMB Substrate Kit (Ref. 34021) was purchased from Thermo Fisher. Polypropylene and polystyrene plates were purchased

from Costar and Nunc (Maxisorp, Roskilde, DK) respectively. The ELISA plates (Nunc MaxiSorp™ flat-bottom Ref. 44-2404-21) were purchased from Invitrogen. Taqman probes and reagents for the qPCR were purchased from Thermo Fisher Scientific, Taqman Advanced miRNA cDNA Synthesis kit (ref. A28007), TaqMan Fast Advanced Master Mix (ref. 4444557), and the probes, hsa-27a-3p (ref. 478384_mir), hsa-21-5p (ref. 477975_mir) and hsa-let-7a-5p (ref.478575_mir).

For scaffold assembling, magnetic particles oligo(dT)-MPs (Dynabeads™ Oligo(dT)25, Ref. 61002) were purchased from ThermoFisher Scientific. The synthetic miRNAs, the scaffold and the probes were purchased in Merck (Darmstadt, DE), and the sequences are described in Table 3.1.

Buffers and solutions

Bovine serum albumin (BSA, ref. A4503), sodium phosphate dibasic (ref. 71636), potassium phosphate dibasic (ref. 795496), sodium chloride (ref. S3014), potassium chloride (ref. P3911) and magnesium chloride (ref. M8266) were purchased in Sigma-Aldrich (Merck KGaA, DE). Sodium carbonate (ref. 131648) and sulfuric acid (ref. 131058) were purchased from Panreac (ES).

The composition of the solutions used for:

Scaffold assembly on Oligo(dT) magnetic particles

- PBS 1X buffer: 10 mmol L^{-1} Na_2HPO_4, 137 mmol L^{-1} NaCl, 2.7 mmol L^{-1} KCl, 1.8 mmol L^{-1} K_2HPO_4, pH 7.4.
- Washing buffer/ Oligo(dT) magnetic particles washing buffer: 0.5% w/v BSA in PBS 1X buffer.
- Storage buffer: 0.1% w/v BSA in PBS 1X buffer.

ELISA and ELmiRNA assay

- PBS 1X buffer: 10 mmol L^{-1} Na_2HPO_4, 137 mmol L^{-1} NaCl, 2.7 mmol L^{-1} KCl, 1.8 mmol L^{-1} K_2HPO_4, pH 7.4.
- Washing buffer: 0.5% w/v BSA in PBS 1X buffer.
- Carbonate/bicarbonate buffer: 100 mmol L^{-1} Na_2CO_3, pH 9.6.

- Blocking buffer: 3% w/v BSA in PBS 1X buffer.
- Stopping solution: Sulfuric acid 2 mol L^{-1} solution.

Cell culture

Cell lines MDA-MD-231 (breast adenocarcinoma, ATCC, ref. HTB-26), MCF-7 (breast adenocarcinoma, ATCC, ref. HTB-22) were cultured in Dulbecco's Modified Eagle Medium (DMEM) medium supplemented with a 10% of decomplemented exosome-free fetal bovine serum (FBS) and with a 100 U mL^{-1} of penicillin-streptomycin. Cells were maintained at controlled temperature (37°C) and CO_2 concentration (5%) with a humidified atmosphere.

Exosome isolation and characterization by nanoparticle tracking analysis and transmission electronic microscopy

The exosomes were purified by differential ultracentrifugation from cell line cultured supernatant[23]. Cells were trypsinitzed when the flask was at a 70-80% confluence. Several centrifugation steps were performed: first, the supernatant was centrifuged at 10,000 *g* for 30 min to remove cellular debris, then it was ultracentrifuged at 100,000 *g* during 60 min twice to pellet the exosomes. After ultracentrifugation, the pellet was resuspended 40-fold concentrated into PBS 1X buffer (pH 7.4, sterile 0.22 µm filtered). For the determination of the concentration and characterization, nanoparticle tracking analysis (NTA) was performed. The analysis was carried out with a tuned 405 nm laser at 24.8°C. NTA software analyzed raw data videos by triplicate during 60 s with 50 frames per sec. From the analyzed data, a histogram of the size distribution and the concentration of exosomes was obtained. The characterization of the morphology of the exosomes was used the cryogenic transmission electronic microscopy (Cryo-TEM) technique at a voltage of 200 kV. Samples were dropped upon a Formvar-Carbon EM grid and frozen with liquid nitrogen avoiding the water crystal formation. The sample was maintained at a -182°C temperature during the assay.

3.6.2. Scaffold assembly on Oligo(dT) magnetic particles

Before conducting the competitive magneto enzyme-linked miRNA (ELmiRNA) assay, scaffold assembly was prepared, as illustrated in Figure 3.1, Panel A. Initially, 5 pmols double-tagged miRNA-27a and/or miRNA-21 probes were hybridized on 2.5 pmol ODN miRNA 21/27a backbone. The hybridization involved a mixture of the ODN backbone and the tagged probes at a two-fold concentration ratio. This solution was heated at 95°C for 5 minutes, followed by a controlled gradual cooling to 20°C over 2 h. The mixture was then incubated with 75 µg oligo$(dT)_{25}$-MPs in a 100 µL final volume for 30 min at 20°C with gentle rotation, to achieve hybridization of the ODN backbone by its polyA end. Probes in excess were then removed by washing (2X). Afterwards, the scaffold was stored at 4°C until use as a reagent in the ELmiRNA assay. The optimization of all the concentration, as well as the use of 15 µg per assay of the oligo(dT) MP (thus containing 0.5 pmol of the ODN backbone miRNA 21/27a and 1 pmol of each of the double-tagged probes) is shown in the next section of 3.6.2 supplementary data.

Characterization of the reagents for the scaffold assembly

The tagged-probes including double-tagged miRNA27a and miRNA21 and the labelling antibodies were firstly set up using a conventional ELISA. Maxisorp microplates were coated overnight at 4°C either with antiDigoxigenin (ref. 11333089001, Roche) or antiFlurescein (ref. MAB045, Roche) antibodies, followed by washing (3X). The microplate was then incubated with blocking solution during 4 h at RT. After that, either double-tagged miRNA27a or miRNA21 were added to the plate at concentrations ranging from 0 to 0.16 nM and incubated for 2 h at RT. The enzymatic labelling was then performed incubating with streptavidin-HRP at 5 x 10^{-3} U mL^{-1} for 30 min at RT. Finally, the optical readout was performed using TMB substrate kit (Ref. 34021,- Thermo Fisher Scientific) following the supplier recommendations. Next, the absorbance measurement of the supernatants was thus performed with the microplate reader using a 450 nm filter, and the results are shown in Figure3.5.

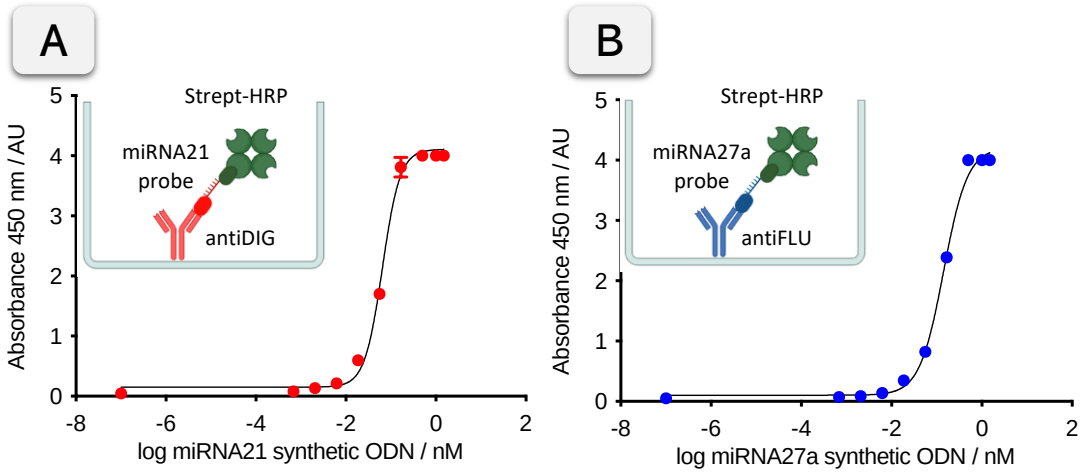


Figure 3.5. Characterization of the double-tagged microRNAs probes by conventional ELISA. Calibration plot of the double-tagged miRNA21 (Panel A) and miRNA27a (Panel B) are shown, at concentration ranging from 0 to 0.16 nM. The absorbance values were fitted using a nonlinear regression (four Parameter logistic curve), with a R^2 of 0.9969 and 0.9930 respectively. The concentration of capture antibodies, antiDIG and antiFLU respectively, was set to a final working concentration of 2 $mg{\cdot}mL^{-1}$ and Strep-HRP concentration was set to a 5 x 10^{-3} U mL^{-1}. The error bars show the standard deviation for n=3.

The displacement of the probes in the ELmiRNA is proportional to the concentration of the specific miRNA sequences. Depending on this concentration, the remaining probes will also vary allowing the antibody interaction. Thereby, varying the absorbance values as represented in Fig. 3.6.

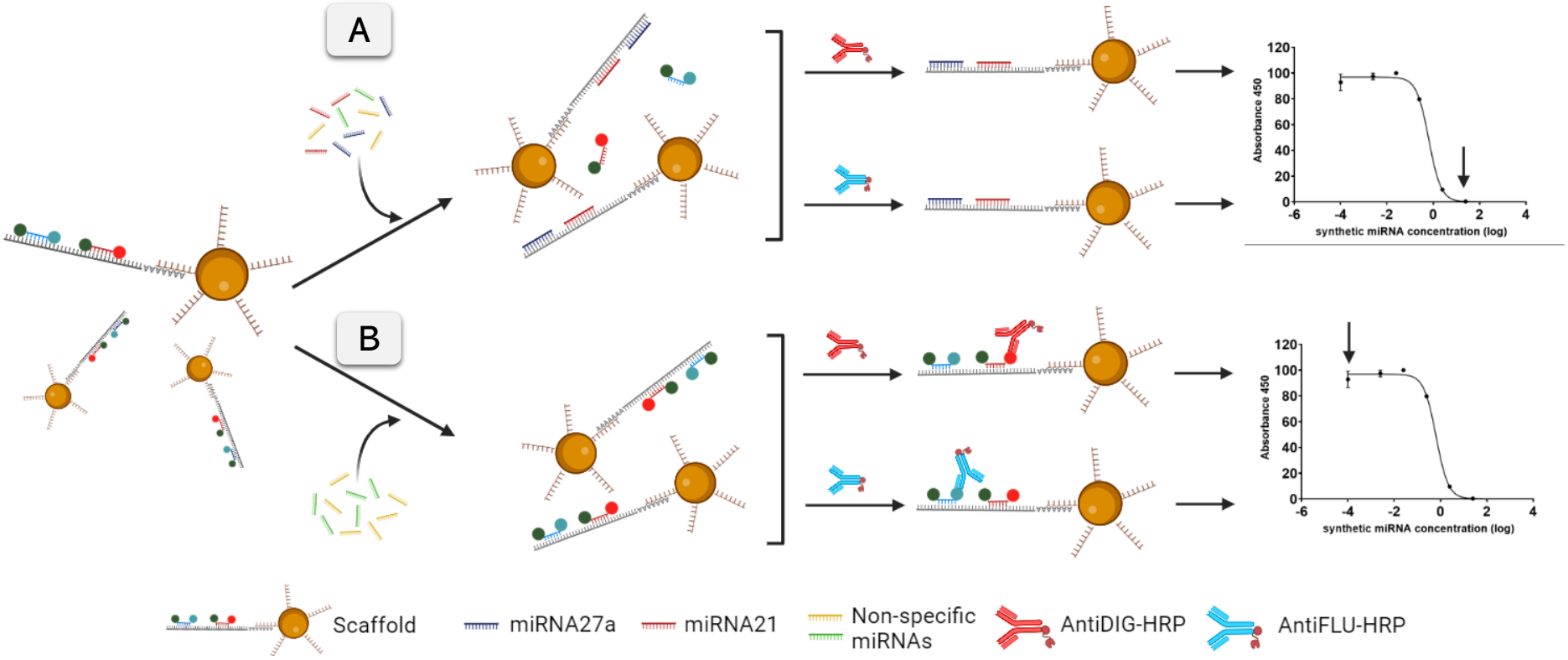


Figure 3.6. Schematic representation of different casuistic of the competitive magneto enzyme-linked miRNA (ELmiRNA) assay for the detection of miRNA27a and miRNA21. Panel A, competitive assay in presence of miRNA21 and/or miRNA27a. that would displace the probes Panel B, competitive assay without the presence of miRNA21 and/or miRNA27a, with the consequent non-displacement of the probes. Created with biorender.com.

Optimization of the reagents for the scaffold assembly: double-tagged probes and oligo(dT)-MPs

Prior to the competitive magneto enzyme-linked miRNA assay, different ratio concentrations for the scaffold assembly, including combinations of amounts of the double-tagged probes (5, 25 and 50 pmol) and oligo(dT)-MP (5, 25, and 75 µg) were tested while keeping a constant amount of ODN miRNA 21/27a backbone in 2.5 pmol. Also, two different concentrations of the enzymatic reporter strep-HRP (5×10^{-2} U mL^{-1} and 5×10^{-3} U mL^{-1}) were evaluated for each condition. The magneto enzyme-linked miR27a assay, without competition, was performed for each condition in a 100 µL reaction volume. Additionally, the negative control for each condition was also assessed.

The scaffolds prior assembled with the different conditions described before were deposited into the polypropylene 96-well plate. Positive controls were added to the corresponding wells and all the samples were brought up to 100 µL final volume. The microplate was then placed into a thermomixer and heated for 5 minutes at 37°C and slowly cooled down for 30 min until it reaches 10°C, followed by washing (3X). The remaining tagged probes on the scaffold were then incubated with streptavidin-HRP (ref. 11089153001, Roche) for 30 min. at 10°C and 750 rpm. Then, the microplate was three-times washed for 3 minutes in the thermomixer at 750 rpm with washing buffer. Finally, the optical readout was performed with the TMB substrate kit mixing 1:1 volume of TMB and H_2O_2 and 100 µL added to each well. After 30 min of reaction, a volume of stop solution was added. The microplate was placed into the magnet to allow the sample placement into a polystyrene plate for the subsequently measurement. Finally, the absorbance measurement of the supernatants was thus performed with the microplate reader using a 450 nm filter. After each incubation or washing step, a 96-well magnet plate separator was positioned under the microtiter plate until pellet formation on the bottom corner, followed by supernatant separation.

Bar plots in Fig. 3.7 show the absorbance values for each assessed condition using 5×10^{-3} U mL^{-1} (Panel A) and 5×10^{-2} U mL^{-1} (Panel B) of strept-HRP, respectively. These results state that, while the use of higher amounts of double-tagged probes has no significant effect since they are clearly in excess, the use of an increased amount of oligo(dT)-MPs

considerably improves the final readout. Consequently, 5 pmols of double-tagged probe (50 nM), 75 µg of oligo(dT)-MPs and 2.5 pmol ODN miRNA 21/27a backbone (25 nM) were selected for all further experiments. This condition is chosen because it offers the optimal balance between a higher signal and the minimal probe quantity, while keeping an enhanced background signal ratio.

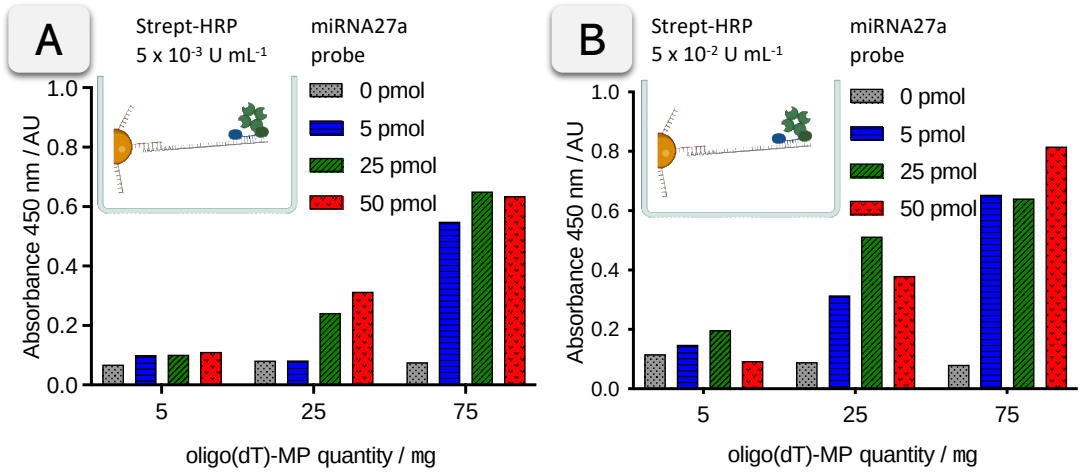


Figure 3.7. Magneto enzyme-linked miRNA assay for the optimization of the reagent for assembling the scaffold, including double-tagged miRNA27a probe (ranging from 0 to 500 nM), oligo(dT)-MPs (ranging from 5, 25 to 75 mg) and enzymatic reporter strept-HRP (5 x 10^{-3} U mL^{-1} for Panel A and 5 x 10^{-2} U mL^{-1} for Panel B), while keeping the ODN miRNA 21/27a backbone in 25 nM in all cases.

Competitive magneto enzyme-linked miRNA assay. Optimization of the scaffold amount

Once the assembly of the scaffold was established including the optimal concentration of each of the reagents, the evaluation of the optimal amount of scaffold per assay was tested. To achieve that, a competitive magneto enzyme-linked miRNA assay was designed to assess the performance of the test in terms of tagged-probe displacement. The first approach, instead of using microRNAs, 25 pmol synthetic ODN counterpart for miRNA21 and miRNA27a was used. The negative samples i. e. the scaffold with the double-tagged probes were in all instances also assessed.

Different concentrations of the scaffold were placed into a polypropylene plate as well as positive and negative samples for miRNA21 and miRNA27a separately with a 100 µL final

volume. Then, the plate was placed into a thermomixer for 5 minutes at 37°C for the sample heating and then slowly cooled down during 30 minutes until 10°C were reached. Three washing steps of 3 minutes were performed before the incubation with 100 µL of antiDIG-HRP (10 mU mL^{-1}) or antiFLU-HRP (7.14 mU mL^{-1}) conjugates during 30 minutes at 750 rpm and 10°C into the thermomixer. Then, the microplate was three-times washed for 3 minutes in the thermomixer at 750 rpm with washing buffer. The optical readout was then performed with the TMB substrate kit adding 100 µL of 1:1 TMB:H_2O_2 mix to each well. After 30 min of reaction, a volume of stop solution was added. The sample was transferred to a polystyrene plate to permit the absorbance and the measurement of the supernatants was performed with the microplate reader using a 450 nm filter. After each incubation or washing step, a 96-well magnet plate separator was positioned under the microtiter plate until pellet formation on the bottom corner, followed by supernatant separation.

Results shown in Fig. 3.8 correspond to the absorbance values of each amount of oligo(dT)-MP with the scaffold (from 7.5 to 75 µg). The 75 µg oligo(dT)-MP containing 2.5 pmol of the ODN backbone miRNA21/miRNA27a and 5 pmol of each of the double-tagged probes in 100 µL. The positive signals were obtained with enough synthetic miRNA to displace the double-tagged probes in its totality showing a decrease of absorbance intensity compared to the negative control. From de results, it was determined that 15 µg of the oligo(dT)-MP (thus containing 0.5 pmol of the ODN backbone miRNA 21/27a and 1 pmol of each of the double-tagged probes) will be used in all further experiments, resulting in a good signal-background ratio for both probes.

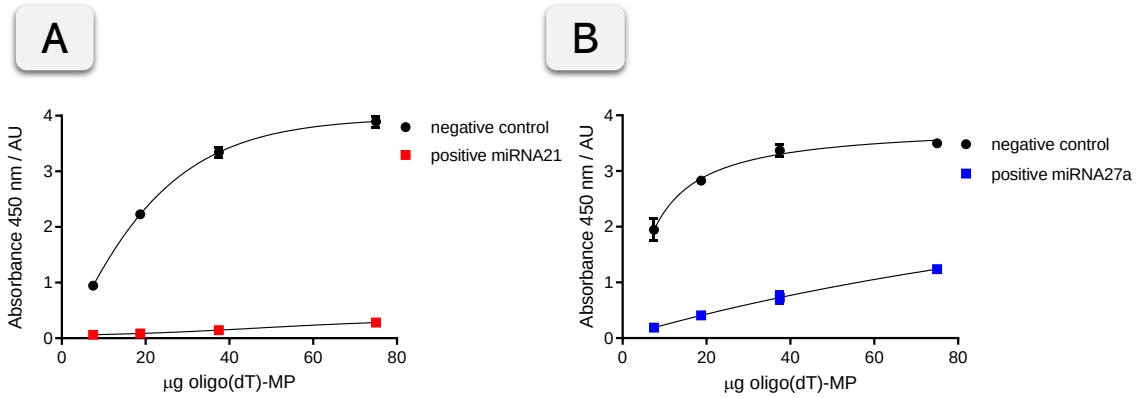


Figure 3.8. Optimization of the scaffold amount in a competitive magneto enzyme-linked miRNA assay. The test was carried out with four different final amounts of the oligo(dT)-MP corresponding to 7.5, 18.75, 37.5 and 75 µL of the oligo(dT)-MP (100 µL oligo(dT)-MP with the scaffold contains 2.5 pmol of the ODN backbone miRNA 21/27a and 5 pmol of each of the double-tagged probes). For each condition, the positive control incubated with excess of miRNA21 (Panel A) or miRNA27a (Panel B) synthetic ODN counterpart is shown, as well as the negative control. As an enzymatic reporter, 5 x 10^{-3} U mL^{-1} Strept-HRP was used. The error bars show the standard deviation for n=3.

3.6.3. miRNA extraction and quantification

miRNA extraction and quantification from MCF-7 and MDA-MB-231 cells

The miRNAs of the cell pellets and the exosomes were isolated with their corresponding isolation kits. Cells pellets were processed using the mirVana™ miRNA Isolation Kit with phenol (ref. AM1560, Invitrogen). First, the pellet was disrupted using 600 µL of lysis/binding buffer provided by the manufacturer and vortexing the sample. 60 µL of miRNA Homogenate Additive were added to the cell lysate and incubated 10 minutes in ice. A volume of Acid-Phenol:Chloroform equal to the lysis/binding buffer (600 µL) was added to each sample and the mixture vortexed. Subsequently the sample was centrifuged for two phase separation at 10000 g for 10 minutes. The aqueous phase containing the RNA was recovered and 1/3 volume of 100% ethanol added. The mix was passed through a filter Cartridge. For the mixture pass through samples were centrifuged 15 seconds at 10000 g. The filtrated was collected and 2/3 of 100% ethanol added. The mixture was then passed through a new filter Cartridge centrifuging 15 seconds at 10000 g. The small RNAs were then placed into the filter and three washing steps were subsequently carried out. The first washing step was performed with 700 µL of washing

buffer 1 and the next ones with 500 µL of washing buffer 2/3. Finally, the small RNAs were eluted applying 100 µL of preheated (95°C) elution buffer. Eluted samples were stored at -80°C for its further use. All the reagents and buffers were provided by the manufacturer in exception of the ethanol (ref. 1085430250, Sigma Aldrich).

miRNA extraction and quantification from exosomes-derived from MCF-7 and MDA-MB-231 cells

For the isolation of the miRNAs in purified exosomes samples Total Exosome RNA and Protein Isolation Kit (ref. 4478545, Invitrogen) was used. Volume was added up to 200 µL with PBS 1X to the preconcentrated exosomes samples. One volume of preheated (37°C) 2X Denaturing Solution was added to the mix with a subsequently 5 minutes incubation in ice. Once the incubation was performed one volume of Acid-Phenol:Chloroform was added and the mixture centrifuged 5 minutes at 10000 g after vortexing. Two phases were separated, and the upper aqueous phase transferred into a new tube. Then, 1/3 volume of 100% tempered ethanol was added to the sample and the mixture transferred into a filter cartridge. The tubes were centrifuged at 10000 g 30 seconds for liquid to passing through. The flowthrough was collected, and 2/3 volume of 100% ethanol added. The mixture was placed into a new filter cartridge and centrifuged 30 seconds at 10000 g. The flowthrough was discarded, and the filter washed. First, it was washed with 700 µL of washing buffer 1 and subsequently it was twice washed with 500 µL of washing buffer 2/3. Finally, the miRNAs were eluted dropping 50 µL of preheated (95°C) elution buffer into the filter and centrifuged 30 seconds at 10000 g. The eluate was then storage for further use at -80°C.

Quantification of the miRNA samples were performed with Qubit 4 using the microRNA assay kit (ref. Q32880, Invitrogen). The set up of the assay required the use of two standards provided by the manufacturer. The working solution was prepared mixing the microRNA reagent 1:200 with the microRNA buffer. Then, 10 µL of standard solutions were added to the tubes with 190 µL working solutions and 2 µL of the samples to 198 µL working solutions. The mixtures were incubated at RT for 2 minutes after vortexing them. Finally, the samples were read with the appropriate program into the Qubit 4.

It was quantified for the MCF-7 cells a total miRNA concentration of 66 µg mL^{-1} and a total miRNA concentration for the MDA-MB-231 of 63 µg mL^{-1}. Total miRNA concentrations of 3.54 µg mL^{-1} and 0.235 µg mL^{-1} were quantified for MCF-7 and MDA-MB-231 derived exosomes respectively.

3.6.4. qPCR

qPCR was used as the gold standard method for miRNA detection in whole cells and exosomes. All the miRNA samples were tested by ELmiRNA assay and further validated by qPCR. During the qPCR determination, a reference miRNA was used for the normalization of the expression of the target miRNAs ($2^{-\Delta Ct}$). First, the TaqMan™ Advanced miRNA Human Endogenous Controls Card (Applied biosystems, ref. A34716) qPCR assay was performed to determine the best miRNA candidate to be used for expression normalization. This assay included 32 miRNAs known to be endogenous controls for human samples. Thus, it was used to find a suitable candidate to be used in exosomes. For this assay exosomes from four different cell lines were included, containing three samples derived from breast cancer cell lines (MCF-7, MDA-MB-231 and SKBR-3) plus one neuroblastoma cell line (SH-SY5Y).

Prior to the qPCR performance, samples were pretreated to match the optimal conditions of the assay. Thus, the previously isolated miRNAs were retrotranscribed using the TaqMan™ Advanced miRNA cDNA Synthesis Kit (AppliedBiosystems, ref. A28007). First, a poly(A) tailing reaction was performed. A reaction mix composed by 0.5 µL 10X Poly(A) buffer, 0.5 µL ATP, 0.3 µL Poly(A) enzyme and 1.7 µL of RNase-free water and 2 µL of miRNA sample for each tube were mixed into a PCR tube. The mix reactions were then placed into the thermocycler and ran with the poly(A) program (37°C for 45 minutes, 65°C for 10 minutes and 4°C on hold). Subsequently, the adaptor ligation was carried out into the same tubes, were 10 µL of the following reaction mix was added: (i) 3 µL of 5X DNA ligase buffer, (ii) 4.5 µL 50% PEG 8000, (iii) 0.6 µL 25X Ligation adaptor, (iv) 1.5 µL RNA ligase and (v) 0.4 µL RNase-free water. The tubes were then placed into a thermocycler and incubated (16°C for 60 minutes and then 4°C on hold). The reverse transcription reaction was then performed by transferring 15 µL of the reaction mix (6 µL 5X RT buffer, 1.2 µL dNTP mix (25 nM each), 1.5 µL 20X universal RT primer, 3 µL 10X RT enzyme mix and 3.3 µL RNase-free water) to each tube. Tubes were then placed into the thermal cycler and incubated

(42°C for 15 minutes, 85°C for 5 minutes and 4°C on hold). The product was stored at -20ºC until use. An amplification step was then performed as recommended by the manufacturer. miR-Amp reaction mix (25 µL 2X miR-Amp master mix, 2.5 µL 20X miR-Amp primer mix and 17.5 µL RNase-free water) was mixed with 5 µL of the RT reaction product. Tubes were placed into a thermal cycler and incubate with the following settings: (i) 95°C for 5 minutes, (ii) 14 cycles of 95°C for 3 seconds and 60°C for 30 seconds, (iii) stopping step of 99°C for 10 minutes, and (iv) 4°C on hold. For the TaqMan™ Advanced miRNA Human Endogenous Controls Card assay, samples were diluted 1:10, mixed with the TaqMan® Fast Advanced Master Mix (2X), and introduced into the assay card.

The obtained results determined that from a total of 32 miRNAs analyzed, 53.125% were detected at least in one of the exosomes samples, as shown in the miRNA expression levels represented in Fig. 3.9. The results also showed that 4 of the assayed miRNAs (miRNA320a, miRNA19a, miRNAlet-7a and miRNA423) could be used as endogenous controls for further assays, due their similar expression in all the exosomes cell lines (MCF-7, MDA-MB-231, SKBR-3 and SH-SY5Y). After comparing our results with the literature, we chose the miRNAlet-7a, as it has been previously used as a control in other studies[39–41], and it presents a higher expression compared to other candidates as miRNA320a and miRNA19a, which were also previously found to be used as controls[42,43].

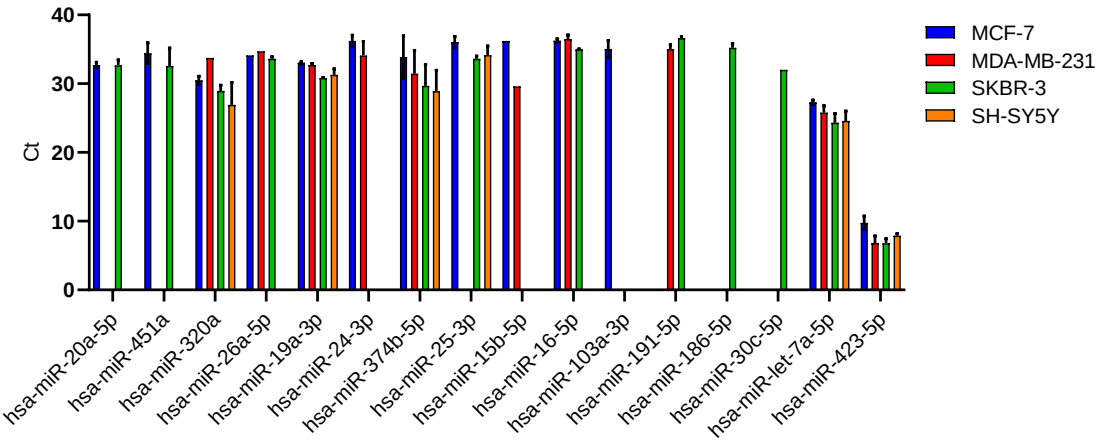


Figure 3.9. TaqMan™ Advanced miRNA Human Endogenous Controls Card assay for the determination of an endogenous control for the exosomes. Bar plot of the Ct for each of the miRNA evaluated in the assay expressed in the exosomal miRNA samples derived from MCF-7, MDA-MB-231. SKBR-3 and SH-SY5Y cell lines.

Once the adequate control for the assay was determined, we continued with the analysis of the miRNA samples of MCF-7 and MDA-MB-231 cell lines. For this experiment, miRNAs were previously retrotranscribed using the TaqMan™ Advanced miRNA cDNA Synthesis Kit and the qPCR performed with the same parameters as mentioned before. However, in this case the Taqman probes were not deposited into the microplates but added into the PCR master mix composed by 10 µL TaqMan® Fast Advanced Master Mix (2X), 1 µL TaqMan® Advanced miRNA Assay (20X) and 4 µL RNase-free water with 5 µL of the previously diluted (1:10) cDNA previously synthetized. The relative expression of the miRNA21 and miRNA27a for the breast cancer cell lines and their derived exosomes are represented in Figure 3.4. Both were normalized with the miRNAlet-7a ($2^{-\Delta Ct}$).

3.7 References

(1) Lee, R. C.; Feinbaum, R. L.; Ambros, V. The C. Elegans Heterochronic Gene Lin-4 Encodes Small RNAs with Antisense Complementarity to Lin-14. *Cell* **1993**, *75* (5), 843–854. https://doi.org/10.1016/0092-8674(93)90529-Y.

(2) Tribolet, L.; Kerr, E.; Cowled, C.; Bean, A. G. D.; Stewart, C. R.; Dearnley, M.; Farr, R. J. MicroRNA Biomarkers for Infectious Diseases: From Basic Research to Biosensing. *Front. Microbiol.* **2020**, *11*, 1197. https://doi.org/10.3389/FMICB.2020.01197.

(3) da Silva, D. C. P.; Carneiro, F. D.; Almeida, K. C. de; Bottino, C. F. D. S. Role of MiRNAs on the Pathophysiology of Cardiovascular Diseases. *Arq. Bras. Cardiol.* **2018**, *111* (5), 738–746. https://doi.org/10.5935/ABC.20180215.

(4) Li, Y.; Yin, Z.; Fan, J.; Zhang, S.; Yang, W. The Roles of Exosomal MiRNAs and LncRNAs in Lung Diseases. *Signal Transduct. Target. Ther.* **2019**, *4* (1), 47. https://doi.org/10.1038/S41392-019-0080-7.

(5) O'Brien, J.; Hayder, H.; Zayed, Y.; Peng, C. Overview of MicroRNA Biogenesis, Mechanisms of Actions, and Circulation. *Front. Endocrinol. (Lausanne).* **2018**, *9*, 402. https://doi.org/10.3389/fendo.2018.00402.

(6) Weber, J. A.; Baxter, D. H.; Zhang, S.; Huang, D. Y.; Huang, K. H.; Lee, M. J.; Galas, D. J.; Wang, K. The MicroRNA Spectrum in 12 Body Fluids. *Clin. Chem.* **2010**, *56* (11), 1733. https://doi.org/10.1373/CLINCHEM.2010.147405.

(7) Chevillet, J. R.; Kang, Q.; Ruf, I. K.; Briggs, H. A.; Vojtech, L. N.; Hughes, S. M.; Cheng, H. H.; Arroyo, J. D.; Meredith, E. K.; Gallichotte, E. N.; Pogosova-Agadjanyan, E. L.; Morrissey, C.; Stirewalt, D. L.; Hladik, F.; Yu, E. Y.; Higano, C. S.; Tewari, M. Quantitative and Stoichiometric Analysis of the MicroRNA Content of Exosomes. *Proc. Natl. Acad. Sci. U. S. A.* **2014**, *111* (41), 14888–14893. https://doi.org/10.1073/PNAS.1408301111/.

(8) Abramowicz, A.; Story, M. D. The Long and Short of It: The Emerging Roles of Non-Coding RNA in Small Extracellular Vesicles. *Cancers (Basel).* **2020**, *12* (6), 1445. https://doi.org/10.3390/cancers12061445.

(9) Moura, S. L.; Martín, C. G.; Martí, M.; Pividori, M. I. Multiplex Detection and Characterization of Breast Cancer Exosomes by Magneto-Actuated Immunoassay. *Talanta* **2020**, *211*, 120657. https://doi.org/10.1016/j.talanta.2019.120657.

(10) Cano, A.; Muñoz-Morales, Á.; Sánchez-López, E.; Ettcheto, M.; Souto, E. B.; Camins, A.; Boada, M.; Ruíz, A. Exosomes-Based Nanomedicine for Neurodegenerative Diseases: Current Insights and Future Challenges. *Pharmaceutics* **2023**, *15* (1), 298. https://doi.org/10.3390/pharmaceutics15010298.

(11) Condrat, C. E.; Thompson, D. C.; Barbu, M. G.; Bugnar, O. L.; Boboc, A.; Cretoiu, D.; Suciu, N.; Cretoiu, S. M.; Voinea, S. C. MiRNAs as Biomarkers in Disease: Latest Findings Regarding Their Role in Diagnosis and Prognosis. *Cells* **2020**, *9* (2), 276. https://doi.org/10.3390/cells9020276.

(12) Yaylak, B.; Akgül, B. Experimental MicroRNA Detection Methods. *Methods Mol. Biol.* **2022**, *2257*, 33–55. https://doi.org/10.1007/978-1-0716-1170-8_2.

(13) Sun, L.; Chen, Y.; Yi, P.; Yang, L.; Yan, Y.; Zhang, K.; Zeng, Q.; Guo, A. Serological Detection of Mycobacterium Tuberculosis Complex Infection in Multiple Hosts by One Universal ELISA. *PLoS One* **2021**, *16* (10), e0257920. https://doi.org/10.1371/journal.pone.0257920.

(14) Vengesai, A.; Midzi, H.; Kasambala, M.; Mutandadzi, H.; Mduluza-Jokonya, T. L.; Rusakaniko, S.; Mutapi, F.; Naicker, T.; Mduluza, T. A Systematic and Meta-Analysis Review on the Diagnostic Accuracy of Antibodies in the Serological Diagnosis of COVID-19. *Syst. Rev.* **2021**, *10* (1), 155. https://doi.org/10.1186/s13643-021-01689-3.

(15) Kim, S. E.; Van Tieu, M.; Hwang, S. Y.; Lee, M. H. Magnetic Particles: Their Applications from Sample Preparations to Biosensing Platforms. *Micromachines* **2020**, *11* (3), 302. https://doi.org/10.3390/mi11030302.

(16) Kurozumi, S.; Yamaguchi, Y.; Kurosumi, M.; Ohira, M.; Matsumoto, H.; Horiguchi, J. Recent Trends in MicroRNA Research into Breast Cancer with Particular Focus on the Associations between MicroRNAs and Intrinsic Subtypes. *J. Hum. Genet.* **2017**, *62* (1), 15–24. https://doi.org/10.1038/jhg.2016.89.

(17) Mertens-Talcott, S. U.; Chintharlapalli, S.; Li, X.; Safe, S. The Oncogenic MicroRNA-27a Targets Genes That Regulate Specificity Protein Transcription Factors and the G2-M Checkpoint in MDA-MB-231 Breast Cancer Cells. *Cancer Res.* **2007**, *67* (22), 11001–11011. https://doi.org/10.1158/0008-5472.CAN-07-2416.

(18) Stevic, I.; Müller, V.; Weber, K.; Fasching, P. A.; Karn, T.; Marmé, F.; Schem, C.; Stickeler, E.; Denkert, C.; Van Mackelenbergh, M.; Salat, C.; Schneeweiss, A.; Pantel, K.; Loibl, S.; Untch, M.; Schwarzenbach, H. Specific MicroRNA Signatures in Exosomes of Triple-Negative and HER2-Positive Breast Cancer Patients Undergoing Neoadjuvant Therapy within the GeparSixto Trial. *BMC Med.* **2018**, *16* (1), 1–16. https://doi.org/10.1186/s12916-018-1163-y.

(19) Liu, L. Z.; Li, C.; Chen, Q.; Jing, Y.; Carpenter, R.; Jiang, Y.; Kung, H. F.; Lai, L.; Jiang, B. H. Mir-21 Induced Angiogenesis through AKT and ERK Activation and HIF-1α Expression. *PLoS One* **2011**, *6* (4), e19139. https://doi.org/10.1371/journal.pone.0019139.

(20) Liébana, S.; Lermo, A.; Campoy, S.; Barbé, J.; Alegret, S.; Pividori, M. I. Magneto Immunoseparation of Pathogenic Bacteria and Electrochemical Magneto Genosensing of the Double-Tagged Amplicon. *Anal. Chem.* **2009**, *81* (14), 5812–5820. https://doi.org/10.1021/ac9007539.

(21) Ben Aissa, A.; Jara, J. J.; Sebastián, R. M.; Vallribera, A.; Campoy, S.; Pividori, M. I. Comparing Nucleic Acid Lateral Flow and Electrochemical Genosensing for the Simultaneous Detection of Foodborne Pathogens. *Biosens. Bioelectron.* **2017**, *88*, 265–272. https://doi.org/10.1016/j.bios.2016.08.046.

(22) Lermo, A.; Liébana, S.; Campoy, S.; Fabiano, S.; Inés García, M.; Soutullo, A.; Zumárraga, M. J.; Alegret, S.; Isabel Pividori, M. A Novel Strategy for Screening-out

Raw Milk Contaminated with Mycobacterium Bovis on Dairy Farms by Double-Tagging PCR and Electrochemical Genosensing. *Int. Microbiol.* **2010**, *13* (2), 91–97. https://doi.org/10.2436/20.1501.01.114.

(23) Théry, C.; Amigorena, S.; Raposo, G.; Clayton, A. Isolation and Characterization of Exosomes from Cell Culture Supernatants and Biological Fluids. *Curr. Protoc. Cell Biol.* **2006**, *30* (1), 3–22. https://doi.org/10.1002/0471143030.cb0322s30.

(24) Wang, H.; He, D.; Wan, K.; Sheng, X.; Cheng, H.; Huang, J.; Zhou, X.; He, X.; Wang, K. In Situ Multiplex Detection of Serum Exosomal MicroRNAs Using an All-in-One Biosensor for Breast Cancer Diagnosis. *Analyst* **2020**, *145* (9), 3289–3296. https://doi.org/10.1039/d0an00393j.

(25) Balcells, I.; Cirera, S.; Busk, P. K. Specific and Sensitive Quantitative RT-PCR of MiRNAs with DNA Primers. *BMC Biotechnol.* **2011**, *11* (1), 1–11. https://doi.org/10.1186/1472-6750-11-70.

(26) Weber, J. A.; Baxter, D. H.; Zhang, S.; Huang, D. Y.; Huang, K. H.; Lee, M. J.; Galas, D. J.; Wang, K. The MicroRNA Spectrum in 12 Body Fluids. *Clin. Chem.* **2010**, *56* (11), 1733–1741. https://doi.org/10.1373/clinchem.2010.147405.

(27) Mitchell, P. S.; Parkin, R. K.; Kroh, E. M.; Fritz, B. R.; Wyman, S. K.; Pogosova-Agadjanyan, E. L.; Peterson, A.; Noteboom, J.; O'Briant, K. C.; Allen, A.; Lin, D. W.; Urban, N.; Drescher, C. W.; Knudsen, B. S.; Stirewalt, D. L.; Gentleman, R.; Vessella, R. L.; Nelson, P. S.; Martin, D. B.; Tewari, M. Circulating MicroRNAs as Stable Blood-Based Markers for Cancer Detection. *Proc. Natl. Acad. Sci. U. S. A.* **2008**, *105* (30), 10513–10518. https://doi.org/10.1073/pnas.0804549105.

(28) Jet, T.; Gines, G.; Rondelez, Y.; Taly, V. Advances in Multiplexed Techniques for the Detection and Quantification of MicroRNAs. *Chem. Soc. Rev.* **2021**, *50* (6), 4141–4161. https://doi.org/10.1039/d0cs00609b.

(29) Chen, C.; Ridzon, D. A.; Broomer, A. J.; Zhou, Z.; Lee, D. H.; Nguyen, J. T.; Barbisin, M.; Xu, N. L.; Mahuvakar, V. R.; Andersen, M. R.; Lao, K. Q.; Livak, K. J.; Guegler, K. J. Real-Time Quantification of MicroRNAs by Stem-Loop RT-PCR. *Nucleic Acids Res.* **2005**, *33* (20), e179–e179. https://doi.org/10.1093/nar/gni178.

(30) Pritchard, C. C.; Cheng, H. H.; Tewari, M. MicroRNA Profiling: Approaches and Considerations. *Nat. Rev. Genet.* **2012**, *13* (5), 358–369. https://doi.org/10.1038/nrg3198.

(31) Stevanato, L.; Thanabalasundaram, L.; Vysokov, N.; Sinden, J. D. Investigation of Content, Stoichiometry and Transfer of MiRNA from Human Neural Stem Cell Line Derived Exosomes. *PLoS One* **2016**, *11* (1), e0146353. https://doi.org/10.1371/JOURNAL.PONE.0146353.

(32) He, Y.; Deng, F.; Yang, S.; Wang, D.; Chen, X.; Zhong, S.; Zhao, J.; Tang, J. Exosomal MicroRNA: A Novel Biomarker for Breast Cancer. *Biomark. Med.* **2018**, *12* (2), 177–188. https://doi.org/10.2217/bmm-2017-0305.

(33) Hannafon, B. N.; Carpenter, K. J.; Berry, W. L.; Janknecht, R.; Dooley, W. C.; Ding, W. Q. Exosome-Mediated MicroRNA Signaling from Breast Cancer Cells Is Altered by

the Anti-Angiogenesis Agent Docosahexaenoic Acid (DHA). *Mol. Cancer* **2015**, *14* (1), 1–13. https://doi.org/10.1186/s12943-015-0400-7.

(34) Pallares-Rusiñol, A.; Moura, S. L.; Martí, M.; Pividori, M. I. Electrochemical Genosensing of Overexpressed GAPDH Transcripts in Breast Cancer Exosomes. *Anal. Chem.* **2023**, *95* (4), 2487–2495. https://doi.org/10.1021/acs.analchem.2c04773.

(35) Qin, X.; Yu, S.; Xu, X.; Shen, B.; Feng, J. Comparative Analysis of MicroRNA Expression Profiles between A549, A549/DDP and Their Respective Exosomes. *Oncotarget* **2017**, *8* (26), 42125–42135. https://doi.org/10.18632/oncotarget.15009.

(36) Mittelbrunn, M.; Gutiérrez-Vázquez, C.; Villarroya-Beltri, C.; González, S.; Sánchez-Cabo, F.; González, M. Á.; Bernad, A.; Sánchez-Madrid, F. Unidirectional Transfer of MicroRNA-Loaded Exosomes from T Cells to Antigen-Presenting Cells. *Nat. Commun.* **2011**, *2* (1), 1–10. https://doi.org/10.1038/ncomms1285.

(37) Schwarzenbach, H.; Gahan, P. B. MicroRNA Shuttle from Cell-to-Cell by Exosomes and Its Impact in Cancer. *Non-coding RNA* **2019**, *5* (1), 28. https://doi.org/10.3390/ncrna5010028.

(38) Groot, M.; Lee, H. Sorting Mechanisms for MicroRNAs into Extracellular Vesicles and Their Associated Diseases. *Cells* **2020**, *9* (4), 1044. https://doi.org/10.3390/cells9041044.

(39) Peltier, H. J.; Latham, G. J. Normalization of MicroRNA Expression Levels in Quantitative RT-PCR Assays: Identification of Suitable Reference RNA Targets in Normal and Cancerous Human Solid Tissues. *RNA* **2008**, *14* (5), 844–852. https://doi.org/10.1261/rna.939908.

(40) Drobna, M.; Szarzyńska-Zawadzka, B.; Daca-Roszak, P.; Kosmalska, M.; Jaksik, R.; Witt, M.; Dawidowska, M. Identification of Endogenous Control Mirnas for RT-QPCR in T-Cell Acute Lymphoblastic Leukemia. *Int. J. Mol. Sci.* **2018**, *19* (10), 2858. https://doi.org/10.3390/ijms19102858.

(41) Davoren, P. A.; McNeill, R. E.; Lowery, A. J.; Kerin, M. J.; Miller, N. Identification of Suitable Endogenous Control Genes for MicroRNA Gene Expression Analysis in Human Breast Cancer. *BMC Mol. Biol.* **2008**, *9* (1), 1–11. https://doi.org/10.1186/1471-2199-9-76.

(42) Li, Y.; Zhang, L.; Liu, F.; Xiang, G.; Jiang, D.; Pu, X. Identification of Endogenous Controls for Analyzing Serum Exosomal MiRNA in Patients with Hepatitis B or Hepatocellular Carcinoma. *Dis. Markers* **2015**, *2015*, 893594. https://doi.org/10.1155/2015/893594.

(43) Drobna, M.; Szarzyńska-Zawadzka, B.; Daca-Roszak, P.; Kosmalska, M.; Jaksik, R.; Witt, M.; Dawidowska, M. Identification of Endogenous Control Mirnas for RT-QPCR in T-Cell Acute Lymphoblastic Leukemia. *Int. J. Mol. Sci.* **2018**, *19* (10). https://doi.org/10.3390/ijms19102858.

Chapter 4.

Rapid diagnostic test for assessment of cellular immune response in a viral infection as a model

4.1. Abstract

During the recent SARS-CoV-2 outbreak, there has been a recognized need of evaluating the adaptative immunological status, not only in infected individuals, but also in the vaccinated population. While the humoral immune response has been extensively assessed, the cellular immune response has received less attention due to the challenges of transferring it into a rapid diagnostic test. Consequently, there is a demand for the development of a rapid and user-friendly test for detecting activated T cells. This study is based on measuring interferon-gamma production as an indirect assessment of specific T cells. It uses the early expression of transcripts, amplifying them through PCR to targeted it in a paper-based rapid test. SARS-CoV-2 infection serves as a model for evaluating IFNγ transcripts in COVID-19 patients using a lateral flow assay. Whole blood of infected and non-infected individuals (both vaccinated) is incubated with Spike and Nucleocapsid peptide mixture followed by an immunomagnetic separation of the CD3+ T cells and IFNγ double-tagging RT-PCR. In parallel, non-stimulated blood sample are included as IFNγ basal expression. IFNγ increment is assessed by comparing the intensity of LFA signal from stimulated versus basal samples with a smartphone. Moreover, a time course is conducted to track the signal over time in the individuals with a specific T cell response. In summary, IFNγ-LFA is a one-day test, capable of assessing the cellular immune response up to two months and suitable for point-of-care applications as it requires minimal equipment.

4.2. Introduction

The increasing significance of disease outbreaks in health care accentuate the need of their early diagnosis and the monitoring of the evolution of infected patients. The immune system has evolved to provide protection to multiple pathogens by using different effector mechanisms. The final goal is to eliminate the pathogen and generate immunological memory through the activation of pathogen-specific B and T lymphocytes. B cells lead the humoral immune response secreting pathogen-specific antibodies that help neutralizing and opsonizing the target. On the other hand, cellular immune response is based on the activation of pathogen specific CD3+ T cells. Including; CD8+ T cells responsible for the recognition and lysis of target-infected cells, and CD4+ T cells critical due to their implication in the immune response including B-cell activation[1,2]. Antigen-specific T cells

are activated by the recognition of pathogen derived peptides bound to presenting molecules known as MHC (major histocompatibility complex) molecules. This recognition is mediated by the expression of MHC molecules by professional antigen-presenting cells or infected cells which are detected by the antigen specific receptor of T-cells (T-cell receptor)[3]. One of the T-cell activation consequences is the release and production of soluble mediators as cytokines. For cytotoxic T cells activation, the release of IFN-gamma (IFNγ) is crucial. It is defined as a pro-inflammatory cytokine belonging to the interferon family. In addition, IFNγ is also produced by activated Th1 cells (a subtype of Th cells), NK cells, and NKT cells[4].

The determination of cytokine production as indirect evidence of T-cell activation by specific antigens was performed for the first time by the so-called IGRA test (interferon gamma release assay). Different approaches have been developed for its detection, but there are two that are approved by the FDA, QuantiFERON®-TB Gold Plus (QFT-Plus, FDA P010033) and T-SPOT®.*TB* test (T-Spot, FDA P070006). Briefly, the QFT-Plus test consists of an ELISA that measures IFNγ released into the plasma after an overnight incubation of whole blood pulsed with pathogen-derived immunogenic peptides. In contrast, T-Spot quantifies the IFNγ-producing cells, therefore it requires a previously isolation and overnight stimulation of the mononuclear peripheral cells (PBMCs). However, other alternative assays have been developed as the determination of IFNγ by intracellular flow cytometry in CoVITEST[5], or through the IFNγ transcript amplification and detection by electrochemical genosensing, as previously published in our group[6], among others (Table 4.6, Supp. data).

One of the crucial features to set-up an IGRA test is the previous knowledge of the pathogen-immunogenic peptides. The evaluation of the cellular immune response provides information of the quality and long-lasting of the immune response through and after infection, and vaccination[7–9]. On March 2020, a global pandemic caused by a novel coronavirus (SARS-CoV-2 virus) was declared by WHO (World Health Organization) highlighting the need of evaluating the immunological status of the population. The at-home rapid tests were focused on the detection of the virus, but the immune response of the infected individuals was not determined. While the humoral response against SARS-CoV-2 had been widely assessed by the first *in vitro* diagnostic tests at the hospitals[10], the

cellular response had been more difficult to setup because it means to handle PBMCs but also due to the absence of immunogenic targets when the outbreak started. Some of the most severe COVID-19 manifestations were associated to disfunction of the immune response[11,12]. The possibility to stratify patients based on their prognosis at the point-of-care (POC) would have been a key test to prevent the collapse suffered at the hospital urgencies. Thus, the development of rapid and user-friendly test for the detection of the activated specific T cells was considered at that time as a major need.

In the current study, we demonstrate that the combination of antiCD3 and oligo(dT)-modified magnetic particles enhances the original IGRA design by: i) reducing the time required for peptide incubation of whole blood through the use of mRNA as analyte instead of IFNγ protein; ii) improving efficacy by selecting IFNγ producing T-cells using antiCD3-modified magnetic particles; iii) gaining sensitivity as IFNγ mRNA is detected after amplification; and iv) minimizing the instrumentation needed. In addition, the readout has been performed in parallel with CNP (carbon nanoparticles) and AuNP (gold nanoparticles) which is the current gold standard redout system in these tests. Overall, the IFNγ-LFA allows the detection of specific T cells on infected individuals seven hours after sample collection without the need of trained personnel and with minimal instrumentation.

4.3. Experimental

4.3.1. Instrumentation

The deposition of the antibody into the nitrocellulose membrane for the lateral flow assay (LFA) was carried out by Isoflow reagent dispensing system (Claremont Bio, Upland, CA, USA), coupled with a syringe bomb KDS LegatoTM 200 (KD Scientific Inc., Holliston, MA, USA) at a flow rate of 38 µL min^{-1}. The PCR was performed by the SimpliAmp Thermal Cycler (Applied biosystems, Thermo Fisher Scientific, Foster City, CA, USA). For the preparation of carbon black nanoparticles, an Eppendorf Thermomixer C (Eppendorf AG, DE, Hamburg, Germany), a microtube centrifuge Sprectrafuge 24D (Labnet, Madrid, Spain, ref. LA-C2400-230V), and a probe sonicator (Sonics Materials, Newtown, CT, USA Ref. VCX130PB220) were used. The separation of the magnetic particles for the washing steps were performed using the magnet DynaMag-2 (Invitrogen™, Thermo Fisher Scientific, WA,

USA, ref. 12321D). The agarose gel read out was performed with the GelDoc XR imaging system from Bio-Rad. Pictures were taken with a smartphone with 48 megapixels camera.

4.3.2. Chemicals and biochemicals

The carbon nanoparticles (CNPs) obtained from carbon black (CB) Spezial Schwartz 4 (Degussa AG, Essen, Germany, Ref.7088) and avidin (Thermo Scientific, Waltham, MA, USA, Ref. 21121) were used to prepare the avidin-modified carbon nanoparticles (Av-CNPs). Commercial streptavidin-modified 40 nm gold nanoparticles were obtained from Expedeon (Cambridge, UK, Ref. 250–1000). Bovine serum albumin (BSA, Ref. A5403), sucrose (Ref. S0389), and Tween® 20 (Ref. P9416) were purchased from Sigma-Aldrich (St. Louis, MO, USA). For the T lymphocytes Dynabeads™ CD3 were used, purchased from Invitrogen (ref. 11151D) All solutions were prepared with ultrapure Milli-Q water (Millipore® System, Burlington, MA, USA, resistivity 18.2 MΩ·cm). The RNA capture carried out with Dynabeads™ Oligo(dT)25 purchased from Thermo Fisher (ref. 61002). For the double-tagging PCR, the tagged primers were obtained from Sigma-Aldrich. Platinum™ II Taq Hot-Start DNA Polymerase (Ref. 14966001) and nuclease-free water (Ref. AM9937) were purchased from Thermo Fisher (Waltham, MA, USA). Standard reaction buffer 10× with MgCl2 (Ref. 20.034-4182) was purchased from Biotools, Madrid, Spain. Deoxynucleotide Mix 10 mM (Ref. D7295) was purchased from Sigma-Aldrich, St. Louis, MO, USA. The IFNγ forward and reverse modified were primers used for the amplification; 5'- [BIO] TGACCAGAGCATCCAAAA-3' and 5'- [DIG] CTCTTCGACCTCGAAACAGC-3' respectively, were purchased at the custom primer platform from Sigma Aldrich. For the cell culture the medium Iscove's Modified Dulbecco's Medium (IMDM) was purchased to Gibco™ ref. 12440-053 and the penicillin/streptomycin in Thermo Fisher (ref. 15140122). Dynabeads™ Human T-Activator CD3/CD28 for T Cell Expansion and Activation was purchased from Thermo Fisher (ref 11161D) and PHA (Roche, ref. 11249738001) was used as positive control. The SARS-CoV-2 derived peptides from Spike and Nucleocapsid were purchased from (Miltenyi ref 130-126-701 and 130-126-698 respectively).

For the construction of LFA strips, adhesive backing cards were purchased from Kenosha C.V., Amstelveen, The Netherlands (Ref. KN-2211). Nitrocellulose membrane (Ref. FF120H) and absorbent pads (CF7) were purchased from GE Healthcare Europe, Chicago, IL, USA. The cellulose sample pads (CFSP203000) and glass fiber conjugate pads (GFCP083000)

were purchased from Millipore, Burlington, MA, USA. Anti-digoxigenin Fab fragments (anti-DIG antibody) (Roche, Basilea, Switzerland, Ref. 11214667001) were used in the test line at 0.5 mg·mL^{-1}. As a control line, biotinylated protein was used at 0.5 mg·mL^{-1} (BSA-biotin, Thermo Scientific Ref. 29130).

4.3.3. Rapid diagnostic test for assessment of cellular immune response

All the solutions and biochemicals are detailed on Supp. data, § 4.6.1. The procedure from blood stimulation to visual readout based on a paper-based immunochromatography test is schematically described in Figure 4.1.

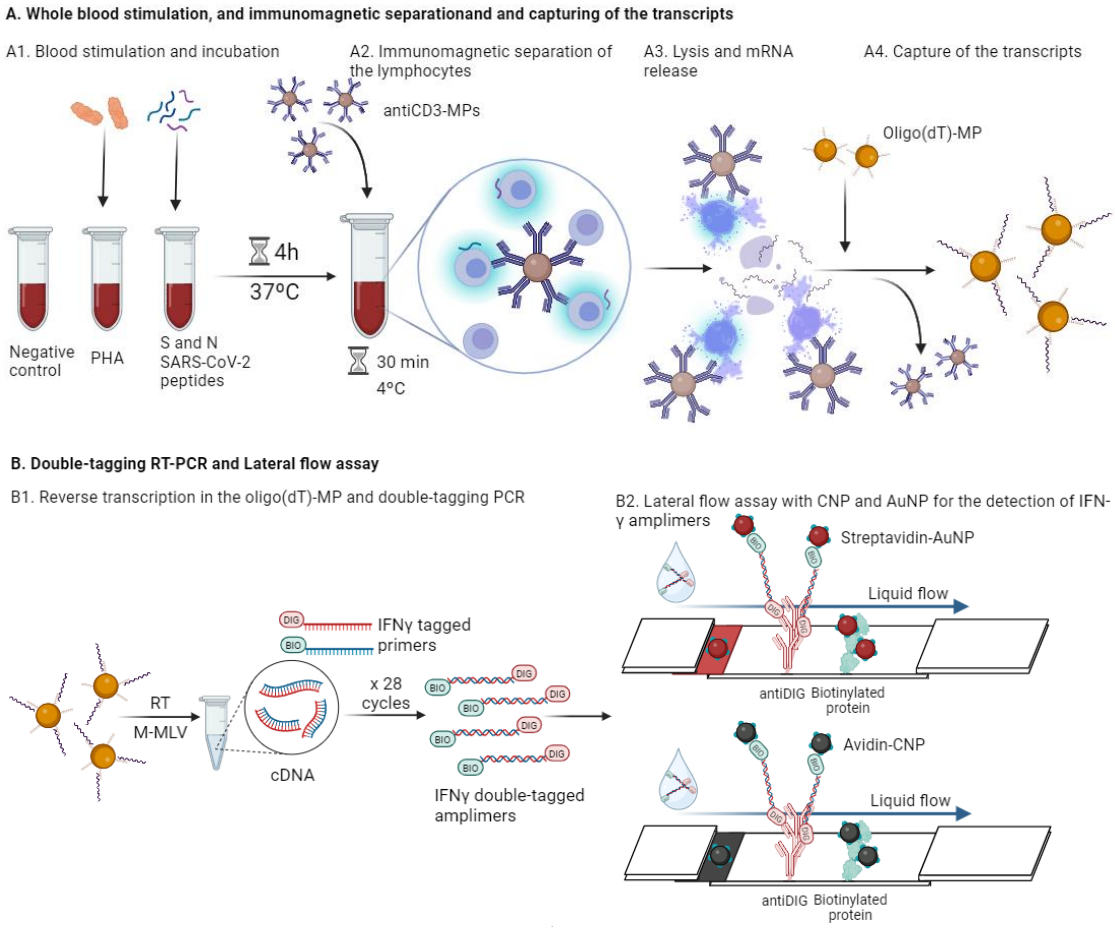


Figure 4.1. Schematical representation of the rapid diagnostic test for assessment of cellular immune response based on the IFNγ mRNA transcripts, involving the subsequently steps: whole blood stimulation, immunomagnetic separation of the lymphocytes and capturing of the mRNA (Panel A) and double-tagging RT-PCR and lateral flow assay (Panel B). Created with Biorender.com.

4.3.4. Whole blood stimulation, immunomagnetic separation of the lymphocytes and capturing of the transcripts

The assay was tested with heparinized whole blood from SARS-CoV-2 infected patients 10 days after negativity of an antigen test, as well as and non-infected donors considered as control. Each sample (1 mL) was processed by incubation at 37°C during 4 h in three different conditions (shown in Figure 4.1, Panel A1). Non-stimulated blood as a negative control, stimulated with phytohemagglutinin (PHA, 5 µg mL^{-1}) as a positive control, and stimulated with peptides from the two main SARS-CoV2 antigens, (spike (S) and nucleocapsid (N) proteins, used at 2.5 µg mL^{-1} each). Next, the immunomagnetic separation of T lymphocytes was performed, as shown in Figure 4.1, Panel A2, by incubating directly with 1×10^7 antiCD3-MPs for 30 min with rotation at 4°C (Figure 4.1, Panel A2). CD3+ T cells were then washed with isolation buffer twice. Isolated CD3+ T cells were resuspended with 1 mL of Lysis/Binding buffer and disrupted using a 21 G needle in order to release the genetic material (Figure 4.1, Panel A3). The antiCD3-MP were discarded, and the supernatant was kept for further mRNA isolation. In all instances, after incubation or washing step, a magnetic separator was positioned under the tubes until pellet formation on the tube side wall, followed by supernatant separation.

The mRNA capture was carried out with oligo(dT)-MP following the manufacturer protocol. Briefly, 15 µL of oligo(dT)-MP were added into the supernatant and the mixture was incubated 5 min at 750 rpm at RT. mRNA attached to oligo(dT)MP were washed with 500 µL of buffer A and then 500 µL of washing buffer B and with 100 µL of RNase-free water (Figure 4.1, Panel A4). Finally, the MPs were resuspended in 12 µL RNase-free water to perform the cDNA retrotranscription protocol.

4.3.5. Double-tagging RT-PCR on magnetic beads

dNTPs were added to the mRNA attached to oligo(dT)-MP and incubated 5 min at 65°C. Then the master mix was added and incubated 2 minutes at 37°C. The M-MLV retrotranscriptase was finally added at 200 U to the mixture with final volume of 20 µL (Figure. 4.1, Panel B1). Reverse transcription was performed for 50 min at 37°C, 15 min at 70°C.

Double-tagging PCR was performed to amplify IFNγ cDNA using double-tagged Digoxigenin/Biotin-labelled primers. The PCR was performed in 15 µL of reaction mixture per sample. Master mix was added to 2 µL of the cDNA (Figure 4.1 Panel B1). Amplification was performed after incubation 2 min at 94°C with 28 cycles (94°C for 15 s, 60°C for 15 s, 68°C for 15 s) and analyzed with conventional agarose gel electrophoresis on 2% agarose gel in TAE buffer 1× Syber Safe dye and by Lateral Flow assays.

4.3.6. Lateral flow assay

The strips for the lateral flow assay (LFA) were prepared by dispensing anti-digoxigenin (0,5 $mg \cdot mL^{-1}$) as a test line and BSA-biotin (1 $mg \cdot mL^{-1}$) as control line onto a nitrocellulose membrane with an Isoflow reagent dispensing system. CNP modified with avidin (prepared as described in § 4.6.2, Supp data) or AuNP were diluted 1/5 with conjugation buffer and 25 µL of the mixture were dropped on the conjugate pad and air dried. Both components as well as the sample and the absorbent pads were deposited into a 5 mm adhesive backing pad as well as the previously cut sample pad and absorbent pad.

On to the sample pad, 5 µL of the PCR product (double-tagged IFNγ amplimers) diluted with 20 µL of running buffer were dropped and followed by 200 µL of running buffer (Figure 4.1, Panel B2). The result was registered after 15 min of the buffer deposition through a photograph, taken with a smart phone. To ensure consistent image quality and eliminate luminosity-related biases, all pictures were taken under the same conditions. This process involved using a portable photographic studio equipped with 1100 lm LED lights maintaining a colour temperature of 6000–6500 K and the picture taken with a smartphone camera (12 megapixels). Then, the pictures were analyzed through the ImageJ gel analysis toolbox. LFA without a visible control line would be invalidated.

4.3.7. Study design and ethics

This is a prospective observational and control study that includes twelve individuals. This cohort was divided in individuals that were vaccinated but presumably not infected with SARS-CoV-2 virus (n=5), and individuals that were vaccinated and infected (n=7). The infection with SARS-CoV-2 was checked with an antigen test and blood samples were collected after the antigen test switched to negative. The infected individuals have mild disease with less than two weeks symptomatology. Demographic information of the study

is collected in Table 4.1 supp. data). The longitudinal study was conducted with the infected individuals recruited the first month after the infection. Blood was drawn at the Autonomous University of Barcelona Health Care Service and informed consent was signed by all volunteers included in the study.

All works were performed in a Biosafety cabinet, and all material was decontaminated by autoclaving or disinfected before discarding following US Department of Health and Human Services guidelines for level 2 laboratory Biosafety.

4.3.8. Statistical Analysis

The statistical analyzes and calculations were performed using Prism v 10.0.1 (GraphPad, San Diego, USA). The calibration curves were adjusted to a non-linear regression fitting, using the log(inhibitor) vs. response (three parameters). The limit of detection was calculated considering the values of negative controls for each curve, using the one-tailed test with a significance level of $p < 0.05$ (t Student, $p < 0.05$). Two-way ANOVA was performed to determine statistical differences between the different conditions in a specificity study with a significance level of $p < 0.05$.

4.4. Results and discussion

4.4.1. Rapid diagnostic test for the assessment of cellular immune response

The optimization of the lateral flow, including the readout system based on CNP and the analytical performance, are discussed in supplementary data (Figure 4.6). The Limit of Detection (LOD) for the lateral flow assay was established at 695 cells for the AuNP and 1929 cells for the CNP, by using the smartphone readout, while the LOD for the visual redout was found to be 10,000 cells in both signal generating systems. Accordingly, both detection systems are suitable for the sample evaluation, being CNP a competitive readout method considering cost and ease of preparation. Whole blood samples were evaluated by the two readout methods, based on AuNP and CNP as signal generating system in the LFA. (Figure 4.6, Supp. data). Moreover, the conditions of the assay procedure were also optimized as detailed in § 4.6.5, supp. data (Figures 4.7-4.9). Two groups of vaccinated individuals were examined i.e., individuals which, presumably, have not been previously infected with SARS-CoV-2 and individuals recently infected. For each individual, 1 mL

whole blood was processed for each stimulation condition, as schematically described in Figure 4.1. The results were obtained by analyzing the area under the curve of the test lines through ImageJ software. For each condition the values shown were the mean of LFA duplicates (Figure 4.10, supp. data).

The comparison of the IFNγ production of infected individuals between basal and peptide stimulated samples indicated that the rapid test based on the lateral flow was able to detect the presence of activated specific T cells after only 4 h incubation. In contrast, no statistical differences were obtained when comparing the IFNγ production of the basal and the stimulated blood samples of non-infected individuals, as shown in Figure 4.2, Panels A and B. This result was as expected considering that the vaccine administrated to all the population (regardless the manufacturer) was based only on the spike (S) protein or mRNA, as it was focused to induce the immune response against this viral protein. In this approach, the nucleocapsid (N) was also included as recently published results showed that is also an important immunogenic protein of SARS-CoV-2 virus[13,14]. Positive controls showed significative difference compared to the basal expression for all the individuals included in the study with both readout methods (in all cases, the corresponding strips are shown in Figure 4.10, Supp. data). Moreover, an additional significant difference was observed among the stimulated samples when comparing both groups (Infected versus Non-Infected), indicating the semiquantitative readout of this test, as confirmed also by the statistical data showed in Table 4.2, Supp. data).

In order to evaluate the response of each individual, Figure 4.2, Panels C and D, show the results for Student's *t*-test at the 95% significance level. Variances in IFNγ expression were noted between basal and stimulated samples of the infected individuals, while no significant differences were observed in the non-infected group. Consistent results were obtained with both detection methods (Fig. 4.2, Panels C and D).

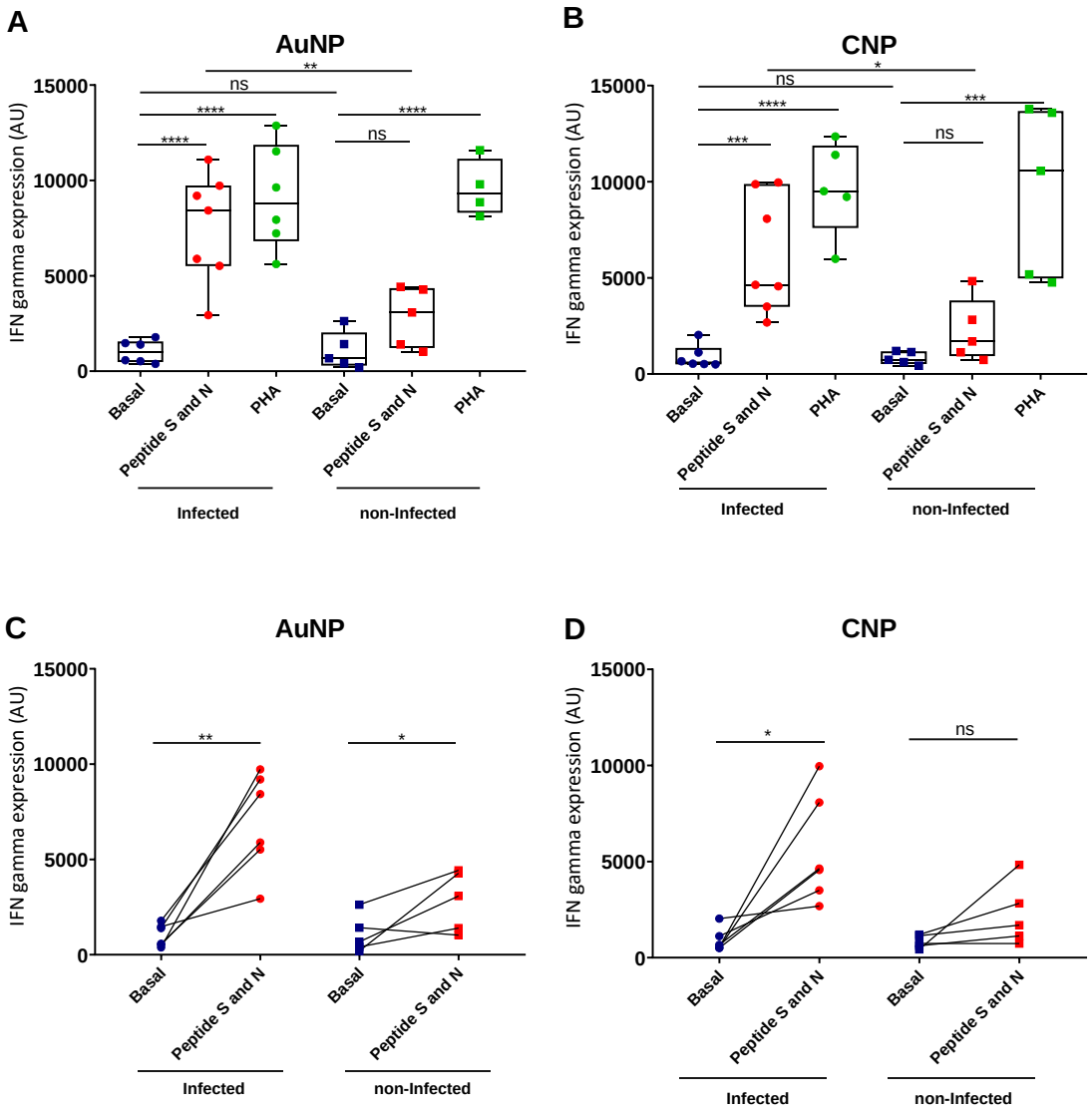


Figure 4.2. Graphical representation for the signal obtained with the LFA test line, showing the expression of the IFNγ. Box plots with circles belonged to the Infected group while squares, the non-Infected group. For both groups, the basal expression of the cytokine obtained by non-stimulated whole blood is shown in blue, as well as the expression after 4h-stimulated whole blood, incubated with S and N peptides derived from SARs-CoV-2 (in red) and with PHA (in green). Panels A and B show the signals obtained with the LFA based on AuNP and CNP, respectively. Panels A and B show the results for the statistical analysis performed by a multiparametric ANOVA, comparing the basal IFNγ expression values as well as those obtained after peptide stimulation for LFA based on sAvAuNP and AvCNP, respectively. Panels C and D, show the results for Student's *t*-test at the 95% significance level, in order to evaluate the performance of each individual. One value of the basal Infected group was excluded after a Grubbs' test for the identification of outlier values.

The outcome of the results using AuNP and CNP was comparable as well as their statistical analysis (Figure 4.2, Panels A and B). When comparing both methods, it was noticed a tendency of a higher dispersion for CNP in the stimulated samples of the infected

individuals. Nevertheless, interindividual differences were observed in both detection methods and groups (infected and non-infected). The observed variability among individuals may arise from various factors, including: i) the heterogeneity of blood leukocyte population, and ii) the capture of entire CD3+ T cell populations, encompassing both activated and non-activated T lymphocytes, being the activated a variable percentage of the total population which could induce a bias.

4.4.2. Rapid diagnostic test for the follow up of cellular immune response

The next objective was to analyze to what extent the IFNγ-LFA was able to detect circulating SARS-CoV-2 memory T cells. A follow up of the group of infected individuals was performed over eight months, i.e. blood samples were extracted at the beginning, two, and eight months after infection.

As demonstrated in Figure 4.2, at the time of infection (0 months), all samples exhibited significant differences between basal and SARS-CoV-2 peptide-stimulated samples. Figure 4.3 illustrates that this difference persisted for at least two months. The detectable amount of circulating memory T cells via the IFNγ-LFA decreased between two- and eight-months post-infection. Additionally, the positive control was examined under all conditions, and its variance from basal expression was found to be statistically significant. The results were subjected to one-way ANOVA (refer to Table 4.4 in the supp data).

Considering this, a Student's *t*-test was carried out to determine the differential expression for each individual (Figure 4.3, Panels C and D) as confirmed also by the statistical data showed in Table 4.5, Supp. data). T cell responses were detected up to 2 months in all the individuals, but at 8 months the responses dropped correlating with previous studies where the T cell response have been determined to be decreased faster than the humoral response[13]. The longitudinal study was conducted with recently infected individuals. Under these stimulation conditions, reactivity against specific peptides was observed for up to 2 months, considering interpopulation variability in the immune response that has been widely observed in SARS-CoV-2-infected individuals[14–16].

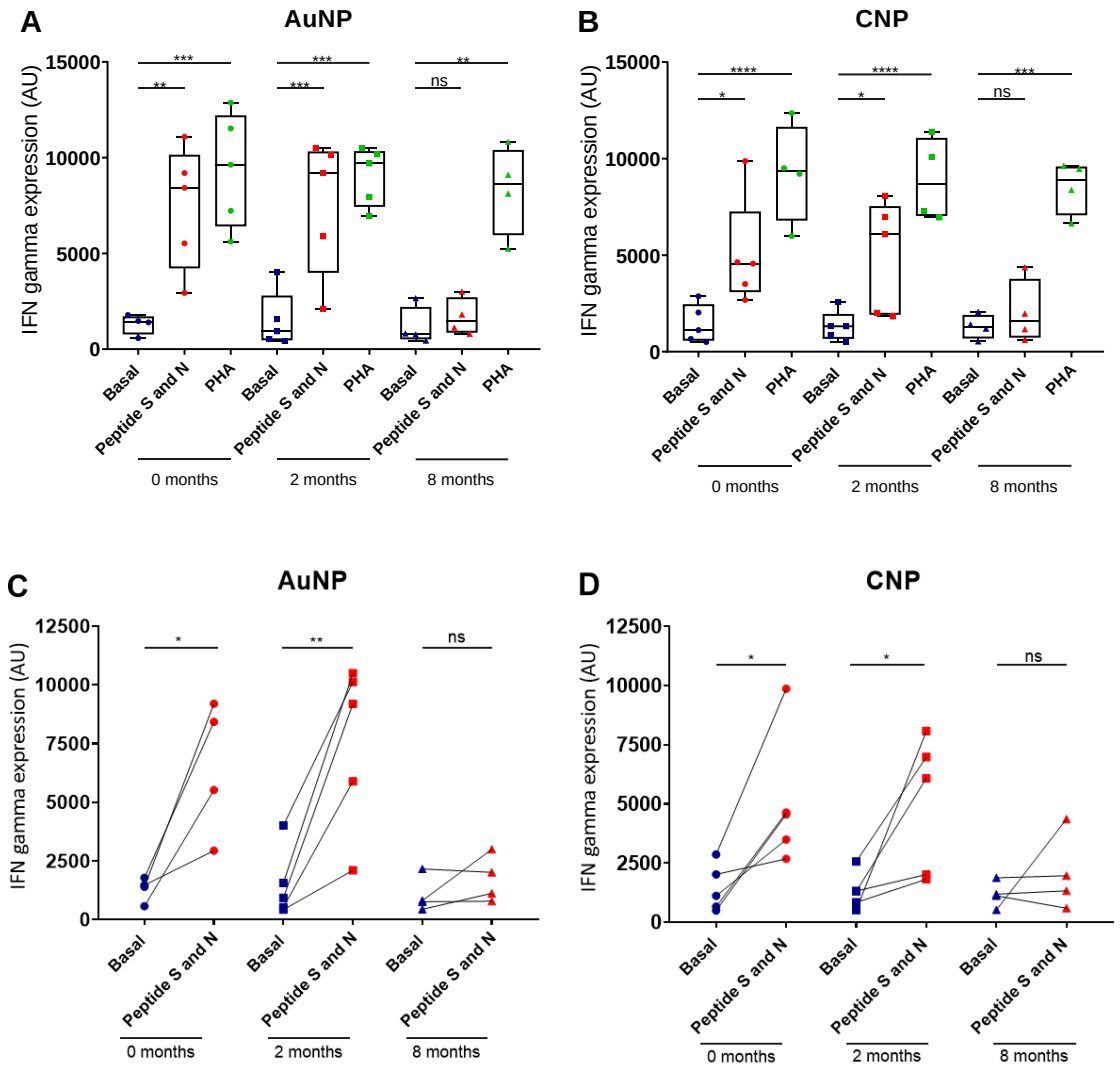


Figure 4.3. Graphical representation for the signal obtained with the LFA test line in the follow up experiment, showing the expression of the IFNγ in infected individuals over 0 month (circles), 2 month (squares) and 8 months (triangles). The basal expression of the cytokine obtained by non-stimulated whole blood is shown in blue, as well as the expression after 4h-stimulated whole blood incubated with S and N peptides derived from SARs-CoV-2 (in red) and with PHA (in green). Panels A and B show the signals obtained with the LFA based on AuNP and CNP, respectively. Panels C and D show the results for the statistical analysis performed by a Student's *t*-test at the 95% significance level, in order to evaluate the performance of each individual for LFA based on AuNP and CNP, respectively.

Even though there is no significative difference between both groups in the 8 month follow up, in one of the individuals there is an increasing of the expression higher than 5-fold. This suggests the contact of the individual with the virus even it was in an asymptomatic infection.

The fundamentals and the analytical features of the IGRA test currently in the market are summarized and compared with other approaches recently developed and with this work in § 4.6.9 Supp. data, and Table 4.6. A shortened protocol time is achieved through a reduced incubation period, thanks to the evaluation of mRNA levels rather than the released cytokine[8,15] compared with the other approaches. The entire protocol takes approximately 7 h from sample collection to the delivery of the results. In comparison to the current gold standard techniques for tuberculosis, such as QFT-GIT and T-Spot (Table 4.6, supp. Data), this LFA design significatively reduces the time as results can be obtained the same day of blood sample extraction. In fact, the gold standard technique for the T specific cell activation and detection is the QFT-GIT, requires 16-24 h stimulation. Moreover, the T-spot protocol require a previous PBMC isolation as well as an overnight stimulation. In addition, both protocols require trained personnel. Novel detection methods with a comparable time performance is based on the detection of the intracellular IFNγ protein and the cytometry as the readout method[5,17]. They offer high sensitivity due to fluorescence, but the use of expensive equipment and well-trained personnel limits its application in low-resource settings. In the proposed LFA, blood sample stimulation follows the previously published methodology[5]. In fact, the approach used in the IFNγ-LFA are based on CoVITEST but avoiding the addition of Fastimmune™ CD28/CD49d cocktail (a costimulatory stimulus to reinforce T-cell activation), demonstrating the robustness of this approach. On the other hand, the absence of CD28 signalling during the stimulation could explain that specific T-cells were not detected further than two months in this test. Moreover, it requires no equipment for the readout, even though the LFA interpretation can be linked to a smartphone integrating it with mHealth technology for results delivery and analysis.

In addition to the analytical performance, a test needs to be safe and affordable. In this study, the use of non-invasive sample such as blood, as well as the low amount required (3 mL) makes it feasible to be used as a diagnostic test for paediatric population. In addition, the aim of designing an affordable test for all countries, the use of CNP is consistently used throughout the study. The results have demonstrated that the use of the AvCNP performs comparably to the widely considered gold standard readout sAvAuNP in the LFA. Moreover, the AvCNP offers a better cost-effective alternative due to its lower

price. Thus, it reduces the total cost of the assay maintaining a comparable level of analytical performance.

The use of antiCD3-MP allows for the broad capture of CD4+ and CD8+ T cells but does not differentiate between activated and non-activated cells. This extensive T cell capture, over extended periods following infection, results in a lower frequency of effector memory T cells in the CD3+ T cell fraction over time. This limitation could be addressed by employing MPs for the capture of more specific populations, such as CD69+, an activation marker used in CoVITEST[5] (§ 4.6.9 supp. data). Although these specific MPs are commercially available, they present a less cost-effective alternative compared to the MPs currently used in the assay. Consequently, the specific T lymphocyte response was successfully evaluated using a broad capture in whole blood samples for up to 2 months after infection. However, adjustments to the procedure could be applied for longer-term evaluations, including during the incubation co-stimulatory molecules, or mixture of peptides from more antigenic targets, to enhance the long-term predictive value of the test. As well as further optimizations as the reduction of the assay performance time as explored in the § 4.6.8 supp. data.

4.5. Conclusions

The development of *in vitro* diagnostic tests to assess the cellular immune response has become essential due to the increasing frequency of infectious disease outbreaks and the need for patient stratification to prevent the collapse of hospital emergency services. Furthermore, such tests could provide a broader overview of the immune response for immunocompromised individuals. Therefore, this study introduces an alternative version to the Interferon-Gamma Release Assay, based on the determination of IFNγ transcript expression by antigen-specific T cells through LFA. Compared to other test in the market, the approach described here shows improved analytical features, including a significantly reduced incubation time, from overnight to as low as 4 hours, achieved by using transcripts instead of released proteins. Additionally, sensitivity is increased through the amplification and double-tagging of IFN-γ transcripts. The incorporation of magnetic preconcentration for CD3+ T lymphocytes reduces interference from clinical samples during stimulation by isolating the target within the containing cells. Finally, the visual

readout is achieved in a paper-based LFA, reducing costs. Due to the methodology versatility, changing the stimulating peptides allows for the evaluation of the cellular immune response to any other pathogens. This adaptability facilitates faster test development for upcoming disease outbreaks. In summary, infectious diseases are a priority in low resource settings, and the design of an alternative IGRA test amenable to a LFA is presented as a more versatile technique as it eliminates the need for expensive benchtop equipment and specialist personnel to be implemented at the POC.

4.6. Supplementary data

4.6.1. Experimental

Chemicals and biochemicals

Diethyl pyrocarbonate (DEPC, ref. D5758), ethylenediaminetetraacetic acid (EDTA, ref. E9884), glycine (ref. 410225), lithium chloride (ref. 746460), lithium dodecyl sulfate (LiDS, ref. L9761), tris(hydroxymethyl)aminomethane (TRIS, ref. 252859), Tween 20 (ref. P9416), sucrose (Ref. S0389), boric acid (ref. B6768), sodium phosphate dibasic (ref. 71636), potassium phosphate dibasic (ref. 795496), sodium chloride (ref. S3014), potassium chloride (ref. P3911) and magnesium chloride (ref. M8266), Polyvinylpyrrolidone (ref. PVP360) were purchased from Sigma-Aldrich (Merck KGaA, DE). DL-Dithiothreitol (DTT, ref. 46819) was purchased from Fluka (Thermo Fisher Scientific). All buffer solutions used in RNA extraction were prepared with 0.1% diethylpyrocarbonate (DEPC) treated with Ultrapure water (Millipore® System, resistivity 18.2 MΩ cm) to prevent RNA degradation.

Buffer and solution composition

The composition of the buffers used in this work are described below:

The composition of the solutions was:

- PBS 1X buffer: 10 mmol L^{-1} Na_2HPO_4, 137 mmol L^{-1} NaCl, 2.7 mmol L^{-1} KCl, 1.8 mmol L^{-1} K_2HPO_4, pH 7.4.

For the carbon nanoparticles preparation and storage:

- Borate buffer 1: 100 mmol·L^{-1} borate, pH 8.8
- Borate buffer 2: 5 mmol·L^{-1} borate, pH 8.8.
- Washing buffer: 5 mmol·L^{-1} borate, pH 8.8, 1% w/v BSA, 0.1% w/v casein.
- Storage buffer: 100 mmol·L^{-1} borate, pH 8.8 with 0.1% *w/v* casein and 0,1% *w/v* PVP.

For the LFA the solutions were:

- CNP Conjugate buffer: 10 mmol·L^{-1} borate, pH 8.8, 20% w/v sucrose, 0.1% w/v casein.

- CNP Running buffer: 100 mmol·L^{-1} borate, pH 8.8, 1% w/v BSA, 0.05% v/v Tween 20®.
- AuNP Conjugate buffer: 10 mmol·L^{-1} borate, pH 8.8, 20% w/v sucrose.
- AuNP Running buffer: PBS 10 mmol·L^{-1}, pH 7.4, 0.05% v/v Tween 20®, 1% w/v BSA.

For the RNA extraction with poly(dT)-MPs, the solutions were:

- RNase-free water: 0.1% v/v DEPC.
- Isolation buffer: 0.1 M PBS, 2 mM EDTA and 0.1% BSA w/v
- Binding Buffer: 20 mmol L^{-1} TRIS-HCl, pH 7.5, 1.0 mol L^{-1} LiCl, 2 mmol L^{-1} EDTA.
- Lysis/Binding buffer: 100 mmol L^{-1} Tris-HCl, 500 mmol L^{-1} LiCl, 10 mmol L^{-1} EDTA, 1% w/v LiDS, 5 mmol L^{-1} DTT.
- Washing buffer A: 10 mmol L^{-1} TRIS-HCl, pH 7.5, 0.15 mol L^{-1} LiCl, 1 mmol L^{-1} EDTA, 0.1% w/v LiDS.
- Washing buffer B: 10 mmol L^{-1} TRIS-HCl, pH 7.5, 0.15 mol L^{-1}, LiCl, 1 mmol L^{-1} EDTA.

The composition for the RT-PCR was:

- RT master mix: 5X FS buffer, 0.1 M DTT and 40 U RNase OUT.
- PCR master mix: 200µM of each deoxynucleotide triphosphate, 0.2 µM of each tagging primers for IFN-γ transcripts and 1X of Platinum™ II Taq Hot-Start DNA Polymerase.

4.6.2. Carbon nanoparticle modification with avidin

For carbon nanoparticle synthesis 10 mg·mL^{-1} carbon black (Degussa AG, Essen, Germany) solution was sonicated for 5 min at 27 W, 5-fold diluted in borate buffer (pH 8.8) and sonicated again. Then, 1 mL of the carbon solution was mixed with 150 µL of avidin (Thermo Scientific, Waltham, MA, USA) (5 mg·mL^{-1}) and incubated 3 h at 550 rpm in the Eppendorf Thermomixer C (Eppendorf AG, DE, Hamburg, Germany). To eliminate the excess of avidin, the suspension was twice centrifuged and washed with washing buffer (5 mM borate, pH 8.8, 1% w/v BSA, 0.1% w/v casein). Ultimately, the Av-CNPs were resuspended in 1 mL storage buffer (100 mM borate, pH 8.8 with 0.1% w/v casein and

0,1% w/v PVP). The performance and the stability study of the CNP was then carried out and the results presents in Supp data § 4.6.4.

4.6.3. Demographic information of the study

Results of both groups were comparable in age and sex. Both groups have a higher percentage of females.

Table 4.1 Demographic data of the vaccinated individuals tested, divided in infected and non-infected.

CODE	STATUS	AGE	SEX	VACCINES				DAYS FROM VAC.	DAYS FROM NEG. TEST
				Astra Zeneca	**Janssen**	**Moderna**	**Pfizer**		
COV2.01	Infected	27	M	-	-	1	2	NA	1
COV2.02	Infected	25	F	2	-	1	-	NA	14
COV2.03	Infected	71	F	-	-	3	-	NA	2
COV2.08	Infected	40	F	-	-	-	3	NA	45
COV2.09	Non-Infected	52	F	-	-	2	-	126	-
COV2.10	Infected	50	F	-	-	1	2	NA	10
COV2.11	Non-Infected	28	F	-	1	1	-	276	-
COV2.12	Non-Infected	21	M	-	-	-	3	319	-
COV2.13	Non-Infected	58	F	-	-	3	-	314	-
COV2.14	Infected	24	M	-	-	3	-	NA	18
COV2.17	Infected	71	F	-	-	-	3	149	-
COV2.19	Infected	31	M	-	-	3	-	NA	11
COV2.20	Infected	27	M	-	-	3	-	NA	14
COV2.21	Infected	27	F	-	-	-	2	NA	19
COV2.24	Non-Infected	51	F	-	-	1	2	364	-

4.6.4. Optimization of the rapid diagnostic test for the assessment of cellular immune response

Optimization of the readout system based on carbon nanoparticles

Avidin-modified carbon nanoparticles (AvCNP) were employed as the readout method in lateral flow assays (LFA), as previously described, in a dipstick format[18,19]. In this work, the LFA was enhanced by introducing the nanoparticles into a conjugate pad instead of pre-incubating them with the sample. This optimization made the LFA ready-to-use for sample

deposition onto the strip, rendering it comparable to commercial devices that use gold nanoparticles (AuNP) for the readout.

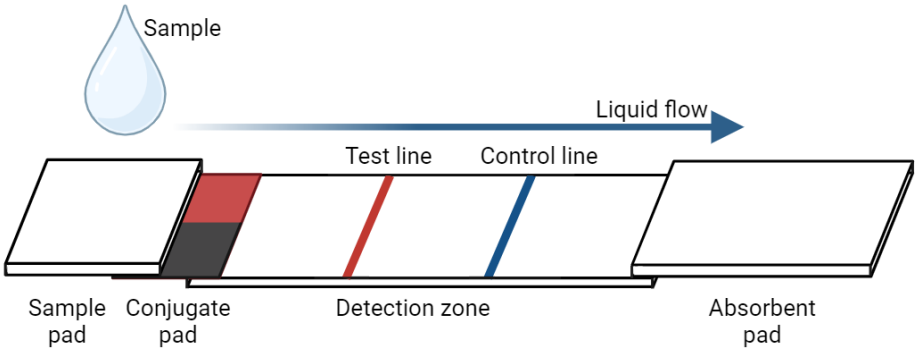


Figure 4.4. Scheme of the strip assembly, showing all the parts. The strip is composed by the different parts: i) sample pad, ii) conjugate pad containing the readout nanoparticles, being sAvAuNP or AvCNP represented as red and black in the scheme, iii) detection zone, containing the test and control line, and iv) absorbent pad. Created with Biorender.com.

After its integration into the strip as a signal generating system, their stability was assessed by evaluating test robustness over time in a humidity-controlled atmosphere. Over eight weeks, positive and negative control assays were conducted, and the intensity of the LFA strips was analyzed using ImageJ software. The results from the test-line analysis are shown in Figure 4.5, revealing no false positive signals in any of the negative test lines and no false negative signals throughout the entire assay performance. Positive controls were performed in all cases using double-tagged amplicon from transcripts of the same cDNA sample, aliquoted to ensure an equivalent transcript amount and prevent refreezing. The stability of LFAs was established for six weeks, and a statistically significant signal diminishment was observed from week eight onwards (Figure 4.5). LFAs were maintained in a humidity-controlled atmosphere during the assay procedures. However, it is important to highlight that this assay is not performed as optimization of the shelf life of the strips but for the robustness of the AvCNP generated, since they are not kept in dry conditions which are the usual conditions for commercialization and the optimal.

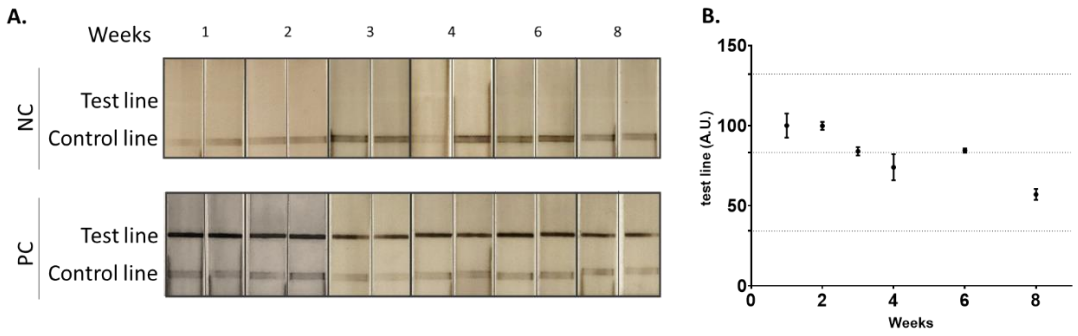


Figure 4.5. Stability assay for the determination of the stability of the AvCNP as a readout method after its incorporation into the LFA. Panel A. negative and positive LFA strips (NC and PC). Panel B. graphical representation of the intensity of the test lines of the positive controls during the 8 weeks assay. The error bars show the standard deviation for n=2. These values were obtained after the LFA photographed with a smart phone and the images processed with the ImageJ software. One replicate at week 5 was eliminated for an observable problem into the test line deposition.

Study of the analytical performance

PB100.2i cells were serially diluted, captured with antiCD3-MP, and directly lysed for mRNA extraction using oligo(dT)-MP. cDNA was further obtained by reverse transcription. Next, cDNA was amplified and double-tagged amplimers for the IFNγ were obtained, allowing its further detection through the sAvAuNP or AvCNP into the LFA. Fifteen minutes after dropping the amplified sample on top of the path sample, the results of the LFA were obtained, and images shown in Figure 4.6 were taken with a smartphone camera.

T cell culture

T cell clone PB100.2i was obtained by cloning the infiltrating T lymphocytes from a pancreatic donor organ[20] This clone was previously characterized and selected based on its IFNγ secretion. T cells were cultured with Iscove's Modified Dulbecco's Medium (IMDM) supplemented with 10% of complement inactivated Human Serum and 1% of penicillin/streptomycin. T-cell activation was done with IL-2 (80 U mL^{-1}) and Dynabeads™ Human T-Activator CD3/CD28 at a ratio of 1 cell:10 beads and maintained at 37°C and 5% CO_2. After 72h of stimulation, T cells were collected to perform the calibration plot[6].

To assess the analytical performance of the lateral flow assay for sAvAuNP and AvCNP, the limit of detection (LODs) for both approaches were calculated. For this, IFN-γ secreting T-cell clone PB100.2i cells were stimulated with anti-CD3 and anti-CD28 beads[6]. The

intensity of the lines from each lateral flow strip was processed by ImageJ software and the values were used to determine the differences in intensity obtained because of the dilutions in the processed cells. Areas under the peak obtained by the analysis tool were fitted into a non-linear regression curve (three parameters variable slope, R^2= 0.9827 and 0.9654 for sAvAuNP and AvCNP respectively) (Figure 4.6). The Limit of Detection (LOD) for the lateral flow assay was established at 695 cells for the AuNP readout and 1929 cells for the CNP. This determination was made by calculating the threshold as the sum of the negative value plus three times the standard deviation. However, the visual LOD for both methods would be determined at 10,000 cells. Even though the in-house produced CNP had a higher LOD compared to the gold standard AuNP, the signal obtained in the samples show intensities above 2500 AU. Thus, both detection LOD are suitable for the sample evaluation, being CNP a competitive readout method.

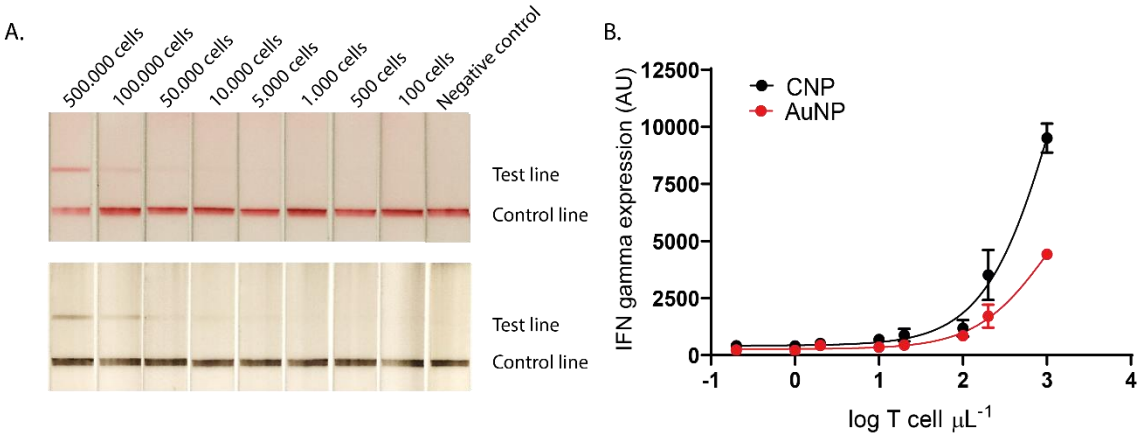


Figure 4.6. A. Lateral flow strips performed with streptavidin-modified AuNP (sAvAuNP) and avidin-modified CNP (AvCNP) using a range of stimulated cells between 500,000 and 100 cells. Negative control performed with a negative PCR sample B. Fitting of the values of the IFN-γ expression obtained with both readouts, sAvAuNP and AvCNP (n=3).

4.6.5. Detection of IFN-γ expression by lateral flow assay in whole blood samples. Optimization of the assay conditions

Prior of the whole blood samples performance of the assays the conditions were set up. First, the incubation time for the blood had to be set up. For that purpose, two different control samples were evaluated at different times comparing stimulated and non-stimulated conditions. For each condition 1 mL of whole blood was used. To simulate peptide stimulation, PMA in combination with ionomycin were used in suboptimal concentrations (PMA 10 ng mL^{-1} ionomycin 0.25 µg mL^{-1}). After the incubation time the

lymphocytes were captured with anti-CD3-MP and subsequently lysed. Moreover, the mRNA was captured with oligo (dT)-MP, washed and retrotranscribed, amplified through a PCR (x 28 cycles). The results obtained shown in the time course graphic of the production of the cytokine mRNA demonstrates that at 4h the increase of mRNA can be detected. These results were in concordance with the bibliography where it is described the time course of the mRNA production and accumulation after different stimulation methods[21,22]. The incubation time for the carry out of the subsequent experiments was determined to be 4h. Thus, compared with the gold standard methods for the detection of IFN-γ expression it means the reduction of the incubation time compared to them. This reduction was probably mainly produced for the detection of the mRNA instead of the protein which production and release was slower than the mRNA expression increasing.

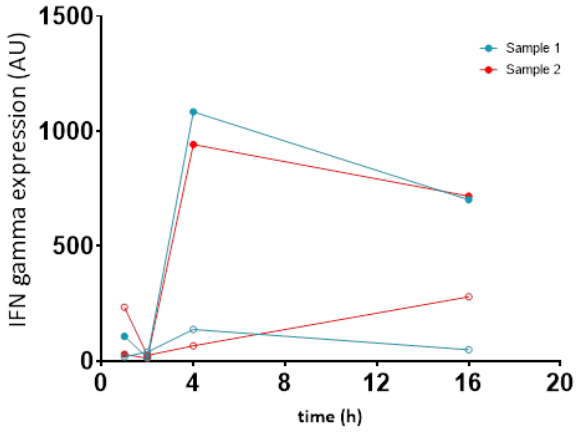


Figure 4.7. Time course evaluation of the IFN-γ expression levels obtained at different times ranged from 0 to 16 h of incubation. Values obtained through the analysis of the agarose gel performed after the PCR with the ImageJ software. The assay was carried out at different conditions (stimulated and non-stimulated) at different times (from 1 h to 16 h). Stimulated samples (with PMA and ionomycin) represented with full circles and the non-stimulated with empty open circles.

Optimization of the positive controls

For the validation of assay performance, a positive control must be conducted in parallel to determine lymphocyte activation capacity. Phytohemagglutinin (PHA) was employed for this purpose, as it is a mitogen known to stimulate cell division and cytokine synthesis. Various concentrations ranging from 0 to 10 µg mL^{-1} were tested. IFN-γ expression was normalized with GAPDH, a housekeeping gene, to mitigate bias arising from differences in cell quantity. As depicted in the results (Fig. 4.8), the concentration that induced the

highest expression of IFNγ was found to be 5 µg mL^{-1}. Consequently, this concentration was selected for further experiments as the positive control.

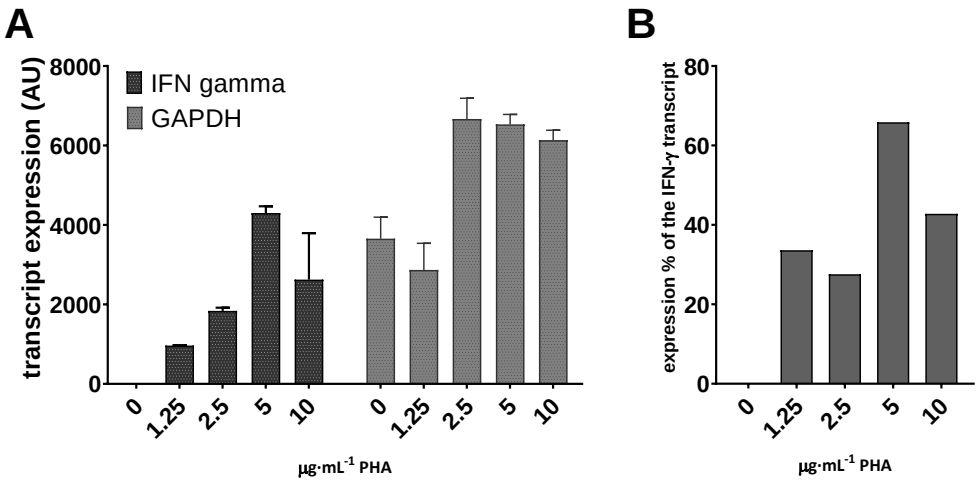


Figure 4.8. mRNA expression bar plot of the IFNγ and GAPDH amplimers. Data obtained through the analysis of a 2% agarose gel with the ImageJ software. Panel A. bar plot expression of IFNγ and GAPDH mRNAs culturing 400,000 cells per well after a 24h incubation at 37 ºC and 5% CO_2 with constant humidity, with different PHA conditions, concentrations ranged from 0 to 10 µg mL^{-1}. Panel B. relative expression bar plot of IFNγ regarding to GAPDH mRNA for each of the PHA concentration conditions.

Detection of IFNγ expression by lateral flow assay in PBMCs

Before of the carry out of the protocol with whole blood samples the stimulation with viral peptides was validated with PMBCs avoiding the complex matrix that the use of blood adds to the assay. PBMCs were obtained through a density gradient centrifugation. First, the blood was diluted 1-fold with PBS 1 X (100 mM). Once the blood was diluted it was gently poured, avoiding the mix between the blood and the gradient centrifugation medium (Lymphoprep, ref 07801, Stem Cell technologies). The proportion between Lymphoprep and diluted blood was 1:3. Then, the sample was centrifuged during 30 minutes at 600 *g* and RT without acceleration or break. After the centrifugation, the different blood components could be observed into the tub. At the bottom the erythrocytes and granulocytes were deposited, the Lymphoprep solution upon them, in the middle part a white ring containing the PBMCs was observed, and the plasma above all. The PBMCs ring must be aspired with a pipette and transferred into a clean tube with PBS 100 mM to wash them. After two washing 15 minutes centrifugations at 200 *g*, the

cells can be resuspended into preheated IMDM medium, counted, and seeded for further experiments.

Once their obtention was performed, they were quantified and 400,000 cells per well incubated during 4 hours at three different conditions (without stimulation, PHA stimulation 5 µg mL^{-1} and stimulation with spike COVID derived peptide 1 µg mL^{-1}). Three donors recently infected were evaluated and their IFNγ expression was determined (COV02.01, 02, 03 with antigen negative tests 1, 14 and 7 days before the sample collection respectively). The results show the activation of the T specific cells against the peptides represented as a higher expression of the IFNγ compared to the basal expression.

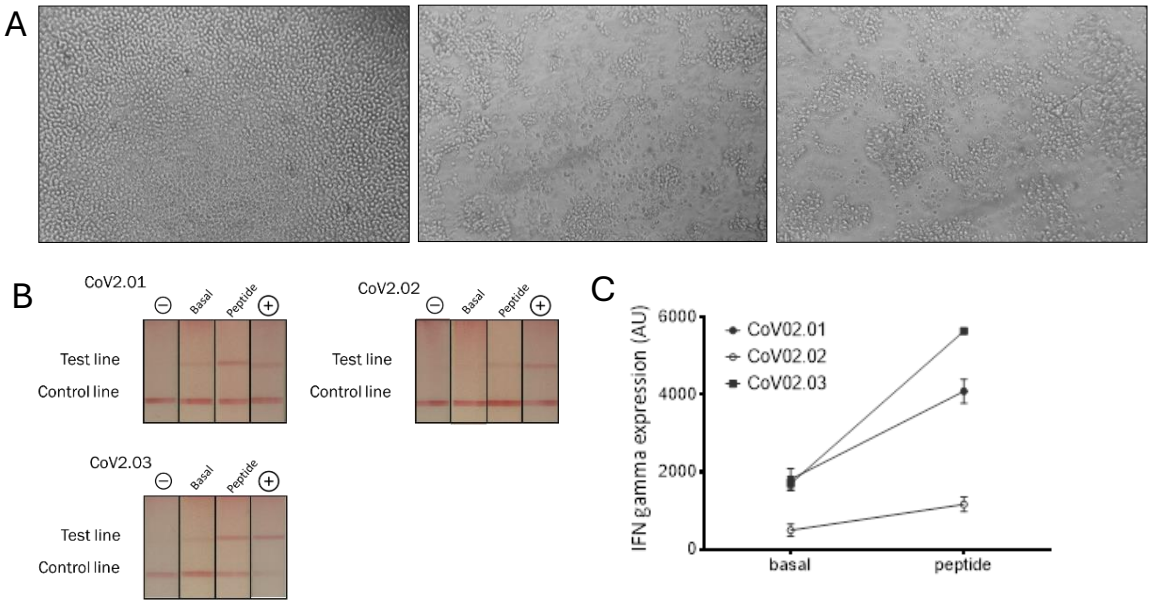


Figure 4.9. Panel A. pictures of the PBMCs after 4 h incubation from left to right first the PBMCs incubated without stimulation, the ones incubated with PHA and the peptide incubated. Panel B. LFA pictures of the three individuals for the different conditions, a negative and a positive control, the basal expression and the expression after the incubation with the SARS-COV-2 derived peptides. Panel C. comparative of the expression levels between the basal and the peptide stimulated. Results obtained through the image processing with the Image J software. The error bars show the standard deviation for n=2.

4.6.6. Rapid diagnostic test for the assessment of cellular immune response

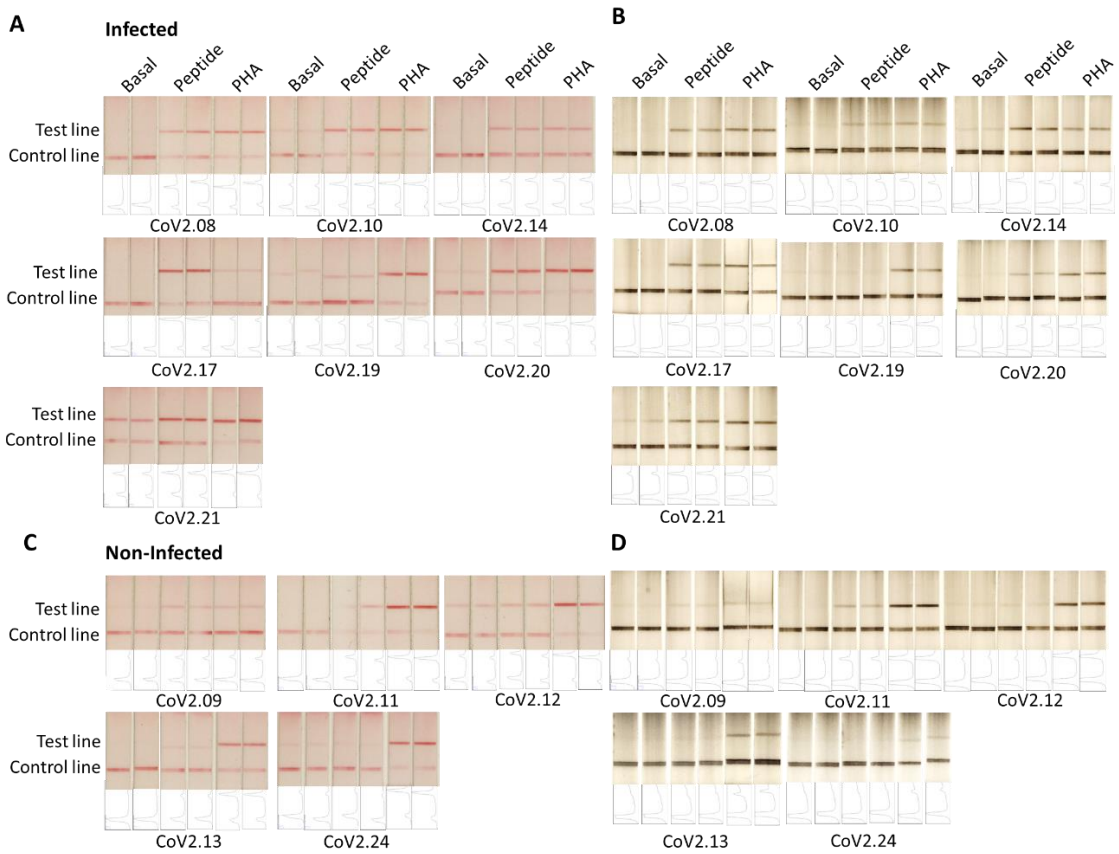


Figure 4.10. LFA images of the infected (Panels A and B) and the no-infected (Panels C and D) individuals using the sAvAuNP (Panels A and C) and the AvCNP (Panels B and D) as readout methods. For each individual, different conditions have been evaluated including the basal expression using non-stimulated samples, a positive control stimulating the samples with PHA and a sample stimulated with SARS-CoV-2 derived peptides (S and N) (n = 2).

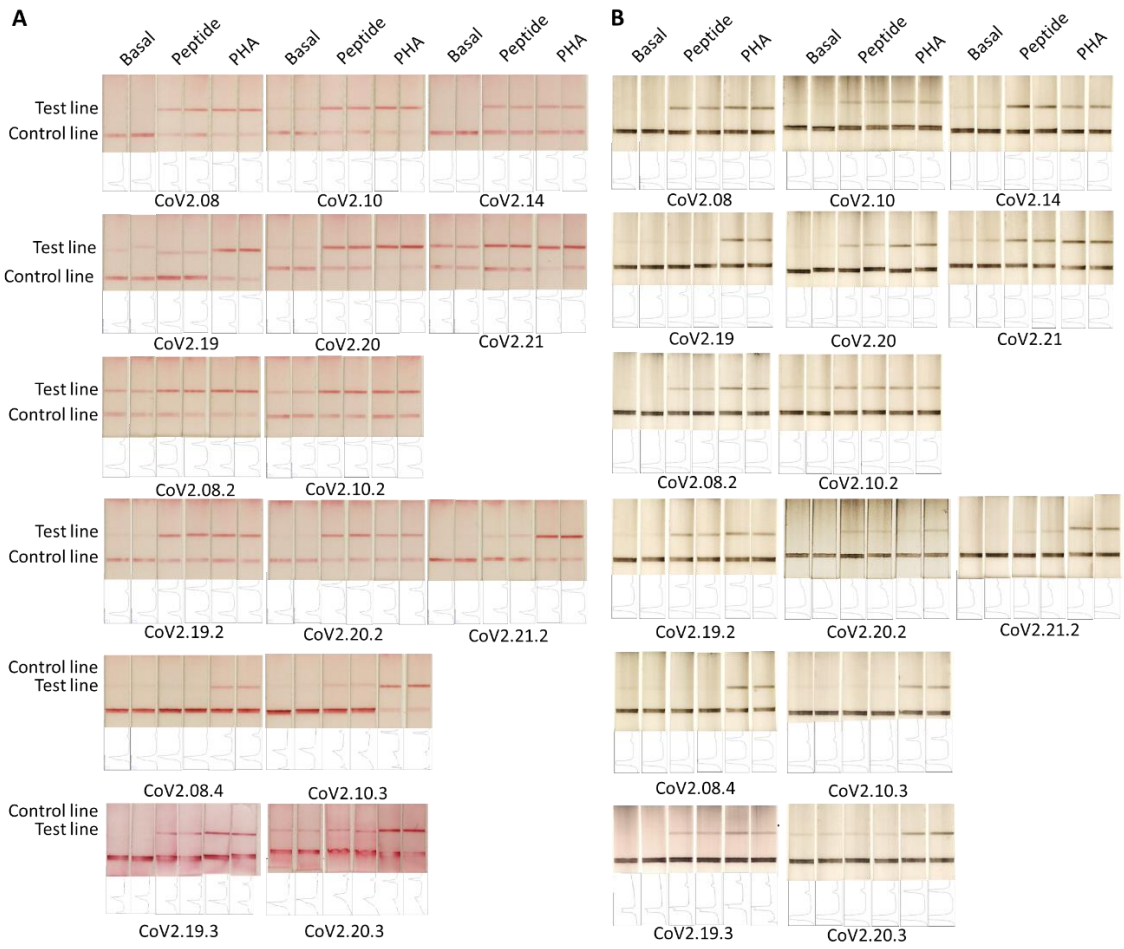


Figure 4.11. LFA images of the follow up of each infected individuals using the AuNP (Panel A) and the CNP (Panel B) as readout methods. For each individual, different conditions were evaluated including the basal expression using non-stimulated samples, a positive control (by stimulating the samples with PHA) and a sample stimulated with SARS-CoV-2 derived peptides (S and N) (n = 2).

4.6.7. Statistical analysis

The ANOVA test performed for the determination of the differences between the infected and vaccinated (Infected) and the vaccinated but not infected (Non-Infected) is summarized in the following Table 4.2 for both signal generating systems. With a significance of 95%.

Table 4.2. One-way ANOVA test multiple comparisons result for both detection methods.

	Streptavidin-AuNP		**Avidin-CNP**	
	Adjusted P value	**Summary**	**Adjusted P value**	**Summary**
Basal Infected vs Peptide Infected	<0.0001	****	0,0004	***
Basal Infected vs Basal Non-Infected	>0.9999	ns	0,9999	ns
Basal Infected vs PHA Infected	<0.0001	****	<0.0001	****
Basal Non-Infected vs Peptide Non-Infected	0.4436	ns	0,6493	ns
Peptide infected vs Peptide Non-Infected	0.0018	**	0,0109	*
Basal No-Infected vs PHA Non-Infected	<0.0001	****	0.0001	***

For the same set of values, a Student's *t*-test was conducted to assess whether individual results correlated with the group tendency.

Table 4.3. Student's *t*-test results for both detection methods and groups.

	Streptavidin-AuNP		**Avidin-CNP**	
	Adjusted P value	**Summary**	**Adjusted P value**	**Summary**
Infected	0,0031	**	0,0171	*
Non-Infected	0,0747	ns	0,1478	ns

The results of the one-way ANOVA for the follow-up of the individuals was summarized in the Table 4.4.

Table 4.4. One-way ANOVA test multiple comparisons result for both detection methods.

	Streptavidin-AuNP		**Avidin-CNP**	
	Adjusted P value	**Summary**	**Adjusted P value**	**Summary**
0 months; Basal vs Peptide S and N	0,0011	**	0,0243	*
0 months; Basal vs PHA	0.0003	***	<0.0001	****
2 months; Basal vs Peptide S and N	0,0006	***	0,0180	*
2 months; Basal vs PHA	0.0003	***	<0.0001	****
8 months; Basal vs Peptide S and N	0,9655	ns	0,9935	ns
8 months; Basal vs PHA	0.0031	**	0.0004	***

Moreover, the results of the Student's *t*-test were summarized in the following table 4.5.

Table 4.5. Student's *t*-test results for the all the time points.

	Streptavidin-AuNP		Avidin-CNP	
Basal vs Peptide S and N	**Adjusted P value**	**Summary**	**Adjusted P value**	**Summary**
0 months	0,0325	*	0,0263	*
2 months	0,0090	**	0,0454	*
8 months	0,2337	ns	0,3895	ns

4.6.8. Future perspectives

For the reduction of assay time and handling, aiming to provide faster and more robust results, a one-step reverse transcription PCR (SuperScript™ IV One-Step RT-PCR System, ref: 12594025) was used. The assay performance was conducted in parallel with the standard methodology using samples COV2.08.02, CoV2.20.2, COV2.15.3, COV2.19.3, and COV2.08.3. Preliminary results from the analysis of five samples were obtained, indicating no significant differences in the signal ratio (peptide N and S stimulation vs. basal expression) between the samples analyzed with the previously presented protocol and the one-step RT-PCR approach (statistical analysis performed using Student's t-test at the 95% significance level). Further analysis, including a larger number of samples, should be performed.

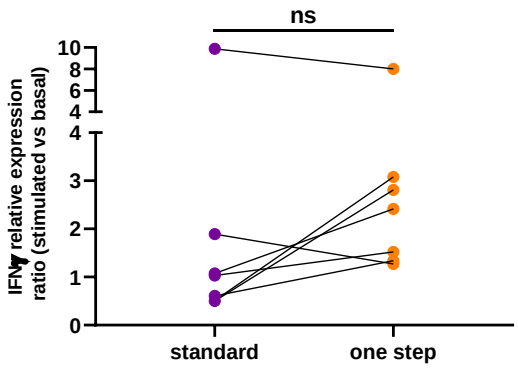


Figure 4.11. Comparative between the IFNγ ratio of the stimulated with peptides N and S and the basal expression of the standard method previously presented and the one-step RT-PCR procedure. The graphic shows the result for Student's t-test at the 95% significance level, in order to evaluate the performance of each individual.

4.6.9. Interferon gamma release assays

Interferon gamma release assays (IGRA) are blood tests used for the detection of the cell-mediated immune response against specific pathogens. They are mainly based for the detection of latent tuberculosis, but it can be used for different pathogens which its immunogenic derived peptides are available. For this purpose, there are two commercial tests approved for the FDA available, but there are also alternative assays being developed overcoming the limitations that these tests have. Both commercial tests are developed for the tuberculosis detection.

The two commercial tests are QuantiFERON®-TB Gold Plus (QFT-Plus) and T-SPOT®.*TB* test (T-Spot). QFT-Plus (Qiagen, The Netherlands) is based on the IFNγ release from previously sensitized lymphocytes. TB derived peptides (from ESAT-6 and CFP-10 proteins) are coating the tubes where whole blood samples are deposited activating the specific previously mentioned cells. The kit also provides a negative control tube and a positive control tube containing PHA. The samples are then incubated between 16 to 24 h and the plasma collected for the released IFNγ detection by ELISA. Due to the SARS-CoV-2 pandemic Qiagen has adapted their kit to a QuantiFERON SARS-CoV-2 RUO which nowadays is only available for research purposes. It uses a mix of SARS-CoV-2 peptides and the protocol performed is the same as the QuantiFERON®-TB Gold Plus with 16 to 24 h of incubation.

On the other hand, there is the T-SPOT®.is an enzyme linked immunospot that determines the number of IFNγ producing cells. It is based in the specific lymphocytes' stimulation with pathogenic derived peptides previously separated and deposited into a membrane. Since these membranes are precoated with antiIFNγ when the cells release the cytokine, this is going to get attached near the producing cell. The number of cultured cells is known to determine the concentration of IFNγ producing cells. In this assay there is a positive and a negative control but differently of the QFT-Plus there is not a mix of peptides. Instead, each peptide mix was deposited into a different well.

The SARS-CoV-2 pandemic has highlighted the need of these assays for the immune response evaluation and novel detection methods have been developed. One of the most used strategies is the cytokine detection through intracellular flow cytometry. Briefly, the stimulation protocol is similar to the protocol used by QFT-Plus using whole blood samples

and incubating them with pathogen derived peptides but also adding Brefeldin A to avoid the release of the cytokines and Fastimmune™ CD28/CD49d cocktail (BD Bioscience®) as a costimulatory signal, allowing shorter incubation times (6h). Once the samples are stimulated, the red blood cells are lysed, and the lymphocytes stained with extracelullar and intracellular markers. The gating strategy for the sample analysis is different in each study, nevertheless all start with a CD3 selection for the lymphocyte selection and a CD8 and a CD4 separation. As well as the flow cytometry approach also, electrochemical approaches have been developed. However, even though the detection devices have been developed they have not been validated with real samples.

Table 4.6. Comparison of the main characteristics of commercial test available, the previous developed test in our group, the flow cytometry methodology and our current developed test.

	QuantiFERON®-TB Gold Plus	***T-SPOT®.***	***Flow cytometry IFNγ detection***	***IFNγ transcript detection on T cells based on electrochemical genosensing (previous work)***	***LFA for specific activated T cells detection (this work)***
Target	IFNγ protein released	IFNγ protein released by previously separated PBMCs	Intracellular IFNγ protein	IFNγ transcripts	IFNγ transcripts
Readout technology	ELISA	ELISPOT	Flow cytometry	magneto-actuated biosensors with electrochemical readout	Paper-based LFA
Sample	Whole blood. Up to 4 mL (1 mL per tube)	Whole blood requiring the PBMCs isolation	Whole blood. Between 250 µL to 1 mL per tube depending on the protocol	Whole blood. 100 µL per tube requiring immunomagnetic separation with antiCD3-MP	Whole blood. Up to 3 mL (1 mL per tube) requiring immunomagnetic separation with antiCD3-MP
Incubation time	16 – 24 h	16 – 20 h	5-6 h	48 h (with high expression / lower times were no tested)	4 h
Assay time	~ 4 h	~ 2 h	~ 2 h	3 h	3h
Information provided by the test	Concentration of IFNγ protein released	Number of IFNγ producing cells	Number of IFNγ producing cells (depending on the gating can be more specific populations)	IFNγ transcript concentration produced by cells	IFNγ expression (semi-quantitative)
Equipment required	Centrifuge and spectrophotometer	Centrifuge and spectrophotometer	Centrifuge and flow cytometer	Thermocycler and amperometric controller	Thermocycler and paper-based LFA

4.7. References

(1) Vivier, E.; Malissen, B. Innate and Adaptive Immunity: Specificities and Signaling Hierarchies Revisited. *Nat. Immunol.* **2005**, *6* (1), 17–21. https://doi.org/10.1038/ni1153.

(2) Natoli, G.; Ostuni, R. Adaptation and Memory in Immune Responses. *Nat. Immunol.* **2019**, *20* (7), 783–792. https://doi.org/10.1038/s41590-019-0399-9.

(3) Roche, P. A.; Furuta, K. The Ins and Outs of MHC Class II-Mediated Antigen Processing and Presentation. *Nat. Rev. Immunol.* **2015**, *15* (4), 203–216. https://doi.org/10.1038/nri3818.

(4) Lin, Q.; Rong, L.; Jia, X.; Li, R.; Yu, B.; Hu, J.; Luo, X.; Badea, S. R.; Xu, C.; Fu, G.; Lai, K.; Lee, M. chun; Zhang, B.; Gong, H.; Zhou, N.; Chen, X. L.; Lin, S. hai; Fu, G.; Huang, J. D. IFN-γ-Dependent NK Cell Activation Is Essential to Metastasis Suppression by Engineered Salmonella. *Nat. Commun.* **2021**, *12* (1), 1–15. https://doi.org/10.1038/s41467-021-22755-3.

(5) Egri, N.; Olivé, V.; Hernández-Rodríguez, J.; Castro, P.; De Guzman, C.; Heredia, L.; Segura, A. C.; Fernandez, M. D.; de Moner, N.; Torradeflot, M.; Ballús, J.; Martinez, R.; Vazquez, M.; Costa, M. V.; Dobaño, C.; Mazza, M.; Mazzotti, L.; Pascal, M.; Juan, M.; González-Navarro, E. A.; Calderón, H. CoVITEST: A Fast and Reliable Method to Monitor Anti-SARS-CoV-2 Specific T Cells From Whole Blood. *Front. Immunol.* **2022**, *13*, 848586. https://doi.org/10.3389/fimmu.2022.848586.

(6) Carinelli, S.; Xufré, C.; Martí, M.; Pividori, M. I. Interferon Gamma Transcript Detection on T Cells Based on Magnetic Actuation and Multiplex Double-Tagging Electrochemical Genosensing. *Biosens. Bioelectron.* **2018**, *117*, 183–190. https://doi.org/10.1016/j.bios.2018.05.030.

(7) Combadiere, B.; Boissonnas, A.; Carcelain, G.; Lefranc, E.; Samri, A.; Bricaire, F.; Debre, P.; Autran, B. Distinct Time Effects of Vaccination on Long-Term Proliferative and IFN-γ-Producing T Cell Memory to Smallpox in Humans. *J. Exp. Med.* **2004**, *199* (11), 1585–1593. https://doi.org/10.1084/jem.20032083.

(8) Arnaboldi, P. M.; D'Arco, C.; Hefter, Y.; Nolan, S.; Jobe, D. A.; Callister, S. M.; Dattwyler, R. J. Detection of IFN-ΓSecretion in Blood Samples Collected before and after Treatment of Varying Stages of Lyme Disease. *Clin. Infect. Dis.* **2021**, *73* (8), 1484–1491. https://doi.org/10.1093/cid/ciab503.

(9) Mutnal, M. B.; Hu, S.; Little, M. R.; Lokensgard, J. R. Memory T Cells Persisting in the Brain Following MCMV Infection Induce Long-Term Microglial Activation via Interferon-γ. *J. Neurovirol.* **2011**, *17* (5), 424–437. https://doi.org/10.1007/s13365-011-0042-5.

(10) Whitman, J. D.; Hiatt, J.; Mowery, C. T.; Shy, B. R.; Yu, R.; Yamamoto, T. N.; Rathore, U.; Goldgof, G. M.; Whitty, C.; Woo, J. M.; Gallman, A. E.; Miller, T. E.; Levine, A. G.; Nguyen, D. N.; Bapat, S. P.; Balcerek, J.; Bylsma, S. A.; Lyons, A. M.; Li, S.; Wong, A. W. yi; Gillis-Buck, E. M.; Steinhart, Z. B.; Lee, Y.; Apathy, R.; Lipke, M. J.; Smith, J. A.; Zheng, T.; Boothby, I. C.; Isaza, E.; Chan, J.; Acenas, D. D.; Lee, J.; Macrae, T. A.; Kyaw,

T. S.; Wu, D.; Ng, D. L.; Gu, W.; York, V. A.; Eskandarian, H. A.; Callaway, P. C.; Warrier, L.; Moreno, M. E.; Levan, J.; Torres, L.; Farrington, L. A.; Loudermilk, R. P.; Koshal, K.; Zorn, K. C.; Garcia-Beltran, W. F.; Yang, D.; Astudillo, M. G.; Bernstein, B. E.; Gelfand, J. A.; Ryan, E. T.; Charles, R. C.; Iafrate, A. J.; Lennerz, J. K.; Miller, S.; Chiu, C. Y.; Stramer, S. L.; Wilson, M. R.; Manglik, A.; Ye, C. J.; Krogan, N. J.; Anderson, M. S.; Cyster, J. G.; Ernst, J. D.; Wu, A. H. B.; Lynch, K. L.; Bern, C.; Hsu, P. D.; Marson, A. Evaluation of SARS-CoV-2 Serology Assays Reveals a Range of Test Performance. *Nat. Biotechnol.* **2020**, *38* (10), 1174–1183. https://doi.org/10.1038/s41587-020-0659-0.

(11) Yazdanpanah, F.; Hamblin, M. R.; Rezaei, N. The Immune System and COVID-19: Friend or Foe? *Life Sci.* **2020**, *256*, 117900. https://doi.org/10.1016/j.lfs.2020.117900.

(12) Brodin, P. Immune Determinants of COVID-19 Disease Presentation and Severity. *Nat. Med.* **2021**, *27* (1), 28–33. https://doi.org/10.1038/s41591-020-01202-8.

(13) Dan, J. M.; Mateus, J.; Kato, Y.; Hastie, K. M.; Yu, E. D.; Faliti, C. E.; Grifoni, A.; Ramirez, S. I.; Haupt, S.; Frazier, A.; Nakao, C.; Rayaprolu, V.; Rawlings, S. A.; Peters, B.; Krammer, F.; Simon, V.; Saphire, E. O.; Smith, D. M.; Weiskopf, D.; Sette, A.; Crotty, S. Immunological Memory to SARS-CoV-2 Assessed for up to 8 Months after Infection. *Science.* **2021**, *371* (6529), eabf4063. https://doi.org/10.1126/science.abf4063.

(14) Zuo, J.; Dowell, A. C.; Pearce, H.; Verma, K.; Long, H. M.; Begum, J.; Aiano, F.; Amin-Chowdhury, Z.; Hallis, B.; Stapley, L.; Borrow, R.; Linley, E.; Ahmad, S.; Parker, B.; Horsley, A.; Amirthalingam, G.; Brown, K.; Ramsay, M. E.; Ladhani, S.; Moss, P. Robust SARS-CoV-2-Specific T Cell Immunity Is Maintained at 6 Months Following Primary Infection. *Nat. Immunol.* **2021**, *22* (5), 620–626. https://doi.org/10.1038/s41590-021-00902-8.

(15) Guo, L.; Wang, G.; Wang, Y.; Zhang, Q.; Ren, L.; Gu, X.; Huang, T.; Zhong, J.; Wang, Y.; Wang, X.; Huang, L.; Xu, L.; Wang, C.; Chen, L.; Xiao, X.; Peng, Y.; Knight, J. C.; Dong, T.; Cao, B.; Wang, J. SARS-CoV-2-Specific Antibody and T-Cell Responses 1 Year after Infection in People Recovered from COVID-19: A Longitudinal Cohort Study. *The Lancet Microbe* **2022**, *3* (5), e348–e356. https://doi.org/10.1016/S2666-5247(22)00036-2.

(16) Sherina, N.; Piralla, A.; Du, L.; Wan, H.; Kumagai-Braesch, M.; Andréll, J.; Braesch-Andersen, S.; Cassaniti, I.; Percivalle, E.; Sarasini, A.; Bergami, F.; Di Martino, R.; Colaneri, M.; Vecchia, M.; Sambo, M.; Zuccaro, V.; Bruno, R.; Sachs, M.; Oggionni, T.; Meloni, F.; Abolhassani, H.; Bertoglio, F.; Schubert, M.; Byrne-Steele, M.; Han, J.; Hust, M.; Xue, Y.; Hammarström, L.; Baldanti, F.; Marcotte, H.; Pan-Hammarström, Q. Persistence of SARS-CoV-2-Specific B and T Cell Responses in Convalescent COVID-19 Patients 6–8 Months after the Infection. *Med* **2021**, *2* (3), 281-295.e4. https://doi.org/10.1016/j.medj.2021.02.001.

(17) Le Bert, N.; Clapham, H. E.; Tan, A. T.; Chia, W. N.; Tham, C. Y. L.; Lim, J. M.; Kunasegaran, K.; Tan, L. W. L.; Dutertre, C. A.; Shankar, N.; Lim, J. M. E.; Sun, L. J.; Zahari, M.; Tun, Z. M.; Kumar, V.; Lim, B. L.; Lim, S. H.; Chia, A.; Tan, Y. J.; Tambyah,

P. A.; Kalimuddin, S.; Lye, D.; Low, J. G. H.; Wang, L. F.; Wan, W. Y.; Hsu, L. Y.; Bertoletti, A.; Tam, C. C. Highly Functional Virus-Specific Cellular Immune Response in Asymptomatic SARS-CoV-2 Infection. *J. Exp. Med.* **2021**, *218* (5). https://doi.org/10.1084/JEM.20202617.

(18) Porras, J. C.; Bernuz, M.; Marfa, J.; Pallares-rusiñol, A.; Martí, M.; Pividori, M. I. Comparative Study of Gold and Carbon Nanoparticles in Nucleic Acid Lateral Flow Assay. *Nanomaterials* **2021**, *11* (3), 1–11. https://doi.org/10.3390/nano11030741.

(19) van Amerongen, A.; Wichers, J. H.; Berendsen, L. B. J. M.; Timmermans, A. J. M.; Keizer, G. D.; van Doorn, A. W. J.; Bantjes, A.; van Gelder, W. M. J. Colloidal Carbon Particles as a New Label for Rapid Immunochemical Test Methods: Quantitative Computer Image Analysis of Results. *J. Biotechnol.* **1993**, *30* (2), 185–195. https://doi.org/10.1016/0168-1656(93)90112-Z.

(20) Xufré, C.; Costa, M.; Roura-Mir, C.; Codina-Busqueta, E.; Usero, L.; Pizarro, E.; Obiols, G.; Jaraquemada, D.; Martí, M. Low Frequency of GITR+ T Cells in Ex Vivo and in Vitro Expanded Treg Cells from Type 1 Diabetic Patients. *Int. Immunol.* **2013**, *25* (10), 563–574. https://doi.org/10.1093/intimm/dxt020.

(21) Fan, J.; Nishantan, P.; Breen, E. C.; Mcdonald, M.; Fahey, J. L. Cytokine Gene Expression in Normal Human Lymphocytes in Response to Stimulation. *Clin. Diagn. Lab. Immunol.* **1998**, *5* (3), 335–340. https://doi.org/10.1128/cdli.5.3.335-340.1998.

(22) Radke, L.; López Hemmerling, D. A.; Lubitz, A.; Giese, C.; Frohme, M. Induced Cytokine Response of Human PMBC-Cultures: Correlation of Gene Expression and Secretion Profiling and the Effect of Cryopreservation. *Cell. Immunol.* **2012**, *272* (2), 144–153. https://doi.org/10.1016/j.cellimm.2011.10.018.

Chapter 5.

Detection and characterization of neuroblastoma exosomes by magneto-actuated immunoassay for Alzheimer's Disease diagnosis

5.1. Abstract

Alzheimer's disease (AD) is the most prevalent neurodegenerative disorder associated with dementia, constituting a significant global health concern. It is characterized by cognitive and functional decline and has two main pathological hallmarks; extracellular amyloid plaques and intracellular tau tangles, which eventually drives into neuronal dysfunction and cell death. The challenge lies in the fact that these pathological changes precede clinical symptoms. Thus, early detection before cognitive decline should be crucial for its diagnosis and its effective treatment. Current approaches, like the AT(N) system, focus on biomarkers as well as cognitive evaluation allowing a classification of the patients, however, approaches involving less invasive procedures are being explored. Neuron-derived exosomes, small vesicles carrying specific markers, including proteins and nucleic acids, have emerged as promising AD biomarkers due to its cargo relation with their oncoming cells. In addition, exosomes are able to cross the blood-brain barrier, offering the possibility of being obtained from liquid biopsies.

This study develops a magneto-actuated immunoassay for detecting neuron-derived exosomes as a minimally invasive approach for central nervous system information obtention. The proposed AD biomarker, β-secretase (BACE1), is involved in amyloid plaque formation, thus, explored for its potential as a screening test for AD. The method involves a magnetic capture with functionalized magnetic particles with antibodies against neuronal markers to preconcentrate neuron-derived exosomes, offering a potential approach for AD diagnosis and screening.

5.2. Introduction

Alzheimer's disease (AD) is a neurodegenerative condition causing the 60-70% of the dementia cases according to World Health Organization (WHO). AD was first described by Alois Alzheimer in 1907[1] (for the English translation[2]) and it is characterized by a cognitive and functional decline. It is distinguished from other dementias by two pathological hallmarks: a) extracellular accumulation of amyloid plaques, mainly formed by amyloid-β peptide, and b) intracellular tangles formed by hyperphosphorylated tau protein[3]. Amyloid plaques, in addition to tau tangles, lead to neuronal disfunction and eventually to cell death. Pathological changes occur long before the appearance of the earliest clinical

symptoms. However, the number of the amyloid plaques present in the brain do not always correlate with the degree of cognitive impairment[4].

In AD, as in most of the diseases, the pathology does not only arise from a single cause. Even though most of the cases have a sporadic etiology, there are familiar forms leaded by autosomal dominant mutations on mainly three gens involved in formation of the amyloid plaques (amyloid precursor protein (APP), presenilin 1 (PSEN1) and presenilin 2 (PSEN2)). Moreover, the familiar form of the AD is characterized by an early onset compared to the sporadic form[5,6].

Currently available AD treatments as cholinesterase inhibitors However, these therapies are not able to reverse the neuronal degeneration but to modify its progression. Hence, an early detection before the cognitive decline appearance is critical for a timely and successful treatment[7].

Due to the symptomatic similarities of the AD with other types of dementias, the differential diagnosis between them is the major handicap in the clinics. Moreover, they are usually diagnosed at later stages when treatments are less effective[8]. Thus, even though the clinical symptom-based diagnosis, new approaches are committed to earlier and more accurate diagnosis criteria. Nowadays, individuals are being categorized by the AT(N) system (amyloid-β (Aβ) pathway (A), tau-mediated pathophysiology (T) and neurodegeneration (N)), which combines seven main AD pathophysiological biomarkers from which 3 binary combinations are defined[9]. These criteria has been in constant revision since it was proposed. Nowadays, the measure of the Aβ is determined by the aβ42 to aβ40 ratio with higher concordance with the amyloid pathway dyshomeostasis and the results shown with the amyloid PET. The total Tau and the neurofilament light chain indicated neuron degeneration[3]. Nevertheless, it serves more as a classification method than a diagnostic framework. Which make it important to keep researching for new biomarkers for an accurate and early diagnosis, and less invasive procedures to achieve population screening such as neurogranin[10], miRNAs[11,12], among others. Plasma biomarkers have been studied in deep, as soluble proteins or miRNAs profiling among others[13], but neuron-derived exosomes, due to their characteristics, have been recently proposed as suitable candidate biomarkers for AD diagnosis[14].

Exosomes are small bilipid nanovesicles with a diameter between 30-200 nm secreted by mainly all cell types, including central nervous system cells. They come from multivesicular bodies and are present in biological fluids as blood, saliva, urine, cerebrospinal fluid (CSF), among others[15,16]. These vesicles were first believed to be cellular waste resulting from cell damage, or products of cell homeostasis with no significant biological function, but it has been described that nanovesicles are involved in cell-to-cell communication and can carry active molecules to proximal and distal cells of the body[17]. Exosomes carry specific markers such as proteins related to transport and fusion (e.g., flotillin, caveolin-1), proteins involved in exosome release (e.g., Alix, TSG101), tetraspanins (e.g., CD81, CD63, CD9), heat shock proteins (e.g., Hsp90), lipid-related proteins and nucleic acids (e.g., microRNAs, messenger RNAs or DNA)[18]. Besides, during their biogenesis, their cargo can acquire cell-derived molecules (including proteins and nucleic acids). For this reason, exosomes can be considered a multiplexed biomarker as they carry specific markers that indicate certain cell signature. Moreover, exosomes are known to pass the blood-brain barrier (BBB) allowing the putative prediction of neuron information on plasma, opening the possibility of using minimally invasive procedures as liquid biopsies[19].

In this chapter, a magneto-actuated immunoassay for the detection of neuron-derived exosomes (NDE) was developed for the AD diagnosis. The design consists in the use of magnetic particles functionalized with antibodies against neuronal markers to preconcentrate NDE from different samples including biological fluids as plasma or serum. This protocol allows the use of a minimally invasive procedure for the obtention of central nervous system information. For this purpose, the magneto-actuated immunoassay was set up using the exosomes from a neuroblastoma cell line that were first purified for their further use as a model for the capture and detection of AD related biomarkers.

The potential novel AD biomarker used in this study was β-secretase (BACE1), which was selected due its implication in the amyloid plaque formation (Figure 5.1). BACE1 is a transmembrane enzyme involved in the Aβ peptides formation through the cleavage of the amyloid precursor protein (APP) together with the γ-secretase[20,21]. This is an alternative processing of the APP which is more frequently cleaved by α-secretase together with γ-secretase. Moreover, it is located in the cellular membrane but also into the endosomal compartments being possibly expressed in the exosomes membranes[21]. In

addition, the BACE1 overexpression in AD and mild cognitive impairment (MCI), has been previously described in the literature[22–24]. Because of that, the detection of BACE1 on NDE is a promising biomarker for the development of a screening test for AD.

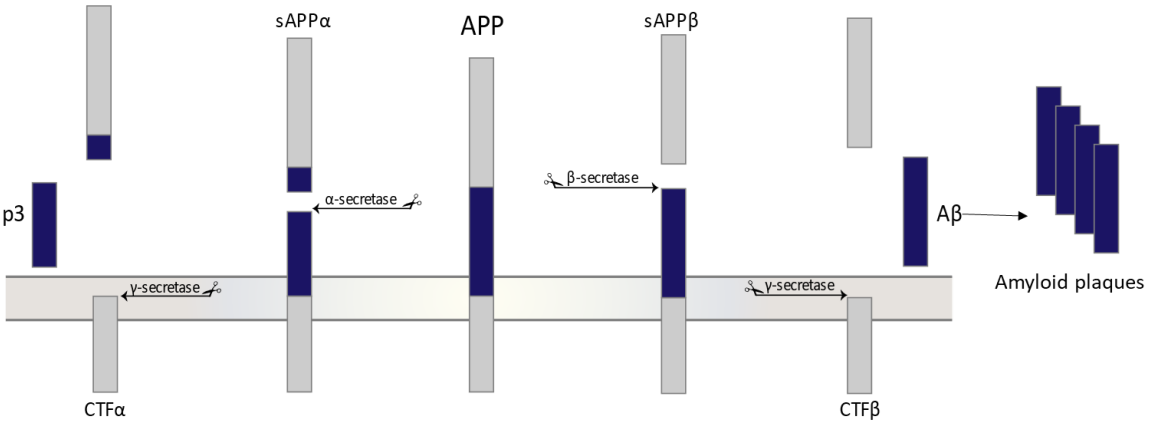


Figure 5.1. Graphical abstract of the cleavage variations of the APP protein through different secretase isoforms and the amyloid plaques formation.

5.3. Experimental

5.3.1. Instrumentation

The exosome ultracentrifugation was performed using the ultracentrifuge Beckman Coulter OptimaTM L-80XP. Nanoparticle tracking analysis (NTA) was performed using the NanoSight LM10- HS system (NanoSight Ltd, Malvern, GB). The cryogenic transmission electron microscopy (CryoTEM) images were collected by a Jeol JEM 2011 (JEOL USA Inc., MA, US) microscope. Flow cytometry were performed using BD FACSCANTO II (BD Biosciences, NJ, US) equipment and the cytometer for the direct exosomes acquisition was performed with MacsQuant 10 (Miltenyi Biotec). Mean Fluorescence Intensity (MFI) and beads count data were obtained by FlowJo analysis software (FlowJo LLC, BD Biosciences). Magnetic separation was performed with a magnetic separator DynaMag™-96 Side Skirted Magnet (ref. 12027, Thermo Fisher Scientific). Optical measurements were performed on the spectrophotometer (Infinite F50) purchased from Tecan (Männedorf, CH) microplate reader with Magellan v7.0 software.

5.3.2. Chemicals and biochemicals

For cell culture the following reagents were purchased, Dulbecco's Modified Eagle Medium (DMEM, ref. 31966-047, Thermo Fisher Scientific) medium, fetal bovine serum

(FBS, ref. 12007C, Sigma-Aldrich) and penicillin-streptomycin (ref. 15140122, Thermo Fisher Scientific). Tosylactivated magnetic particles (MPs) (Dynabeads M450 Tosylactivated, ref. 14013) were purchased from Thermo Fisher Scientific (Waltham, MA, US). All the antibodies purchased are listed in Table 5.1 below. For the optical readout, Pierce™ TMB Substrate Kit (Ref. 34021) was purchased from Thermo Fisher. Polypropylene and polystyrene plates were purchased from Costar and Nunc (Maxisorp, Roskilde, Denmark) respectively. The ELISA plates (Nunc MaxiSorp™ flat-bottom Ref. 44-2404-21) were purchased from Invitrogen.

All buffer and solutions were prepared with ultrapure water and all other reagents were in analytical reagent grade (supplied from Sigma Aldrich, St. Louis, MO, USA), and the composition are described in § 5.7.1 (Supp. data).

Table 5.1. Summary of the antibodies used in this study.

Antibody	Target	Clonality	Conjugate	Host	Source	Reference
Anti-CD81	CD81	Monoclonal	No	Mouse	Thermo Fisher	10630D
Anti-CD81	CD81	Polyclonal	No	Rabbit	Sigma	HPA007234
Anti-CD63	CD63	Monoclonal	No	Mouse	Thermo Fisher	10628D
Anti-CD63	CD63	Polyclonal	No	Rabbit	Abcam	Ab68418
Anti-CD63-HRP	CD63	Monoclonal	HRP	Mouse	Novus Biologicals	NBP2-42225H
Anti-CD63-PE	CD63	Monoclonal	PE	Mouse	Miltenyi Biotec	130-100-153
Anti-CD9	CD9	Monoclonal	No	Mouse	Thermo Fisher	10626D
Anti-CD9	CD9	Polyclonal	No	Rabbit	Abcam	Ab97999
Anti-CD9-APC	CD9	Monoclonal	APC	Mouse	Miltenyi Biotec	130-128-037
Anti-L1CAM	L1CAM (CD171)	Monoclonal	No	Mouse	Thermo Fisher	14-1719-82
Anti-BACE1	BACE1 (β-secretase)	Recombinant monoclonal	No	Rabbit	Thermo Fisher	MA5-29048
Anti-NF-L	Neurofilament light chain	Monoclonal	No	Mouse	Sigma Aldrich	MAB1615
Anti-CD54	CD54 (ICAM-1)	Monoclonal	No	Mouse	Abcam	Ab2213
Anti-CD32	CD326 (EpCAM)	Monoclonal	No	Mouse	Abcam	Ab7504
Anti-CD34	CD340 (erbB2)	Monoclonal	No	Mouse	Abcam	Ab30
Anti-CD44	CD44	Monoclonal	No	Mouse	eBioscience	BMS113
Anti-CD56	CD56 (NCAM)	Monoclonal	No	Mouse	Invitrogen	MA5-11563
Anti-Vinculin	Vinculin	Monoclonal	No	Mouse	Invitrogen	MA5-11690
Anti-TAU	TAU	Monoclonal	No	Mouse	Invitrogen	13-6400
Anti-mouse-Cy5	Mouse IgG	Polyclonal	Cy5	Rabbit	Abcam	Ab97037
Anti-rabbit-A488	Rabbit IgG	Polyclonal	Alexa Fluor 488	Goat	Invitrogen	A11034
Anti-rabbit-HRP	Rabbit IgG	Polyclonal	HRP	Goat	BioRad	1706515

5.3.3. Cell culture

Neuroblastoma cell line SH-SY5Y (ATCC, ref. CRL-2266) was cultured in Dulbecco's Modified Eagle Medium (DMEM) supplemented with a 10% of exosome-free fetal bovine serum (FBS) and with a 100 U mL^{-1} of penicillin-streptomycin. The maintenance of the cells was done at a controlled temperature (37 ºC) and CO_2 concentration (5%) with a humidified atmosphere. Cells were seeded at a concentration of 300.000 cells mL^{-1} and maintained

for four days then the culture medium was obtained for the purification of exosomes. The supernatant was centrifugated at 2000 *g* during 10 minutes for the residual removal of the cells before its storage at -20 ºC until use.

5.3.4. Exosomes isolation and purification

The exosomes were concentrated and purified through differential ultracentrifugation from cell line cultured supernatant based on protocol published [25] with small modifications. All the ultracentrifugation steps were performed with Beckman Coulter Optima L-80XP Ultracentrifuge and the 70Ti rotor and the regular centrifugations were performed with a Beckman Coulter Avanti J-26 XPI centrifuge with the JA25.50 rotor. Centrifugation steps were performed: first, the supernatant was centrifuged at 10,000 g for 30 minutes to remove cellular debris, then it was ultracentrifuged at 100,000 *g* during 60 min twice to pellet the exosomes. After the first ultracentrifugation the pellet was washed with filtered PBS 1X (pH = 7.4) and then ultracentrifuged again. The exosomes pellet was resuspended concentrating 200-fold from the initial supernatant volume into filtered PBS 1X buffer (pH 7.4, sterile 0.22 μm filtered).

5.3.5. Exosomes characterization for nanoparticle tracking analysis and cryogenic transmission electronic microscopy

To measure the exosomes concentration of the sample, a nanoparticle tracking analysis was performed (NTA). First, the samples were diluted in sterile filtered buffer 50 to 1000-fold. Then, the analysis was carried out using a NanoSight LM10-HS system with a tuned 405 nm laser at 24.8 ºC. NTA software analyzed raw data videos by triplicate during 60 s with 50 frames per second. From the analyzed data a histogram of the size distribution and the exosomes concentration was obtained.

The cooling of the samples into cryogenic temperatures allows the preservation of their structure avoiding artefacts. For the sample preparation, exosomes sample was dropped upon a Formvar-Carbon EM grid and frozen with liquid ethane avoiding the water crystal formation. During the assay's performance the sample was maintained at a -182°C temperature. The characterization of the morphology of the exosomes was obtained by the pictures taken through cryogenic transmission electronic microscopy (Cryo-TEM) using a Jeol JEM 2011 transmission electron microscope at a voltage of 200 kV.

5.3.6. Immobilization of antibodies on magnetic particles

Different antibodies were immobilized on the surface of Dynabeads M-450 tosylactivated superparamagnetic beads. Their immobilization was carried out following the manufacturer protocol. Briefly, magnetic particles (MP) were firstly washed with borate buffer (pH 8.5, 0.1 mol L^{-1}) and resuspended in this buffer with the initial volume. The specific antibody was then added at 200 µg x mL^{-1} as well as 3 mol x L^{-1} ammonium sulphate in borate buffer (100 µL). For the coupling of the antibody to the MP, an incubation for 20 hours at 37ºC was performed. Subsequently, a blocking step was carried out incubating the particles 4 hours at 37 ºC in a 0.5 mol x L^{-1} glycine solution. After this step, the MP were washed and resuspended up to a final concentration of 1 x 10^7 MP x mL^{-1} for further use.

5.3.7. Flow cytometry

The analysis of the biomarkers for the cells and the exosomes was carried out through fluorescence labelled antibodies detected by flow cytometry. The protocol was applied for both cells and exosomes with slight modifications., due to the small size of the exosomes, a previous step of exosomes capture with MP was mandatory to perform the acquisition by the flow cytometer and further analysis. Briefly, exosomes were captured by modified MP modified with antibodies. This was performed through an incubation for 1h at RT with gentle rotation. This produces an increase in their size, permitting their detection. Moreover, the washing steps for cells were performed through centrifugation for 3 minutes at 300 g while the exosomes attached to the MP were washed using a magnetic field. After that, the samples were incubated with the primary antibodies (listed in Table 5.1) during 30 minutes with gentle rotation at RT, followed by further washing (3x). and incubation with a secondary labelled antibody for 30 minutes at RT with gentle rotation. Lastly, the samples were resuspended in 1X PBS and acquired by the FACSCanto cytometer. Of note, the same antibodies were used for both type of samples, and the level of protein expression was quantified. The protocol is fully detailed in the supplementary in § 5.7.2 (Supp. data).

5.3.8. Magneto-actuated immunoassay

Direct and indirect formats of the magneto-actuated immunoassay were performed for the exosome detection. Both formats were carried out in polypropylene 96 well flat

bottom plates. Moreover, the exosomes were captured with MP previously immobilized with antibodies (1 x 10^6 per assay). The immobilized antibodies used were i) antiCD81 antibody, towards a general exosome marker for the total exosome capture and ii) antiL1CAM antibody towards a neuronal marker for the specific capture of the neuronal derived exosomes. For their capture, the mixture of the MP and the exosome sample (5 x 10^8 exosomes per assay) were incubated 1h at RT with gentle rotation. After this initial incubation, two strategies of detection were performed: the direct and the indirect labelling. Regarding the direct format, exosomes were attached to the functionalized MP and incubated for 40 minutes with a CD63 HRP conjugated antibody. Additional three washing steps of 3 minutes each were carried out with washing buffer before adding the substrate TMB and H_2O_2 used for the optical readout. Differently, the indirect format consists of the use of two antibodies. First, the sample was incubated with a primary antibody (BACE1) was for 30 minutes at RT and 750 rpm. Subsequently, three washing steps were performed and later, the sample was incubated with a secondary antibody labelled with HRP for 30 minutes at RT and 750 rpm. As before, three additional and final washing steps were performed with washing buffer previously, to incubate the sample with a mixture of TMB and H_2O_2 for the optical readout. For both formats, 2 M sulfuric acid was used to stop the reaction. Finally, samples were pated on an Infinite F50 Tecan microplate reader for the read at 450 nm (Figure 5.2).

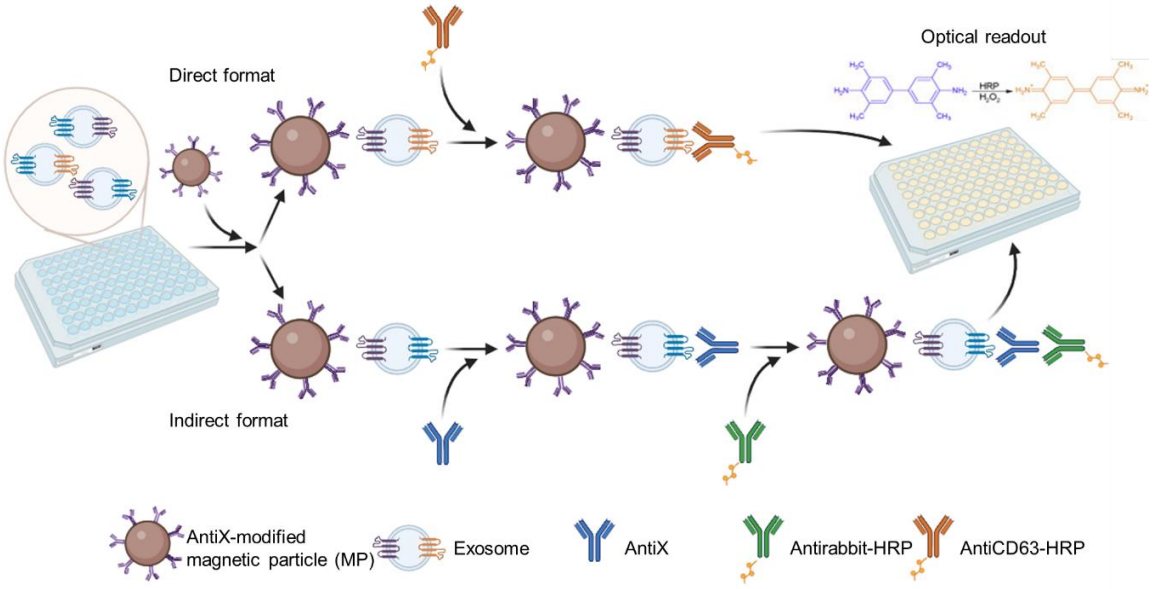


Figure 5.2. graphical representation of the direct and indirect format for the magneto-actuated immunoassay. Created with biorender.com.

5.3.9. Statistical Analysis

The statistical analyses and calculations were performed using Prism v 10.0.1 (GraphPad, San Diego, USA). The calibration curves were adjusted to a non-linear regression fitting, using the four-parameter logistic curve, abbreviated 4PL. The limit of detection was calculated considering the number of negative controls for each curve, using the one-tailed test with a significance level of $p > 0.05$ (t Student, $p > 0.05$).

5.3.10. Safety Considerations

All works were performed in a biosafety cabinet, and all material decontaminated by autoclaving or disinfected before discarding in accordance with U.S. Department of Health and Human Services guidelines for level 2 laboratory Biosafety.

5.4. Results and discussion

5.4.1. Characterization of exosomes by nanoparticle tracking analysis and cryogenic transmission electron microscopy

Purified and concentrated exosomes from the neuroblastoma cell line SH-SY5Y were characterized. The size and concentration of exosomes were estimated by nanotracking analysis assay (NTA), which showed a diameter size distribution from 35 to 350 nm with higher peaks at 125 nm and 165 nm (Figure 5.3 Panel A). The obtained results were in accordance with the expected exosomes size range i.e. between 30-200nm[17]. Moreover, a low peak at around 405 nm was observed, probably corresponding to aggregates. NTA analysis also determined a concentration of 1.1×10^{11} (SD 2.6×10^{9}) particles mL^{-1} (Figure 5.3 Panel A). In addition, images of shape and integrity of exosomes were obtained through cryogenic transmission electron microscopy (Cryo-TEM). The micrographics show round shape bilipidic membrane vesicles isolated and in aggregates (Figure 5.3 Panel B).

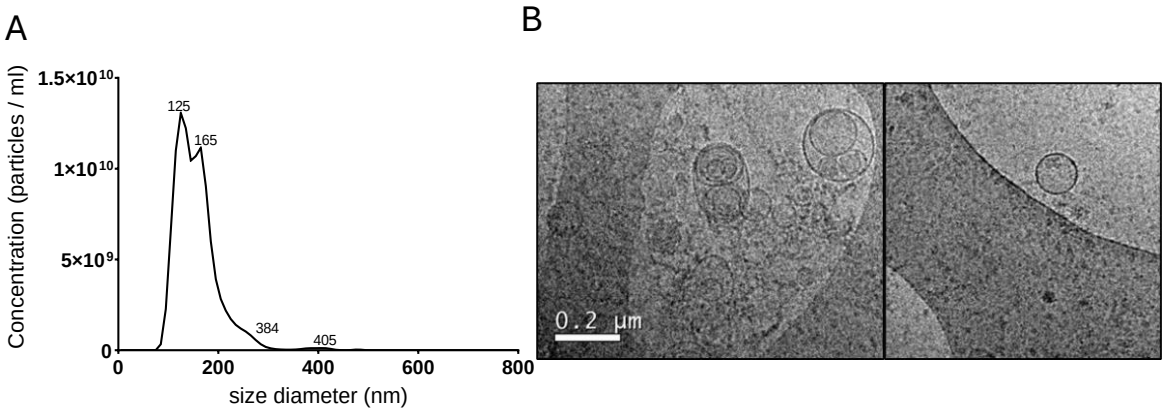


Figure 5.3. Characterization of the purified SH-SY5Y exosomes through NTA (Panel A) and CryoTEM (Panel B). Nanosight NTA Software analyzed raw data videos by triplicate during 60 s with 50 frames per second and the temperature of the laser unit set at 24.8 ºC. Cryo-TEM images of purified exosomes at an acceleration voltage of 200 kV.

5.4.2. Characterization and comparative of the biomarkers expressed by SH-SY5Y cells and their derived exosomes.

First, the expression of the biomarkers of the neuroblastoma cells and their derived exosomes was assessed by using a combination of general exosome biomarkers (tetraspanins such as CD81, CD63 and CD9)[26], adhesion molecules and neuronal biomarkers. The adhesion neuronal marker L1CAM was selected among other neuronal markers for further separation of neuronal exosomes in preclinical AD plasma samples[27]. Moreover, other groups have used this biomarker *a posteriori* for the enrichment of the samples into neuronal exosomes for further analysis as miRNAs detection among others[28–30]. The results of the characterization of the cell line through flow cytometry show a wide expression of the tetraspanins and the neuronal adhesion molecule L1CAM (Figure 5.4). However, the other adhesion molecules tested were not expressed in the cell surface except for the CD24 which was also highly expressed (Figure 5.4). CD24 is an adhesion molecule with several pattern of cellular expression as it is mainly expressed by B cells but it is also a marker for a high-risk neuroblastoma which has been previously described to be highly expressed in the SH-SY5Y cell line (Supp. data, Figure 5.10)[31]. and it is also considered a marker for cancer stem cells[32,33]. The analysis of the samples and the gating of the populations is described in the supplementary data, Figures 5.8 and 5.9.

Afterwards, exosome biomarkers were characterized by performing a bead-based flow cytometry technique, using the biomarkers previously assessed in the neuroblastoma cells. However, this technique only allowed the determination of extracellular biomarkers

in the exosomes samples but not the biomarkers inside them. For the bead-based flow cytometry, exosomes were previously captured with antiCD81-MP and then detected with primary and secondary antibodies (Figure 5.4 and in supp. data, Figure 5.11). Tetraspanins were the higher expressed markers, and among them, CD81 the most expressed. Moreover, L1CAM was the most expressed adhesion molecule with a >80% of expression in the exosomes previously captured with the antiCD81MP (Figure 5.4). The expression pattern determined with the cells was not always the same as the one observed in the exosomes. Both tetraspanins and L1CAM were detected in the exosomes as well as in the cells. However, even though the adhesion molecules CD24 and CD56 were detected in the cells, no adhesion molecule but the L1CAM was detected in the exosomes (Figure 5.4).

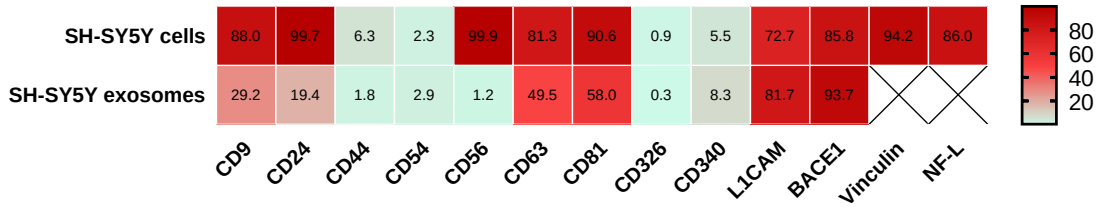


Figure 5.4. Heat map of the expression of the biomarkers comparative between cells and their derived exosomes by flow cytometry, expression determined as the percentage of the positive signal compared to a negative control (n=2). All exosome samples were captured with antiCD81-MP.

5.4.3. Design of a combination of biomarkers for the neuronal derived exosomes detection

Once the exosomes of the SH-SY5Y cell line were characterized, the next step was to assess the expression of an AD-related biomarker on the exosomes with the purpose to set up a combination of markers that allowed a specific capture and detection of neuronal derived exosomes (NDE). The neuronal biomarker selected was the β-secretase (BACE1) for its implication in the amyloid plaque formation and its previously described upregulation in AD (Figure 5.5 Panel A)[34,35]. The BACE1 expression was determined and compared between the parental cell line and the exosomes by flow cytometry.

First, the presence of the BACE1 protein was determined by flow cytometry onto the cells and later onto the exosomes. Results determined a high expression of BACE1 in the cells surface and, in the exosomes, (Figure 5.5 Panel A and B). For the bead-based cytometry, the exosomes were captured with antiCD81-MP. Thus, the BACE1 biomarker was selected

to be used for the further set-up of the magneto-actuated immunoassay as an AD related biomarker.

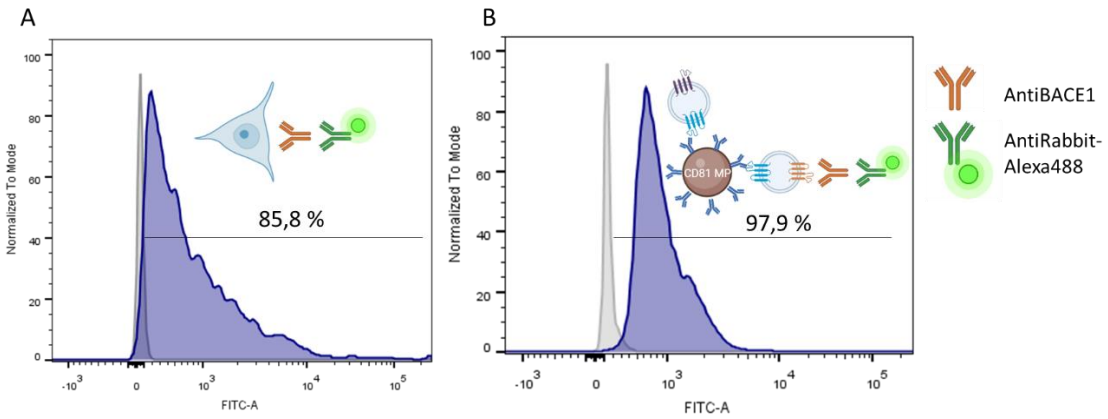


Figure 5.5. Panel A. Histogram of the expression of the BACE1 biomarker in the SH-SY5Y cell line. Panel B. Histogram of the BACE1 expression in the SH-SY5Y derived exosomes by flow cytometry. Cells and exosomes were selected from the single cell dot plot and the bead dot plot described respectively in the supplementary data (Figure 5.8 and 5.9). In the bead-based flow cytometry antiCD81-MP were used for the exosomes capture.

5.4.4. Magneto-actuated immunoassay

For the magneto-actuated immunoassay, two different capture methods were designed. First, antiCD81-MPs were used to capture of exosomes with a ubiquitous marker and antiL1CAM-MPs to specifically capture neuronal exosomes. For Both systems the captured exosomes were revealed with an antiCD63-HRP antibody. Moreover, to better identify NDE captured by the antiL1CAM-MP a readout with an antiBACE1 antibody was performed. Even though BACE1 was previously proposed as a biomarker, it had a limitation because its expression is not only restricted to the brain[36]. This challenge was overcome by combining the capture of the NDE with a neuronal specific biomarker, followed by a second labelling with BACE1, which although not exclusive, mainly expressed by neuronal cells.

As a control setting was include the capture and the detection of all the exosomes using antibodies against a general marker. The capture was performed with antiCD81-MP and exosomes detection with a direct labelled antiCD63-HPR. Tetraspanins are known to be widely present in the exosomes and CD81 and CD63 were determined to be co-expressed in their surface through the previous flow cytometry experiments (Figure 5.4). Different

exosomes concentrations were used for the determination of the LOD of the detection of exosomes. Calculated by processing the negative samples without exosomes and obtaining the mean value for each plot. The cutoff value was then determined in all cases with a one-tailed t-test at a 95% confidence level. These values were interpolated in each plot to obtain the LODs Calibration curve for SH-SY5Y exosomes from 10^4 to 10^7 exosomes μL^{-1} was performed (calculated from the NTA concentration). The plots obtained for the detection of SH-SY5Y derived exosomes were represented by a Four Parameter logistic Equation and are shown in Figure 5.6. The limit of detection (LOD) was 1.26×10^5 exosomes μL^{-1} ($R^2 = 0.9955$) for the direct format using antiCD63-HRP.

This assay demonstrates, in agreement with the flow cytometry study, that the capture and detection of exosomes with two general markers results in a massive exosome detection, since the CD81-CD63 co-expression is high on their membranes.

Subsequently, capture of exosomes with a neuronal marker (L1CAM) and a read-out with a tetraspanin for the demonstration of the exosome capture using this NDE enrichment approach was set up (Figure 5.6 Panel B). With this approach, the capacity of the functionalized MP for capturing and enriching exosomes samples was demonstrated. Values were fitted into a four-parameter logistic curve $R^2 = 0{,}9415$ (Figure 5.6). The LOD was 1.01×10^6 exosomes μl^{-1}. Compared to the LOD obtained using a general marker for the capture it can be observed a diminishment of the capture. This can be due to the higher co-expression of the general markers compared to the neuronal.

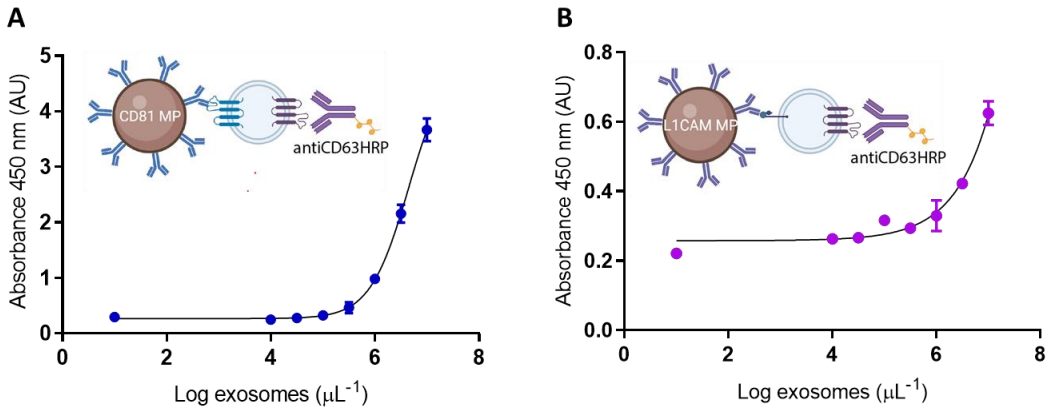


Figure 5.6. Calibration plot for the magneto-actuated immunoassay with a direct format using antiCD63-HRP (0.11 µg mL^{-1}) for the detection. Panel A. calibration plot for the total exosome determination from 0 to 10^7 exosomes μL^{-1} using antiCD81-MP. Panel B. calibration plot for the total NDE determination from 0 to 10^7 exosomes μL^{-1} using antiL1CAM-MP (n=3).

Next, the capture with L1CAM-MP as a neuronal biomarker was validated by using an antiBACE1 antibody for the optical readout. As described before, BACE1 was the biomarker selected for the readout after the NDE enrichment, and a calibration curve from 10^4 to 10^7 exosomes μl^{-1} was performed (Figure 5.7). The values were fitted into a four-parameter logistic equation with a $R^2 = 0.9248$. LoD was calculated as previously described resulting into 9,64 x 10^5 exosomes μl^{-1} (Figure 5.7).

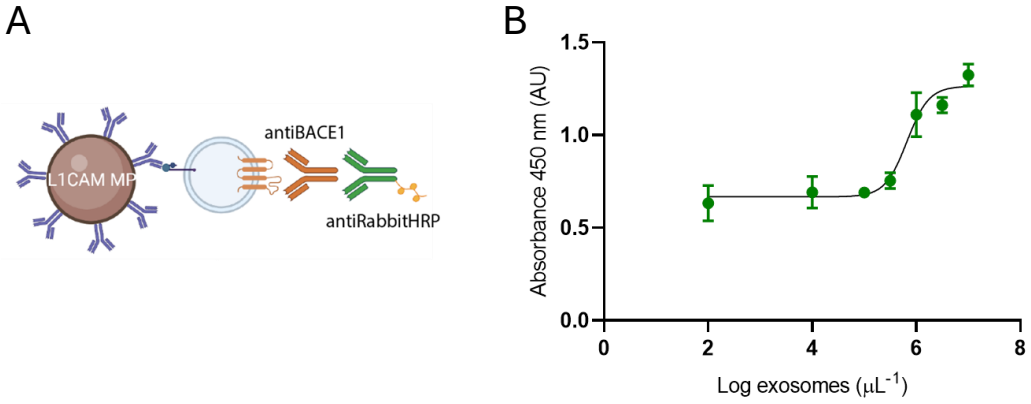


Figure 5.7. Calibration plot for the magneto-actuated immunoassay. Panel A graphical representation created with biorender.com, Panel B calibration plot determining from 0 to 10^7 exosomes μL^{-1} using antiL1CAM-MP and BACE1 and antirabbit-HRP as a readout (n=3).

The values of the obtained LODs are compatible with the exosome concentration in serum samples, as previous reports have determined that the exosomes concentration in serum is around 10^9 exosomes μL^{-1} [37] leaving a significant range to work with. With this approach,

information related to the neurodegenerative process occurring into the oncoming cells is expected to be determined directly in plasma or serum samples. Although, previous studies in our group had demonstrated the minimal impact of the matrix using this isolation strategy[38]. Further steps should include the evaluation of the matrix effect due to the capture of the exosomes from the serum or plasma, a high complex matrix.

5.5. Future perspectives

Once the magneto-actuated immunoassays were set up it remained to validate them with human samples. Regarding the human samples that would be used, they would include CSF, for the obtention of neuronal non-biased results, and plasma, for less invasive procedures for sample obtention. Exosomes from both sample types were isolated and characterized before their further use in the magneto-actuated immunoassays. Results obtained for the isolation and characterization are described in the § 5.7.5 (Supp. data).

5.6. Conclusions

Current AD diagnostic tools are expensive and procedures are invasive. It has become clear that in prodromal phases there is a pressing need to discover new biomarkers that are minimally invasive and low cost. Thus, blood-based biomarkers are thought to be the most suitable option. However, they have limitations to show good specificity and sensitivity as they are non-tissue specific. To overcome this drawback, exosomes have emerged as promising biomarkers due to their characteristics[17]. Exosomes reflect cellular processes happening in the cell because their cargo is related to their oncoming cells. Moreover, they are capable to go through the blood brain barrier (BBB) allowing them to arrive to the blood stream[39]. Thus, the idea of using cell-specific exosomes from a liquid biopsy as serum holds great promise.

In this thesis chapter, the SH-SY5Y cell line and its derived exosomes have been characterized. The exosomes isolated from cell culture supernatant revealed a size distribution with a major peak at 125 nm and an estimated concentration of 10.10×10^{11} exosomes mL^{-1}. Different combinations of biomarkers were studied for the capture and detection of the neuronal-derived exosomes. BACE1 was decided to be selected as an AD-related biomarker due to its involvement in amyloid plaque formation and previous

studies relating its upregulation with the pathology[23,24]. A magneto-actuated immunoassay was set up for the capture and detection of exosomes. Two different approaches were tested: (a) general capture using antiCD81-MPs and detection with antiCD63HRP, and (b) specific neuronal exosome capture using antiL1CAM-MPs and detection with antiCD63HRP or antiBACE1. The limit of detection (LOD) for the general capture approach was estimated at 1.26 x 10^5 exosomes μL^{-1}, while for the specific neuronal exosome capture approach, the LOD was determined to be 1.01 x 10^6 exosomes μL^{-1}. Demonstrating the capacity of the antiL1CAM-MP to capture neuron-derived exosomes an enrich exosome samples with the selected population. The capture, however, is not as efficient as when a general marker is used.

The magneto-actuated immunoassay combining the neuronal capture and the BACE1 (AD-related biomarker) showed promising results with a LOD of 9.64 x 10^5 exosomes μl^{-1}. It opens the possibility of an early diagnostic test for AD with minimally invasive procedures. In addition, plasma samples have been characterized demonstrating the capacity of exosome purification and showing the presence of the biomarkers. Nevertheless, it remains to be elucidated if BACE1 is a suitable biomarker for the stratification of the individuals with the first AD symptoms performing the magneto-actuated immunoassay with plasma samples.

It is noteworthy that exosomes from CSF could be measured and characterized following our approach. Although our data is preliminary, with the analysis of few human samples, we could determine the same order of exosomes concentration in all the CFS samples (mean of 6.5x10^9 particles mL^{-1}) being all the samples over the LOD of the magneto-actuated immunoassay described in this study. Moreover, their CD63 and CD9 expression was determined by flow cytometry and their neural origin is guaranteed by their source. Thus, it is expected that CSF-derived exosomes could be analyzed by the neural biomarker approach, L1CAM and BACE1, proposed in our in vitro magneto-actuated immunoassay design for AD early diagnose.

5.7. Supplementary data

5.7.1. Experimental

Buffers and solutions

Bovine serum albumin (BSA, ref. A4503), sodium phosphate dibasic (ref. 71636), potassium phosphate dibasic (ref. 795496), sodium chloride (ref. S3014), potassium chloride (ref. P3911), saponin (ref 47036) and magnesium chloride (ref. M8266) were purchased in Sigma-Aldrich (Merck KGaA, DE). Sulfuric acid (ref. 131058) was purchased from Panreac (ES).

The composition of the solutions was:

- PBS 1X buffer: 10 mmol L^{-1} Na_2HPO_4, 137 mmol L^{-1} NaCl, 2.7 mmol L^{-1} KCl, 1.8 mmol L^{-1} K_2HPO_4, pH 7.4.
- Washing buffer: 0.5% w/v BSA in PBS 1X buffer.
- Stopping solution: Sulfuric acid 2 mol L^{-1} solution

5.7.2. Flow cytometry set up

Standard protocol

For the determination of the expression of the different biomarkers they can be labelled with fluorescence and read out with a flow cytometer. Depending on if the samples are cells or exosomes the protocol differs slightly. The protocol for the labelling of the exosomes was as follows:

10^9 exosomes per well and 1×10^6 MPs (previously functionalized with the desired capture antibody) were placed in a polypropylene 96-well microtiter plate. The mix was incubated 1h at 750 rpm at RT. A washing step was then carried out placing the plate into the magnet (DynaMagTM-96 Side Skirted Magnet (Product Nº 12027, ThermoFisher), discarding the liquid and washing the MP with the exosomes immunocaptured with washing buffer. The samples were indirect labelled using a primary antibody and a secondary labelled antibody. To the solution containing the previously modified MPs with the exosomes attached were added 100 µL (at 5 µg mL^{-1}) of the antibodies antiCDX (for instance antiCD81 monoclonal antibody, Ref 10630D, Thermo Fisher) and incubated for 30 minutes at RT and 750 rpm. Three washing steps were carried out with 180 µL washing buffer.

Afterwards, 100 µL of secondary antibody (at 2 µg mL^{-1}) were added, for instance, Goat Anti-Mouse IgG H&L (Cy5 ®, ref ab97037, Abcam), and incubate for 30 min at RT °C and 750 rpm. The MP were washed with 180 µL of washing buffer under shaking for 3 min at RT and 750 rpm for three times. Finally, the readout was carried out resuspending the MP with 100 µL of PBS 1X and acquired using the FacsCanto cytometer.

For the cell labelling two different protocols were performed, the membrane protein labelling and the intracellular protein labelling. Both were performed depositing between 1 to $3x10^5$ cells plated into a polystyrene 96 well with conical (V) bottom plate (Thermo Scientific, ref. 277143). Differing of the exosomes protocol all the washing steps were performed by centrifuging 3 minutes at 800 g. Both protocols had the same staining steps but the intracellular protein labelling had a previous cell pretreatment for the membrane permeabilization. Firstly, the cells from culture were fixed with 200 µL of diluted formaldehyde 4% in PBS 1X for 10 minutes at RT. Then, the microplate was centrifuged for the cell pelleting, supernatant was discarded. After washing steps cells were incubated with 200 µL of PBS 1X containing 2% of FBS and 0.1% of saponin, for 10 minutes at RT. The plate was centrifuged, and the supernatant discarded. Then, the cells were resuspended in FBS containing 0.3% of saponin for permeabilization of cellular membranes. At this point both protocols converge. The samples with or without the cells pretreated are incubated 30 minutes at RT with primary antibodies (5 µg mL^{-1}). Cells are three times washed and subsequently incubated with secondary labelled antibody (2 µg mL^{-1}) for 30 minutes at RT in the dark. Finally, after three washing steps, the cells were resuspended into 200 µL of PBS 1X and measured with a flow cytometer.

Gating selection and analysis

For the flow cytometry analysis, the different gates had to be determined. For cytometry analysis of the cell line, first, the cells had to be selected using the side scattering channel (SSC) and the forward scattering channel (FSC) plot, leaving unselected the cell debris. Then, the single cells were selected separating them from the aggregates. And finally, using the negative control it was determined the threshold intensity in the green channel for the further biomarkers expression determination. The analysis was performed with FlowJo software.

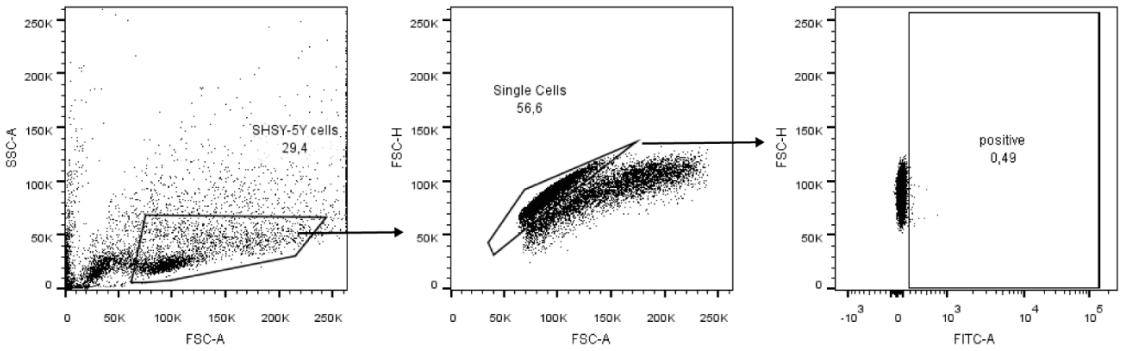


Figure 5.8. SH-SY5Y cells were selected first with the SSC-A / FSC-A then the single cells were separated to the aggregates in the FSC-H / FSC-A. Finally choosing this gate the positivity for the specific marker was selected using the negative control (cells with secondary antibody only lacking the primary antibody) with the green fluorescence in the X axis.

For the bead-based exosomes flow cytometry the gate selection procedure works almost the same way as the cells. The main difference is the presence of beads instead of cells, visualizing them in the first plot (SSC / FSC) as dot clouds depending on if they are single beads or couples. Once the beads selected the green channel (FITC) threshold is determined using the negative control.

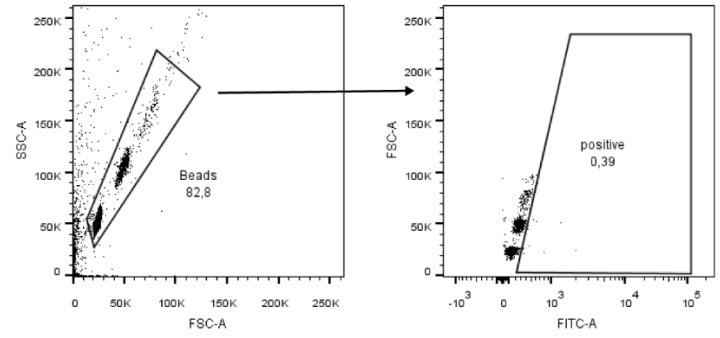


Figure 5.9. SH-SY5Y exosomes attached to the tosylactivated dynabeads functionalized with antiCD81 were selected first with the SSC-A / FSC-A. After choosing this gate the positivity for the specific marker was selected using the negative control (exosomes with the MP and the secondary antibody only lacking the primary antibody) with the green fluorescence in the X axis.

5.7.3. Characterization of the SH-SY5Y and their derived exosomes

Flow cytometry plots of the SH-SY5Y cell line and SH-SY5Y derived exosomes characterization

The SH-SY5Y cell line was characterized by flow cytometry using an indirect format with a primary and a secondary antibody labelled with Cy-5.

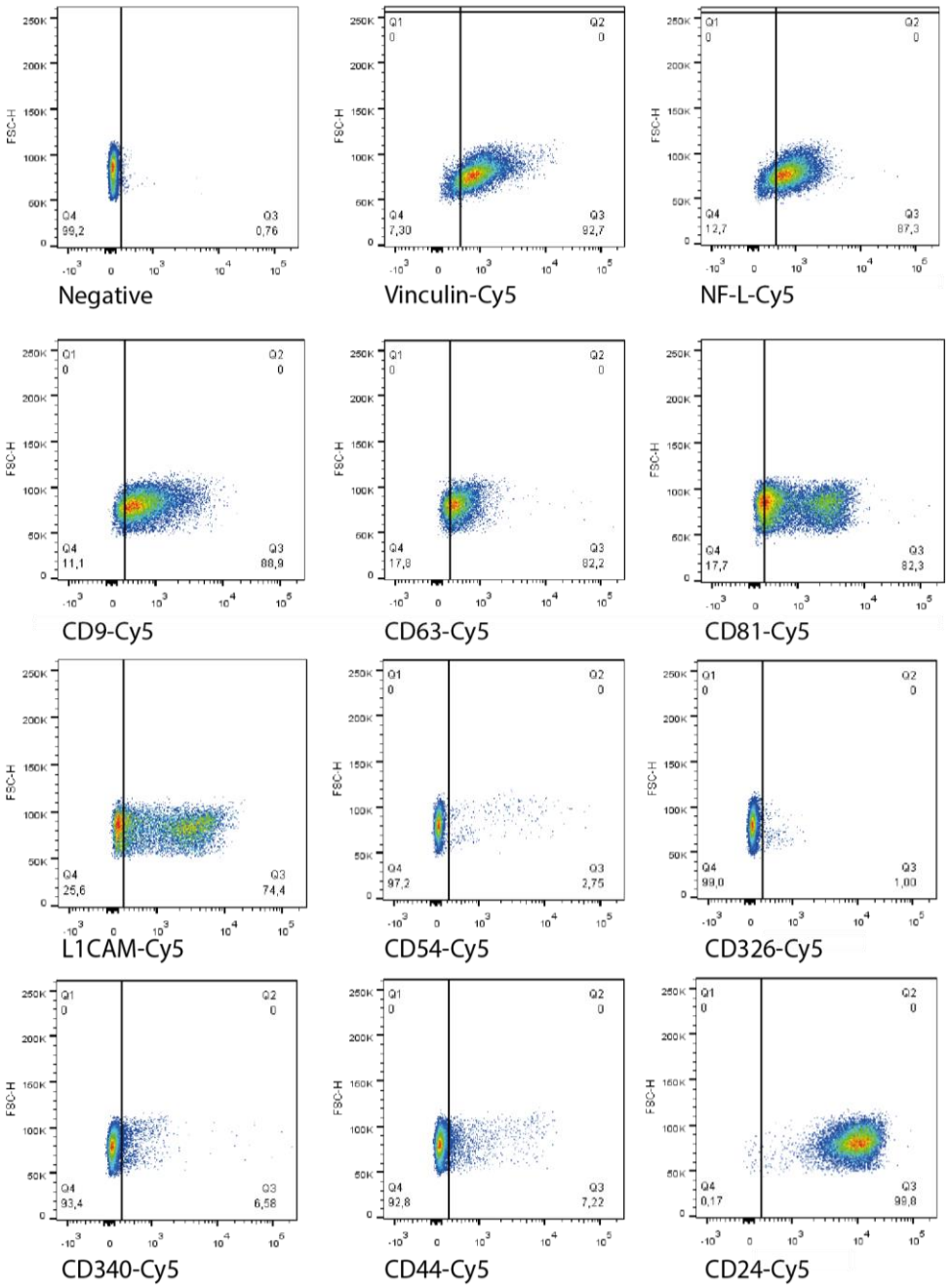


Figure 5.10. dot plots of the characterization of the SH-SY5Y cell line by flow cytometry of surface and intracellular biomarkers. On the Y axis FSC-H was represented and on the X axis was represented the fluorescence of the antimouse-Cy5 fluorochrome of the secondary antibody.

Exosomes characterization by bead-based flow cytometry

Once the SH-SY5Y cell line was characterized the same surface biomarkers were evaluated for their derived exosomes. The exosomes were first captured with antiCD81-MP and then incubated with primary and secondary antibodies for the biomarker detection.

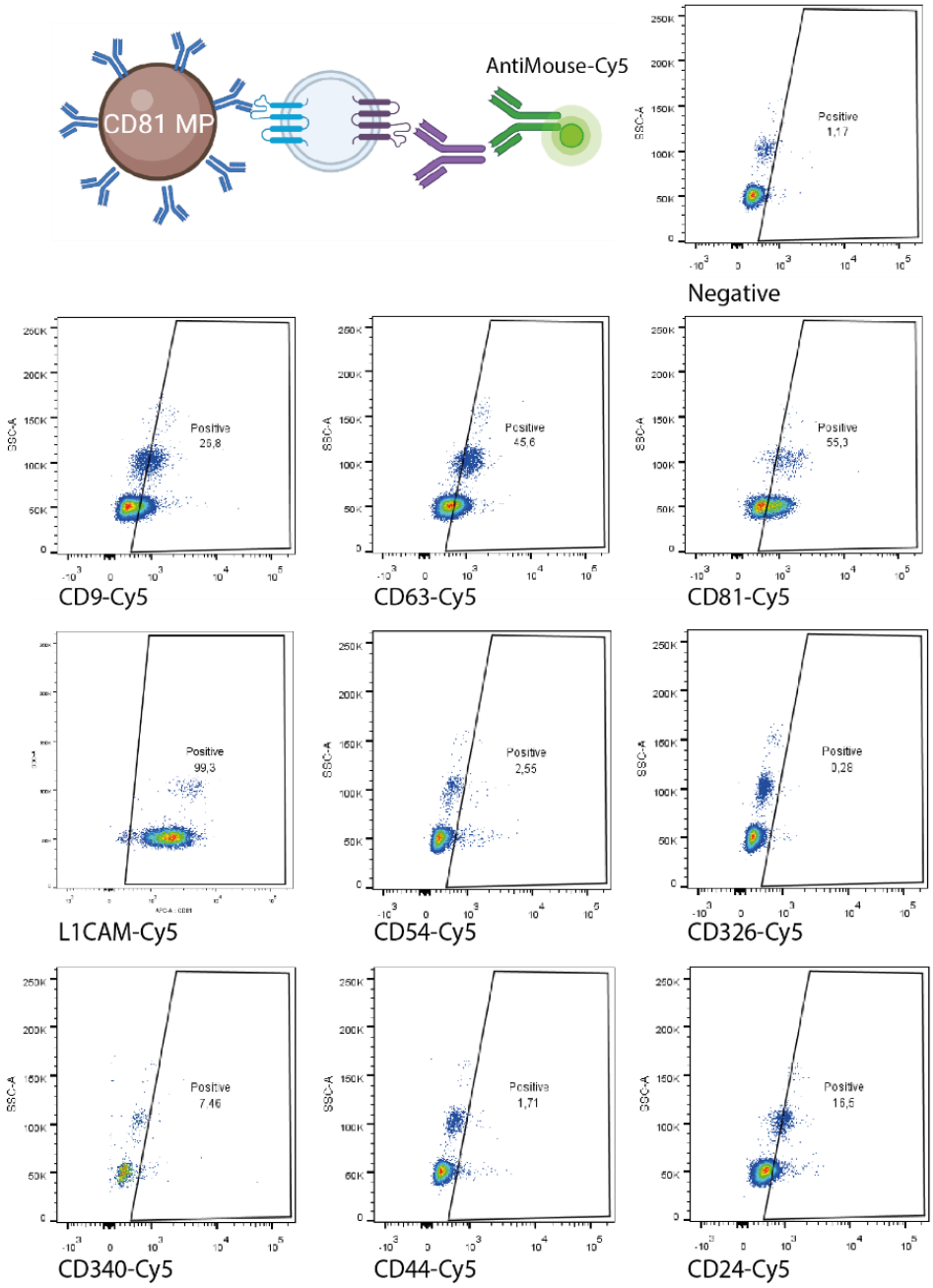


Figure 5.11. dot plots of the characterization of the SH-SY5Y cell line derived exosomes by bead-based flow cytometry (antiCD81-MP). On the Y axis the SSC-A was represented and on the X axis represented the fluorescence of the antimouse-Cy5 fluorochrome of the secondary antibody.

Confocal microscopy

Confocal microscopy was used for the assessment of tetraspanins expression, L1CAM and BACE1. For this purpose, 5 x 10^5 cells were plated in a 24-well plate containing coverslips and were let to adhere and grow overnight at 37ºC in a humidified atmosphere with 5% CO_2. Cells were washed in PBS and then fixed with 4% paraformaldehyde for 20 minutes. After fixation, cells were washed with PBS and then incubated for 30 minutes with a blocking solution (PBS with 5% of FBS). Next, cells were incubated for 1 h with the primary antibody (1:100) against CD81, CD63 and CD9. Following this, cells were washed again with PBS plus 2% of FBS and incubated for 1h (in the dark) with the secondary antiRabbit Alexa 488 or antiMouse-Cy5 (1:400). Six final washes with PBS were performed before carefully removing the coverslips from the plate to mount them on the slides. One drop of mounting medium containing DAPI dye was placed on the slide and the coverslip was carefully placed over it. Slides were left overnight at a 4ºC chamber and then the edges were sealed with lacquer. Confocal images were collected on a Leica, TCS SP5 microscope (Leica Microsystems, Wetzlar, Germany) (Servei de Microscopia, UAB). Results were analyzed using Image J software.

In the upper Panel of figure 5.12 is shown a doble staining with CD81 Cy5 and BACE1 Alexa488; and in the lower a double staining with CD63 Alexa488 and L1CAM Cy5. Pattern of staining differs depending on the biomarker analyzed. CD81 also showed a dotted pattern but with a higher concentration in the membranes. Differently, the BACE1 which also showed a dotted pattern in the cytoplasm also show accumulations of the protein in certain parts of the cytoplasm. This accumulation in the cytoplasm correspond to their previously described subcellular localization, where it was described to be in the Golgi apparatus as well as in the secretory pathway [40]. L1CAM and CD63 protein shown a dotted patter in the cytoplasm for the as well as in the plasmatic membrane, concurring to their presence in the exosomes membrane.

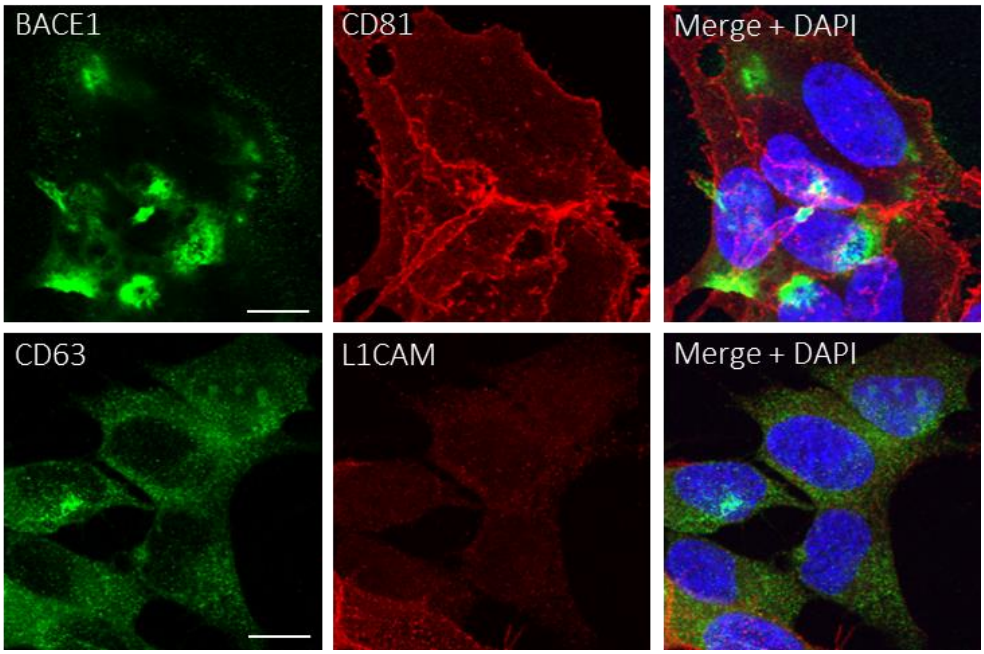


Figure 5.12. Confocal micrographs of SH-SY5Y cells immunostained with antiBACE1 antibody (green), antiCD81 antibody (red), antiCD63 (green) and antiL1CAM (red). Scale corresponding to 10 µm. Images analyzed with FIJI image J software.

5.7.4. SH-SY5Y cell line differentiation

For a better performance of the set up immunomagnetic assay the cell line was differentiated in a single-step protocol. Adherent cells were seeded into 6well plates coated with 0.5 mg x mL^{-1} Bovine collagen I (Sigma, ref. A10644-01) at 2 x 10^5 cells mL^{-1} in 10 mL of complete culture medium further supplemented with 10 µM all-trans retinoic acid (RA, Sigma ref. R2625). Cells were incubated at 37 ºC in a humidified atmosphere with 10% CO_2 for 7 days.

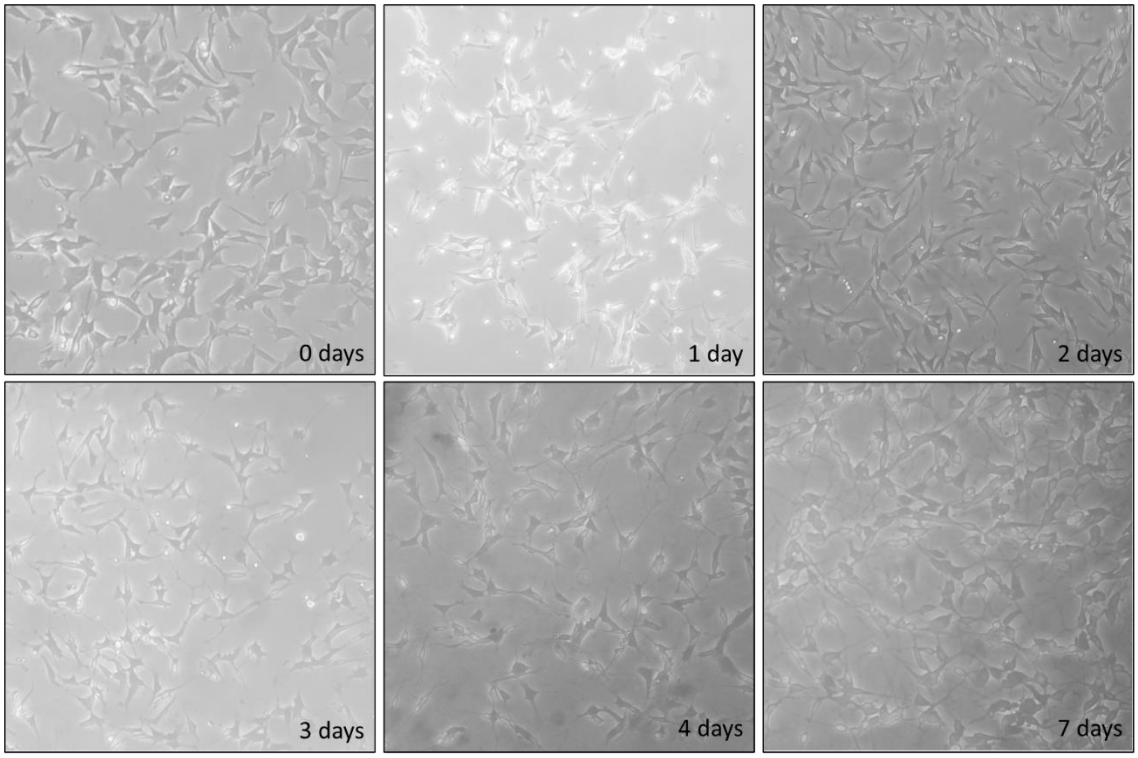


Figure 5.13. Micrographs of SH-SY5Y cells during their differentiation with RA and collagen. differentiation.

Some of their neuronal markers were determined as TAU by flow cytometry and western blot (WB) with no significant differences. Results of the flow cytometry showed a percentage of positivity for the intracellular TAU protein of 80.5% and 80.1% for non-differentiated and differentiated cells, respectively (Figure 5.13 Panel A). Vinculin was used as a positive control of the staining.

TAU expression was also determined by an alternative technique to confirm that the exosomes of differentiated cells using collagen I and RA did not contain TAU as undifferentiated cell line. Western blot was performed charging the exosomes lysed samples into a sodium dodecyl sulphate polyacrylamide gel electrophoresis (SDS-PAGE, 12%). Proteins were separated electrophoretically and transferred onto polyvinylidene difluoride (PVDF) membrane (Millipore) previously activated with methanol (5 minutes) for 45 minutes at a voltage of 100 V. Non-specific binding sites on the PVDF membranes were blocked incubating with 5% skim milk for 1 h with gentle shaking. The PVDF membranes were then incubated with antiVinculin and antiTAU antibodies overnight at 4 °C. After washing with PBS-Tween20 0.05% (v/v) Tween 20, the membranes were incubated with goat anti-rabbit IgG-peroxidase for 1 h. After three washing steps a

detection reagent was applied (1: 1 Clarity Western ECL kit Blotting Substrate ref: 1705061 (BioRad ™)) and the membrane visualized through VersaDoc (Bio-rad). Each membrane was exposed for 20 minutes, and 3 pictures taken. The TAU expression in exosomes was not detected by western blot neither in both differentiated and non-differentiated cells. The detection of vinculin as positive control showed similar expression levels in both indicating that the same amount of protein was added in both samples tested in the assay (Fig 5.14 Panel B).

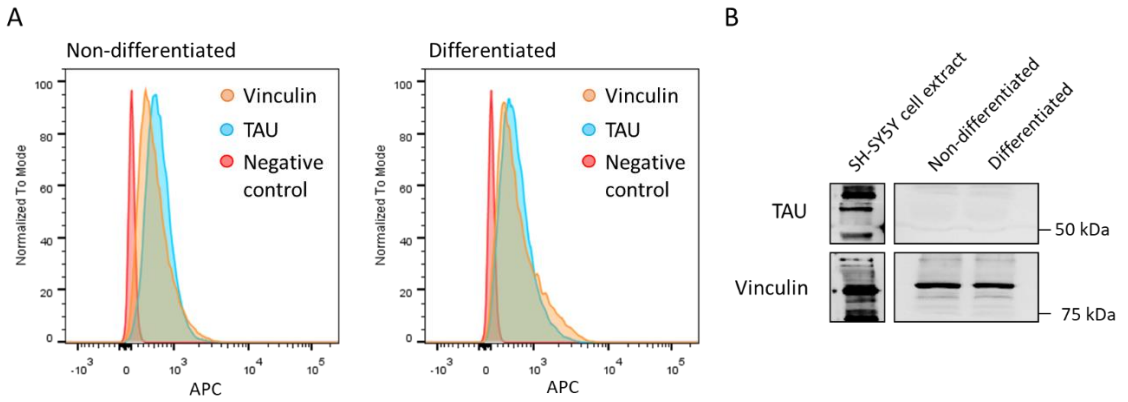


Figure 5.14. Panel A. histograms of the flow cytometry expression of the neuronal biomarker TAU and vinculin as a positive control for SH-SY5Y differentiated and non-differentiated cells. Panel B. western blot of the exosomes the differentiated and non-differentiated SH-SY5Y cell line.

5.7.5. Characterization of human-derived exosomes from cerebrospinal fluid and plasma samples

Exosomes from cerebrospinal fluid (CSF) from 4 individuals were isolated and characterized. Samples included an individual with subjective memory complains (SMC), two with mild cognitive impairment (one with positive beta amyloid 1-42 MCI- and the other with a negative beta amyloid 1-42 MCI+) and one with dementia (DEM+) (Table 5.2).

Table 5.2. AD clinical characterization of the samples by ELISA.

	AB1-42 (pg/ml)	AB1-40 (pg/ml)	tTau (pg/ml)	pTau (pg/ml)	AB42/AB40
SMC-	1006	8565	260	37.4	0.117
MCI-	1081	9900	393	51.3	0.109
MCI+	480	8628	619	106.1	0.056
DEM+	489	8434	777	129.2	0.058

Once the exosomes were isolated by differential ultracentrifugation they were characterized through NTA and Cryo-TEM. The highest peaks were enriched with exosomes and correspond to 125 nm in diameter for SMC and MCI+ samples, 145 nm for MCI- and 25 nm for DEM+ which also have two other high peaks at 92 and 140 nm. The particle concentration after preconcentration by ultracentrifugation in the sample was determined by NTA, being approximately 4.76×10^9 (SD 6.14×10^8) exosomes mL^{-1}, 6.40×10^9 (SD 4.18×10^8) particles mL^{-1}, 7.97×10^9 (SD 1.09×10^9) particles mL^{-1}, and 6.86×10^9 (SD 2.57×10^9) expsomes mL^{-1}, respectively, for exosomes derived from SMC, MCI-, MCI+ and DEM+ respectively. Further information of size diameter distribution was obtained by Cryo-TEM. Micrographs of the exosome sample show well-shape exosome vesicles with closed circular lipid bilayers revealing the presence of single exosomes but also exosome aggregates (Figure 5.15).

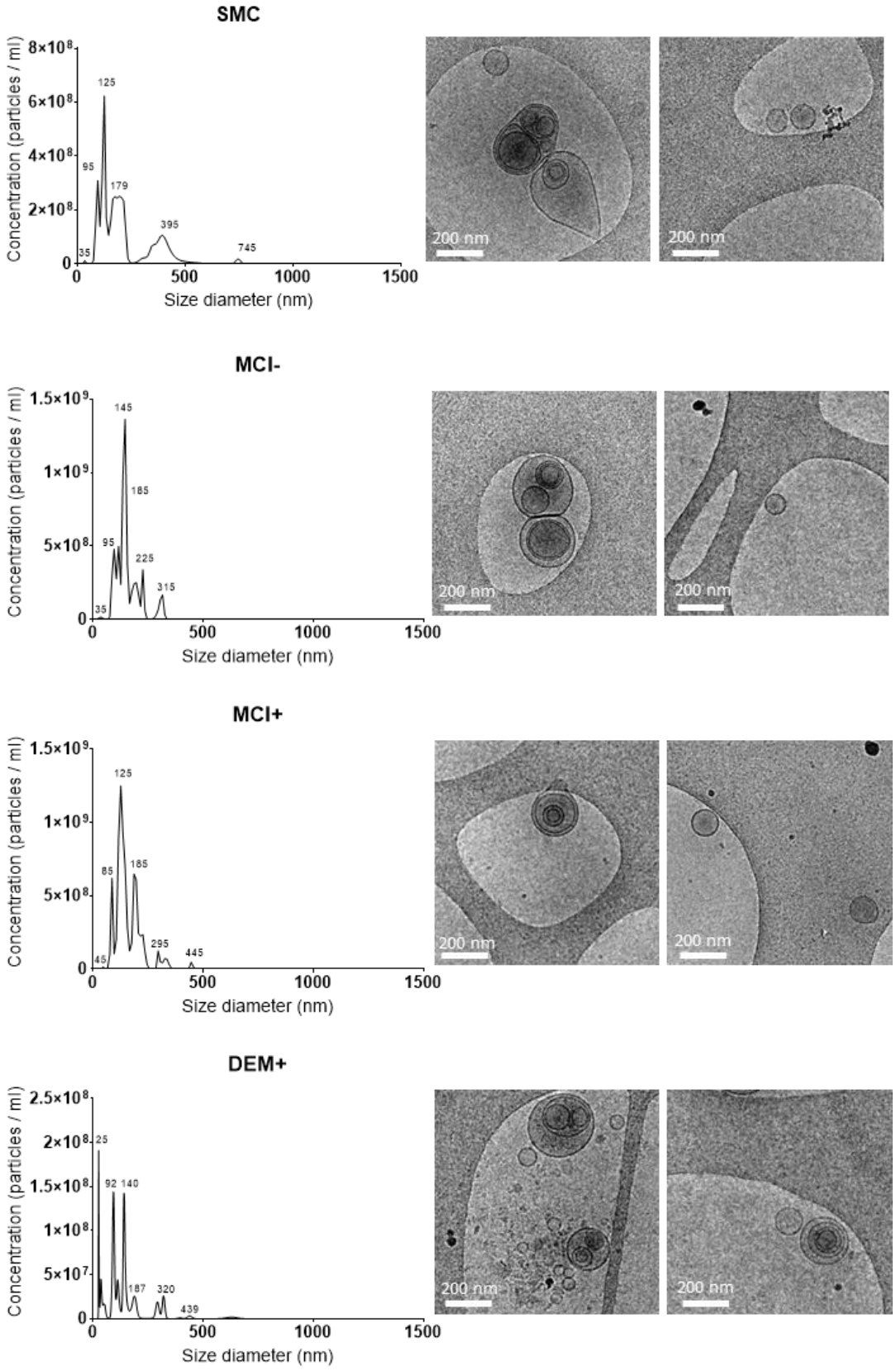


Figure 5.15. Characterization by NTA of purified exosomes derived from the CSF samples; SMC, MCI-, MCI+ and DEM. In addition. cryo-TEM images of purified exosomes at an acceleration voltage of 200 kV.

For the validation of the nanovesicle source flow cytometry was performed demonstrating they were exosomes. Tetraspanins were used as exosomal biomarkers (CD9-APC and CD63-PE). Due to the low volume of the CSF samples other biomarkers were not tested. CD63 was expressed in all the samples compared to CD9 which was only detected in MCI samples. The SMC sample showed lower exosomes concentration and the biomarkers expression could not be determined properly (Figure 5.16).

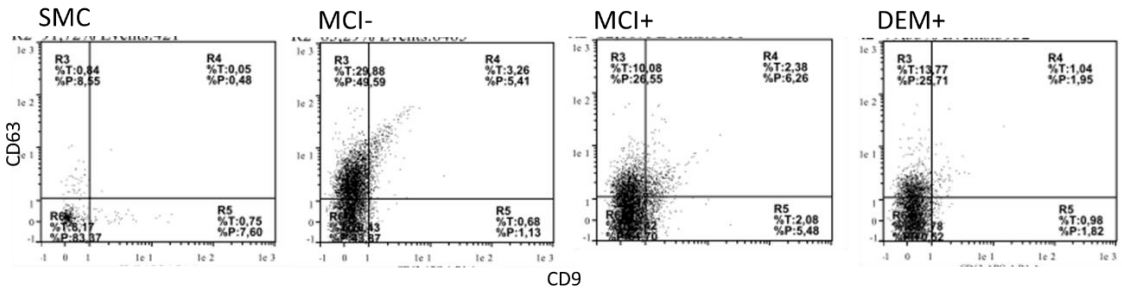


Figure 5.16. dot plots of the CSF exosomes samples for their validation through the detection of the tetraspanins as biomarkers of the exosomes.

On the other hand, exosomes from plasma samples were purified including a universal plasma (UP) sample (a pool of individual samples mixed) and a plasma sample of an individual with mild cognitive impairment (MCI). The exosomes of both samples were isolated with differential ultracentrifugation and characterized through NTA and Cryo-TEM. Figure 5.17 shows the diameter size distribution UP sample (Figure 5.17 Panel A) and MCI sample (Figure 5.17 Panel B). The highest peaks are enriched with exosomes and correspond to 95 and 125 nm in diameter, respectively (Figure 5.17 Panel A and C). The particle concentration after preconcentration by ultracentrifugation in the sample was determined by NTA, being approximately 3.51 x 10^{10} (SD 2.81 x 10^{9}) exosomes x mL^{-1} and 2.21 x 10^{10} (SD 1.51 x 10^{9}) exosomes x mL^{-1}, for UP and MCI samples respectively (Figure 5.17 Panel A and C). Further information of size diameter distribution was obtained by Cryo-TEM. Micrographs of the exosome sample show well-shape exosome vesicles with closed circular lipid bilayers in both samples PU (Figure 5.17 Panel B) and MCI (Figure 5.17 Panel D).

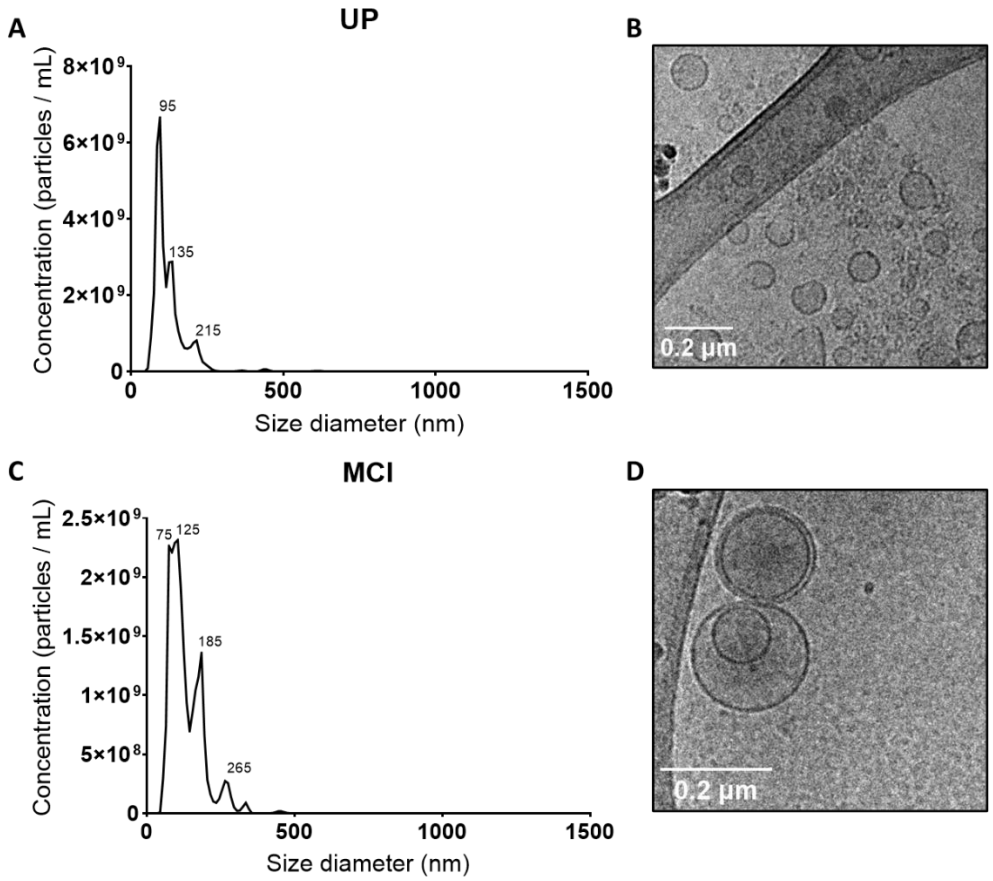


Figure 5.17. Panel A and C. Characterization by NTA of purified exosomes derived from the human serum samples with mild cognitive impairment (MCI) and universal plasma (UP, a pool of different plasma samples). Panels B and D. Cryo-TEM images of purified exosomes at an acceleration voltage of 200 kV.

The expression of surface exosome biomarkers was studied through bead-based flow cytometry. Both exosome samples were captured with antiCD81-MP and then detected with an indirect format for the detection of the tetraspanins, L1CAM and BACE1. All the tetraspanins were detected for both samples with a similar expression pattern, having a higher expression of CD9. In addition, the results show also similar expressions of L1CAM and BACE1 with a slightly higher expression of both in MCI sample (Figure 5.18).

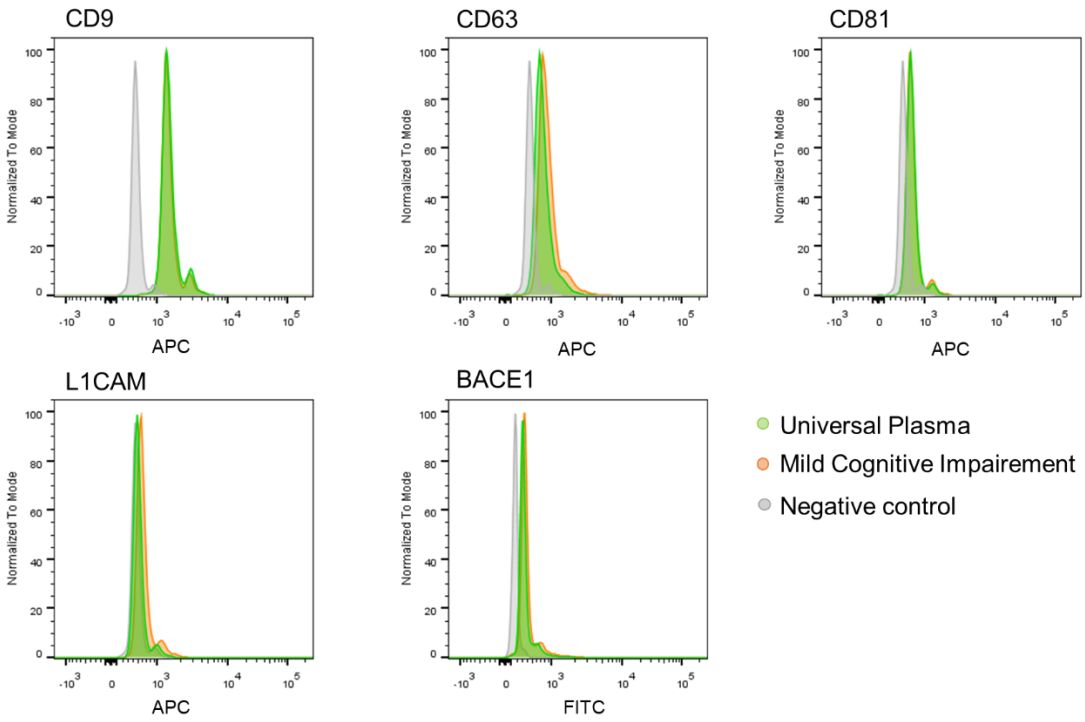


Figure 5.18. histograms of the characterization of the plasma samples by bead-based flow cytometry of surface biomarkers of the exosomes for both universal plasma and mild cognitive impairment samples.

Once the plasma exosomes isolation was performed and they were characterized, it remains to be elucidated if the BACE1 differential expression in neurons, previously described, is translated into significant expression changes in their exosomes at early AD stages in plasma samples through magneto-actuated immunoassay. Then, becoming a potential screening approach for early diagnostic test for AD with minimally invasive procedures.

5.8. References

(1) Alzheimer, A. Uber Eine Eigenartige Erkrankung Der Hirnrinde. *Allg Zeitschr f Psychiatr. u Psych-Gerichtl Med* **1907**, *64* (64), 146–148. https://doi.org/10.1002/ca.980080612.

(2) Stelzmann, R. A.; Norman Schnitzlein, H.; Reed Murtagh, F. An English Translation of Alzheimer's 1907 Paper, "Uber Eine Eigenartige Erkankung Der Hirnrinde." *Clin. Anat.* **1995**, *8* (6), 429–431. https://doi.org/10.1002/CA.980080612.

(3) Hampel, H.; Cummings, J.; Blennow, K.; Gao, P.; Jack, C. R.; Vergallo, A. Developing the ATX(N) Classification for Use across the Alzheimer Disease Continuum. *Nat. Rev. Neurol.* **2021**, *17* (9), 580–589. https://doi.org/10.1038/s41582-021-00520-w.

(4) Jack, C. R.; Holtzman, D. M. Biomarker Modeling of Alzheimer's Disease. *Neuron* **2013**, *80* (6), 1347. https://doi.org/10.1016/J.NEURON.2013.12.003.

(5) Sun, D. K.; Kim, J. Sequence Analyses of Presenilin Mutations Linked to Familial Alzheimer's Disease. *Cell Stress Chaperones* **2008**, *13* (4), 401. https://doi.org/10.1007/S12192-008-0046-0.

(6) Nikolac Perkovic, M.; Pivac, N. Genetic Markers of Alzheimer's Disease. *Adv. Exp. Med. Biol.* **2019**, *1192*, 27–52. https://doi.org/10.1007/978-981-32-9721-0_3.

(7) Passeri, E.; Elkhoury, K.; Morsink, M.; Broersen, K.; Linder, M.; Tamayol, A.; Malaplate, C.; Yen, F. T.; Arab-Tehrany, E. Alzheimer's Disease: Treatment Strategies and Their Limitations. *Int. J. Mol. Sci.* **2022**, *23* (22), 13954. https://doi.org/10.3390/ijms232213954.

(8) Nitrini, R. Preclinical Diagnosis of Alzheimer's Disease: Prevention Or? *Dement. Neuropsychol.* **2010**, *4* (4), 259. https://doi.org/10.1590/S1980-57642010DN40400002.

(9) Jack, C. R.; Bennett, D. A.; Blennow, K.; Carrillo, M. C.; Feldman, H. H.; Frisoni, G. B.; Hampel, H.; Jagust, W. J.; Johnson, K. A.; Knopman, D. S.; Petersen, R. C.; Scheltens, P.; Sperling, R. A.; Dubois, B. A/T/N: An Unbiased Descriptive Classification Scheme for Alzheimer Disease Biomarkers. *Neurology* **2016**, *87* (5), 539–547. https://doi.org/10.1212/WNL.0000000000002923.

(10) Goetzl, E. J.; Kapogiannis, D.; Schwartz, J. B.; Lobach, I. V.; Goetzl, L.; Abner, E. L.; Jicha, G. A.; Karydas, A. M.; Boxer, A.; Miller, B. L. Decreased Synaptic Proteins in Neuronal Exosomes of Frontotemporal Dementia and Alzheimer's Disease. *FASEB J.* **2016**, *30* (12), 4141–4148. https://doi.org/10.1096/fj.201600816R.

(11) Nagpal, N.; Kulshreshtha, R. MiR-191: An Emerging Player in Disease Biology. *Front. Genet.* **2014**, *5*, 87209. https://doi.org/10.3389/fgene.2014.00099.

(12) Zeng, Q.; Zou, L.; Qian, L.; Zhou, F.; Nie, H.; Yu, S.; Jiang, J.; Zhuang, A.; Wang, C.; Zhang, H. Expression of MicroRNA-222 in Serum of Patients with Alzheimer's Disease. *Mol. Med. Rep.* **2017**, *16* (4), 5575–5579. https://doi.org/10.3892/MMR.2017.7301.

(13) Swarbrick, S.; Wragg, N.; Ghosh, S.; Stolzing, A. Systematic Review of MiRNA as

Biomarkers in Alzheimer's Disease. *Mol. Neurobiol.* **2019**, *56* (9), 6156–6167. https://doi.org/10.1007/S12035-019-1500-Y.

(14) Cano, A.; Ettcheto, M.; Bernuz, M.; Puerta, R.; de Antonio, E. E.; Sánchez-López, E.; Souto, E. B.; Camins, A.; Martí, M.; Pividori, M. I.; Boada, M.; Ruiz, A. Extracellular Vesicles, the Emerging Mirrors of Brain Physiopathology. *Int. J. Biol. Sci.* **2023**, *19* (3), 721. https://doi.org/10.7150/IJBS.79063.

(15) Chen, W. W.; Balaj, L.; Liau, L. M.; Samuels, M. L.; Kotsopoulos, S. K.; Maguire, C. A.; LoGuidice, L.; Soto, H.; Garrett, M.; Zhu, L. D.; Sivaraman, S.; Chen, C.; Wong, E. T.; Carter, B. S.; Hochberg, F. H.; Breakefield, X. O.; Skog, J. Beaming and Droplet Digital Pcr Analysis of Mutant Idh1 Mrna in Glioma Patient Serum and Cerebrospinal Fluid Extracellular Vesicles. *Mol. Ther. - Nucleic Acids* **2013**, *2*, e109. https://doi.org/10.1038/mtna.2013.28.

(16) Kaczor-Urbanowicz, K. E.; Wei, F.; Rao, S. L.; Kim, J.; Shin, H.; Cheng, J.; Tu, M.; Wong, D. T. W.; Kim, Y. Clinical Validity of Saliva and Novel Technology for Cancer Detection. *Biochim. Biophys. acta. Rev. cancer* **2019**, *1872* (1), 49. https://doi.org/10.1016/J.BBCAN.2019.05.007.

(17) Zhang, Y.; Liu, Y.; Liu, H.; Tang, W. H. Exosomes: Biogenesis, Biologic Function and Clinical Potential. *Cell Biosci.* **2019**, *9* (1), 1–18. https://doi.org/10.1186/s13578-019-0282-2.

(18) Vlassov, A. V.; Magdaleno, S.; Setterquist, R.; Conrad, R. Exosomes: Current Knowledge of Their Composition, Biological Functions, and Diagnostic and Therapeutic Potentials. *Biochim. Biophys. Acta* **2012**, *1820* (7), 940–948. https://doi.org/10.1016/J.BBAGEN.2012.03.017.

(19) Cano, A.; Esteban-de-Antonio, E.; Bernuz, M.; Puerta, R.; García-González, P.; de Rojas, I.; Olivé, C.; Pérez-Cordón, A.; Montrreal, L.; Núñez-Llaves, R.; Sotolongo-Grau, Ó.; Alarcón-Martín, E.; Valero, S.; Alegret, M.; Martín, E.; Martino-Adami, P. V.; Ettcheto, M.; Camins, A.; Vivas, A.; Gomez-Chiari, M.; Tejero, M. Á.; Orellana, A.; Tárraga, L.; Marquié, M.; Ramírez, A.; Martí, M.; Pividori, M. I.; Boada, M.; Ruíz, A. Plasma Extracellular Vesicles Reveal Early Molecular Differences in Amyloid Positive Patients with Early-Onset Mild Cognitive Impairment. *J. Nanobiotechnology* **2023**, *21* (1), 1–19. https://doi.org/10.1186/S12951-023-01793-7.

(20) Luo, Y.; Bolon, B.; Kahn, S.; Bennett, B. D.; Babu-Khan, S.; Denis, P.; Fan, W.; Kha, H.; Zhang, J.; Gong, Y.; Martin, L.; Louis, J. C.; Yan, Q.; Richards, W. G.; Citron, M.; Vassar, R. Mice Deficient in BACE1, the Alzheimer's β-Secretase, Have Normal Phenotype and Abolished β-Amyloid Generation. *Nat. Neurosci.* **2001**, *4* (3), 231–232. https://doi.org/10.1038/85059.

(21) Vassar, R.; Bennett, B. D.; Babu-Khan, S.; Kahn, S.; Mendiaz, E. A.; Denis, P.; Teplow, D. B.; Ross, S.; Amarante, P.; Loeloff, R.; Luo, Y.; Fisher, S.; Fuller, J.; Edenson, S.; Lile, J.; Jarosinski, M. A.; Biere, A. L.; Curran, E.; Burgess, T.; Louis, J. C.; Collins, F.; Treanor, J.; Rogers, G.; Citron, M. β-Secretase Cleavage of Alzheimer's Amyloid Precursor Protein by the Transmembrane Aspartic Protease BACE. *Science.* **1999**, *286* (5440), 735–741. https://doi.org/10.1126/SCIENCE.286.5440.735.

(22) Guglielmotto, M.; Aragno, M.; Autelli, R.; Giliberto, L.; Novo, E.; Colombatto, S.; Danni, O.; Parola, M.; Smith, M. A.; Perry, G.; Tamagno, E.; Tabaton, M. The Up-Regulation of BACE1 Mediated by Hypoxia and Ischemic Injury: Role of Oxidative Stress and HIF1α. *J. Neurochem.* **2009**, *108* (4), 1045–1056. https://doi.org/10.1111/J.1471-4159.2008.05858.X.

(23) Holsinger, R. M. D.; McLean, C. A.; Beyreuther, K.; Masters, C. L.; Evin, G. Increased Expression of the Amyloid Precursor β-Secretase in Alzheimer's Disease. *Ann. Neurol.* **2002**, *51* (6), 783–786. https://doi.org/10.1002/ANA.10208.

(24) Fukumoto, H.; Cheung, B. S.; Hyman, B. T.; Irizarry, M. C. β-Secretase Protein and Activity Are Increased in the Neocortex in Alzheimer Disease. *Arch. Neurol.* **2002**, *59* (9), 1381–1389. https://doi.org/10.1001/ARCHNEUR.59.9.1381.

(25) Théry, C.; Amigorena, S.; Raposo, G.; Clayton, A. Isolation and Characterization of Exosomes from Cell Culture Supernatants and Biological Fluids. *Curr. Protoc. cell Biol.* **2006**, *Chapter 3* (1), 3–22. https://doi.org/10.1002/0471143030.CB0322S30.

(26) Rana, S.; Zoller, M. The Functional Importance of Tetraspanins in Exosomes. In *Emerging Concepts of Tumor Exosome-Mediated Cell-Cell Communication*; Springer New York, 2013; pp 69–91. https://doi.org/10.1007/978-1-4614-3697-3_4.

(27) Goetzl, E. J.; Boxer, A.; Schwartz, J. B.; Abner, E. L.; Petersen, R. C.; Miller, B. L.; Kapogiannis, D. Altered Lysosomal Proteins in Neural-Derived Plasma Exosomes in Preclinical Alzheimer Disease. *Neurology* **2015**, *85* (1), 40. https://doi.org/10.1212/WNL.0000000000001702.

(28) Dunlop, R. A.; Banack, S. A.; Cox, P. A. L1CAM Immunocapture Generates a Unique Extracellular Vesicle Population with a Reproducible MiRNA Fingerprint. *RNA Biol.* **2023**, *20* (1), 140. https://doi.org/10.1080/15476286.2023.2198805.

(29) Eren, E.; Leoutsakos, J. M.; Troncoso, J.; Lyketsos, C. G.; Oh, E. S.; Kapogiannis, D. Neuronal-Derived EV Biomarkers Track Cognitive Decline in Alzheimer's Disease. *Cells* **2022**, *11* (3), 436. https://doi.org/10.3390/cells11030436.

(30) Jiang, C.; Hopfner, F.; Berg, D.; Hu, M. T.; Pilotto, A.; Borroni, B.; Davis, J. J.; Tofaris, G. K. Validation of A-Synuclein in L1CAM-Immunocaptured Exosomes as a Biomarker for the Stratification of Parkinsonian Syndromes. *Mov. Disord.* **2021**, *36* (11), 2663. https://doi.org/10.1002/MDS.28591.

(31) Ferlemann, F. C.; Menon, V.; Condurat, A. L.; Rößler, J.; Pruszak, J. Surface Marker Profiling of SH-SY5Y Cells Enables Small Molecule Screens Identifying BMP4 as a Modulator of Neuroblastoma Differentiation. *Sci. Rep.* **2017**, *7* (1). https://doi.org/10.1038/S41598-017-13497-8.

(32) Al-Hajj, M.; Wicha, M. S.; Benito-Hernandez, A.; Morrison, S. J.; Clarke, M. F. From the Cover: Prospective Identification of Tumorigenic Breast Cancer Cells. *Proc. Natl. Acad. Sci. U. S. A.* **2003**, *100* (7), 3983. https://doi.org/10.1073/PNAS.0530291100.

(33) Tang, M. R.; Guo, J. Y.; Wang, D.; Xu, N. Identification of CD24 as a Marker for Tumorigenesis of Melanoma. *Onco. Targets. Ther.* **2018**, *11*, 3401–3406. https://doi.org/10.2147/OTT.S157043.

(34) Cervellati, C.; Trentini, A.; Rosta, V.; Passaro, A.; Bosi, C.; Sanz, J. M.; Bonazzi, S.; Pacifico, S.; Seripa, D.; Valacchi, G.; Guerini, R.; Zuliani, G. Serum Beta-Secretase 1 (BACE1) Activity as Candidate Biomarker for Late-Onset Alzheimer's Disease. *GeroScience* **2020**, *42* (1), 159–167. https://doi.org/10.1007/s11357-019-00127-6.

(35) Shen, Y.; Wang, H.; Sun, Q.; Yao, H.; Keegan, A. P.; Mullan, M.; Wilson, J.; Lista, S.; Leyhe, T.; Laske, C.; Rujescu, D.; Levey, A.; Wallin, A.; Blennow, K.; Li, R.; Hampel, H. Increased Plasma BACE1 May Predict Conversion to Alzheimer's Disease Dementia in Individuals With Mild Cognitive Impairment. *Biol. Psychiatry* **2018**, *83* (5), 447. https://doi.org/10.1016/J.BIOPSYCH.2017.02.007.

(36) Meakin, P. J.; Mezzapesa, A.; Benabou, E.; Haas, M. E.; Bonardo, B.; Grino, M.; Brunel, J. M.; Desbois-Mouthon, C.; Biddinger, S. B.; Govers, R.; Ashford, M. L. J.; Peiretti, F. The Beta Secretase BACE1 Regulates the Expression of Insulin Receptor in the Liver. *Nat. Commun.* **2018**, *9* (1), 1–14. https://doi.org/10.1038/s41467-018-03755-2.

(37) Kumar, S. R.; Kimchi, E. T.; Manjunath, Y.; Gajagowni, S.; Stuckel, A. J. RNA Cargos in Extracellular Vesicles Derived from Blood Serum in Pancreas Associated Conditions. *Sci. Rep.* **2020**, *10* (1), 1–10. https://doi.org/10.1038/s41598-020-59523-0.

(38) Pallares-Rusiñol, A.; Moura, S. L.; Martí, M.; Pividori, M. I. Electrochemical Genosensing of Overexpressed GAPDH Transcripts in Breast Cancer Exosomes. *Anal. Chem.* **2023**, *95* (4), 2487–2495. https://doi.org/10.1021/acs.analchem.2c04773.

(39) Banks, W. A.; Sharma, P.; Bullock, K. M.; Hansen, K. M.; Ludwig, N.; Whiteside, T. L. Transport of Extracellular Vesicles across the Blood-Brain Barrier: Brain Pharmacokinetics and Effects of Inflammation. *Int. J. Mol. Sci.* **2020**, *21* (12), 1–21. https://doi.org/10.3390/IJMS21124407.

(40) Cole, S. .; Vassar, R. The Basic Biology of BACE1: A Key Therapeutic Target for Alzheimer's Disease. *Curr. Genomics* **2007**, *8* (8), 509. https://doi.org/10.2174/138920207783769512.

Chapter 6.

Final remarks

6. Final remarks

Over the past decades, the outbreaks of communicable diseases highlight the need of implementing rapid diagnostic tests in primary health care facilities in low and medium-income countries. Thus, there is a necessity to identify novel biomarkers and to simplify and reduce the cost of the tests aligning to the features outlined in the acronym REASSURED (Real-time connectivity, Erase of specimen collection, Affordable, Sensitive, Specific, User-friendly, Rapid and robust, Equipment-free and Deliverable to end-users), as proposed by the World Health Organization. Designing tests for healthcare presents a challenging task, involving several considerations and integrating multiple disciplines as bioanalytical chemistry, molecular biology, biochemistry, immunology, material science, biomedicine, TICs, among many others. Rapid and affordable testing may lead to an early diagnosis of communicable or non-communicable diseases, a better stratification of individuals and an improved monitoring during treatment, reducing the disease burden. The recent COVID-19 pandemic outbreak highlighted the urgency of addressing all these concerns in diagnosis.

In this dissertation, three distinct biomarkers were explored as alternative detection approaches for both communicable and non-communicable diseases. These biomarkers were incorporated into innovative diagnostic platforms. Throughout all chapters, magnetic particles have been integrated to achieve specific isolation and preconcentration of the biomarkers while maintaining analytical simplification on the protocol and the instrumentation. Due to their versatility, magnetic particles tailored with different bioreceptors were used both for capturing the targets and downstream procedure, acting as a solid surface in biosensing approaches. Furthermore, all the methodologies were devised for application in liquid biopsies, using minimally invasive procedures for sample collection.

In Chapter 3, the exploration of miRNAs encapsulated in exosomes as biomarker was studied as the non-coding RNA cargo in exosomes primarily consists of miRNAs. The dysregulation of miRNA expression is extensively linked to pathology. Consequently, the detection of miRNAs within circulating exosomes opens novel routes for identifying changes in their expression by processing the exosomes isolated from sera or plasma.

Current methodologies for miRNA detection are technically complex and resource-intensive, limiting their applicability in specialized facilities. To overcome these constraints, a competitive magneto enzyme-linked miRNA (ELmiRNA) assay was developed. This approach exhibits promising features in enhancing the analytical simplification and cost-effectiveness of miRNA detection, offering an alternative diagnostic methodology. For this purpose, synthetic ODN counterparts were used in the assay, for the detection of miRNA21 and miRNA27a, both of which associated with breast cancer due to their upregulation. Hence, these biomarkers are suitable for detection in breast cancer cell lines and their derived exosomes as a first model. The assay performance was optimized with the synthetic ODN counterparts. Afterwards, miRNAs were detected in breast cancer cell lines (MCF-7 and MDA-MB-231) and their derived exosomes. The performance of the method was demonstrated by successfully detecting both miRNAs in the exosomes of both cell lines. The concentrations obtained for miRNA21 and miRNA27a were 27,821 and 32,440 copies per cell in MCF-7 cell line, and in the case of MDA-MB-231 cell line, the concentration corresponded to 21,077 and 54,920 copies per cell respectively. The quantification of these miRNA on the samples of exosomes was possible using the designed biosensor, being 17 and 12 copies per MCF-7 derived exosome and 11 and 15 copies per MDA-MB-231 derived exosome, for miRNA21 and miRNA27a, respectively. Thereby, the competitive ELmiRNA provides an alternative to the current miRNA detection methods, offering simplified performance and a reduced cost compared to qPCR, the standard method. The lack of amplification in the ELmiRNA assay not only simplify the analytical procedure but reduces the sample processing which can cause handling bias. Moreover, the versatility of the scaffold offers the adaptation to other miRNAs detection for other healthcare purposes. As future perspectives, the developed assay should be validated with complex samples such as human serum. Additionally, exploring the detection of different miRNAs by modifying the scaffold sequences for the use of novel biomarkers should be considered in future studies.

In Chapter 4, interferon-gamma (IFNγ) transcripts were used as a biomarker of cellular immune response. IFNγ is widely used for the detection of specific cellular immune response, and commercially available kits for its determination, such as QuantiFERON®-TB and T-SPOT®, have received FDA approval. These assays rely on detecting IFNγ released

from specific T cells after their stimulation with pathogen-derived peptides. The detection of the cellular immune response is important for determining the immunological status of the individuals as well as the possible outcome of a patient after an infection. While the evaluation of humoral response is equally important, there are now several rapid detection methodologies available for it, unlike those used for cellular immune response, which still tend to be complex and time-consuming. The proposed approach combines the detection of transcripts, rather than the released protein, to achieve a shorter incubation time, along with the use of magnetic particles to reduce the complexity of required instrumentation. Additionally, a lateral flow assay served as the readout after transcript amplification. Transcripts were double-tagged using labelled primers, enabling their detection through the lateral flow assay with avidin-modified carbon nanoparticles and the results compared to commercial streptavidin gold nanoparticles. COVID-19 was employed as a model for viral infection during the assay setup, given its recent outbreak. Analysis of vaccinated individuals recently infected and non-infected were included in the analysis. Our in vitro diagnostic platform was able to demonstrate the capability of the assay to detect specific T cells, distinguishing between both groups. Furthermore, the effectiveness in specific T cell detection without adding any T-cell activator to the blood sample, was up to two months after infection. This *in vitro* diagnostic was a one-day assay, but preliminary data using the reverse transcription and amplification in one step, suggest that the assay could be reduced in almost one hour.

This assay simplifies existing methodologies and shortens the time between sample collection and result outcome. This hallmark is essential to provide a fast patient stratification in highly infected populations to avoid the hospitals collapse. Moving forward, it is mandatory to test a larger number of individuals to validate these promising results. Additionally, individuals with a weak humoral response should be included to assess the suitability of this assay for their analysis. Furthermore, exploring the adaptation of this methodology for other pathogens using other peptides would be of interest.

In Chapter 5, exosomes were used as biomarkers due to their ability to traverse the blood-brain barrier, rendering them accessible targets for neurodegenerative diseases. These vesicles carry information from their originating cells, making them ideal candidates for assessing neuronal cell status. The synergy of both properties enables the detection of

Alzheimer's disease (AD) biomarkers in liquid biopsies such as plasma or sera. A magneto-actuated immunoassay was developed for capturing the exosomes from the sample and further detection in an ELISA platform. L1CAM was used for the capture of neuron-derived exosomes, given its neural origin, while beta-secretase (BACE1) was employed for the detection due to its implication in the generation of the amyloid plaques, a hallmark of AD. Thus, the combination of these biomarkers holds the potential for early AD diagnosis.

Neuroblastoma cell line (SH-SY5Y) was used for the optimization of the assay performance. First, the cell line and their derived exosomes were characterized, and then the magneto immune-actuated assay optimized. Then, the neuroblastoma derived exosomes were captured with a neuronal biomarker (L1CAM) and first detected with a general biomarker followed with an AD related biomarker. The LODs were inside the range of neuronal exosomes detected in human plasma, making the assay suitable for being validated with complex samples. Further research is needed to follow the project. On one hand, it is imperative to translate the findings from the *in vitro* model to patient samples. To achieve this, a matrix effect evaluation must be conducted on plasma samples to determine if it interferes with the capture of exosomes, a step previously undertaken by our group with breast cancer exosomes. On the other hand, there is a need for research in novel biomarker discovery. Several studies are currently examining the cargo of neuron-derived exosomes, which been shown to contain molecules associated with AD pathology, such as Tau, β-amyloid, CTFs, among others. Additionally, there is a promising research line focusing on the detection of miRNAs, as their content appears elevated in exosome cargo. Several miRNAs correlating with AD were found to be indicative of MCI conversion to AD in small studies. Combining the previously developed competitive magneto enzyme-linked miRNA assay with these concepts could be intriguing for a screening test to be conducted as point-of-care, detecting a combination of AD-related miRNAs. Moreover, this study has been the starting point of a research line within our group on the study of exosomes in neurodegenerative diseases. In the subsequent stages of this project, plasma samples of individuals with mild cognitive impairment and AD will be analyzed for the development of a biosensor aimed at detecting early onset Alzheimer's disease.

In conclusion, this thesis addresses the urgent need for rapid diagnostic tests in primary healthcare settings, particularly in low and medium-income countries grappling with communicable diseases. These studies contribute to advancing diagnostics by introducing innovative biomarkers and methodologies, emphasizing simplicity, cost-effectiveness, and adaptability for diverse healthcare purposes. The promising results warrant further validation and exploration, positioning these approaches as potential candidates for point-of-care applications.